

INFORMATION TO USERS

This manuscript has been reproduced from the microfilm master. UMI films the text directly from the original or copy submitted. Thus, some thesis and dissertation copies are in typewriter face, while others may be from any type of computer printer.

The quality of this reproduction is dependent upon the quality of the copy submitted. Broken or indistinct print, colored or poor quality illustrations and photographs, print bleedthrough, substandard margins, and improper alignment can adversely affect reproduction.

In the unlikely event that the author did not send UMI a complete manuscript and there are missing pages, these will be noted. Also, if unauthorized copyright material had to be removed, a note will indicate the deletion.

Oversize materials (e.g., maps, drawings, charts) are reproduced by sectioning the original, beginning at the upper left-hand corner and continuing from left to right in equal sections with small overlaps.

ProQuest Information and Learning
300 North Zeeb Road, Ann Arbor, MI 48106-1346 USA
800-521-0600

UMI[®]

NOTE TO USERS

This reproduction is the best copy available.

UMI[®]

University of Alberta

**GUSSET PLATES AS ENERGY DISSIPATERS IN SEISMICALLY LOADED
STRUCTURES**

by



Dean Thomas Mullin

A thesis submitted to the Faculty of Graduate Studies and Research in partial fulfillment
of the requirements of the degree of Doctor of Philosophy
in
Structural Engineering

Department of Civil and Environmental Engineering

Edmonton, Alberta
Spring 2005



Library and
Archives Canada

Bibliothèque et
Archives Canada

0-494-08278-X

Published Heritage
Branch

Direction du
Patrimoine de l'édition

395 Wellington Street
Ottawa ON K1A 0N4
Canada

395, rue Wellington
Ottawa ON K1A 0N4
Canada

Your file *Votre référence*

ISBN:

Our file *Notre référence*

ISBN:

NOTICE:

The author has granted a non-exclusive license allowing Library and Archives Canada to reproduce, publish, archive, preserve, conserve, communicate to the public by telecommunication or on the Internet, loan, distribute and sell theses worldwide, for commercial or non-commercial purposes, in microform, paper, electronic and/or any other formats.

The author retains copyright ownership and moral rights in this thesis. Neither the thesis nor substantial extracts from it may be printed or otherwise reproduced without the author's permission.

AVIS:

L'auteur a accordé une licence non exclusive permettant à la Bibliothèque et Archives Canada de reproduire, publier, archiver, sauvegarder, conserver, transmettre au public par télécommunication ou par l'Internet, prêter, distribuer et vendre des thèses partout dans le monde, à des fins commerciales ou autres, sur support microforme, papier, électronique et/ou autres formats.

L'auteur conserve la propriété du droit d'auteur et des droits moraux qui protègent cette thèse. Ni la thèse ni des extraits substantiels de celle-ci ne doivent être imprimés ou autrement reproduits sans son autorisation.

In compliance with the Canadian Privacy Act some supporting forms may have been removed from this thesis.

Conformément à la loi canadienne sur la protection de la vie privée, quelques formulaires secondaires ont été enlevés de cette thèse.

While these forms may be included in the document page count, their removal does not represent any loss of content from the thesis.

Bien que ces formulaires aient inclus dans la pagination, il n'y aura aucun contenu manquant.


Canada

Abstract

Gusset plates are elements which connect bracing to beams and/or columns in steel structures. In tests, gusset plates have exhibited load-deformation characteristics desirable of inelastic elements in seismically loaded structures. While the observed load-deformation response indicated potential of gusset plates to act inelastically in seismically loaded structures, they have not been quantitatively assessed in that role. Hence, a program was initiated to investigate gusset plates as inelastic elements in seismically loaded structures. The investigation addressed the interrelationship of gusset plate behavior and overall structural response to earthquakes.

Monotonic tension tests were conducted on six gusset plates of constant thickness and four gussets fitted with a reinforcing plate over the bolted connection. Gusset plates loaded in tension reached ultimate load at first fracture. Unreinforced plates fractured at deformations 2 mm to 5 mm lower than observed in similar reinforced plates. Total deformation at first fracture did not exceed 26 mm in any case. A modified gusset plate arrangement was proposed, employing extended hinge links (EHL), intended to increase deformation at first fracture. Two prototype specimens were tested cyclically. The smaller six link specimen sustained six cycles of loading, to a maximum deformation of 60 mm. The larger ten link specimen sustained 10 cycles of loading with maximum deformation of 120 mm.

Based on test results and analysis, it was concluded that the maximum expected deformation of a standard gusset plate, constructed using readily available materials and

typical propositions, would not be expected to exceed 15 mm. EHL gusset plate tests indicate that modified geometry could be expected to increase maximum cyclic deformation to greater than 60 mm.

Non-linear time history analyses of one, two, four and eight storey steel structures and eight storey seismic retrofit concrete structures were performed using scaled earthquake records. The records were scaled to equal peak zonal acceleration or velocity used in the calculation of seismic forces during structure design. Structures were designed using various bracing configurations zones and force modification factor, R values. One storey structures remained elastic up to design $R = 4$. Two storey structures exhibited inelastic responses, with gusset deformations up to 16 mm for Zone 3 events and for Zone 5 events up to design $R = 2$. For Zone 5 events and structures designed using $R = 3$ and 4, maximum gusset deformations ranged from 18 mm to 28 mm. Four storey steel structures exhibited deformations less than 15 mm (Zone 3, $R = 1.5, 2$), between 15 mm and 16 mm (Zone 3, $R = 3, 4$) and ranging from 18 mm to 30 mm (Zone 5, $R = 1.5, 2, 3$ and 4). For both steel and concrete eight storey structures, maximum gusset deformations ranging from 20 mm to 60 mm were observed in at least one location during one event for the parameters studied (Steel: Zone 3 and 5, $R = 2, 3, 3.5, 4, 6$, Concrete: Zone 5, $R = 2, 3$). Gusset plates typical of current construction practice were predicted to fracture (deform more than 15 mm) during at least one event among all four and eight storey structures. In no case did the predicted deformation demand exceed the deformation sustained in tests of EHL gussets.

Acknowledgements

The author wishes to extend thanks and gratitude to Dr. J.J. Roger Cheng for his guidance and assistance, as supervisor, throughout the course of this study. To the committee members, Drs Chan, Elwi, Jar and Lau, I extend sincere thanks for their insight and guidance.

As always, Larry Burden and Richard Helfrich of the I.F. Morrison Structures Laboratory provided excellent technical assistance and guidance during experimental phases of the study.

This project was conducted with financial assistance from the NSERC Industrial Post Graduate Scholarship Program, in partnership with BP-TEC Engineering Group Ltd. and from the C.W. Carry Fellowship. I wish to thank the individuals and organizations who provided financial assistance to this project, without which, this work would not have been possible. I especially wish to recognize the contributions of the directors of BP-TEC Engineering Group Ltd., who supported this program from the beginning: Bill Hibbard, Stuart Smith, Bob Giebelhaus, John McCune, David Heaton and Scott Donald. I have been honored to work with them as engineer, partner and friend.

Finally, to my family, I express my deepest love and gratitude. To David and Joan, who provided support and assistance in Edmonton – opening their home and hearts to me. To Nicole, Maxwell and Jack for their support, love and understanding – without which this work could not have been done.

Table of Contents

1. INTRODUCTION.....	1
1.1 General	1
1.2 Literature Review – Gusset Plates	6
1.3 Current Gusset Plate Design Practice	9
1.4 References	18
2. SEISMICALLY LOADED CONCENTRICALLY BRACED FRAMES	22
2.1 Introduction	22
2.2 Compatibility of Analysis with CAN/CSA-S16-01	22
2.3 Equivalent Lateral Seismic Loading by NBCC-1995.....	23
2.4 CBF Ductility Design Using CAN/CSA-S16.1-94	25
2.4.1 Ductile Braced Frames (DBF)	25
2.4.2 Braced Frames with Nominal Ductility (NDBF)	26
2.4.3 Strength Braced Frames (SBF)	26
2.5 CBF Ductility Design Using CAN/CSA-S16-01	28
2.5.1 Moderately Ductile (MD) Centrically Braced Frames	29
2.5.2 Limited-Ductility (LD) Centrically Braced Frames	30
2.5.3 Strength Braced Frames (SBF)	30
2.6 CBF Literature Review.....	31
2.6.1 General	31
2.6.2 Response of Braced Steel Structures to Seismic Loading	32
2.6.3 Response of Braced Concrete Structures to Seismic Loading	33
2.7 Conclusions	34
2.8 References	36

3. GUSSET PLATE EXTENSION DEFORMABILITY.....	38
3.1 Introduction.....	38
3.2 Test Specimens And Apparatus.....	39
3.3 Test Results	40
3.3.1 Unreinforced Specimens	40
3.3.2 Reinforced Specimens	42
3.3.3 Comparison of Reinforced to Unreinforced Behaviour	44
3.4 Analysis of Tested Specimens using Modified Block Shear Equations.....	45
3.5 Finite Element Analysis	46
3.5.1 General	46
3.5.2 Analysis of Tested Specimen 12R	47
3.5.3 Reinforced Gussets Analysis	49
3.6 Radial Strip Analysis	50
3.7 Conclusions	53
3.8 References	78
4. DUCTILE GUSSET PLATE – TESTS AND ANALYSIS.....	80
4.1 Introduction	80
4.2 Typical Gusset Behaviour	81
4.3 Gusset Modifications for Increased Deformability	82
4.4 Extended Hinge Link (EHL) Formulation	83
4.4.1 Preliminary Finite Element Analysis	85
4.5 EHL Modeling	85
4.6 EHL Predictive Model	86
4.7 Test Specimens	87
4.8 Test Apparatus	89
4.9 Test Results	90
4.9.1 Ancillary Tests	90
4.9.2 Small Plate Test	90
4.9.3 Large Plate Test	92

4.9.4 Face Plate Restraint	93
4.9.5 Energy Absorption	94
4.10 Discussion	94
4.11 Conclusions	95
4.12 References	121

5. RESPONSE OF SEISMICALLY LOADED LOW RISE STEEL CBF

STRUCTURES WITH INELASTIC GUSSET

PLATE CONNECTIONS	123
5.1 Introduction	123
5.2 Gusset Plate Behaviour	124
5.2.1 Gusset Plate Behaviour in Tension	124
5.2.2 Gusset Plate Behaviour in Compression	125
5.3 Structures Analyzed	126
5.3.1 Proportioning of Structural Members	126
5.3.2 Finite Element Modeling Parameters	127
5.4 Analysis	128
5.5 Results	129
5.5.1 Overall Structure Drift	129
5.5.2 Interstorey Drift	131
5.5.3 Gusset Plate Deformation Demand – General	131
5.5.4 Gusset Plate Deformation Demand – Two Storey Structures	132
5.5.5 Gusset Plate Deformation Demand – Four Storey Structures	133
5.6 Conclusions	134
5.7 References	145

**6. DEFORMATION DEMAND IN SEISMICALLY LOADED
CONCENTRICALLY BRACED STEEL FRAMES**

EMPLOYING INELASTIC GUSSET PLATES.....	148
6.1 Introduction	148
6.2 Gusset Plate Behaviour	149
6.3 Structural Design	150
6.4 Finite Element Analysis	151
6.4.1 General	151
6.4.2 Gusset Plate Modeling	153
6.4 Drift	154
6.4.1 General	154
6.4.2 Cross Braced Structures	154
6.4.3 Single Diagonal Braced Structures	155
6.4.4 M-Braced Structures	155
6.5 Gusset Plate Deformation	156
6.5.1 General	156
6.5.2 Gusset Plate Deformations - Cross Braced CBF	156
6.5.3 Gusset Plate Deformations - Single Diagonal Braced CBF.....	157
6.5.4 Gusset Plate Deformations – M-Braced Structures	158
6.6 Beams and Columns	159
6.7 Comparison of Predicted Behaviour with Published Literature	159
6.8 Discussion – Cross Braced Bay Energy Absorption Characteristics	161
6.9 Conclusions	162
6.10 References	181

7. DUCTILE GUSSET PLATES AS SEISMIC RETROFIT ELEMENTS

IN GRAVITY LOAD DESIGNED CONCRETE FRAMES	183
7.1 Introduction	183
7.2 Gusset Plate Behaviour	185

7.3 Concrete Behaviour and Modeling Parameters	188
7.4 Frame Model	190
7.5 Earthquake Records	191
7.6 Analysis	191
7.7 Results – General	192
7.8 Unbraced Frame	192
7.9 Cross Braced Retrofit with Slender Gussets	193
7.10 Cross Braced Retrofit with Stocky Gussets	194
7.11 M-Braced Retrofit	195
7.12 Column Loads	196
7.13 Conclusions	197
7.14 References	214
8. DISCUSSION, CONCLUSIONS AND RECOMMENDATIONS	218
8.1 General	218
8.2 Deformability of Continuous Gusset Plates	218
8.3 Deformability of EHL Gusset Plates	220
8.4 Gusset Plate Deformation Demand	221
8.4.1 General.....	221
8.4.2 Low Rise Steel Structures	221
8.4.3 Eight Storey Steel Structures	223
8.4.4 Eight Storey Concrete Structures	224
8.5 Conclusions	225
8.6 Recommendations	227
Appendix A – Patch, Beam and Extended Gusset Analysis Results	229
Appendix B – Beam Gusset Analysis Results	246

List of Tables

Table	Page
3.1 – Gusset Plate Ultimate Load Test Results vs. Prediction	54
3.2 – Results Summary – Gusset Plate Deformations	54
4.1 – Distributed Plasticity Gusset Analysis Results	97
5.1 – Member Size Summary	136
5.2 – Summary of Earthquake Records used in Analysis	137
5.3 – Stocky Gusseted Structure – Results Summary	137
6.1 – Member Sizes – Single Diagonal and Cross Braced Structures	164
6.2 – Member Sizes for M-Braced CBF Structures	165
6.3 – Summary of Earthquake Records used in Analysis	166
6.4 – Maximum Inelastic Gusset Deformation (mm) - Cross Braced CBF	167
6.5 – Maximum Inelastic Gusset Compression (mm) - Single Diagonal CBF	168
6.6 – Maximum Inelastic Gusset Extension (mm) - Single Diagonal CBF	169
6.7 – Maximum Inelastic Gusset Compression (mm) – MBF	170
6.8 – Maximum Inelastic Gusset Extension (mm) – MBF	171
7.1 – Gravity Load Design Concrete Frame Member Sizes	199
7.2 – Summary of Earthquake Records Used in Analysis	199
A.1 – Analysis Results	230
B.1 – Analysis Results	246

List of Figures

Figure	Page
1.1 – Typical Gusset Arrangements	12
1.2 – Load - Deformation Hysteresis of Gusset Plates Nominal Thicknesses 6.4 mm, 9.5 mm and 12.7 mm, taken from Walbridge, Grondin and Cheng (1998)	13
1.3 – Whitmore Yield Calculation	14
1.4 – Gusset Block Shear Region	14
1.5 – Test Apparatus, taken from Rabinovitch and Cheng (1993)	15
1.6 – Test Apparatus, taken from Yam and Cheng (1994)	16
1.7 – Thornton Compression Capacity Calculation	16
1.8 – Uniform Force Method, AISC Manual of Steel Construction – Volume II: Connections (1992)	17
3.1 – Test Schematic	55
3.2 – Specimen Dimensions	55
3.3 – Unreinforced Specimens – Experimental Load vs. Deformation	56
3.4 – Experimental Load vs. Deformation – Specimen 4U	57
3.5 – 8U, 8UA and 14U – Post Test	58
3.6a – 12R Post Test	59
3.6 – 12R, 8U, 8UA, 12U and 4U (L to R) Post Test	59
3.7 – Experimental Load vs. Deformation – Specimen 12R	60
3.8 – Experimental Load vs. Deformation – Specimen 12H	61
3.9 – 4U and 4R Load vs. Deformation	62
3.10 – 12 Bolt Specimens – Load vs. Deformation	62
3.11 – Net and Gross Areas Calculation – Definition	63
3.12 – 12R Experimental and FEA Load vs. Displacement	64
3.13 – 12R Gusset – Deformation 3 mm– Principal Stress (ksi).....	65

Figure	Page
3.14 – 12R Gusset – Deformation 3 mm - Inelastic Shear Strain	66
3.15 – 12R Gusset – Deformation 17.4 mm – Plastic Strain	67
3.16 – 12R Gusset – 3 rd Crack Growth Increment (Def. 19.4 mm) Principal Stress	68
3.17 – 12R Gusset – 19th Crack Growth Increment (Def. 26.4 mm) Principal Stress	69
3.18 – Doubler Plate Reinforced Gusset Geometries	70
3.19 – 12D8 Gusset – Deformation 10.2 mm – Maximum Principal Strain	71
3.20 – 12S2 Gusset – Deformation 3.3 mm - Maximum Principal Strain	72
3.21 – 12S2 Gusset – Deformation 10 mm – Principal Stress Vector Plot Includes Radial Lines from Focus	73
3.22 – 12D8 Gusset – Deformation 10.2 mm - Principal Stress Vector Plot Includes Radial Lines from Focus of Gusset	74
3.23 – 12R Gusset – Deformation 17.4 mm – Principal Stress Vector Plot Includes Radial Lines from Focus of Gusset	75
3.24 – Radial Strip Analysis	76
3.25 – Predicted Ultimate Deformations (mm) – FEA vs. Radial Strip	76
4.1 – Gusset Modification to Increase Deformability	98
4.2 – Extended Hinge Link (EHL) Schematic	99
4.3 – Opt9 Gusset Segment – Principal Strain at 394 mm Deformation	100
4.4 – Opt9 Gusset Segment – Principal Stress (ksi) at 394 mm Deformation	101
4.5 – Opt21 Gusset – Principal Strain Deformation 25.4 mm, Cycle1	102
4.6 – Opt21 Gusset – Principal Stress (ksi) – Deformation 25.4 mm, Cycle 1	103
4.7 – Face Plate Dimensions.....	104
4.8 – Small Plate Core Dimensions	104
4.9 – Large Plate Core Dimensions	105

Figure	Page
4.10 – Small Plate Hole Dimensions	106
4.11 – Brace Dimensions (As Originally Fabricated)	107
4.12 – Large Plate – Deformation +52 mm	108
4.13 – Edge View of Assembled Specimen	109
4.14 – Large Plate – Pretest	110
4.15 – Small Plate Load – Deformation Hysteresis	111
4.16 – Small Plate Load Deformation Cycles 1 through 3	112
4.17 – Small Plate Load Deformation Cycles 4 through 6	112
4.18 – Small Plate Load Deformation Cycle 7	112
4.19 – Small Plate Galling of Outside Surface of Face Plate	113
4.20 – Small Gusset – Necking of Upper Link, Cycle 7, Def. +60 mm, Load 350 kN	114
4.21 – Small Plate – End of Test – Fractured Links Visible Between Face Plates	114
4.22 – Small Plate with Fractured Link Parts in Contact Compression, Cycle 7	114
4.23 – Small Plate – Post Test Before Disassembly	115
4.24 – Large Plate – Load Deformation Hysteresis	116
4.25 – Large Plate – Load Deformation – Cycles 1 through 3	117
4.26 – Large Plate – Load Deformation – Cycles 4 through 6	117
4.27 – Large Plate – Load Deformation – Cycles 7 through 9	118
4.28 – Large Plate – Load Deformation – Cycles 10 and 11	118
4.29 – Large Plate Core – Post Test	119
4.30 – Large Plate Local Buckle Restrained by Face Plates	119
4.31 – Ductile Gusset Energy Absorption	120

Figure	Page
5.1 – Typical Brace and Gusset Configurations	138
5.2 – One, Two and Four Storey CBF Structure Geometry and Design Parameters	139
5.3 – Gusset Behaviour Modeled using Parallel Nonlinear Elements	140
5.4 – Unscaled LPI Acceleration, Velocity and Displacement	141
5.5 – Maximum, Mean and Minimum Interstorey Drift vs. a/v	142
5.6 – Maximum Gusset Deformation – Two Storey Structures	143
5.7 – Maximum Gusset Deformation – Four Storey Structures	144
6.1 – Gusset Hysteresis, taken from Nast (1999)	172
6.2 – Whitmore (Tension) and Thornton (Compression) Gusset Ultimate Load Models	173
6.3 – Structure General Arrangement and Bracing Configuration	174
6.4 – Loma Prieta (LPI) Event Unscaled Acceleration, Velocity and Displacement	175
6.5 – Gusset Plate Model Employing Parallel Inelastic Bar Elements	176
6.6 – Cross Braced Structures Interstorey Drift Envelopes	177
6.7 – Diagonal Braced Structures Interstorey Drift Envelopes	178
6.8 – M Braced Structures Interstorey Drift Envelopes	179
6.9 – Gusset Inelastic Deformation Envelopes	180
7.1 – GLD Column Behaviour, from Joh, O., Goto, Y., and Shibata, T. (1991)	200
7.2 – Gusset Hysteresis, from Walbridge (1999)	200
7.3 – Concrete Frame Retrofit General Arrangement	201
7.4 – Load - Deformation Behaviour of Gussets of Varying Thickness, from Walbridge, Grondin and Cheng (1998)	202

Figure	Page
7.5 – DRAIN2DX Uniaxial Stress-Strain Relationship for Concrete, from Powell, G.H. (1993)	203
7.6 – DRAIN2DX Type 15 Element Configuration with Non-linear Hinge from Powell, G.H. (1993)	203
7.7 – DRAIN2DX Hinge Fibre Response Modification Factors, from Powell, G.H. (1993)	204
7.8 – DRAIN-2DX Element 15 Patch Test Schematic Test Result, from Saiidi (1982)	205
7.9 – Concrete Frame Model General Arrangement	206
7.10 – Unscaled LPI Event, Acceleration (g), Velocity (m/s), and Displacement (m)	207
7.11 – Unbraced GLD Concrete Frame Response Summary	208
7.12 – Slender Gusset – X Braced Concrete Frame Response Summary	209
7.13 – Stocky Gusset – X Braced Concrete Frame Response Summary	210
7.14 – Stocky Gusset - M Braced Frames Response Summary	211
7.15 – Retrofit Frames, Gusset Deformation Envelopes	212
7.16 – Column Axial Loads , R=2 Structures	213
A.1 – Gusset 12DE Geometry	231
A.2 – Gusset 12DF Geometry	231
A.3 – Gusset 12DG Geometry	232
A.4 – Gusset 12DH Geometry	232
A.5 – Gusset 12DI Geometry	233
A.6 – Gusset 12DJ Geometry	233
A.7 – Gusset 12DK Geometry	234
A.8 – Gusset 16ROM Geometry	234
A.9 – Gusset 20RCL Geometry	235

Figure	Page
A.10 – Gusset 20RCM Geometry	235
A.11 – Gusset 20RCS Geometry	236
A.12 – Gusset 24RCL Geometry	236
A.13 – Gusset 24RCM Geometry	237
A.14 – Gusset 24RCS Geometry	237
A.15 – Gusset EXT1 Geometry	238
A.16 – Gusset EXT2 Geometry	238
A.17 – Gusset EXTEND Geometry	239
A.18 – Gusset 12WM Geometry	239
A.19 – Gusset 12D2 Geometry	240
A.20 – Gusset 12D8 Geometry	240
A.21 – Gusset 12D16 Geometry	241
A.22 – Gusset 12S2 Geometry	241
A.23 – Gusset 12S8 Geometry	242
A.24 – Gusset 12S16 Geometry	242
A.25 – Gusset 12DB Geometry	243
A.26 – Gusset 12DC Geometry	243
A.27 – Gusset 12DD Geometry	244
A.28 – Gusset 12R Geometry	244
A.29 – Gusset 12W Geometry	245
B.1 – bend2 Geometry	247
B.2 – bend3 Geometry	247
B.3 – bend4 Geometry	247
B.4 – bend5 Geometry	248
B.5 – bend7 Geometry	248
B.6 – bend8 Geometry	248

Figure	Page
B.7 – bend9 Geometry	249
B.8 – bend10 Geometry	249
B.9 – bend11 Geometry	249
B.10 – bend12 Geometry	250
B.11 – bend13 Geometry	250
B.12 – bend14 Geometry	250
B.13 – bend15 Geometry	251

List of Symbols

a	Peak horizontal acceleration
A_{vg}	Gross shear area of block tear
A_{vn}	Net shear area of block tear
A_{tg}	Gross tension area of block tear
A_{tn}	Net tension area of block tear
C	Gusset compression strength
C_R	Column compression capacity
E	Modulus of elasticity
EA	Modulus of elasticity times cross section area
e_B	Eccentricity of gusset to beam connection from beam centerline
e_C	Eccentricity of gusset to column from column centerline
E_{SEC}	Secant modulus
F	Foundation factor
F_T	Lateral to force in equivalent static lateral load design
F_y	Yield stress
F_U, F_{ULT}	Ultimate stress
H	Horizontal component of force transmitted through gusset, UFM
H_B	Horizontal force transmitted to beam from gusset, UFM
H_C	Horizontal force transmitted to column from gusset, UFM
h_o	Extended Hinge Link minimum depth
$h(x)$	Extended Hinge Link depth
I	Seismic importance factor
k	Effective length factor
ℓ	Length
$L1$	Column strip length from the upper tip of the Whitmore section to the supported gusset boundary, measured parallel to the brace axis.
$L2$	Column strip length from the center of the Whitmore section to the supported gusset boundary, measured parallel to the brace axis.

List of Symbols (Continued)

L_3	Column strip length from the lower tip of the Whitmore section to the supported gusset boundary, measured parallel to the brace axis.
L_{eff}	Thornton's effective column strip length = $(L_1 + L_2 + L_3) / 3$
L_{vg}	Gross shear length of block tear
L_{vn}	Net shear length of block tear
L_{tg}	Gross tension length of block tear
L_{tn}	Net tension length of block tear
M	Moment in extended hinge link
M_P	Plastic moment of section
M_{RY}	Column weak axis moment capacity
O	Gusset focal point
r	Radius of gyration
r	Distance from gusset focus, O
r_c	Radius of the connection boundary from the focus, O , of a gusset
r_y	Radius of yielded zone from gusset focus, O
R	Force modification factor
R	Vertical component of beam reaction, UFM
R_B	Resultant of reactions along gusset to beam connection, UFM
R_C	Resultant of reactions along gusset to column connection, UFM
S	Seismic response factor
S_{net}	Tension net section for block tearing calculation
t	Thickness
T	Gusset tension strength
T_R	Column tension resistance
v	Zonal velocity ratio, the ratio of the specified horizontal ground velocity to 1 m/s
V	Minimum lateral seismic force at the base of a structure
V	Vertical component of force transmitted through gusset, UFM
V_{ALL}	Allowable shear force in extended hinge link

List of Symbols (Continued)

V_B	Vertical force transmitted to beam from gusset, UFM
V_C	Vertical force transmitted to column from gusset, UFM
W	Structure dead load + 0.25 snow load + 0.6 storage load + tank contents
W_e	Whitmore effective width
x	Distance from extended hinge link origin
Z	Seismic zone
Z_a	Acceleration related seismic zone
Z_v	Velocity related seismic zone
α	Half height of gusset plate, UFM
α	Ratio of average shear stress to yield stress in extended hinge link.
β	Half width of gusset plate, UFM
δ, δ_{ULT}	Gusset deformability parallel to brace axis
ϵ	Strain
ϵ_{ULT}	Ultimate strain
ϵ_Y	Yield strain, Strain at the Proportional Limit
N	Resistance factor
$\sigma(r)$	Principal stress at distance point r from gusset focus, O
σ_c	Buckling stress
σ_i	Principal Stress in the i axis
$\sigma_1, \sigma_2, \sigma_3$	Principal Stress in the 1, 2 and 3 axis
σ_{ULT}	Ultimate strength of gusset plate
σ_Y	Yield strength of gusset plate
Θ	Angle from vertical to brace axis, UFM

List of Abbreviations

ACI	American Concrete Institute.
AISC	American Institute of Steel Construction
ASD	Allowable Stress Design
ASTM	American Society for Testing and Materials
ATC	Applied Technology Council
CANCEE	Canadian National Committee on Earthquake Engineering
CBF	Centrally Braced Frame
CISC	Canadian Institute of Steel Construction
CSA	Canadian standards Association
CTOD	Crack Tip Opening Displacement
CUREe	California Universities for Research in Earthquake Engineering
DBF	Ductile Braced Frame
EHL	Extended Hinge Link
ga.	hole gauge
GLD	Gravity Load Design
HLS.	Holes
kip	kiloPound (Pound x 10 ³)
kN	kiloNewton (Newton x 10 ³)
ksi	kip per square inch
LD	Limited Ductility
LRFD	Load and Resistance Factor Design
LVDT	Linear Varying Displacement Transducer
mm	milliMeter
MD	Moderately Ductile
MPa	MegaPascal (N/mm ²)
MTS	Material Test System
NBCC	National Building Code of Canada
NDBF	Braced Frame of Nominal Ductility
RC	Reinforced Concrete

List of Abbreviations (Continued)

s	second
SAC	A joint venture of SEAOC, ATC and CUREe
SBF	Strength Braced Frame
SEAOC	Structural Engineers Association of California
SRSS	Square Root Sum-of-Squares
UBC	Uniform Building Code
UFM	Uniform Force Method
w.p.	Work Point

1. INTRODUCTION

1.1 General

Gusset plates are those elements, in structural steel frames, which connect lateral load resisting braces to gravity load resisting beams and columns. Gusset plates are typically constructed using a structural steel plate, welded or bolted to the bracing element and welded or bolted to the adjacent beam and column. Common arrangements of gusset plates are shown in figure 1.1.

In previous research by Rabinovitch and Cheng (1993), Nast, Grondin and Cheng (1999) and Walbridge, Grondin and Cheng (1998), gusset plates have exhibited stable and open load deformation hysteresis when cyclically loaded as shown in figure 1.2 – especially when configured with stiffeners along their free edges. This behaviour is desirable in structural elements subjected to seismic loading beyond the elastic range. Of special interest is the combination of bracing which remains elastic during design seismic loading, while inelasticity occurs only in gusset plates. This capacity design system, referred to as “strong brace – weak gusset”, has exhibited better energy absorption characteristics than similar systems, which allow some brace inelasticity in cyclic tests by Nast (1999).

As outlined below, by limiting inelasticity during seismic loading to gusset plates, several benefits may be realized in design, construction, retrofit and post disaster repair of structures. If bracing elements remain elastic, overall and local brace slenderness limitations, normally applied to bracing members to ensure good post-buckling brace behaviour, would no longer be required. Elimination of these slenderness limitations has potential to reduce brace member sizes and increase the number of candidate cross sections available to the designer. Brace end connections in a strong brace – weak gusset system could be designed for loads less than gross cross section yield of the brace member, leading to more economical connections than those designed to develop full

brace cross section yield. For members with end connections designed to resist full cross section yielding, suppressing fracture at reduced net section may require reinforcement in the connection region, connections of large size or elimination of certain connection types from the list of choices available to fabricators. Retrofit of existing structures could be accomplished by installation of new gussets or addition of stiffeners to existing ones, thereby enabling gusset plates to act as “structural fuses” to prevent yielding of existing bracing. Post disaster repair of structures employing “strong brace-weak gusset” lateral load resisting elements would be simplified through localization of damage within the gusset plates – which could easily be replaced after a damaging earthquake while primary members remain in place.

Past research by others has focused primarily on gusset plate behaviour and on gusset – brace member interaction. While component and system behaviour have been found, in previous research, to exhibit characteristics deemed desirable in seismically loaded structures, no research has been conducted relating specifically to the response of structures employing “strong brace – weak gusset” lateral load resisting systems to seismic loading.

The purpose of this research is to quantify the anticipated deformation demand on gussets in a variety of seismically loaded structures, designed using the “strong brace – weak gusset” philosophy. Of additional interest is the distribution of damage in structures, so designed, after a design earthquake event. The ability of gusset plates of various configurations to deform without fracturing is also explored through tests and analyses.

This thesis is presented as a “Paper Based” thesis, using consistent format throughout, and contains six papers, listed below in the order in which they are presented, with a brief summary of each. The first paper (Chapter 2) summarizes the design and behaviour of seismically loaded concentrically braced steel structures. The next two papers (Chapters 3 and 4) present results relating to the ability of gussets to deform without fracturing and their post fracture behaviour. Throughout the subsequent text, the deformation up to first fracture is referred to as deformability. Deformability may be considered, in limit states

design terms, a resistance. The last three papers (Chapters 5, 6 and 7) present results relating to the anticipated deformation demand placed on gussets in seismically loaded “strong brace – weak gusset” systems. Deformation demand may be considered, in limit states design terms, a loading.

Summaries of the papers contained within this thesis, listed by chapter number, are:

2. Literature Review - This chapter provides a summary of the design and behaviour of seismically loaded concentrically braced steel structures. The first section of this chapter presents an overview of the design requirements of the National Building Code of Canada, NRCC (1995) and CAN/CSA S16.1-94, the standards used for calculation of design loads and structural member sizes in chapters 5 through 7. A comparison of the seismic provisions of the new Canadian structural steel design standard, CAN/CSA S16-01 with CAN/CSA S16.1-94 is made. The second section of this chapter is a review of seismically loaded braced frame research relevant to this thesis. Included in the review are summaries of those papers deemed particularly relevant to the non-linear time history analyses conducted as part of Chapters 5, 6 and 7 of this thesis.

3. Gusset Plate Extension Deformability – Tests of gusset plates, bolted to brace members, were conducted. Bolted connections were fabricated with and without reinforcing plates welded to the gusset, around the brace – gusset connection bolt group. Subsequent to testing, non-linear finite element analyses were conducted on plates configured to match test specimens and on other configurations. A predictive model for gusset plate fracture deformation was formulated based on observed gusset behaviour. Fracture deformations calculated using the model were found to correlate with finite element predicted fracture deformations.

4. Ductile Gusset Plate Tests and Analysis – Based on the results of the analyses presented in chapter 2, gusset configurations transferring applied forces in flexure, through deformable links, are expected to provide improved deformability when compared to conventionally configured continuous gusset plates. Gusset plates

configured with flexural links were evaluated analytically and experimentally. Finite element analyses of a variety of gusset configurations are reported. A candidate flexural link shape, referred to as Extended Hinge Link (EHL) is formulated based on maximized yielded volume prior to fracture. Cyclic test results are presented for two gussets employing EHL links. Deformability of tested EHL gussets was 80 mm for the smaller specimen and 120 mm for the larger, compared to 10 mm to 20 mm observed in tests of conventionally configured gussets by Chakrabarti and Bjorhovde (1983), Bjorhovde and Chakrabarti (1985), Gross (1990), Rabinovitch and Cheng (1993) and Mullin (Chapter 3).

5. Response of Seismically Loaded Low Rise Steel CBF Structures with Inelastic Gusset Plate Connections – Steel structures of 1, 2 and 4 storeys were designed and analysed using parameters $R = 1.5, 2, 3$ and 4 in zones 3 and 5. Lateral load resisting systems were proportioned based on the “Strong Brace – Weak Gusset” philosophy. Structures were analysed using non-linear time history analysis, performed using DRAIN-2DX software, Prakash, Powell and Campbell (1993), and nine scaled earthquake records, covering a range of a/v ratios. All structures were cross braced, within a single bay and within each storey. One storey structures responded primarily elastically in all cases. Two storey structure gusset deformations were primarily less than previously observed conventional gusset deformability (up to 20mm). In four storey structures predicted gusset deformations exceeded anticipated conventional gusset plate deformability in several of the cases analysed.

6. Response of Seismically Loaded Eight Storey Steel CBF Structures with Inelastic Gusset Plate Connections – Eight storey steel concentrically braced frames were designed using single diagonal, cross braced and M-braced lateral load resisting systems and design parameters of $Z = 3$ and 5 , $R = 2, 3$ and 4 (X and diagonal) and $R = 3, 4.5$ and 6 (M-Braced). Lateral load resisting systems were proportioned based on the “Strong Brace – Weak Gusset” philosophy. Structures were analysed using non-linear time history analysis, performed using DRAIN-2DX software, Prakash, Powell and Campbell (1993), and nine scaled earthquake records, covering a range of a/v ratios. Gusset deformation demand was found to approach or exceed experimentally observed

deformability of conventionally configured gusset plates in all configurations analysed. Ductile gusset configurations, identified by Mullin (Chapter 4), have exhibited deformability in excess of predicted deformation demand for all retrofit structures analysed.

7. Ductile Gusset Plates as Seismic Retrofit Elements in Gravity Load Designed

Concrete Frames – Using non-linear time history analyses and scaled earthquake

records, gravity load designed concrete frames were analysed in the unbraced state and

with retrofit steel bracing and gusset plates, designed using the “strong brace – weak

gusset” philosophy. Retrofit bracing was provided in three configurations, X-braced with

slender gussets, X-braced with stocky gussets and M-Braced, a steep double chevron

configuration, with stocky gussets. In the analyses, stocky gussets possessed equal

compression and tension proportional limits while in slender gussets, compression

proportional limit was 85% of that in tension. Design parameters were Zone 5 design

events with $R = 2$ and 3 . Unbraced frames were found to suffer “soft storey collapse” or

severe damage within the ground storey during 4 of the 9 events analysed. Storey drift in

structures with retrofit concentric bracing was found to correspond with reduced damage

(< 0.02 radians plastic hinge rotation) in concrete columns. Gusset deformation demand

exceeded the anticipated gusset deformability of 15 mm in X-braced structures but

generally did not exceed that deformability in the M-braced configuration. Ductile gusset

configurations, identified by Mullin (Chapter 4), have exhibited deformability in excess

of predicted maximum gusset deformation demand in all retrofit structures analysed.

The papers presented within this thesis are of an internally consistent format and do not reflect the format requirements of any specific publication. Figures and tables are located at the end of each paper and are followed by a references. A list of variables is provided after the table of contents. Figure and table numbering is sequential within each paper and include the chapter number. Prior to submission for publication, each paper will be reformatted to comply with the requirements of the target publication.

1.2 Literature Review – Gusset Plates

Current gusset plate design practice is based in large measure on the experimental work of Whitmore (1952), which comprised tests of gusset plates using photo-elasticity, strain gauges and brittle lacquer to assess the elastic stress state of loaded gussets. Based on the observations made during the tests, Whitmore concluded that the location of maximum stress in the gusset existed just beyond the end of the brace-gusset connection region. Further, he proposed the effective width concept, defined in figure 1.3, to allow prediction of that maximum stress. The effective width is defined as the length of a line, perpendicular to the brace axis and passing through the center of the fastener nearest the root of the gusset, bounded on two sides by lines extending from the fasteners most distant from the root of the gusset and at 30° to the brace axis. The Whitmore load is defined as the effective width multiplied by gusset thickness and yield strength. This method of prediction of stress in gussets remains widely used.

Subsequent to research by Whitmore, experimental investigations were conducted by Irvan (1957) and Hardin (1958). The investigations by Irvan and Hardin led to a proposed modification of the Whitmore effective width concept where the origin of the 30° line was moved from the fastener most distant from the root of the gusset to the centroid of the fastener group.

The results of linear elastic finite element analytical investigations conducted by Davis (1967) and Vasarhelyi (1971) indicated that the Whitmore effective width concept provided good prediction of maximum stress but poor prediction of the location of maximum stress for the gussets analysed.

Further analytical investigation was performed by Struik (1972) using elastic-plastic finite element analysis which included bolt holes and elastic fastener behaviour. The results of the analysis indicated that the ratio of ultimate to design load was highly variable in gussets using methods of design common at the time.

Six full-scale gusset plate tests were performed by Bjorhovde and Chakrabarti (1985). The results indicated that failure of gussets in tension is typically via block shear failure comprising first fracture across the bolt line closest to the gusset root followed by fracture along the bolts parallel to the brace axis. Fracture circumscribing the connection region in a gusset is commonly referred to as block shear or block tearing and is depicted in figure 1.4. In compression, gusset edge buckling, preceded by in-plane bending was observed.

Additional testing of gussets by Hardash and Bjorhovde (1985) enabled the development of the modified block shear concept utilizing ultimate tension stress on the net section of the gusset along the bolts near the root of the connection and shear yield along the gross section of the sides of the bolted connection, as shown in figure 1.4.

When loaded in compression, the ultimate limit state arises from gusset plate instability rather than fracture. Williams and Richard (1986) performed an analytical study of the compressive behaviour of gusset plates. A parametric study was conducted using elastic finite element analysis. Parameters varied were plate size, mesh size, beam and column boundary fixity, gusset configuration (single brace or K) and frame action. The study revealed that fixity at the beam and column connection to gussets increased the buckling capacity of the gussets analysed. It was also concluded that for similar configurations, K brace gussets had higher compression capacity than single brace gussets.

Hu and Cheng (1987) performed an experimental investigation of the elastic response of gussets, loaded in compression. Tests were conducted on fourteen specimens of two thicknesses (3.1 mm and 6.7 mm) and two sizes (850 mm x 500 mm and 850 mm x 700 mm) which were assembled concentrically and eccentrically with the bracing member. The boundary connections of the gusset to beam and column were restrained from displacement relative to the brace axis in some tests and free to displace out-of plane of the undeformed gusset in others. It was determined from the test results that the concentrically loaded gussets failed by buckling of their free edges. When constrained, maximum out-of-plane displacement of the gussets was near the mid-point of their free

edges. When unconstrained, maximum out-of-plane displacement of the system was that of the brace relative to the plane of the beam and column frame. Failures observed in the eccentrically loaded gussets were similar in nature to those observed in the concentric cases but were observed to occur at lower loads with increasing eccentricity. It was also observed that increasing the stiffness of the splice plates could increase the buckling load, where the gusset-brace assembly was loaded eccentrically.

Rabinovitch and Cheng (1993) performed tests and analysis of five concentrically loaded gusset plate specimens of varying thickness, edge stiffening and geometry, using the apparatus schematically depicted in figure 1.5. Loading was cyclic with maximum cycle deformations increasing in tension but remaining nearly constant in compression during subsequent load cycles. It was determined from the test results that gussets furnished with stiffeners along their free edges exhibited a stable load with increasing post buckling compression deformation. In contrast, tested gussets with unstiffened free edges exhibited an abrupt reduction of load with post-buckling compression deformation.

Yam and Cheng (1993) performed twenty-one compression tests on nineteen gusset plate specimens, varying size, thickness, brace angle, brace eccentricity and out-of-plane restraint using the apparatus depicted schematically in figure 1.6. The effects of frame action were investigated by applying loads to the beam and column to produce moment at the gusset location. Failure of specimens was generally sideways within the gusset accompanied by buckling of the free edges of the plates. Reduced capacity was observed in gussets with eccentrically connected bracing, as observed by Hu and Cheng (1987). Beam and column moment was found to have a negligible effect on gusset strength. Yielding was observed at loads lower than those predicted using the Whitmore effective width. Buckling capacity was found to be well predicted by a modified Thornton method, incorporating an increased 45° dispersion angle as shown in figure 1.7 and described by Yam and Cheng (2002). The beam column equation of S16.1-M89 was used in conjunction with the modified Thornton method to predict capacity with acceptable accuracy.

Nast, Grondin and Cheng (1999) performed an experimental and analytical investigation of four gusset plate assemblies, loaded cyclically through long bracing members. By varying the brace length, specimens were proportioned such that, when compressed, two would buckle within the brace (strong gusset – weak brace) and two would buckle within the gusset (strong brace – weak gusset). Two specimens were edge stiffened and two were unstiffened. It was determined that the strong brace – weak gusset configuration with gusset edge stiffening exhibited stable post-buckling strength and enhanced energy absorption characteristics when compared to the other configurations.

Walbridge, Grondin and Cheng (1998) performed a numerical study of gussets previously tested by Yam and Cheng (1994) and Rabinovitch and Cheng (1993) using the finite element program ABAQUS. The first phase of the analysis was to duplicate as accurately as possible the results obtained in previous tests. The parameters used to accurately model previous tests were then employed to conduct a parametric study of brace-gusset interaction and gusset parameters. The results of the investigation indicated that the strong brace-weak gusset approach would provide stable post-buckling strength and enhanced energy absorption when compared to other configurations.

1.3 Current Gusset Plate Design Practice

The proportions of gusset plates are typically determined through evaluation of three limit states. The first limit state is fracture of the gusset plate material around the perimeter of the brace – gusset connection. Fracture of this nature is frequently referred to as block tearing, block shear failure or net section fracture. In the case of bolted brace connections, fracture is typically assumed to occur along the perimeter of the connection bolt group with initial fracture occurring between the bolts closest to the root of the gusset plate. Equations from Hardash and Bjorhovde (1985) are used, in modified forms, to predict ultimate strength of the block shearing failure mode in both AISC (LRFD J5.2.c ; ASD J4) and CAN/CSA-S16-01 (12.3.1) standards.

The second limit state considered in design of gussets is strength and stability of the gusset. In tension, the maximum stress in the gusset may be predicted using the effective width concept, originally described by Whitmore (1952). In compression, gusset capacity can be predicted using the method described by Thornton (1984) wherein the same effective width approach described by Whitmore (1952) is used but with stress limited to the maximum allowed for the k/r of the gusset, as defined in figure 1.7. These methods are not specifically referenced in clauses of AISC or CISC design standards, but do appear in companion publications. "Connection Design for Steel Structures" (CISC, 1991) specifically describes the Whitmore effective width concept for design and makes reference to the requirement that instability be considered when compression forces are to be applied to gussets by stating "the possibility of local buckling in compression zones must be examined when the (gusset) unsupported length is significant". The AISC Manual of Steel Construction, Volume II, Connections (LRFD/ASD), specifically describes the application of Whitmore's Effective width for tension capacity evaluation and the Thornton method, modified by Gross (1990), using $k = 0.5$ and length either of L_2 , the distance between the innermost row of connectors and the gusset root or the average of L_1 , L_2 and L_3 .

The third limit state considered in the proportioning of gusset plates and their connections to adjacent elements is capacity of the connection of the gusset to beams and/or columns. Three methods are generally applied in connection design practice and have been studied and compared by the AISC Task Group on gusset connections, Thornton (1992). The component method is commonly used and involves resolution of brace force along the faces of gusset plates connected to gravity framing. Connections on those planes are then proportioned for those force components. Application of this method to gusset boundary connection design implies that the line of action of the brace force passes through the intersection of the connected faces, which is rarely the case. To equilibrate forces arising from the eccentricity of the brace axis from the gusset root, the force-couple method includes moment on the boundary of the gusset where boundary conditions are stiffest. The stress distribution along the stiffly connected boundary of the gusset is generally and conservatively assumed to be linear notwithstanding the location of maximum stress has

been shown in tests, e.g. Whitmore (1952), to vary from that predicted by the linear elastic stress distribution. While the location of maximum stress is poorly predicted by linear elastic boundary stress distribution, the magnitude of the maximum stress does not vary significantly between Whitmore (1952) and linear elastic bending. As reported by the AISC Task Group, the force-couple method generally gives rise to smaller gusset size than that obtained using the component method for a given set of design conditions, but requires more effort on the part of the designer.

The uniform force method, recommended as the method giving rise to the most economical brace connections in the AISC Manual of Steel Construction, Volume II, Connections (LRFD/ASD), is the third most common method of proportioning gusset boundary connections. As outlined in figure 1.8, the method is based on the presumption that, at ultimate load, force distributions along the connected boundary of gusset plates are uniform and that resultants of forces acting on those connected boundaries intersect at a point on the brace axis. This arrangement of forces gives rise to no couples on either the beam or column and gives rise to uniform utilization of structural capacity along connected planes. The method requires that a geometric relationship between the column and beam connection planes be satisfied to ensure that uniform boundary force distributions exist at ultimate load.

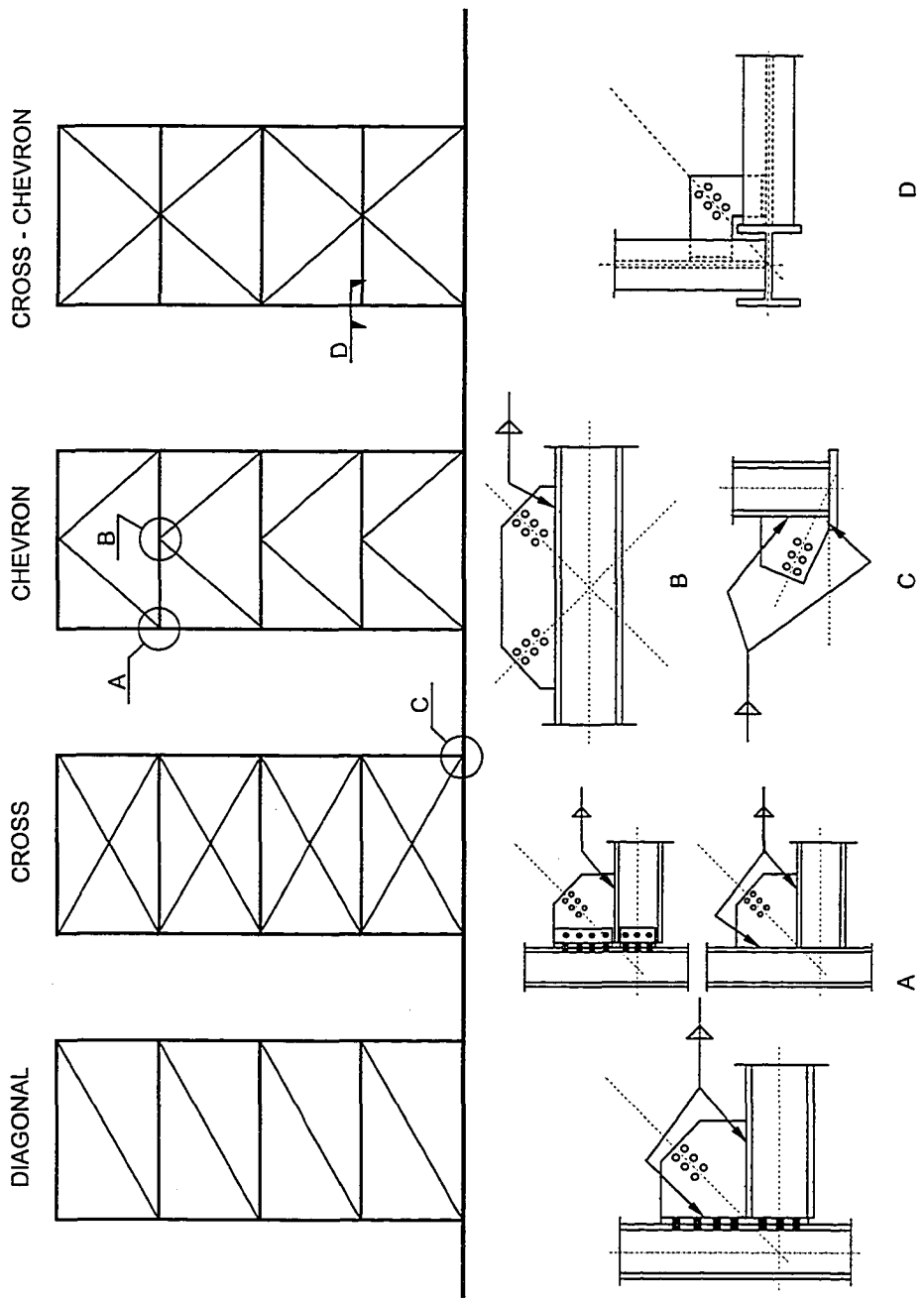
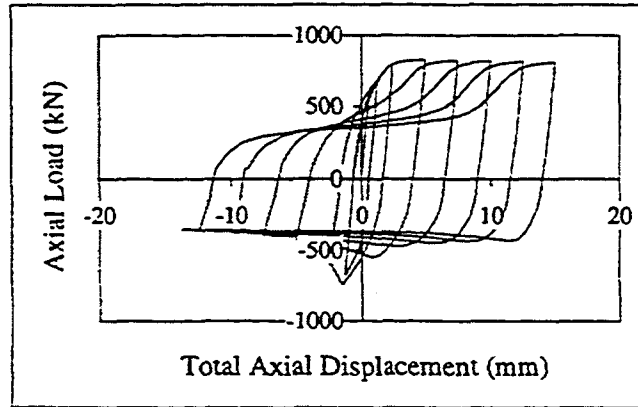
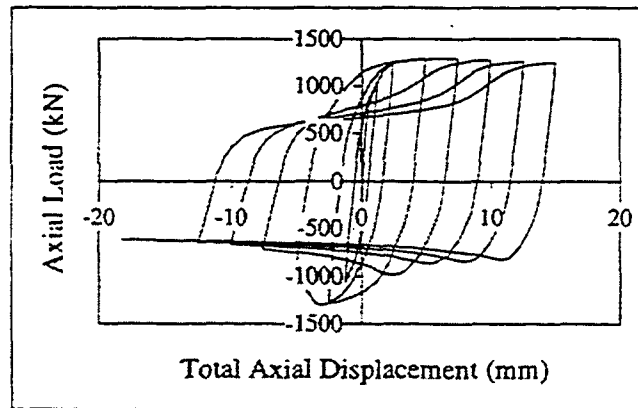


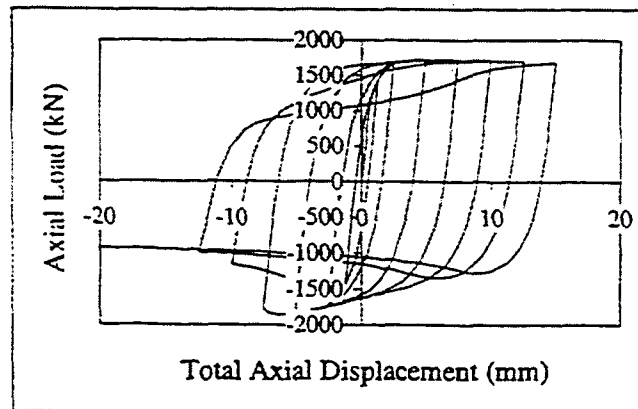
Figure 1.1 - Typical Gusset Arrangements



(a) - Gusset plate GP1 (no brace member): Nominal $t = 6.4$ mm



(b) - Gusset plate GP2 (no brace member): Nominal $t = 9.5$ mm



(c) - Gusset plate GP3 (no brace member): Nominal $t = 12.7$ mm

**Figure 1.2 – Load - Deformation Hysteresis of Gusset Plates
Nominal Thicknesses 6.4 mm, 9.5 mm and 12.7 mm, taken
from Walbridge, Grondin and Cheng (1998)**

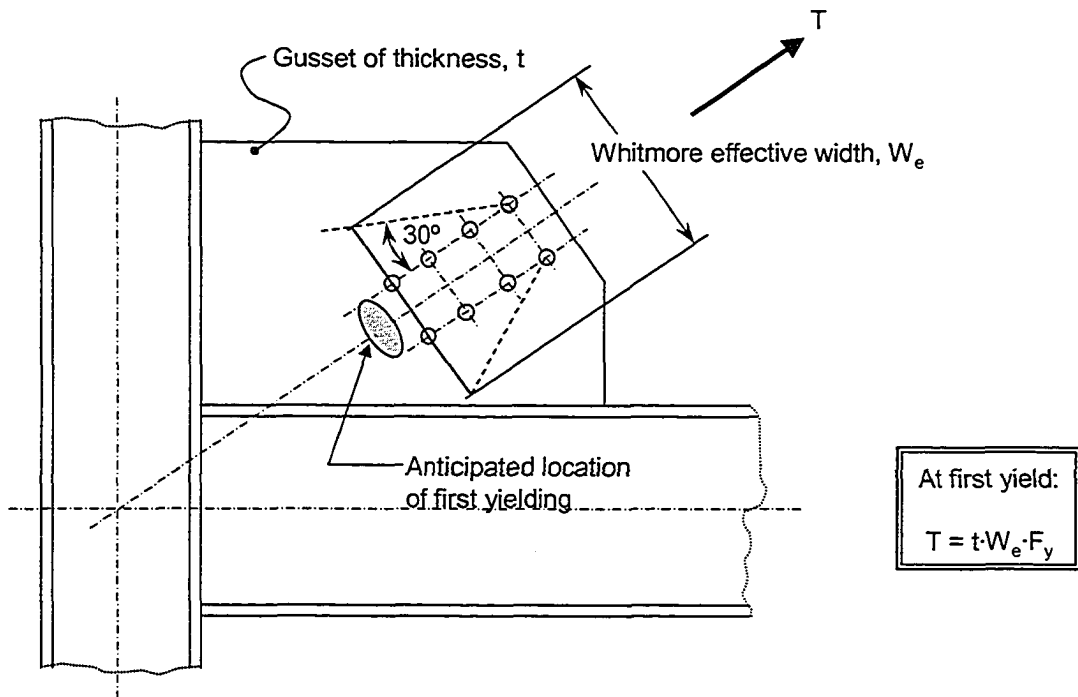


Figure 1.3 - Whitmore Yield Calculation

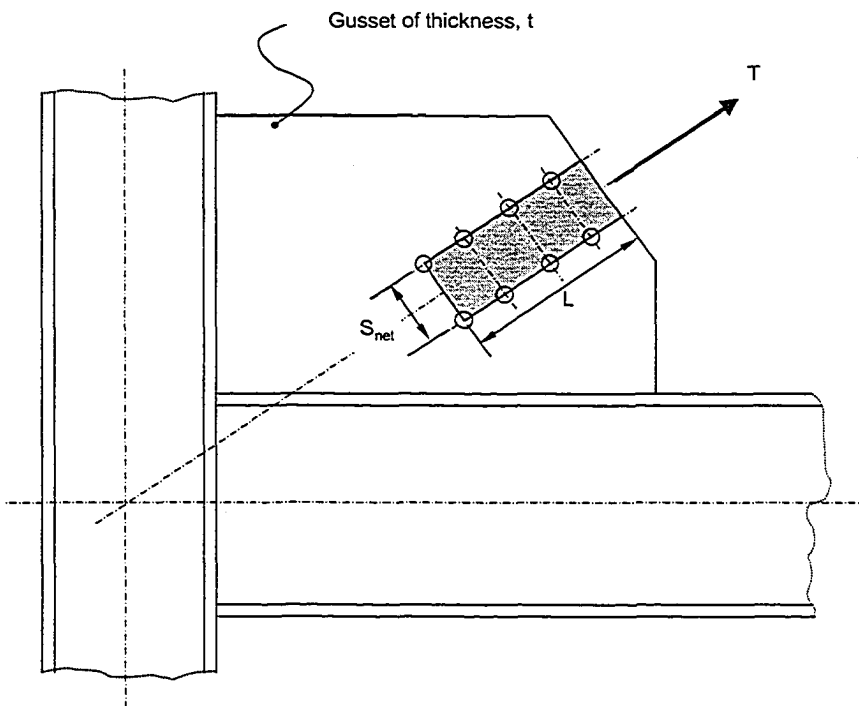


Figure 1.4 - Gusset Block Shear Region

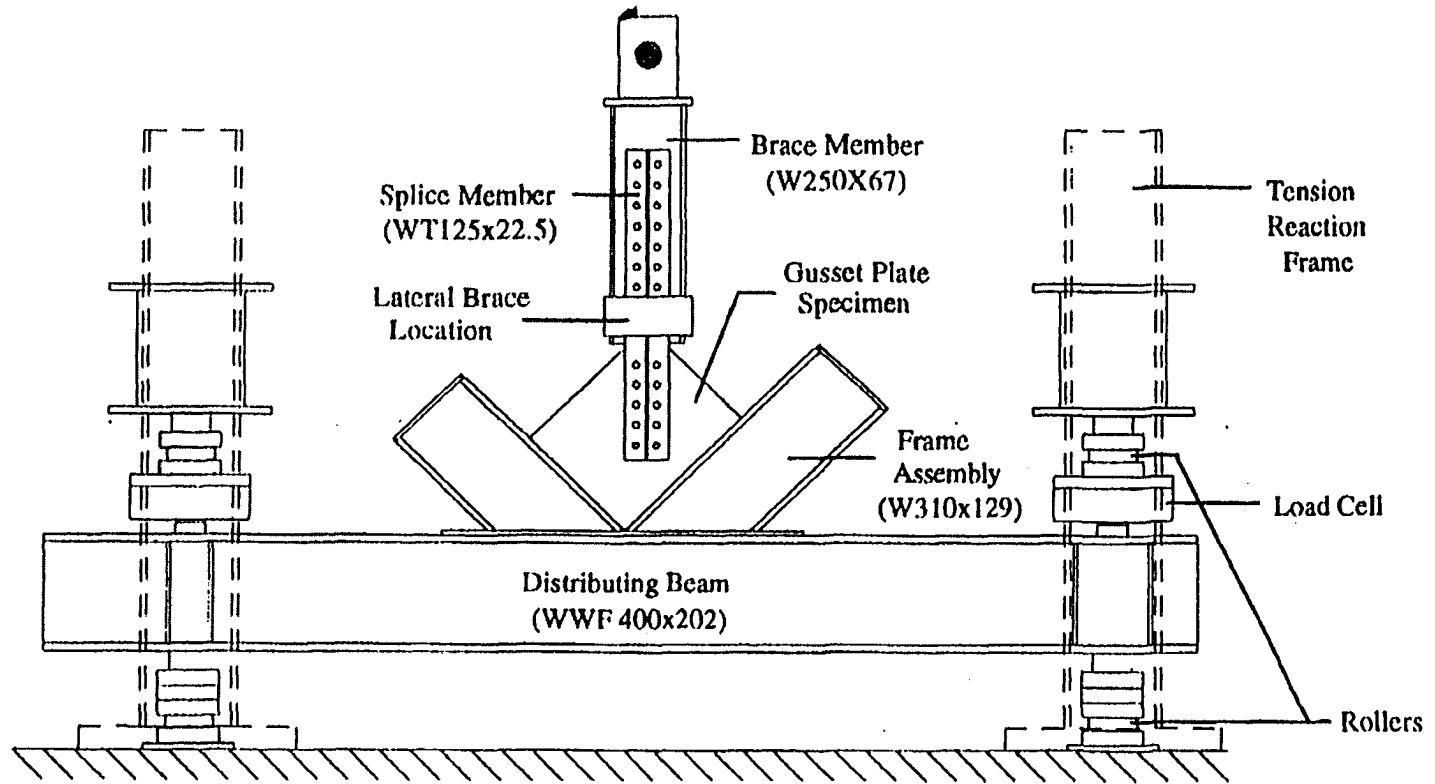


Figure 1.5 - Test Apparatus, from Rabinovitch and Cheng (1993)

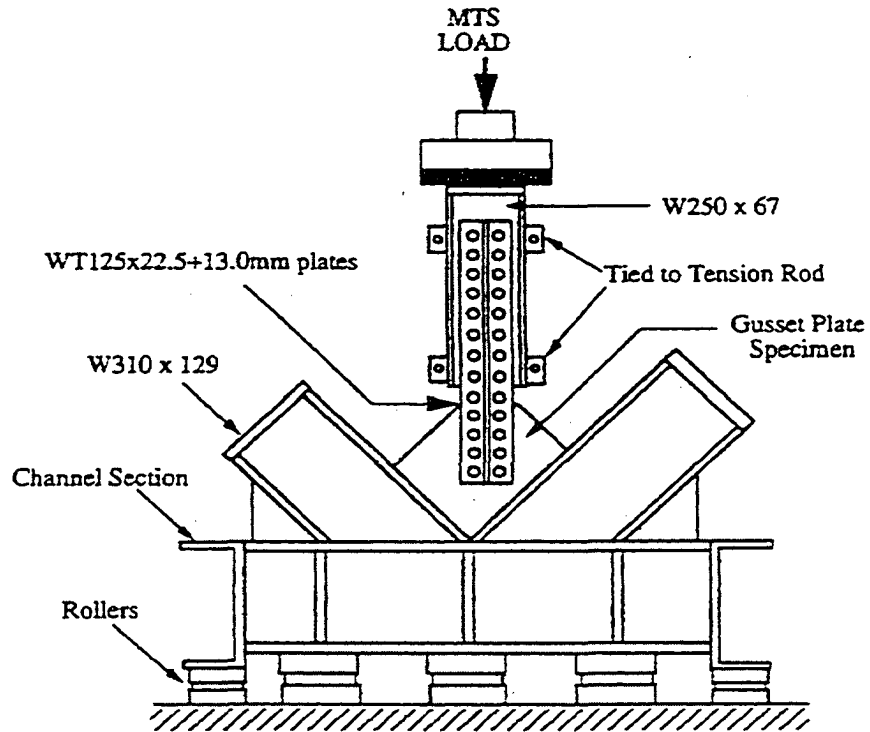


Figure 1.6 - Test Apparatus, from Yam and Cheng (1994)

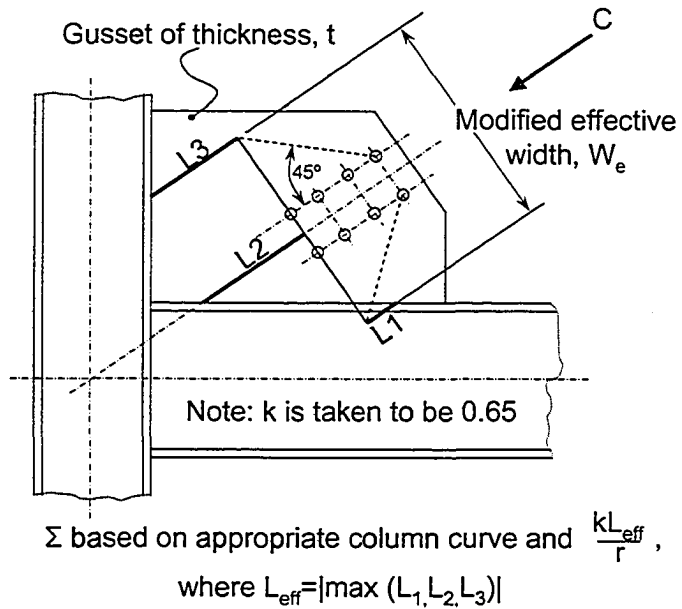


Figure 1.7 - Thornton Compression Capacity Calculation

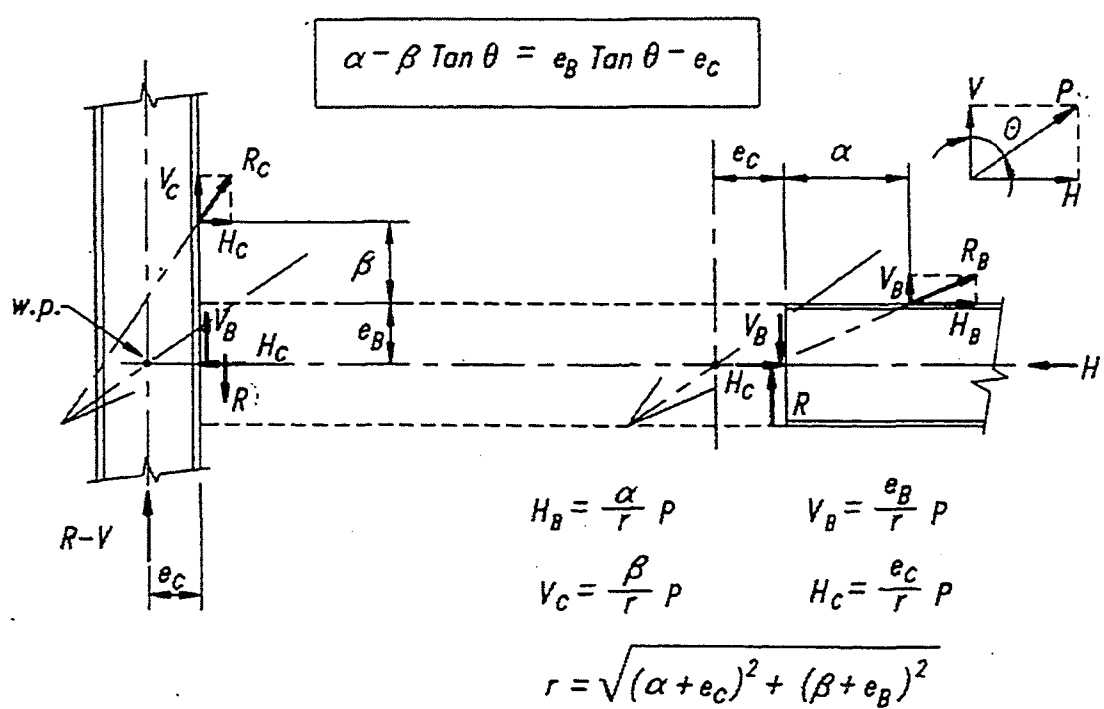
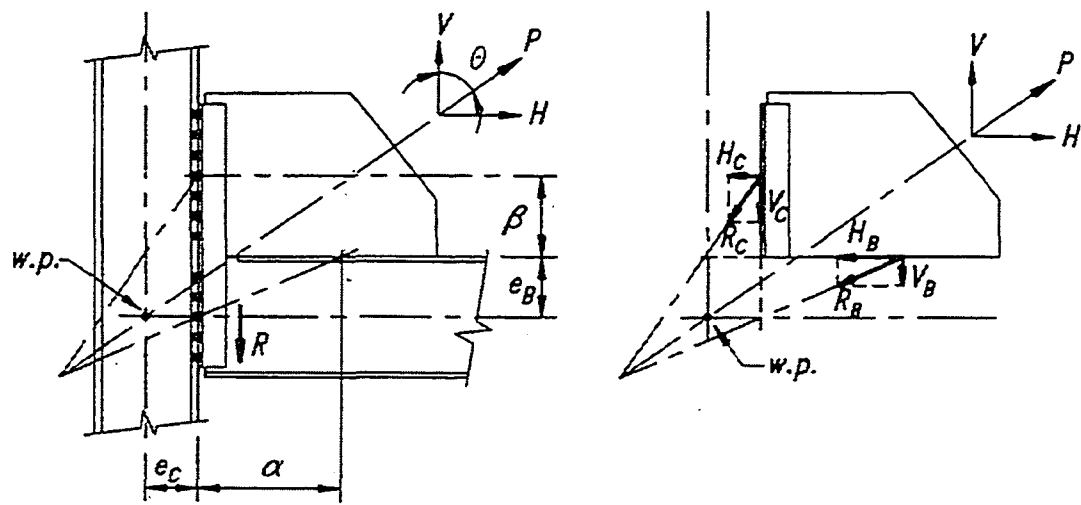


Figure 1.8 - Uniform Force Method, from AISC Manual of Steel Construction – Volume II: Connections (1999)

1.4 References

AISC, 1989. Manual of Steel Construction. Allowable Stress Design. Ninth Edition. American Institute of Steel Construction, Inc., Chicago IL.

AISC, 1995. Manual of Steel Construction. Load and Resistance Factor Design. Second Edition. American Institute of Steel Construction, Inc., Chicago IL.

AISC, 1999. Manual of Steel Construction. Volume II: Connections, LRFD 2nd Ed. American Institute of Steel Construction, Inc., Chicago IL.

Bjorhovde, R., and Chakrabarti, S.K., 1985. "Tests of Full-Size Gusset Plate Connections." Journal of Structural Engineering, ASCE, Vol. 111, No. 3, pp. 667-684.

CISC, 1991. Connections for Steel Structures, Third Printing. Canadian Institute of Steel Construction, Willowdale, Ontario.

CAN/CSA-S16.1-94, 1995. Limit States Design of Steel Structures, Canadian Standards Association, Rexdale, Ontario.

CAN/CSA-S16-01, 2003. Limit States Design of Steel Structures, Canadian Standards Association, Rexdale, Ontario.

Chakrabarti, S.K., and Bjorhovde, R., 1983. "Tests of Full Size Gusset Plate Connections." Research Report, Department of Civil Engineering, University of Arizona - Tuscon, Arizona.

Chakrabarti, S.K., and Richard, R.M., 1990. "Inelastic Buckling of Gusset Plates." Structural Engineering Review, Vol. 2, pp. 13-29.

Davis, C.S., 1967. "Computer Analysis of Stresses in a Gusset Plate." Thesis presented to the University of Washington, at Seattle, Wash., in partial fulfillment of the requirements for the Degree of Master of Science.

Gross, J.L., 1990. "Experimental Study of Gusseted Connections." Engineering Journal, AISC, Vol. 27, No. 3, Third Quarter, pp. 89-97.

Hardash, S.G. and Bjorhovde, R., 1985. "New Design Criteria for Gusset Plates in Tension." Engineering Journal, AISC, Vol. 22, No. 2, pp. 77-94.

Hardin, B.O. 1958. "Experimental Investigation of the Primary Stress Distribution in the Gusset Plates of a Double Plane Pratt Truss Joint with Chord Splice at the Joint." Bulletin No. 49, Engineering Experiment Station, University of Kentucky

Irvan, W.G. 1957. "Experimental Study of Primary Stresses in Gusset Plates of a Double Pratt Truss." Bulletin No. 46, Engineering Experiment Station, University of Kentucky.

Nast, T.E., Grondin, G.Y., and Cheng, J.J.R., 1999, "Cyclic Behaviour of Stiffened Gusset Plate-Brace Member Assemblies." Structural Engineering Report No. 229, Department of Civil Engineering, University of Alberta, Edmonton, Alberta.

NRCC, 1995. National Building Code of Canada. Associate Committee on the National Building Code, National Research Council of Canada, Ottawa, Ontario.

Prakash, V., Powell, G.H., and Campbell, S., 1993. DRAIN-2DX Base Program Description and Users Guide. Ver. 1.10, Report No. UCB/SEMM-93/17, Department of Civil Engineering, University of California, Berkeley, California.

Rabinovitch, J.S., and Cheng, J.J.R., 1993. "Cyclic Behaviour of Steel Gusset Plate Connections." Structural Engineering Report No. 191, Department of Civil Engineering, University of Alberta, Edmonton, Alberta.

Struik, J.H.A., 1972. "Applications of Finite Element Analysis to Non-Linear Plane Stress Problem." Ph.D. Dissertation, Department of Civil Engineering, Lehigh University, Bethlehem, Pa.

Thornton, W.A., 1984. "Bracing Connections for Heavy Construction." Engineering Journal, AISC, Vol. 21, No. 3, pp 139-148.

Thornton, W.A., 1992. "Designing for Cost Efficient Fabrication." Modern Steel Construction, AISC, February, 1992, pp 12-20.

Vasarhelyi, D.D., 1971 "Tests of Gusset Plate Models." Journal of the Structural Division, ASCE, 97(2), pp 665-678.

Walbridge, S.S., Grondin, G.Y., and Cheng, J.J.R., 1998. "An Analysis of the Cyclic Behaviour of Steel Gusset Plate Connections." Structural Engineering Report No. 225, Department of Civil Engineering, University of Alberta, Edmonton, Alberta.

Whitmore, R.E., 1952. "Experimental Investigation of Stresses in Gusset Plates." Bulletin No. 16, Engineering Experiment Station, University of Tennessee.

Williams, G.C., and Richard, R.M., 1986. "Steel Construction Design Based on Inelastic Finite Element Analysis." Report to the Department of Civil Engineering and Engineering Mechanics, the University of Arizona.

Yam, C.H.M, Sheng, N., Iu, V.P., and Cheng, J.J.R., 1998. "Analytical Study of the Compressive Behaviour and Strength of Steel Gusset Plate Connections." Proceedings of the Annual Conference of the Canadian Society for Civil Engineering, Vol IIIa, pp. 97 to 106.

Yam, C.H.M., and Cheng, J.J.R., 1993. "Experimental Investigation of the Compressive Behaviour of Gusset Plate Connections." Structural Engineering Report No. 194, Department of Civil Engineering, University of Alberta, Edmonton, Alberta.

Yam, C.H.M., and Cheng, J.J.R., 1994. "Analytical Investigation of the Compressive Behaviour and Strength of Steel Gusset Plate Connections." Structural Engineering Report No. 207, Department of Civil Engineering, University of Alberta, Edmonton, Alberta.

Yam, C.M.H. and Cheng, J.J.R., 2002. "Behaviour and Design of Gusset Plate Connections in Compression." Journal of Constructional Steel Research 58 (2002), pp. 1143 to 1159

2. SEISMICALLY LOADED CONCENTRICALLY BRACED FRAMES

2.1 Introduction

This chapter provides a summary of the design and behaviour of seismically loaded concentrically braced steel structures. The first section of this chapter presents an overview of the design requirements of the National Building Code of Canada (NBCC), NRCC (1995) and CAN/CSA-S16.1-94, the standards used for calculation of design loads and structural member sizes in chapters 5 through 7. The CAN/CSA-S16.1-94 standard has been superseded by CAN/CSA-S16-01 and with that, the requirements for seismic resistant steel structures (Clause 27) of CAN/CSA-S16.1-94 have been changed in CAN/CSA-S16-01. The differences in between clause 27 of CAN/CSA-S16.1-94 and clause 27 of CAN/CSA-S16-01 are discussed, as they relate to design of concentrically braced frame steel structures.

The second section of this chapter is a review of seismically loaded braced frame research relevant to this thesis. The review includes summaries of those papers particularly relevant to the non-linear time history analyses conducted as part of this thesis. The body of published research relating to structural response to earthquake excitation is vast. This summary is not a detailed literature review but provides an introduction to those particular publications most relevant to the work reported in latter chapters of this thesis.

2.2 Compatibility of Analysis with CAN/CSA-S16-01

Research reported in chapters 5, 6 and 7 was primarily based on the requirements of CAN/CSA-S16.1-94, which was the current standard of design of steel building structures in Canada at the time the research was performed. That standard has since been superseded by CAN/CSA-S16-01. It should be noted that the contents of

CAN/CSA-S16-01 were known to the author during the period of the research and, as much as possible, were considered in that work. Specifically, column continuity requirements, structure height limitations and chevron bracing requirements of CAN/CSA-S16-01 were incorporated in the design of the structures analysed in chapters 5 through 7. Aspects of both CAN/CSA-S16.1-94 and CAN/CSA-S16-01 which relate to inelastic brace behaviour, such as brace slenderness, brace stockiness and brace connection requirements were deemed not relevant to this research since, in this investigation, inelasticity is limited to gusset plates.

2.3 Equivalent Lateral Seismic Loading by NBCC-1995

The National Building Code of Canada, NRCC (1995) provides, in clause 4.1.9, a method for calculation of design forces arising from the action of earthquakes. The method is referred to as the equivalent static lateral force method, whereby lateral loads are applied at each floor level of a structure based on parameters including design earthquake intensity, importance of the structure, structure ductility, foundation type and period of the structure. The method is similar to those employed in many other design standards including the Uniform Building Code and Eurocode. Application of the static forces to each floor of the structure as prescribed in NBCC 4.1.9 allows calculation of storey shears, beam axial forces, column forces and deformations as required to proportion members and connections.

Site specific parameters are used to characterize the intensity and characteristics of design seismic events for a given location. The parameters may be determined through reference to climatic information in appendix C of the NBCC, 1995. Three variables are used to define the characteristics of the design event:

Z_a = Acceleration-related seismic zone, ranging from 0 to 6

Z_v = Velocity-related seismic zone, ranging from 0 to 6

v = zonal velocity ratio, ranging from 0 to 0.4 expressed as a ratio of 1 m/s

Acceleration dominated events are those where $Z_a > Z_v$. Such events are typically centered near the location of the structure and are most damaging to short period structures. Velocity dominated events are those where $Z_a < Z_v$. Such events are typically centered at a large distance from the structure being designed and are most damaging to longer period structures.

The minimum total lateral force applied to a structure for seismic design is calculated by the following formula, shown below in a slightly different form than in the NBCC 4.1.9.1.(4)

$$V = 0.6 \frac{vSIFW}{R}, \text{ where:}$$

v = zonal velocity ratio, ranging from 0 to 0.4 expressed as a ratio of 1 m/s

S = Seismic response factor, a function of period and Z_a/Z_v per NBCC 4.1.9.1.(6)

I = Seismic importance factor per NBCC 4.1.9.1.(10)

F = Foundation factor per NBCC 4.1.9.1.(11)

W = Structure dead load + 0.25 snow load + 0.6 storage load + tank contents

R = Force modification factor, reflecting structural ductility, per NBCC 4.1.9.1.(8)

The above defined lateral load is distributed among the floor levels of the structure by the formulae provided in NBCC 4.1.9.1.(13). The formulae define a top force, F_T applied at the top of the structure, for those structures with periods less than 0.7 seconds. The top force increases the storey shears, beam forces and column loads in the upper storeys of short period structures to account for the effects of higher order modes in their response to earthquake excitation. The top force F_T is then subtracted from the total lateral force V and the remainder is distributed along the height of the structure by the ratio of the mass moment of each floor about the base of the structure with the sum of the mass moments of all levels in the structure taken about the base.

Load effects for design of lateral load resisting elements may be calculated by accumulating the lateral loads at each storey above the level being considered.

Overtuning moments and column forces are calculated based on a reduced moment of lateral loads about the level under consideration as defined in NBCC 4.1.9.1.(23) and 4.1.9.1.(24). The reduction coefficients depend on structure period and the location of the level under consideration as a fraction of the overall building height. The reduction factors reflect the low likelihood of multiple storeys experiencing inertial forces of maximum intensity in one direction simultaneously during earthquake response. Further, overturning reduction factors reflect the reduced overturning moments expected in longer period structures.

2.4 CBF Ductility Design Using CAN/CSA-S16.1-94

Concentrically braced frames (CBF's) are structures composed of truss type bracing, beams and columns. The elements are arranged to form a truss in a vertical plane which serves as the lateral load resisting system. In the existing National Building Code of Canada, NRCC (1995), there are three categories of CBF: ductile braced frames; braced frames with nominal ductility; and strength braced frames with no special provisions to ensure ductility.

General descriptions of the three categories are provided below. It should be noted that some of the specific requirements of CAN/CSA S16.1-94 Clause 27 have not been included for brevity.

2.4.1 Ductile Braced Frames (DBF)

Structures in this category are assigned force modification factor, $R = 3.0$ in NBCC, 1995. Inelasticity is confined to beams and braces. When subject to the design earthquake, braces are likely to undergo significant inelastic straining during multiple

loading cycles in both tension and compression. For bracing, both overall slenderness and cross section component slenderness are limited to ensure post-buckling energy absorption through bending. Brace end connections must be proportioned to resist at least the loads imposed by full yielding of brace cross sections. Some limited inelasticity is anticipated in the beams. While the bracing remains the primary energy absorbing element, beams are required to be class 1 or 2 cross sections to prevent local buckling during inelastic bending.

2.4.2 Braced Frames with Nominal Ductility (NDBF)

Structures in this category are assigned force modification factor, $R = 2.0$ in NBCC, 1995. Inelasticity is confined to the braces and is not anticipated in beams. In the design earthquake, braces are likely to undergo smaller amounts of inelastic straining during fewer load cycles than for the DBF. Post buckling energy absorption is provided in braces by through limiting them to class 1 or 2 sections. As for DBF's, brace end connections must be designed to resist at least the loads imposed by full yielding of the brace cross section.

2.4.3 Strength Braced Frames (SBF)

Structures in this category are assigned force modification factor, $R = 1.5$ in NBCC, 1995. Primarily elastic response is anticipated with a low likelihood that any members will attain full cross section yield during the design earthquake. Connections are proportioned to resist calculated seismic forces and may not be required to resist cross section yield forces. In recognition of the inherent ductility of steel buildings, $R = 1.5$ is used to calculate equivalent static design forces.

The three available design methods are consistent with the capacity design philosophy with the brace as the load limiter. As such, inelasticity is intended to be confined to the

members with the connection capacities exceeding the anticipated loads. The application of this philosophy to the design of CBF's for seismic loading imposes two conditions. First, it is conditional that connection capacity exceeds the maximum load anticipated in the bracing. This condition gives rise to the requirement that connection design capacities equal or exceed the tension yield force of the member in DBF and NDBF structures. For SBF structures, brace end connections must resist the load arising from a fully elastic seismic response. Second, to be effective as ductile elements in DBF and NDBF structures, braces must satisfy limits of overall and cross section element slenderness to ensure good post buckling energy absorption during compression cycles.

For the design of new structures or retrofit of existing structures using the current NBCC, designers are limited to one of the three categories of CBF listed. The implication of using capacity design for the DBF and NDBF structures is that limitations on overall slenderness can give rise to bracing members of excessive cross sectional area.

Limitation of cross section element slenderness reduces the number of cross sections available to the designer and may also increase the required cross sectional area of the brace member. These design conditions may lead to brace over-strength in the final design. Connections must be proportioned to permit the attainment of full yield of the brace cross section, resulting in large connections which can be expensive to fabricate and erect.

For the SBF category, predominantly elastic response is anticipated during the design earthquake. The equivalent static lateral forces which arise from elastic response are very large and result in large bracing members. The large lateral forces can also result in a significant increase in beam and column sizes to eliminate inelasticity in those members. While it is not a requirement that connections be designed to develop brace cross section yield, the large bracing forces arising from elastic response can result in very large connections. In general, SBF structures are not appropriate for zones of high seismic risk.

2.5 CBF Ductility Design Using CAN/CSA-S16-01

The current design standard for steel building structures in Canada is CAN/CSA-S16-01. The design requirements for CBF structures differ substantially between CAN/CSA-S16.1-94 and CAN/CSA-S16-01. The sections of CAN/CSA-S16-01 relevant to CBF design are outlined below, by clause number, with explanatory notes describing the differences between the current and CAN/CSA-S16.1-94 standards. This review is not exhaustive and does not describe the contents of CAN/CSA-S16-01 in detail. It is intended to provide a general comparison of CAN/CSA-S16.1-94 with CAN/CSA-S16-01 to illustrate the changes in seismic resistant design of steel structures.

CAN/CSA-S16-01 27.1.1 General – Use of the National Building Code of Canada, 1995 for calculation of loading is specified, as in CAN/CSA-S16.1-94. In addition to the use of NBCC loading, it is specified that seismic loading may be determined by “non-linear time history analysis using appropriate structural models and ground motions”. While non-linear time history analysis is not specifically identified as an acceptable analysis technique in CAN/CSA-S16.1-94, determination of loading using this method is recommended in the NBCC, 1995 Commentary J-46. The appearance of non-linear time history analysis in Clause 27.1.1 of CAN/CSA-S16-01 does not change the options available to designers, but places more emphasis on advanced analysis techniques in the current structural steel design standard than in the past.

CAN/CSA-S16-01 states specific requirements for column splice design loading, column section class and specifies minimum column continuity of two storeys which were previously not specified in CAN/CSA-S16.1-94. The specific requirements for columns within clause 27 of CAN/CSA-S16-01 are not discussed here in detail. Generally the intent of the column design requirements is to ensure that columns are sufficiently strong and ductile to sustain loads and deformation associated with earthquake loading without loss of capacity.

2.5.1 Moderately Ductile (MD) Concentrically Braced Frames

CAN/CSA-S16-01 Clause 27.5 specifies design requirements for type MD (Moderately Ductile) concentrically braced frames. This category of CBF corresponds with the DBF category of CAN/CSA-S16.1-94, with a corresponding force modification factor, $R = 3.0$. Use of this category in CAN/CSA-S16-01 is limited to chevron (see Figure 1.1 for definition) and tension-compression braced structures not exceeding 8 storeys in height and to tension-only braced structures not exceeding 4 storeys in height. These requirements differ from CAN/CSA-S16.1-94 in two ways. First, CAN/CSA-S16.1-94 did not state height limitations for DBF structures and, second, chevron braced systems were excluded from the DBF category. CAN/CSA-S16-01, in clause 27.5.2.4, has stated requirements for design of beams in chevron braced structures which account for probable forces arising from load redistribution after brace buckling. These requirements were not specifically stated in CAN/CSA-S16.1-94 clause 27.4 since chevron braced systems were not considered within the DBF category in that standard. Consideration of post buckling force redistribution was required to within clause 27.4.6 of CAN/CSA-S16.1, but no specific methods were provided for calculation of post-buckling design forces in beams. The addition of specified design loads in this section of the standard is based on a capacity design philosophy, with design forces for primarily elastic beams being based on “probable capacity” of bracing members. In this manner, inelastic response is limited to bracing members.

Bracing element overall slenderness limitations have been relaxed from $KL/r < 1900/\sqrt{F_y}$ ($KL/r < 109.7$ for $F_y = 300$ MPa; $KL/r < 101.6$ for $F_y = 350$ MPa) in CAN/CSA-S16.1-94 to $KL/r < 200$ in S16-01, reflecting the observed good performance of structures braced with slender members in past earthquakes and in analysis. Whereas CAN/CSA-S16.1-94 required stocky brace members with limited slenderness, giving rise to stable load deformation hysteresis and sustained compression capacity after brace buckling, CAN/CSA-S16-01 allows use of slender brace elements which do not exhibit sustained compression capacity after buckling. Width-to-thickness limitations have been modified in CAN/CSA-S16-01, allowing more slender elements to be present in more

slender bracing. The intent of this provision is to limit strain cycling and fracture at local buckles by reducing the width to thickness ratio of the buckled elements. The ultimate goal of this portion of the specification is to control fracture at local buckles in slender braces which would be expected to experience overall and local buckling early in the design event and undergo significant cyclic inelastic deformation.

2.5.2 Limited-Ductility (LD) Concentrically Braced Frames

CAN/CSA-S16-01 Clause 27.5 specifies design requirements for type LD (Limited-Ductility) concentrically braced frames. This category of CBF corresponds with the CAN/CSA-S16.1-94 NDBF category, using a force modification factor, $R = 2.0$. Use of this category in CAN/CSA-S16-01 is limited to tension-compression and chevron braced structures not exceeding twelve storeys in height and to tension-only braced structures not exceeding eight storeys in height. Brace overall slenderness, KL/r shall not exceed 300, as stated in CAN/CSA-S16-01 clause 27.6.3.1. For bracing with $200 < KL/r < 300$, specific width-to-thickness limitations for seismic design are not applied. The rationale for the dependence of width-to-thickness limitations on brace slenderness is the same for both the LD and MD structure types.

2.5.3 Strength Braced Frames (SBF)

Neither of the CAN/CSA-S16.1-94 and CAN/CSA-S16-01 standards state seismic design requirements for SBF structures ($R = 1.5$), defined in NBCC 1995 as CBF steel structures with no special ductility considerations in their design.

2.6 CBF Literature Review

2.6.1 General

A significant body of literature exists relative to the response of CBF structures to earthquake excitation. The papers summarized herein are only those most relevant to the research presented in the remainder of this thesis. Generally, literature in this area may be divided into two categories; behaviour on individual brace members and behaviour of structural systems.

The anticipated behaviour of individual bracing members during inelastic cyclic loading has been well defined by several researchers. Jain (1978), Popov and Black (1981), Astaneh, Goel and Hanson (1986), and Liu and Goel (1988) described observed hysteresis of various types of steel bracing members subjected to cyclic loading. Generally, as bracing overall slenderness is increased a more marked degradation of post buckling compression capacity and increased pinching of hysteresis is observed during cyclic loading. Similarly, non compact sections exhibit reduced compression capacity and increased pinching of hysteresis with cyclic loading after development of post buckling plastic hinges. With decreasing cross section slenderness, class 1 sections have exhibited more stable post buckling compression capacity. These observations have been the basis for the slenderness limitations applied to ductile braced frame bracing members in CAN/CSA-S16.1-94.

The load deformation behaviour of cyclically loaded bracing is complex and is dependant on member capacity in both tension and compression, overall slenderness and local slenderness. Several empirical models are available to represent the experimentally observed behaviour of inelastic brace members for finite element analysis of structural systems. The model of inelastic brace behaviour proposed by Jain and Goel (1978) is employed in DRAIN-2DX software and is widely used.

2.6.2 Response of Braced Steel Structures to Seismic Loading

Kobeovic and Redwood (1997) performed a study of eccentrically braced frames (EBF) analysed using non-linear time history analysis. Eccentrically braced frames employ diagonal bracing elements similar to those used in CBF structures. The geometry of the bracing is modified such that the bracing work point is located some distance away from the column. Inelasticity, when it occurs due to lateral load, is limited to that segment of beam which is between the brace work point and the gravity structure. That segment is referred to as the link.

A variety of earthquake records were scaled to provide ground motions consistent with NBCC design earthquake intensities for Zone 3 and Zone 5 events. Eight storey structures, designed using NBCC equivalent lateral seismic loading and the structure geometry of the CISC Multi-Storey Building Design Guide, Chien (1987), were analysed. It was observed that, during those events which caused significant inelasticity, the most significant deformations were sustained in the seventh and first stories. It was concluded, based on the observed demand in the upper stories of Zone 5 design event structures, that, brace and column capacities based on the NBCC equivalent static lateral load procedure may be inadequate. Events with intermediate a/v ratios (0.99 to 1.14) were found to be most damaging.

Redwood, Lu, Bouchard and Paultre (1991), using methods similar to those described above, analysed a group of eight and twenty storey concentrically braced frame structures. The structures were designed using $R = 1.5, 2$ and 3 . One group of structures were designed using the recommendations of Redwood and Channagiri (1991), which invoke sizing of gravity framing to resist brace yield. Another group of structures were designed to the requirements of clause 27 of CAN/CSA-S16.1-M89. The structures were analysed using DRAIN 2D with the Jain and Goel (1978) brace hysteresis model and scaled earthquake records covering a range of a/v ratios. Earthquake records were scaled to match the peak velocity of Victoria and Montreal design events.

Among the structures analysed using scaled records representative of a Montreal design event, satisfactory performance was predicted in all cases. Among the structures analysed using Victoria design events, those structures proportioned using CAN/CSA-S16.1-M94 / NBCC experienced demand in the upper storeys which exceeded that implied by the specified design forces. Where upper storey gravity framing was designed based on the method described by Redwood and Channagiri (1991), upper storey performance was satisfactory.

2.6.3 Response of Braced Reinforced Concrete Structures to Seismic Loading

The incorporation of steel bracing within concrete structures to improve seismic performance has been done in many real structures and has been the subject of a large body of research. Steel bracing of concrete structures has been in the form of infill bracing, connected directly to concrete beams and columns and in the form of steel bents complete with steel beams, columns and bracing. Steel lateral load resisting systems within concrete structures have been employed both in new construction and in retrofit of existing structures. Of particular relevance to this research is analytical work performed by Jain (1985). A six storey concrete frame structure, both in an unbraced configuration and retrofit with steel cross and chevron bracing, was analysed using DRAIN 2D. The concrete elements were modelled using the DRAIN2D TYPE15 element P-M interaction, which does not account for stiffness degradation, hysteresis pinching or capacity degradation with inelastic cyclic bending. Steel bracing elements were modelled using the cyclically loaded strut load-deformation model proposed by Jain and Goel (1978). Structures were subjected to base accelerations derived from two acceleration histories, the N-S component of El Centro 1940 and an artificial “B1” earthquake, generated using methods defined by Jennings, Housner and Tsai (1968).

The results of the analyses indicated that brace inelasticity would be mostly confined to the first and second storey of the structures with column and beam inelasticity similarly being restricted to those storeys as well. Storeys three through six did not exhibit

significant inelasticity in any case. Column and beam inelasticity in the “B1” event corresponded to significant structural damage in the bottom two storeys while the damage predicted during the El Centro event was not severe. X-braced frame response was found to be better than the chevron braced frame response. Column axial forces did not exceed tension or compression capacity in any case.

2.7 Conclusions

Design of CBF steel building structures is currently conducted in Canada using the companion NBCC (1995) and CAN/CSA-S16-01 standards. Generally, seismic design loading is determined by the equivalent static lateral load method but, for complicated structures, dynamic analysis may be conducted.

Comparison of the CAN/CSA-S16.1-94 to CAN/CSA-S16-01 steel design standards reveals two recent trends in seismic resistant design of concentrically braced frames in Canada. First, braces designed using the current CAN/CSA-S16-01 standard may be significantly more slender than those allowed by the previous CAN/CSA-S16.1-94. This reflects experimental and field observations of slender braces surviving earthquakes when premature fracture is prevented – which can be accomplished by maintaining thin cross section elements, thus limiting the magnitude of strain cycles at locations of local buckling. Second, more explicit statement of the requirements of capacity design of CBF structures is present in CAN/CSA-S16-01 than in CAN/CSA-S16.1-94. CAN/CSA-S16-01 includes clauses delineating requirements for design and arrangement of column and beam members to ensure that they are sufficiently strong and ductile to sustain the forces and deformations associated with brace inelasticity.

Procedures for design of concentrically braced frame structures for earthquake resistance are clearly defined in companion Canadian standards NBCC and S16.1. Structures, when designed using those standards, have been analysed by various researchers to determine the characteristics of their responses. While many methods of analysis have been used to

assess the response of structures to seismic loading, of particular relevance to this thesis are those studies conducted using non-linear time history analysis performed using DRAIN-2DX software.

In non-linear time history analytical studies of CBF steel structures designed using NBCC and S16 specifications, upper storey bracing and column elements have been found to experience inelastic demand exceeding that predicted by the governing design standards. Lower storey bracing, beam and column elements inelastic demand and foundation loads have been found to be consistent with the predictions of the governing standards.

In similar analytical studies of concrete structures, brace inelasticity and drift in excess of that predicted by NBCC have been predicted in lower storeys, especially the bottom storey. Upper storey brace inelasticity was found to be much less than anticipated, based on the response predicted using NBCC.

2.8 References

Astaneh, A., Goel, S.C., and Hanson, R.D., 1986. "Earthquake Resistant Design of Double Angle Bracings." AISC Engineering Journal, 23(4), pp 133-147.

CAN/CSA-S16.1-M89, 1989. Limit States Design of Steel Structures, Canadian Standards Association, Rexdale, Ontario.

CAN/CSA-S16.1-94, 1995. Limit States Design of Steel Structures, Canadian Standards Association, Rexdale, Ontario.

CAN/CSA-S16-01, 2003. Limit States Design of Steel Structures, Canadian Standards Association, Rexdale, Ontario.

Chien, E., 1987. "Multi-Storey Building Design Aid." Canadian Institute of Steel Construction, Willowdale, Ontario.

Jain, A.K., 1978. "Hysteresis Behaviour of Bracing Members and Seismic Response of Braced Frames with Different Proportions." Ph.D. Thesis, University of Michigan, Ann Arbor, Mi.

Jain, A.K., 1985. "Seismic Response of RC Frames with Steel Braces." ASCE Journal, of Structural Engineering, Vol .111, No. 10 pp 2138 – 2148.

Jain, A.K., and Goel, S.C., 1978. "Hysteresis Models for Steel Members Subjected to Cyclic Buckling or End Moments and Buckling – Users Guide for DRAIN 2D." Report No. UMEE 78R6, Department of Civil Engineering, University of Michigan, Ann Arbor, MI.

Jennings, P.C., Housner, G.W., and Tsai, N.C., 1968. "Simulated Earthquake Motions." E.E.R.L., California Institute of Technology, Pasadena, Ca. April 1968.

Kobeovic, S., and Redwood, R., 1997. "Design and Seismic Response of Shear Critical Eccentrically Braced Frames." *Canadian Journal of Civil Engineering*, 24: 761 – 771.

Liu, Z., and Goel, S.C., 1988. "Cyclic Load Behaviour of Concrete Filled Tubular Braces." *ASCE Journal of Structural Engineering*, 114(7), pp 1488-1506.

NRCC, 1995. National Building Code of Canada. Associate Committee on the National Building Code, National Research Council of Canada, Ottawa, Ontario.

Popov, E.P., and Black, R.G., 1981. "Steel Struts Under Severe Cyclic Loadings." *ASCE Journal of the Structural Division*, 107(ST9), pp 1857-1881.

Redwood, R., and Channagiri, V.S., 1991, "Earthquake Resistant Design of Concentrically Braced Steel Frames." *Canadian Journal of Civil Engineering*, 18, pp 839 – 850.

Redwood, R.G., Lu, F., Bouchard, G., and Paultre, P., 1991. "Seismic Response of Concentrically Braced Steel Frames." *Canadian Journal of Civil Engineering*, 18(6), pp 1062 - 1077.

3. GUSSET PLATE EXTENSION DEFORMABILITY^{1,2}

3.1 Introduction

Damage to infrastructure and loss of human life are commonly associated with intense earthquakes. To mitigate the disastrous consequences of intense earthquakes, new structures in zones of high seismic risk are designed to be earthquake resistant. Additionally, important existing structures such as bridges, hospitals and schools which were originally constructed without proper consideration of earthquake loading have been evaluated and retrofit to improve their earthquake survivability. In both new construction and retrofits, concentrically braced frame (CBF) steel structures are frequently used and have performed well in past earthquakes.

Gusset plates are the most common connecting elements between bracing and gravity framing in CBF structures. With the exception of out-of-plane hinge formation, gussets are typically designed to remain elastic during seismic loading with inelasticity confined to the bracing members. When loaded cyclically beyond yield in tests, however, gusset plates have exhibited stable and open load-deformation hysteresis. As such, gusset plates have been considered as candidate inelastic elements in seismically loaded structures by Rabinovitch and Cheng (1993), Walbridge, Grondin and Cheng (1998) and Nast, Grondin and Cheng (1999). Inelastic gussets furnished with edge stiffeners and combined with braces designed to remain elastic throughout loading have been shown by Nast, Grondin and Cheng (1999) to provide better energy absorption characteristics than other brace-gusset configurations. Systems so configured are referred to as “Strong Brace – Weak Gusset” systems and are of interest because they hold potential to simplify brace end connections and improve the energy absorption characteristics of CBF structures.

¹ A version of this paper is currently under revision for publication in the AISC Engineering Journal.

² Portions of this chapter were presented at the NASCC / PSSC Conference, Long Beach, California, March 2004.

For gussets to be used as inelastic elements in “strong brace – weak gusset” seismically loaded structures, gusset deformation at fracture is significant since it affects the maximum storey and overall structure drift that may be accommodated by the lateral load resisting system. Unfortunately, little information is available regarding prediction of gusset deformation at first fracture or the behaviour of gussets after fracture initiation. The purpose of this research is to explore the relationship between gusset material properties and geometry with deformation at first fracture and to describe the post-fracture behaviour of gusset plates.

A series of physical tests and non-linear finite element analyses have been conducted to determine the effects of gusset reinforcement, gusset configuration and material properties on strength and deformability of gusset plates. Monotonic tension tests were conducted on ten gusset plates, six without reinforcement and four with reinforcing doubler plates, welded over the bolted connection region, as shown in figures 3.1 and 3.2. Subsequent to testing, finite element analyses, using the experimentally determined stress-strain behaviour of the material used in the physical tests, were conducted on models representing the tested specimen geometry and various other reinforced configurations. Based on experimental and analytical observations, a predictive model for gusset deformation at first fracture is derived.

3.2 Test Specimens and Apparatus

Ten gusset plate specimens, configured as shown in figures 3.1 and 3.2, were tested in monotonic axial tension to determine their full load vs. deformation responses. The specimens were of two distinct types. Those designated “nU” and “nUA” were of uniform thickness with n bolts connecting the brace member to the gusset plate. Gussets with reinforcing plates welded over the bolted connection region to suppress block tearing failure through the fastener holes were designated “nR” where specimens were furnished with reinforcing plates on two sides, “nR1” where specimens were furnished with reinforcing plates on only one side and “nH” where specimens were furnished with

reinforcing plates on two sides but gusset continuity was interrupted by drilled holes beside the corners of the reinforcement plates. As in the unreinforced case, n designates the number of bolts in the gusset – brace connection. The specimen dimensions and reinforcing are summarized in figure 3.2. Specimen shape was configured such that the free boundaries were consistent with those of a gusset connected to a brace aligned at 45 degrees to the gravity framing. All specimens were fabricated from a single A517 Gr. 70 plate, with the rolling direction parallel to the loading direction. Three ancillary coupon tests, performed in accordance with ASTM A-370 (1996) indicated mean material properties in the rolling direction of $\sigma_Y = 443$ MPa, $\sigma_{ULT} = 523$ MPa and $\epsilon_{ULT} = 0.27$. The mean measured thickness of the plate was 6.72 mm.

All specimens were whitewashed prior to testing. During testing, stroke controlled monotonic tension loading was applied by an MTS 6000 testing machine at a deformation rate of 1 mm per minute. Load data was collected from the MTS 6000 crosshead load channel. Deformation was measured using an LVDT, connected to the brace member and bearing on the specimen base plate, as indicated in figure 3.1. A second deformation channel, the test machine stroke, was also recorded. Deformations reported herein are those recorded by the LVDT. Bolt deformation, bolt slip and brace deformations within the gauge length of the LVDT are included in the deformation measurement. Loading was paused periodically to permit static conditions to be recorded.

3.3 Test Results

3.3.1 Unreinforced Specimens

The geometry of unreinforced gusset plate specimens are summarized in figure 3.2.

The load-deformation responses of unreinforced specimens are shown in figure 3.3. Consistent with the observations of Chakrabarti and Bjorhovde (1983), unreinforced specimens (4U, 8U, 8UA, 12U, 14U and 16U) were observed to fracture first between the two bolts nearest the end of the brace member at a deformations ranging from 18 mm (8U) to 23.5 mm (14U). In each test, the formation of the first fracture was accompanied by an abrupt reduction in load of approximately 250 kN, which can be seen in each of the load vs. displacement curves in figure 3.3. The observed initial reduction of axial tension from ultimate load to fracture across the first bolt row corresponds with the ultimate strength of the specimens (523 MPa) acting on the gusset thickness (6.72 mm) time the width of the ligament between the bolts (81 mm), or 285 kN.

Generally, very little yielding was observed in the unreinforced gusset plate material surrounding the bolted brace connection at ultimate load. For example, specimen 4U, depicted in figure 3.4, did not shed significant whitewash due to yielding between start of test, $P = 0$ kN (figure 3.4, photo A), and $P_{ULT} = 630$ kN (figure 3.4, photo C). Inelasticity was concentrated within the connection region with no observed yielding in the surrounding gusset plate material. For specimens 8U, 8UA, 12U, 14U and 16U, loading beyond first fracture was accompanied by yielding, concentrated in two visible regions immediately adjacent to the bolted connection. Yielded regions may be seen in specimens 8U, 8UA and 14U in figure 3.5, which shows the specimens after removal from the test apparatus.

After development of yielded regions beside the brace-gusset connection, fractures formed along the lines of bolts parallel to the loading direction in specimens 4U, 8U, 8UA and 12U. The formation of fractures along the sides of the bolt groups was accompanied by continuing reduction in load. After the fracture surface completely circumscribed the gusset material bounded by the bolt holes for specimens 4U, 8U, 8UA and 12U, the specimens continued to carry a small and approximately constant load with further deformation. This residual capacity may be attributed to the contact between the surfaces of the torn block and the adjacent gusset material. Block tearing was complete at deformations ranging from 29 mm to 54 mm.

For specimens 14U and 16U, initial deformation beyond the completion of first fracture was accompanied by increasing load, as seen in the load-deformation responses in figure 3.3. A post-first-fracture maximum load was reached at a deformation of approximately 35 mm for both the 14U and 16U specimens. Specimens 14U and 16U did not develop fractures along the vertical bolt lines to completely circumscribe the bolt group as observed in innumerable previous tests by others and those reported herein. Fractures, extending from the bottom bolt row, grew up and around the adjacent bolt holes, as shown in the upper portion of figure 3.5. The fracture patterns observed in specimens 14U and 16U were inconsistent with those observed in specimens with shorter connection length, as were the post fracture load deformation responses. The post fracture loss of load was much less abrupt in specimens 14U and 16U, which deformed 55 mm and 51 mm respectively at the termination of testing, compared to less than 40 mm of deformation for the specimens with shorter connection lengths: 4U, 8U, 8UA and 12U.

Specimens 14U, 8U and 8UA are shown, post test, in figure 3.5 and specimens 12R, 8U, 8UA, 12U and 4U are shown, post test, in figure 3.6. The region of yielding adjacent to the connection can be seen as two crescent shaped regions of flaked whitewash in the 8 bolt specimens, straddling the second and third bolt rows. The yielded region visible in the 14U specimen, as well as that observed after testing of the 16U specimen (not shown), extends well beyond that observed in the 4, 8 and 12 bolt specimens, intersecting the free edge of the gusset plate.

3.3.2 Reinforced Specimens

The geometry and reinforcement details of reinforced gusset plate specimens are summarized in figure 3.2. Load deformation responses and photographs of specimens 12R and 12H are shown in figures 3.7 and 3.8, respectively. Load-deformation responses of specimens 4R1 and 4U are shown in figure 3.9.

Initial load – deformation response was generally linear up to observed first yield adjacent to the interior corners of reinforcement. After onset of first yield, the yielded region beyond the end of the reinforcing plates was observed to increase in size up to ultimate load. At ultimate load, ductile fracture initiation was observed at deformations ranging from 17 mm (12H) to 26 mm (4R1). Fracture initiation was observed adjacent to the corners of reinforcement in specimens 12R and 12H and across the innermost row of bolts in specimen 4R1.

After initiation of cracks through bolt holes in 4R1 and adjacent to reinforcement in other specimens, crack tips propagated horizontally toward the specimen centerline until inner crack tips joined, or coalesced, near the centerline of the tested specimens. Among reinforced specimens, excluding 12H, the deformation increment between first crack initiation and crack coalescence was typically 5 to 8 mm with an accompanying drop in load of approximately 700 kN. This value corresponds to mean measured ultimate strength of the gusset material (523 MPa) acting on the gusset thickness (6.72 mm) over the width of the reinforcement (203 mm), or 713 kN.

The 12H specimen was furnished with two 21 mm diameter holes at the corners of the reinforcement plate. The holes were introduced at the location of crack initiation in specimen 12R. The purpose of the test was to determine what effect the presence of smooth circular holes in place of a re-entrant corner stress concentration would have on the fracture deformation of gusset plates. During the test of the 12H specimen, in which holes were drilled adjacent to the reinforcement, first fracture occurred at a deformation of 17 mm and progressed to coalescence at a deformation of 20 mm. The presence of the holes in specimen 12H reduced deformation at fracture initiation from 23 mm in test 12R to 17 mm.

Generally, after completion of crack coalescence, the remaining two crack tips continued propagating upward and away from the reinforcement at approximately 45 degrees from the vertical. In test 12R1, the right crack tip followed a path approximately 15 degrees from the vertical while the left crack tip behaved as observed in other tests. With

increasing crack length, load carried by the specimens were observed to decrease. Significant yielding of the gusset was noted in the region surrounding the reinforcement prior to first fracture, as shown in figures 3.7 and 3.8. After crack coalescence the region in front of the advancing crack tips exhibited significant whitewash flaking as shown in the post-test photograph, figure 3.6. Reinforced specimens exhibited yielding over a large area during testing, as illustrated by the significant loss of whitewash in figures 3.6, 3.7 and 3.8. The crack tips reached the free edges of the gussets at deformations ranging from 37.6 mm to 83.8 mm.

3.3.3 Comparison of Reinforced to Unreinforced Behaviour

To assess the effect of reinforcement on the behaviour of the gusset plates tested, the responses of similarly proportioned plates with and without reinforcement are compared. Figure 3.9 shows the load vs. deformation responses of four bolt unreinforced (4U) and four bolt reinforced (4R1) specimens. The deformation at onset of first fracture (taken to be the end of the plateau) increased from approximately 21 mm to 25 mm. The ultimate load increased from 600 kN to 1100 kN with addition of reinforcing. Overall deformation at complete fracture increased from 32 mm to 40 mm with the addition of reinforcing.

Figure 3.10 shows the load vs. deformation responses of 12 bolt specimens for unreinforced (12U), reinforced (12R) and reinforced with holes (12H) configurations. Deformation at first fracture was observed to be similar for the 12R and 12U specimens, at 21 mm while corresponding ultimate loads were 2150 kN and 1475 kN respectively. Addition of holes near the corners of the reinforcement of specimen 12H resulted in deformation at first fracture of 17 mm and ultimate load of 1910 kN. Overall deformation at complete fracture for the unreinforced plate (12U) was 38 mm, 78 mm for the reinforced plate (12R) and 74 mm for the reinforced plate with holes (12H).

3.4 Analysis of Tested Specimens using Modified Block Shear Equations

Test results were compared to predictions of ultimate capacity based on measured dimensions and material properties and five variations of the block shear expressions found in the CAN/CSA S16-01 (2001) and AISC LRFD (1999) design standards, which are based on the recommendations of Hardash and Bjorhovde (1985). The geometric variables used in calculation of the ultimate loads are defined in figure 3.11 and include gross and net section of the tension and shear regions circumscribing the brace connection bolt group. The ultimate loads predicted by the modified block shear expressions and test results are presented and compared in Table 3.1. Unreinforced gusset ultimate loads were best predicted by the sum of the ultimate stress acting over the net tension area and the 0.6 times yield stress acting on the net shear area of the connections tested, with a mean test to predicted ratio of 1.08. That formulation is consistent with the behaviour observed in testing where, at ultimate, significant inelastic deformation was not observed adjacent to the sides of the connection region while the net tension section of the connection was at the point of incipient fracture.

Reinforced gusset ultimate capacity did not correlate well with the sums of ultimate and/or yield stresses acting on the area of the gusset along the reinforcement perimeter. Combinations of yield and ultimate stress acting around the reinforced perimeter provided test-to-predicted ratios ranging from 0.78 to 0.87, as shown in table 3.1. The application of yield or ultimate stress along the full perimeter of reinforcement is inconsistent with the observations made during testing where, at ultimate load, significant yielding had not occurred along the full length of the reinforcement, parallel to the brace member. A modified expression, combining ultimate stress along the net tension area with 0.6 times yield stress acting on 0.75 of the gross shear area provides reasonable correlation with observed test results, with a test to predicted ratio of 1.03. This expression reflects the observed development of an inclined yield band in reinforced specimens extending from the interior corner of the reinforcement to the free edge of the gusset plate, as shown in figure 3.7, photo D.

For both reinforced and unreinforced specimens, initiation of first fracture occurred at ultimate load. The deformation at which this fracture occurred was consistent among all of the test results at approximately 21 mm for all unreinforced specimens, 21 to 25 mm for reinforced specimens 12R, 12R1 and 4R1 and 17 mm for specimen 12H. Increased connection length and reinforcement were observed to increase both deformability and the volume of gusset material having experienced inelasticity upon complete fracture.

3.5 Finite Element Analysis

3.5.1 General

To further explore the effects of reinforcement and of plate configuration on deformability, a series of finite element analyses were conducted on a variety of reinforced gusset configurations, using the stress-strain relationship obtained by ancillary test. As a confirmation of the modelling parameters to be used in that analysis, gusset plates from the physical test series were modelled using CASCA, Swenson, James and Hardeman (1997) and analysed using FRANC2DL (FRacture ANalysis Code 2D Layered) software, Swenson and James (1997). FRANC2DL finite element analysis software models material non-linearity using multi-linear uniaxial stress strain relationships and the von Mises yield criteria. Multiple inelastic 2-D layers were employed to model the interaction of reinforcing plates, gusset plates and bracing. Brace members, reinforcement plates and gusset plates were each modeled as separate layers, connected by forcing consistent displacement for nodes joined by welds and at bolt centrelines. Detailed modelling of inelasticity around bolt holes was not performed since significant inelasticity was not observed around bolt holes during physical tests of reinforced specimens. All plates were modelled using plane stress elements with material properties derived from uniaxial coupon test results.

Ultimate load was assumed to coincide with onset of first fracture, which was assessed using the microvoid coalescence expressions developed by Thomason (1990). In a

highly plastic plane stress problem, attainment of maximum principal stress equal to ultimate engineering stress from a uniaxial stress coupon test is a good predictor of fracture initiation in ductile materials containing impurities and inclusions. The principal stress at fracture initiation was taken to be 523 MPa for the structures analysed, the value obtained from uniaxial tension coupon tests. The orientation of first fracture was taken to be perpendicular to the maximum principal stress vector.

FRANC2DL was also used to model inelastic crack propagation by crack tip opening displacement and automatic fixed increment crack propagation as described by James, (1988).

3.5.2 Analysis of Tested Specimen 12R

To determine appropriate modeling parameters for accurate analysis of reinforced gusset plates, models of tested specimens were analysed using a variety of mesh sizes, and material property relationships. The results of the analyses were compared to measured response to assess the accuracy of the model. Mesh size was varied in preliminary models to determine its effect on solution accuracy, computation time and crack propagation. Guidelines for appropriate mesh size are provided in the FRANC2DL documentation by James (1988). Results for specimen 12R, considered representative of the reinforced specimens, are presented here.

Specimen 12R was analysed using FRANC2DL and the results compared favourably with the experimental response as shown in figures 3.12 through 3.17. The finite element and experimental load-deformation relationship of the 12R specimen are plotted together in figure 3.12 – including the deformations of brace member, base plate connection and bolts. Ultimate load and corresponding deformation, determined by finite element modelling were, 2017 kN and 23.1 mm respectively. These values compare favourably to the experimentally determined ultimate load and deformation of 2006 kN and 21 mm respectively.

Finite element principal stress contour, corresponding to a gusset deformation of 3 mm, is provided in figure 3.13. The zone of maximum stress is located just beyond the end of the brace – gusset connection and is consistent with elastic stress distributions described by Whitmore. Figures 3.14 and 3.15 depict the plastic zone at gusset deformations of 3 mm and 17.4 mm respectively. Plastic zone shape and size closely resemble the yielded region, observed as flaking whitewash, during testing of specimen 12R (figure 3.7, Photos A and C).

Ultimate load in the finite element analysis was considered the load at which the maximum principal stress in the model reached 523 MPa (75.8 ksi), the experimentally determined ultimate strength of the plate used for the physical tests. In the case of the 12R model, this occurred simultaneously adjacent to two interior corners of the reinforcement plate and was consistent with observations made during testing. At the locations of maximum principal stress, cracks were introduced with crack growth parameters of critical crack tip opening displacement, or CTOD = 2.29 mm measured at 12.7 mm from the crack tip, values which were determined by measuring the opening angle of advancing cracks during the physical testing reported in this chapter. The defined crack growth increment was 12.7 mm, a value found to produce stable solutions for a variety of structure geometries in trial models. Crack tip path, shown in figures 3.16 (early in the propagation) and 3.17 (near crack tip coalescence) was found to be similar to that observed in testing and gave rise to similar unloading rates immediately after crack introduction as shown in figure 3.12.

The uncracked and early post-cracking behaviour of the test specimens was reproduced accurately using the finite element modelling procedures described earlier. Crack start location and orientation, as well as early crack growth, were accurately reproduced using the finite element method. In physical tests, when inner crack tips approached each other, the crack tips accelerated toward each other, rapidly joining without significant overall deformation of the specimen. As described by James (1998), crack coalescence is not accurately modelled by a CTOD fixed increment crack propagation model because

the interaction and instability of approaching crack tips are not accurately reflected by a constant CTOD. Given the limitations of the constant CTOD at modelling crack coalescence, gusset behaviour beyond early post-cracking was not explored by finite element analysis.

3.5.3 Reinforced Gussets Analysis

Eleven gusset plates, employing doubler plate reinforcement similar to that used in the reinforced test specimens, were modelled to further assess the effect of size and configuration on gusset deformability. Of interest were the effects of gusset asymmetry and proximity of reinforcing to the connected boundary on the load - deformation response of the plates. All of the plates analysed were reinforced in the connection region to prevent significant inelasticity in the vicinity of the bolted connection, in a manner similar to that employed in specimens 4R1, 12R and 12H. The geometries of a selection of the plates analysed are shown in figure 3.18. The analysis results of all gusset configurations analysed are presented in Table 3.2.

Generally, principal stress concentrations were located just adjacent to the interior corner(s) of the doubler plate reinforcement, as shown in figure 3.19, 3.20 and as observed in tests of similar gussets. The maximum principal strains were equal on each side of the symmetric plates (12D2, 12D8, 12D16), as seen in figure 3.19 but were increased on the side nearest the connected boundary in non-symmetric plates (12S2, 12S8, 12S16), as seen in figure 3.20. Using maximum principal stress = 523 MPa in the structure as the condition corresponding to ultimate load, the range of predicted ultimate gusset displacements in this group was 8.8 mm to 16.4 mm with the largest predicted deformation occurring in the 12R plate, from the experimental series. The range of ultimate loads among doubler plate reinforced gussets was 1348 kN to 2332 kN.

The relationship between proximity of the doubler plate reinforcement to the plate boundary to deformation at first fracture was examined through analysis of six gussets.

Three symmetric configurations, 12D2, 12D8 and 12D16 and three asymmetric configurations, 12S2, 12S8 and 12S16 were analysed to determine the influence of boundary to reinforcement distance on first fracture deformation. In the symmetric cases first fracture deformation decreased from 12.3 mm for 12D16 to 11.4 mm for 12D8 to 8.8 mm for 12D2 (gussets are arranged in order of decreasing distance from boundary to doubler plate reinforcement). In the asymmetric configurations, gusset deformation at first fracture decreased from 13.5 mm for 12S16 to 13.1 mm for 12S8 and to 11.2 mm for 12S2.

3.6 Radial Strip Analysis

The ultimate principal stress vector plots obtained from analysis of reinforced gussets 12S2, 12D8 and 12R are provided in figures 3.21, 3.22 and 3.23 respectively, and are typical of those obtained in other gusset analyses. Referring to figures 3.21 through 3.23, it can be observed that the principal stress directions are generally aligned radially to a central point, O, defined by the intersection of lines extending from the ends of the supported gusset boundaries and through the exterior corners of the doubler plate reinforcement, irrespective of gusset configuration. It was also observed that, at ultimate, minimum principal stresses, shown as vectors perpendicular to the maximum principal stress vectors, were generally very small when compared to the maximum principal stresses at most locations throughout the plates. Based on these observations, a continuous gusset with doubler plate reinforcement may be considered to act, at ultimate load, as an array of axially loaded tapered strips aligned radially about a centre, O, and capable of deformation between the boundaries of the doubler plate reinforcement and the supported boundaries of the gusset plate, as defined in figure 3.24. This approximation of gusset plate behaviour at ultimate load is similar to the Uniform Force Method, used for gusset plate design and described in the AISC Manual of Steel Construction, Volume II: Connections (1999). Idealizing material behaviour as rigid elastic – linear hardening plastic, an expression for the deformation of any radial strip at its' ultimate load may be derived as follows:

$$\sigma(r) = \sigma_{ULT} \cdot \frac{r_c}{r} \quad [1]$$

where,

$\sigma(r)$ is maximum principal stress at any radius, r , from the focus of the gusset

σ_{ULT} is the ultimate strength of the gusset material.

r_c is the radius of the reinforcement boundary from the focus of the gusset

Using the rigid-elastic linear-plastic stress-strain relationship, strain at a location, r , from the origin is defined by the relationship:

$$\varepsilon(r) = \frac{\sigma(r) - \sigma_Y}{E_{SEC}} \quad [2]$$

where,

E_{SEC} is the secant modulus, determined by $(\sigma_{ULT} - \sigma_Y) / (\varepsilon_{ULT} - \varepsilon_Y)$.

σ_Y is the yield strength of the gusset material.

For any gusset idealized using radial strips, the zone of yielded material surrounding the doubler plate reinforcement is finite and extends to a radius r_Y from the focus of the gusset. Within a strip, the dimension r_Y is determined by the relationship:

$$r_Y = r_c \frac{\sigma_{ULT}}{\sigma_Y} \leq r_B \quad [3]$$

where r_B is the distance from O to the supported boundary.

Determining the overall deformation of the strip:

$$\delta = \int_{r_c}^{r_Y} \varepsilon(r) dr$$

$$\delta = \frac{1}{E_{SEC}} (\sigma_{ULT} r_C \ln(r) - \sigma_Y r) \Big|_{r_C}^{r_Y} \quad [4]$$

The ultimate deformability of a reinforced gusset may be estimated by applying [4] at the location of closest proximity of the gusset reinforcement to the supported gusset boundary, i.e. minimum r_{B-r_C}

Gusset ultimate deformations determined by finite element analyses are compared with the values determined using [4] in figure 3.25 and are found to be in good agreement. Parameters used in [4] were $\sigma_{ULT} = 523$ MPa, $\sigma_Y = 443$ MPa, $\epsilon_{ULT} = 0.27$ and $E_{SEC} = 296$ MPa, consistent with the values used in finite element analyses and determined by ancillary tests of steel used in laboratory tests. For the gusset configurations analysed, r_C ranged from 431 mm to 604 mm. For configurations 12S2 and 12D2, gussets with reinforcement positioned closest to the gusset boundary, r_Y found to exceed r_B . For all other configurations, r_Y was contained entirely within the gussets analysed.

The results indicate that for a gusset of with a connection region of a given geometry, increase in overall gusset size beyond the yielded zone would not result in an increase in the deformation at first fracture since increasing gusset size will not increase the size of the yielded region beyond r_Y . The corollary of this is that any gusset with a boundary intersecting the yielded region surrounding the connection would be expected to fracture at a deformation less than that expected for a similar plate with the yielded region fully contained in its' interior. For gussets with asymmetry, fracture would be anticipated first at those locations closest to the restrained boundaries.

Using values of r_C consistent with typical medium rise building gusset plate geometry (300 mm to 400 mm for gussets connecting to braces with 3 rows of two bolts at 76 mm o.c., 100 mm ga.) and material properties representative of currently available structural steel plates ($\sigma_Y = 300$ MPa, $\sigma_{ULT} = 450$ MPa, $\epsilon_{ULT} = 0.25$), predicted gusset deformation at fracture would range from 16 mm to 21 mm based on [4].

3.9 Conclusions

In laboratory monotonic tension tests, gusset plates without reinforcement exhibited block tearing failure consistent with that reported by Chakrabarti and Bjorhovde (1983). Block shear expressions consistent with the CAN/CSA S16-01 (2003), (Equation (3) in table 3.1), and AISC LRFD (1999), (Equations (1) and (2) in table 3.1), modified to incorporate $\Phi=1.0$, were found to correlate well with experimentally determined ultimate loads for the six specimens tested.

Gusset plates with reinforcement over the brace-gusset connection region exhibited tearing around the perimeter of the reinforcement beginning with development of a crack through the gusset plate, perpendicular to the brace axis and just beyond the end of the reinforcement plate. Block shear expressions from the CAN/CSA S16-01 (2003) and AISC LRFD (1995) design standards were found to overestimate experimentally determined ultimate loads when $\Phi=1.0$. A modified expression, with the shear yield contribution reduced to $0.75A_nF_y$ was a good predictor of experimentally determined ultimate load for the four specimens tested.

Gusset plates, when fitted with reinforcing plates over the bolted connection region, exhibit increased ultimate load and marginally increased deformation at first fracture when compared with similar unreinforced gusset plates.

Continuous reinforced gusset plates may be considered analogous to, at ultimate load, concentric inelastic radial strips. Based on the radial strip analogy, gusset deformability is expected to be limited to the deformability of the plastic zone surrounding the brace connection region. Small gussets have exhibited reduced deformability in analysis when the plastic region surrounding reinforcement intersects the connected boundary of the gusset, as predicted by the strip yield analogy.

Reinforced gusset plate deformation may be determined using the strip yield analogy. Predicted deformation using the strip yield analogy agreed well with calculated ultimate deformations, determined using the finite element analysis method.

For reinforced gussets of a size typical of medium rise buildings and constructed using material with properties typical of commonly available structural steel plates, gusset deformation at ultimate load would not be expected to exceed 16 mm to 20 mm based on strip yield analysis.

Table 3.1 - Gusset Plate Ultimate Load Test Results vs. Prediction

Test	Plies	Lvg	Lvn	Ltg	Ltn	(1) $A_{tn}F_u + 0.6A_{vg}F_y$	(2) $A_{tg}F_y + 0.6A_{vn}F_u$	(3) $A_{tn}F_u + 0.6A_{vn}F_u$	(4) $A_{tn}F_u + 0.6A_{vn}F_y$	(5) $A_{tn}F_u + 0.6 * 0.75A_{vn}F_y$	Test Ultimate Load	(1) Test/Pred	(2) Test/Pred	(3) Test/Pred	(4) Test/Pred	(5) Test/Pred
16U	1	572	414	102	82	2352	2050	2034	1767	-	1858	0.80	0.91	0.91	1.05	-
14U	1	495	359	102	82	2057	1818	1802	1571	-	1725	0.84	0.95	0.96	1.10	-
12U	1	419	304	102	82	1785	1586	1570	1374	-	1470	0.82	0.93	0.94	1.07	-
8UA	1	267	193	102	82	1242	1118	1102	978	-	1072	0.86	0.96	0.97	1.10	-
8U	1	267	193	102	82	1242	1118	1102	978	-	1077	0.87	0.96	0.98	1.10	-
4U	1	114	82.8	102	82	695	653	637	584	-	630	0.91	0.96	0.99	1.08	-
						Mean	0.85	0.95	0.96	1.08	-					
12R	3	457	457	203	203	2346	2532	2641	2346	1938	2075	0.88	0.82	0.79	0.88	1.07
12R1	2	457	457	203	203	2346	2532	2641	2346	1938	2076	0.88	0.82	0.79	0.88	1.07
12H	2	457	436	203	182	2272	2443	2478	2197	1804	1857	0.82	0.76	0.75	0.85	1.03
4R1	2	152	152	203	203	1256	1245	1355	1256	1122	1063	0.85	0.85	0.78	0.85	0.95
						Mean	0.86	0.81	0.78	0.87	1.03					

(1) Reflects the requirements of AISC – LRFD (1999) J4-3a.

(2) Reflects the requirements of AISC – LRFD (1999) J4-3b.

(3) Reflects the requirements of CAN/CSA S16-01 (2003) Cl. 12.3.1.

Table 3.2 – Results Summary – Gusset Plate Deformations

Gusset	Finite Element Ultimate Load (kN)	Finite Element Ultimate Displ. (mm)	Radial Strip Ultimate Displ. (mm)	FEM : Radial Strip Displ. Ratio
12R	1989	16.43	14.10	1.165
12S2	1895	11.20	10.41	1.076
12S8	1774	13.13	11.65	1.127
12S16	1777	13.47	11.65	1.156
12D2	1873	8.75	5.38	1.628
12D8	1348	11.37	12.09	0.940
12D16	2017	12.29	12.09	1.016
12DB	1779	11.86	10.06	1.179
12DD	2332	9.65	10.69	0.902
Mean				1.132

Note: Deformations in this table do not include brace member or bolt deformations or bolt slip.

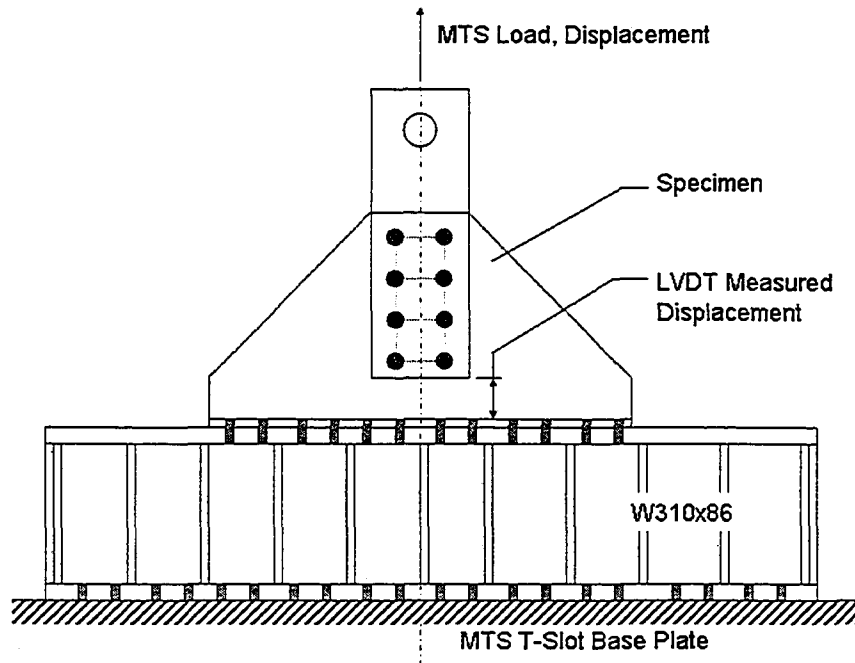
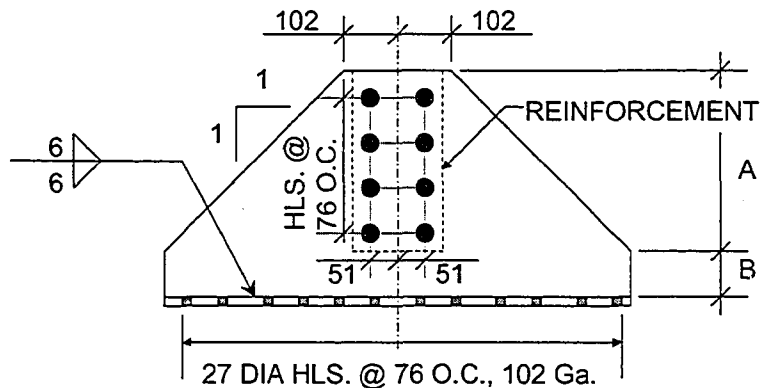


Figure 3.1 – Test Schematic



Specimen	A	B	Reinforcement
4U	330	12.7	None
8U, 8UA	406	76	None
12U	406	228	None
14U	406	381	None
16U	406	381	None
4R1	330	12.7	1 Plate 6.72 mm x 203 mm W x 152 mm H
12R	406	228	2 Plates 6.72 mm x 203 mm W x 456 mm H
12R1	406	228	1 Plate 6.72 mm x 203 mm W x 494 mm H
12H	406	228	2 Plates 6.72 mm x 203 mm W x 456 mm H

Note: A 21 mm diameter hole was provided 12 mm below and outside each corner of the reinforcement.

Note – Brace connections made with 3/4" diameter A325 Bolts in 21mm holes.

Figure 3.2 – Specimen Dimensions

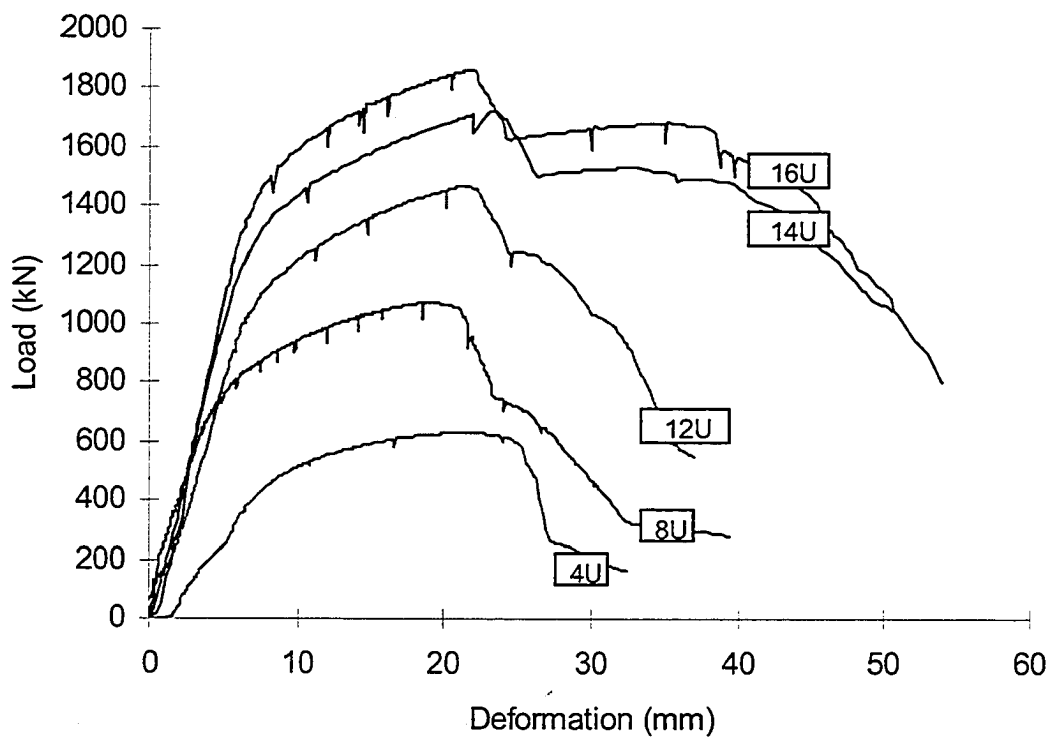


Figure 3.3 – Unreinforced Specimens – Experimental Load vs. Deformation

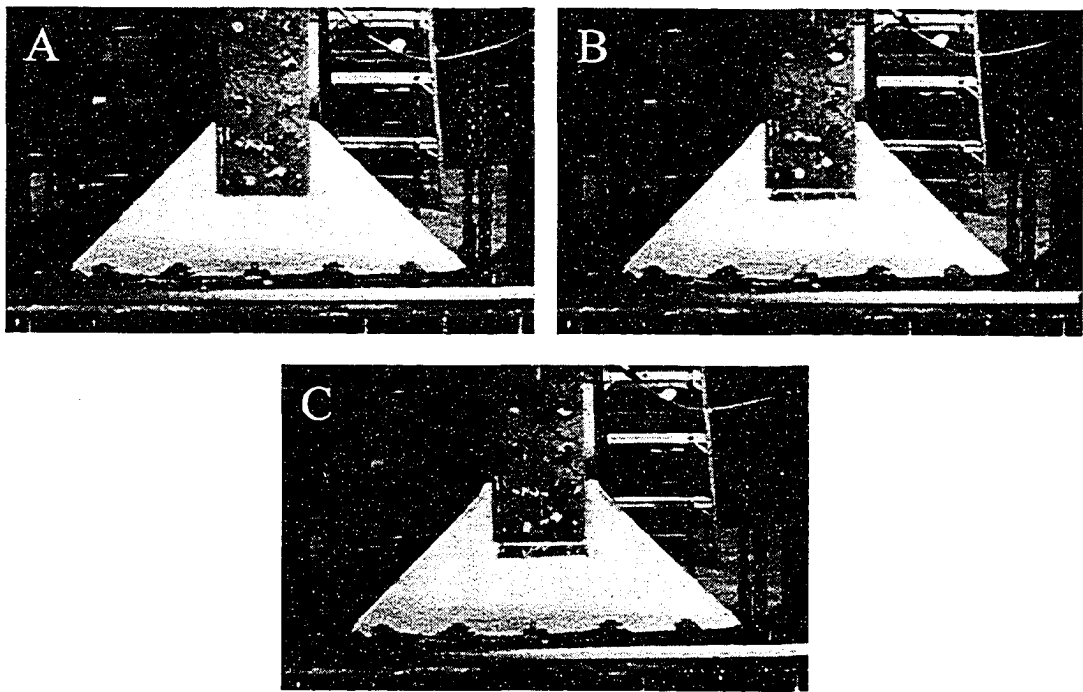
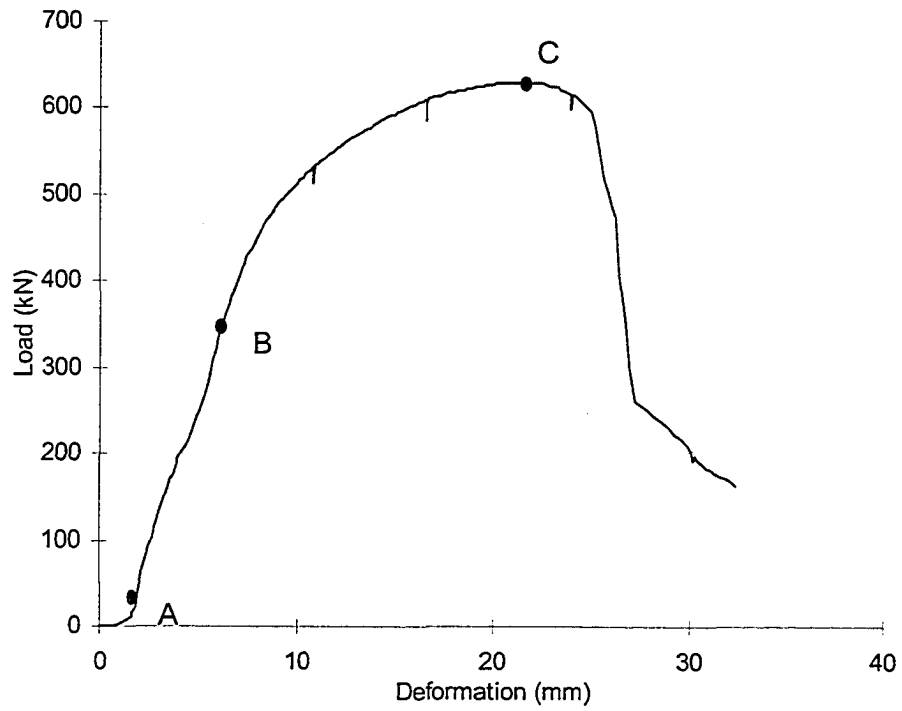


Figure 3.4 – Experimental Load vs. Deformation – Specimen 4U

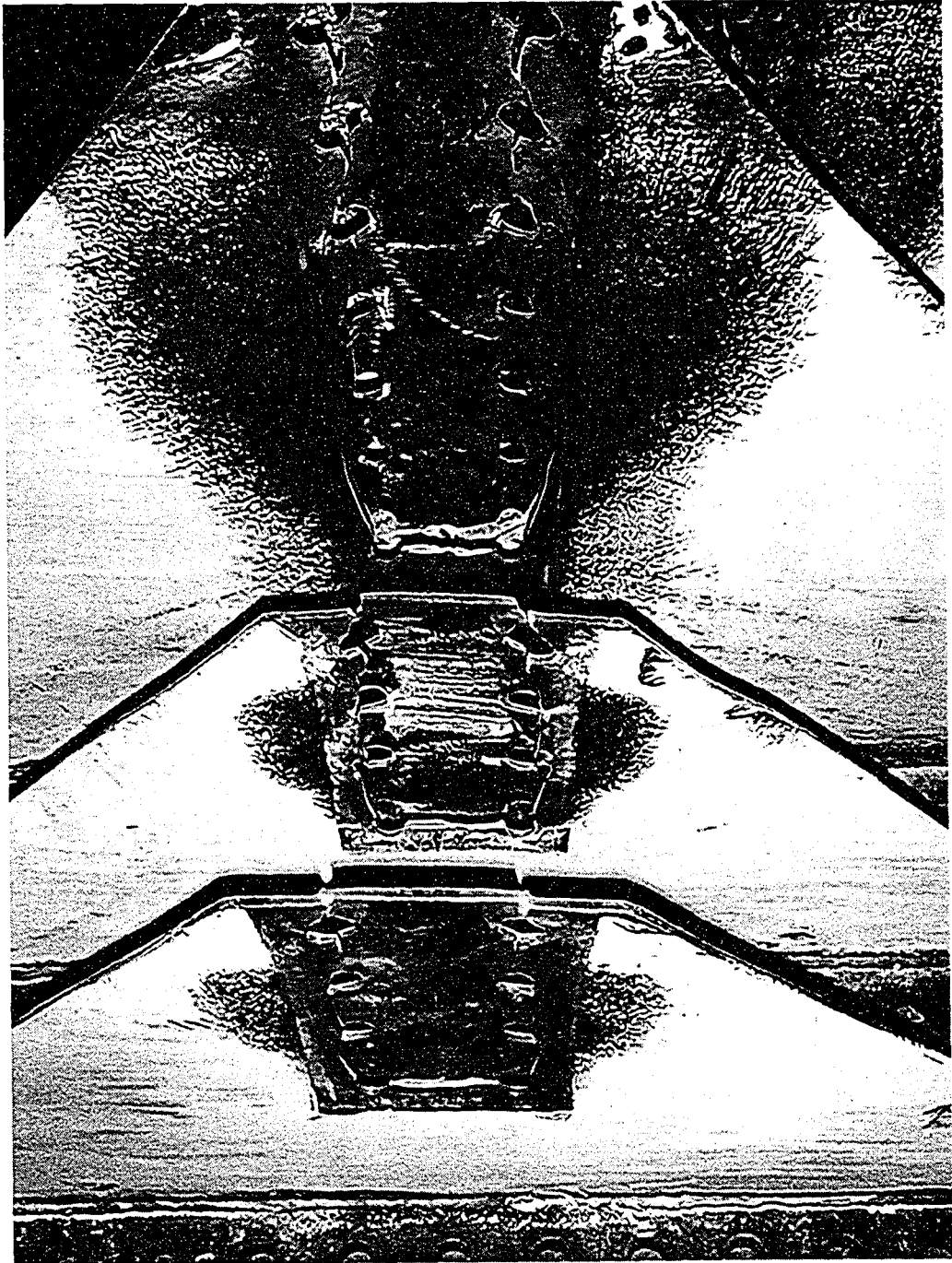


Figure 3.5 – 8U, 8UA and 14U – Post Test

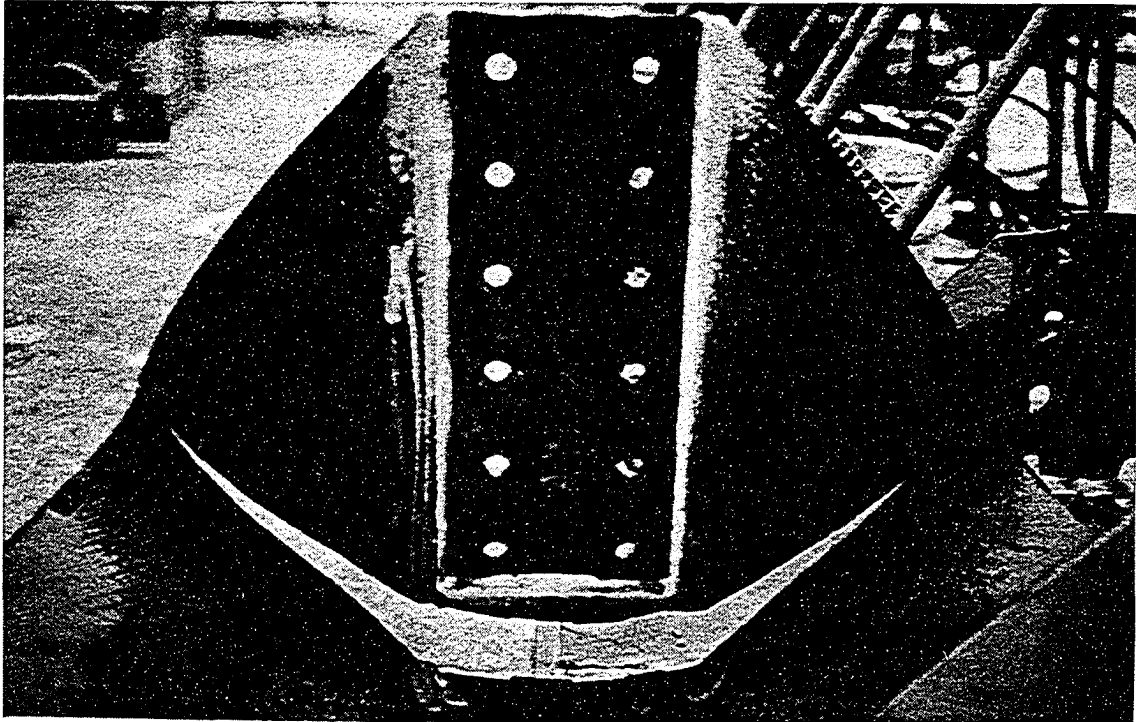


Figure 3.6a - 12R Post Test

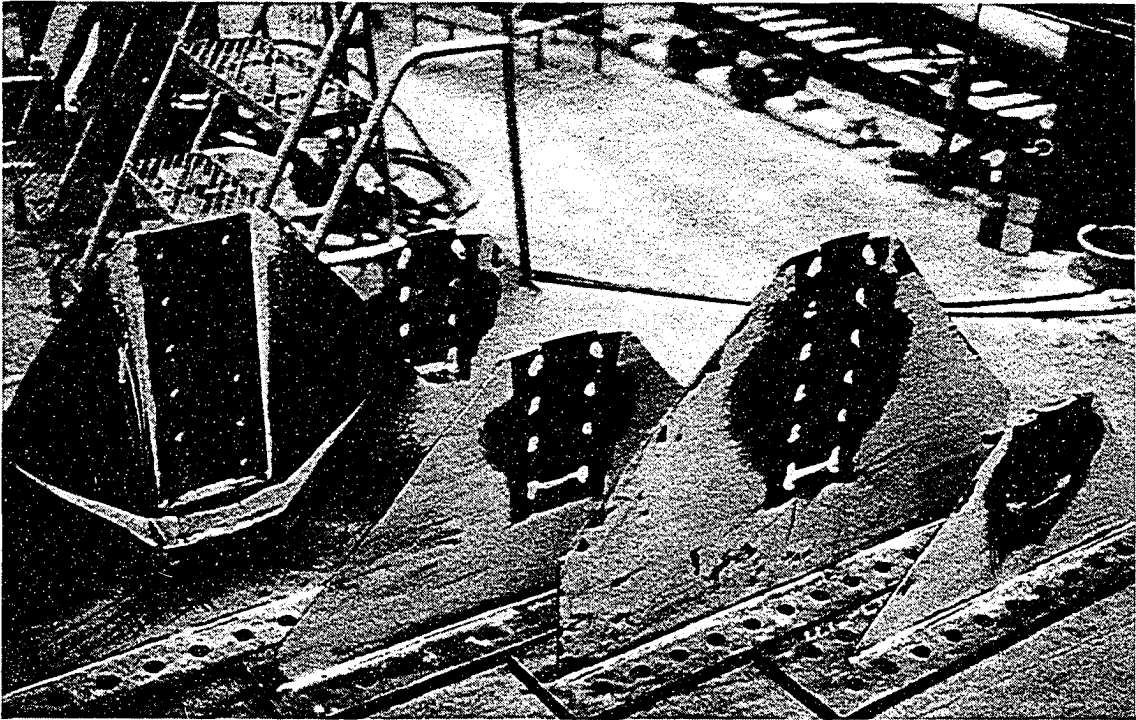


Figure 3.6 – 12R, 8U, 8UA, 12U and 4U (L to R) Post Test

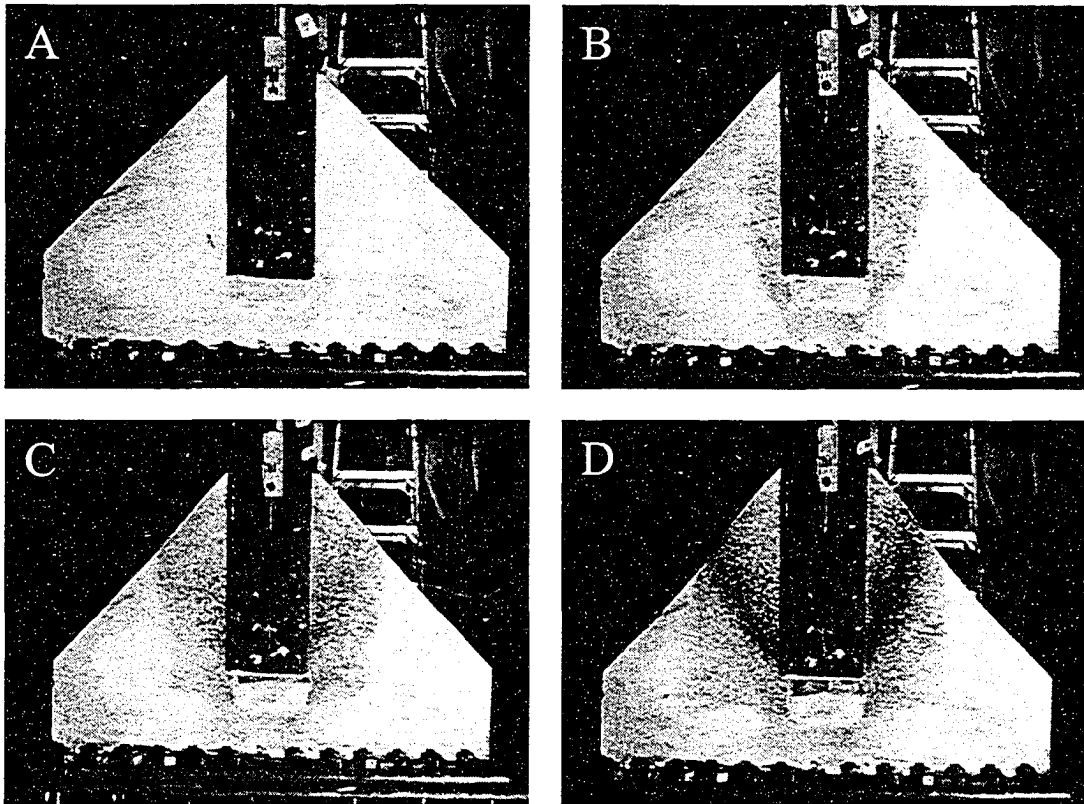
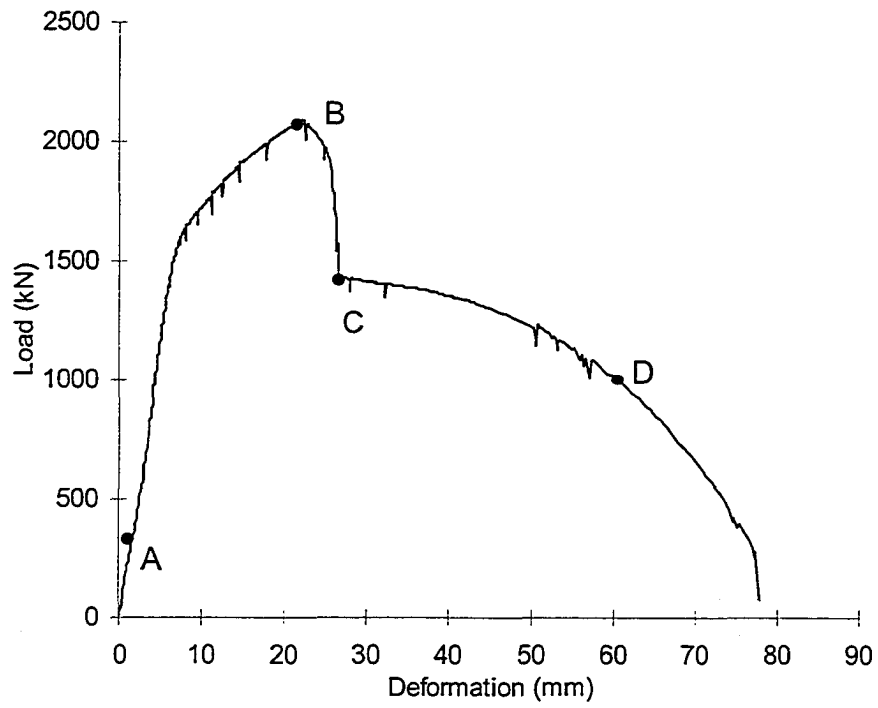


Figure 3.7 – Experimental Load vs. Deformation – Specimen 12R

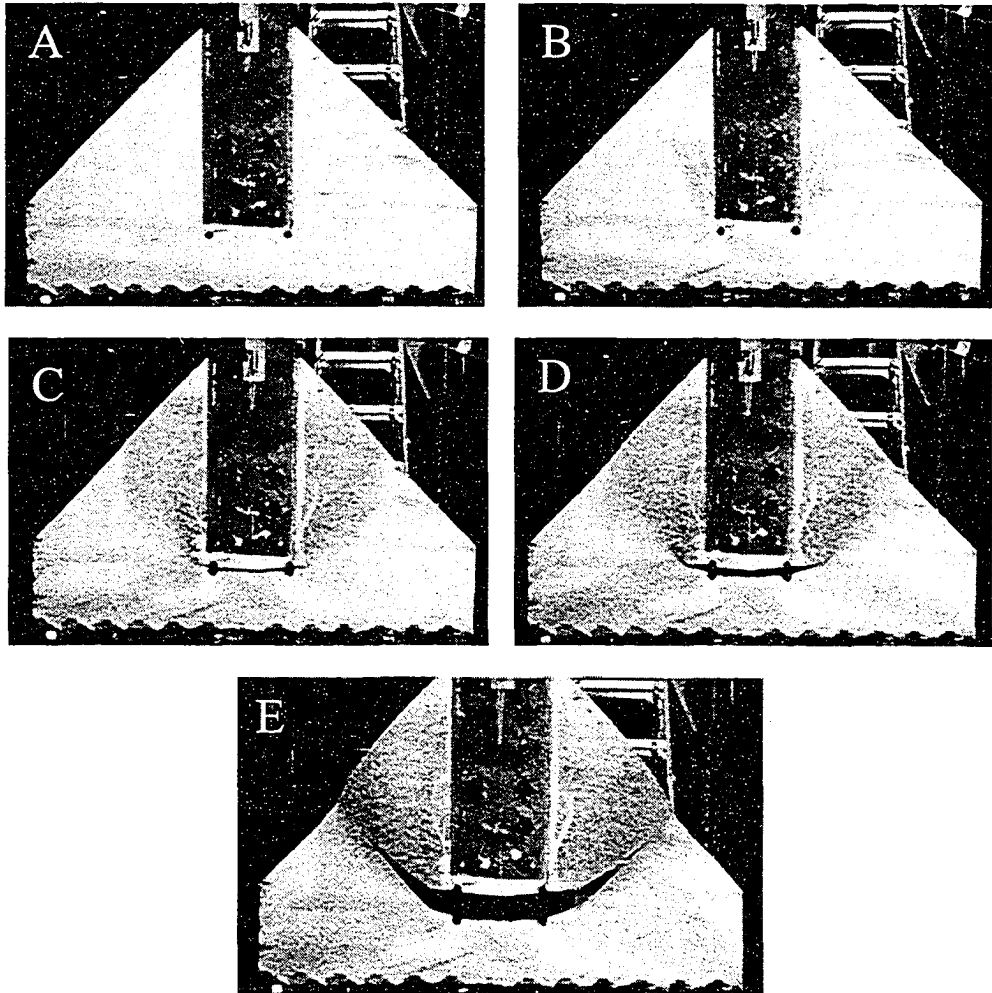
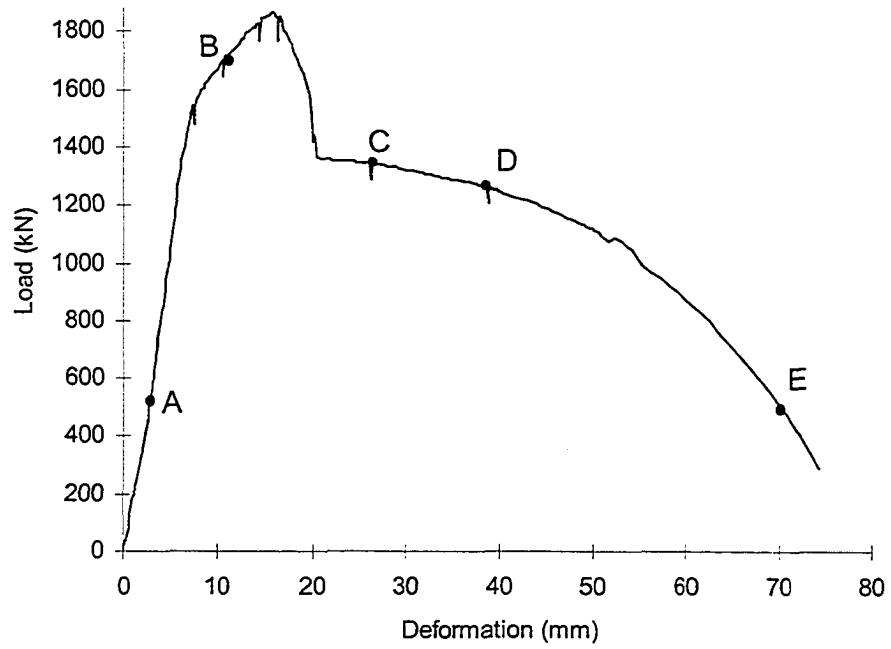


Figure 3.8 – Experimental Load vs. Deformation – Specimen 12H

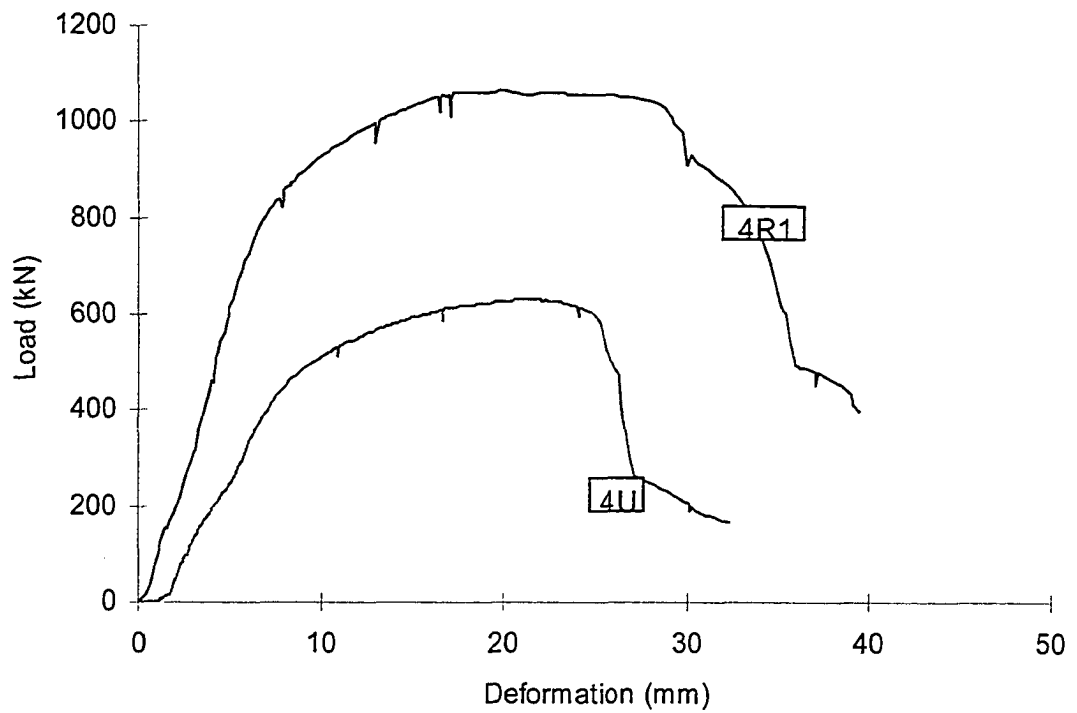


Figure 3.9 – 4U and 4R1 Load vs. Deformation

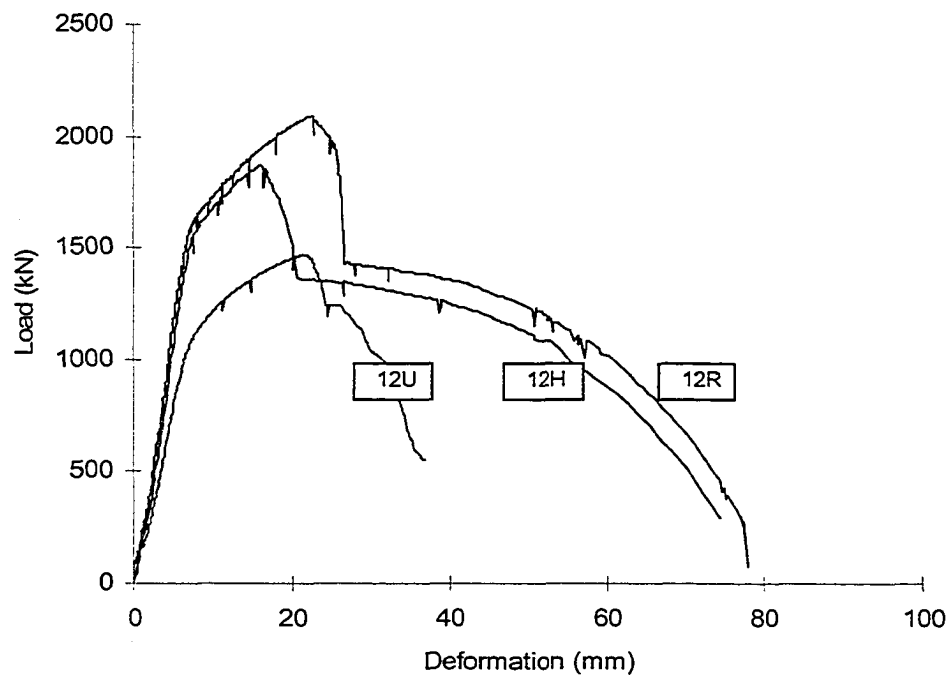


Figure 3.10 – 12 Bolt Specimens – Load vs. Deformation

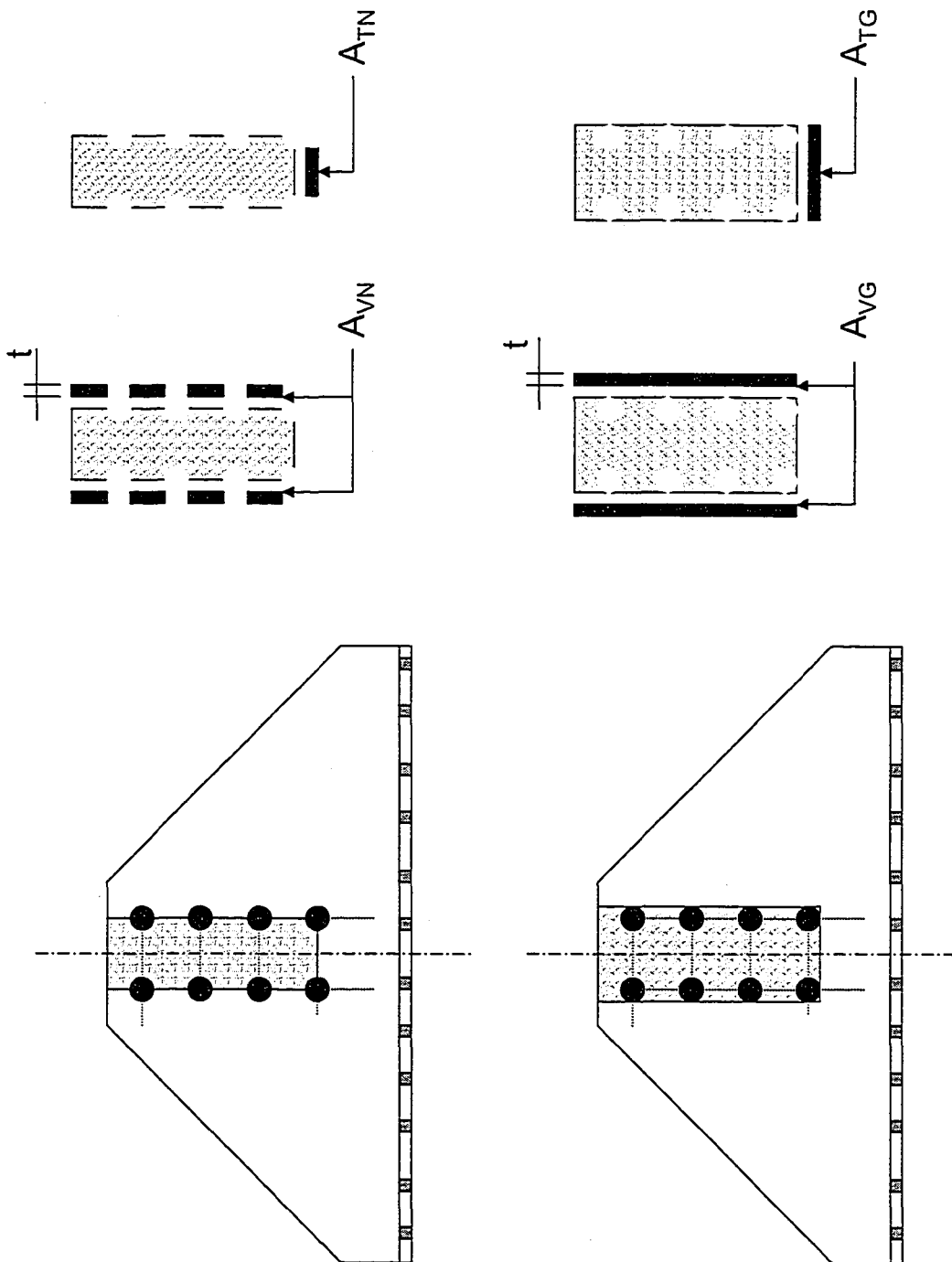


Figure 3.11 – Net and Gross Areas Calculation - Definition

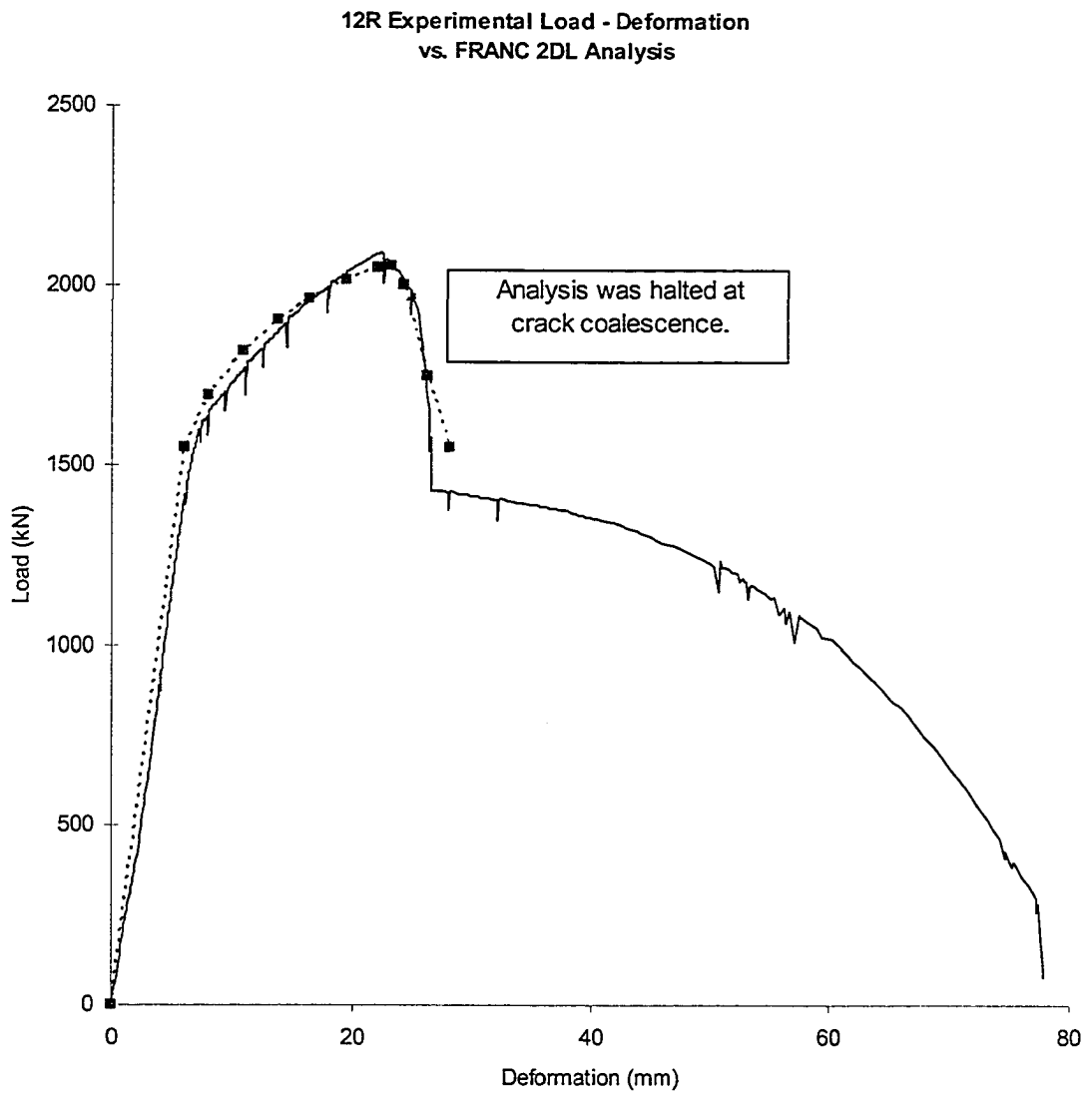


Figure 3.12 – 12R Experimental and FEA Load vs. Displacement

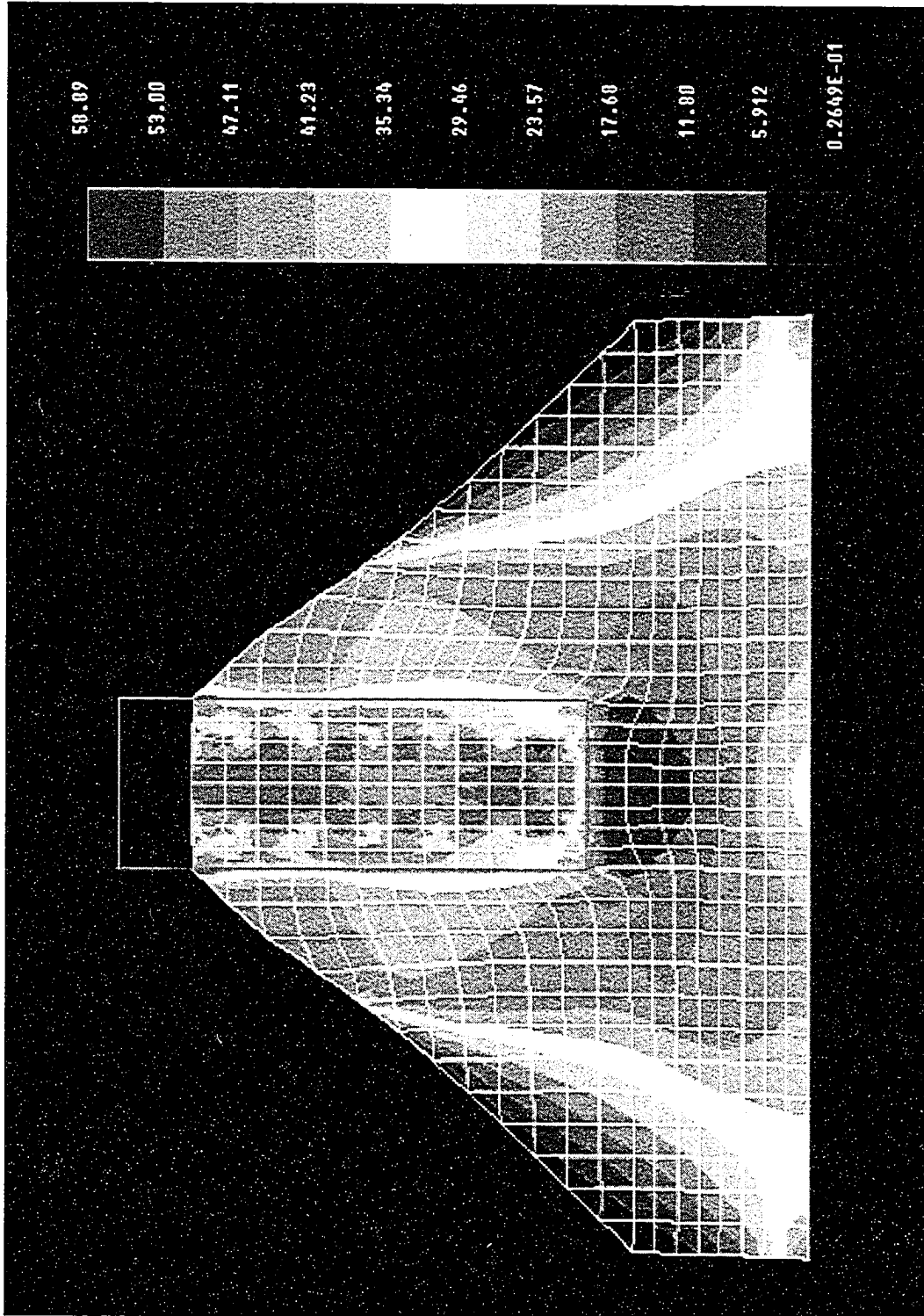


Figure 3.13 - 12R Gusset - Deformation 3 mm-- Principal Stress (ksi)

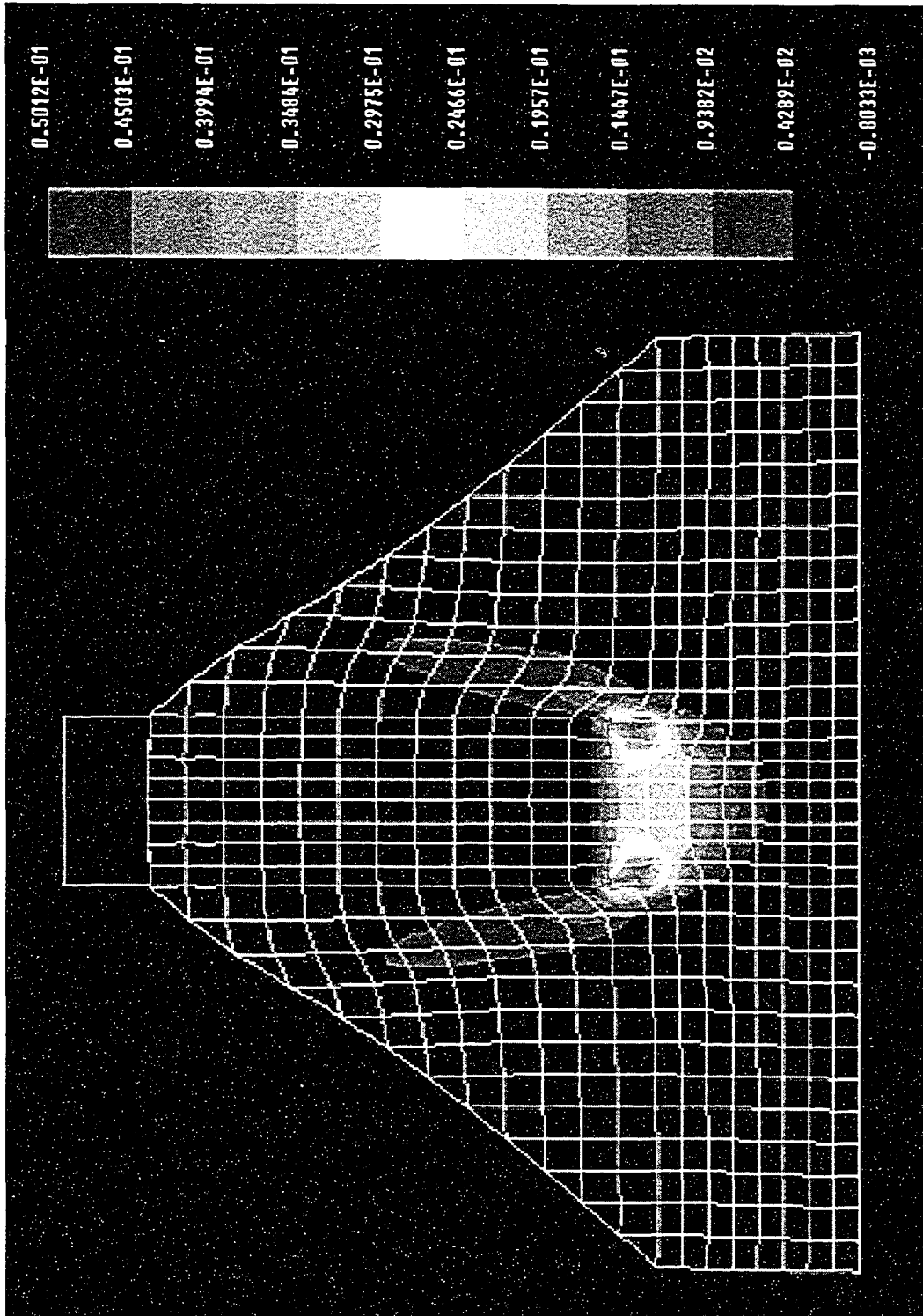


Figure 3.14 - 12R Gusset - Deformation 3 mm - Inelastic Shear Strain

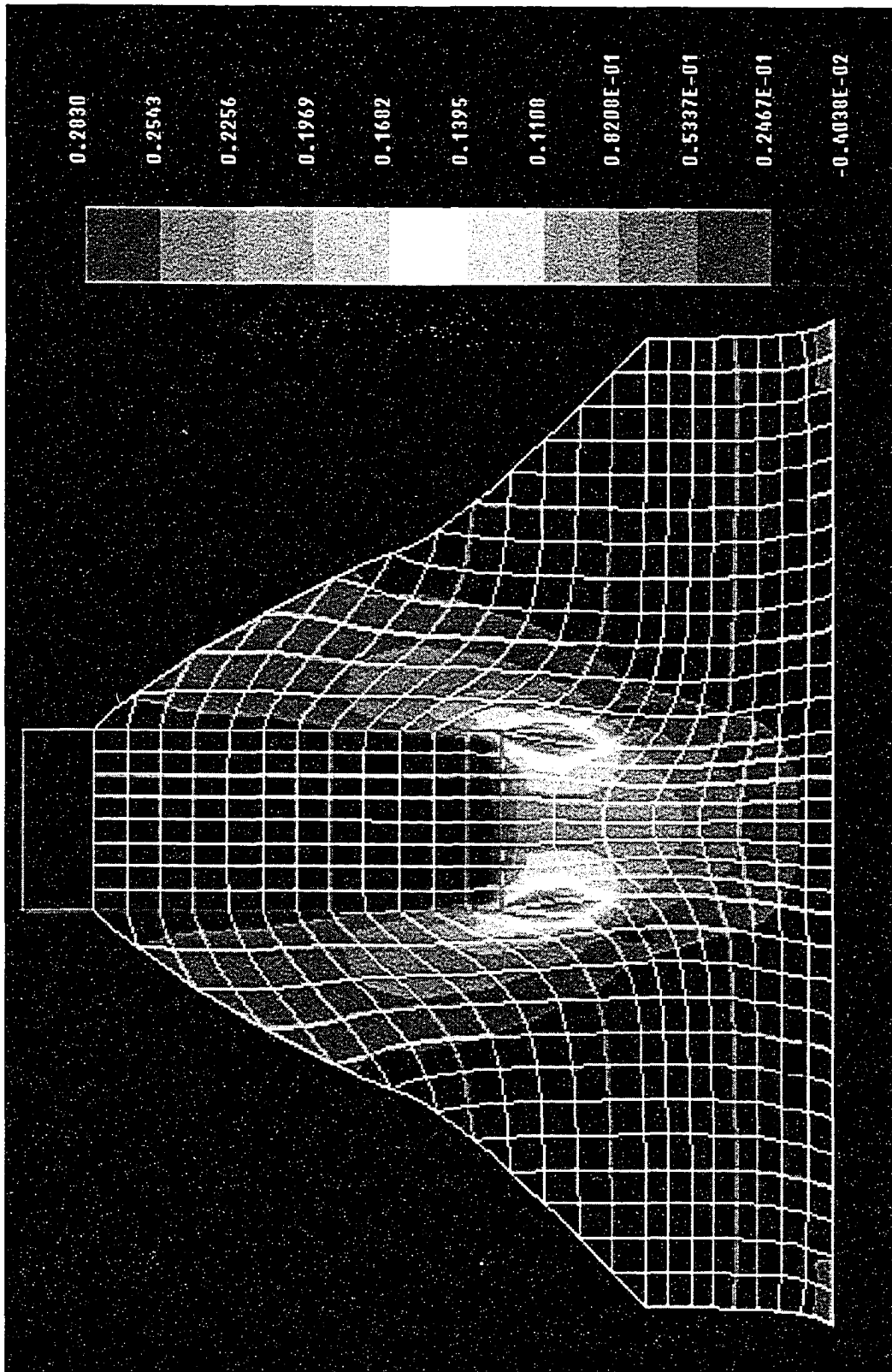


Figure 3.15 - 12R Gusset – Deformation 17.4 mm – Plastic Strain

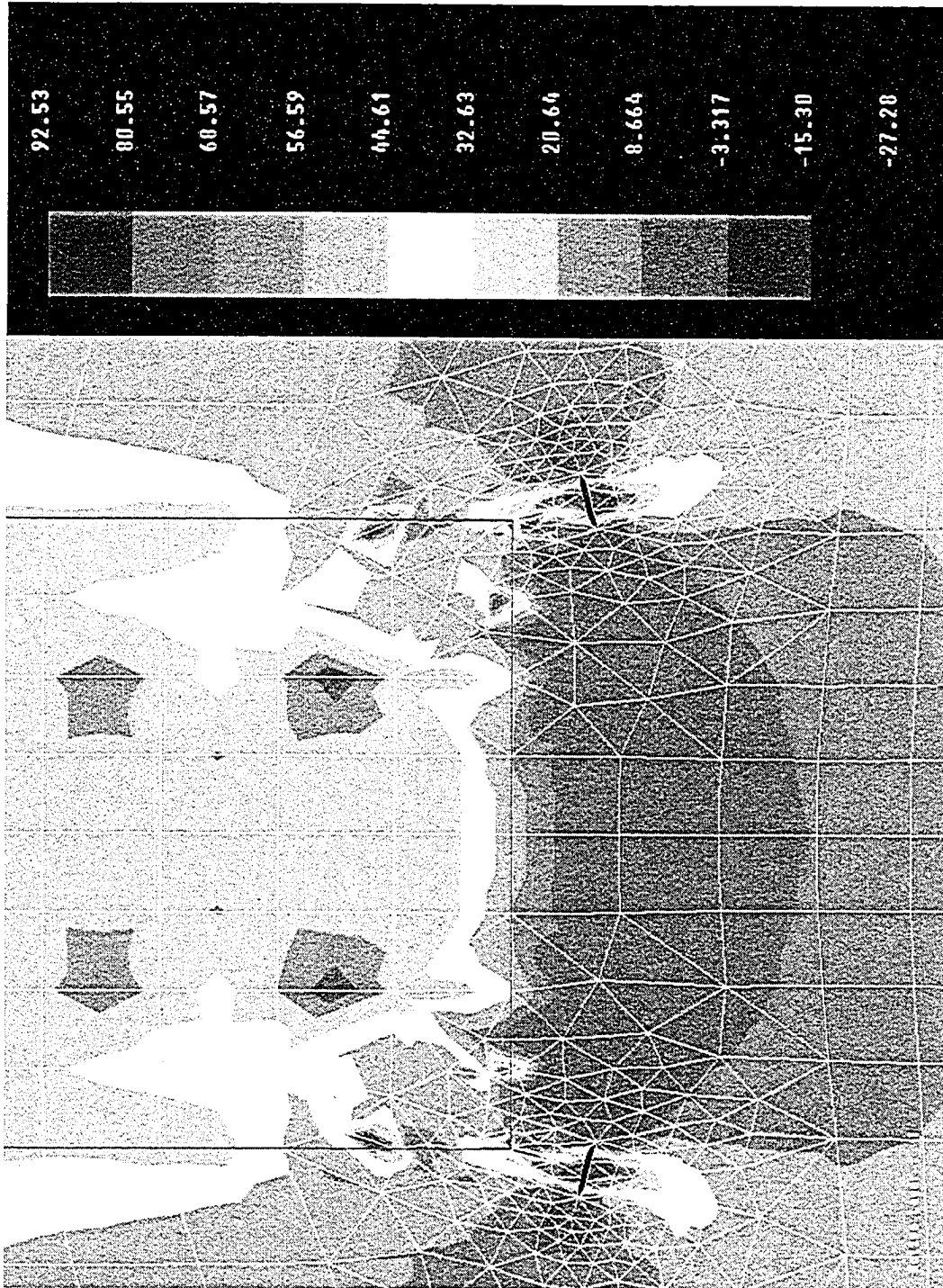


Figure 3.16 - 12R Gusset - 3rd Crack Growth Increment (Def. 19.4 mm) Principal Stress

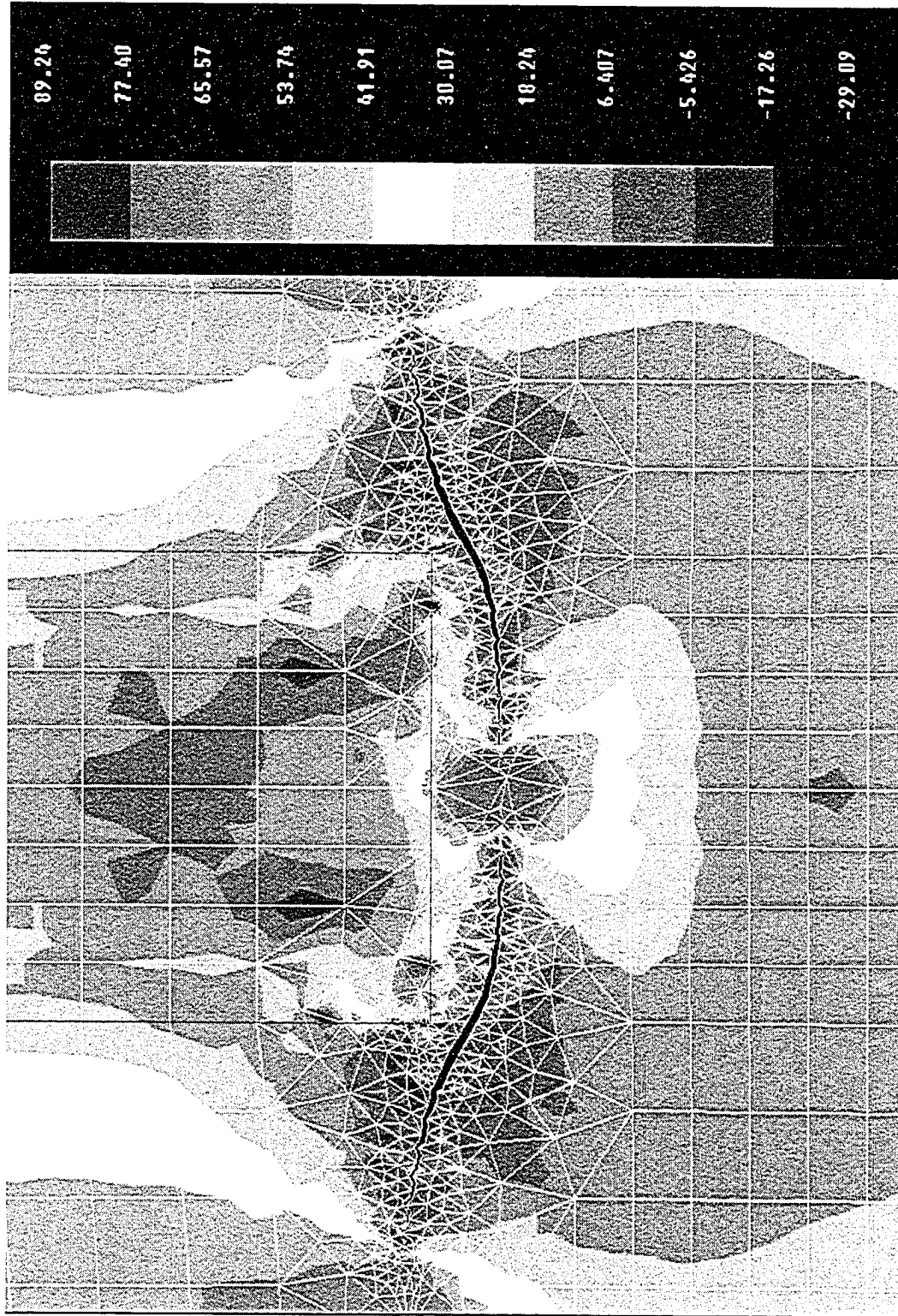


Figure 3.17 - 12R Gusset - 19th Crack Growth Increment (Def. 26.4 mm) Principal Stress

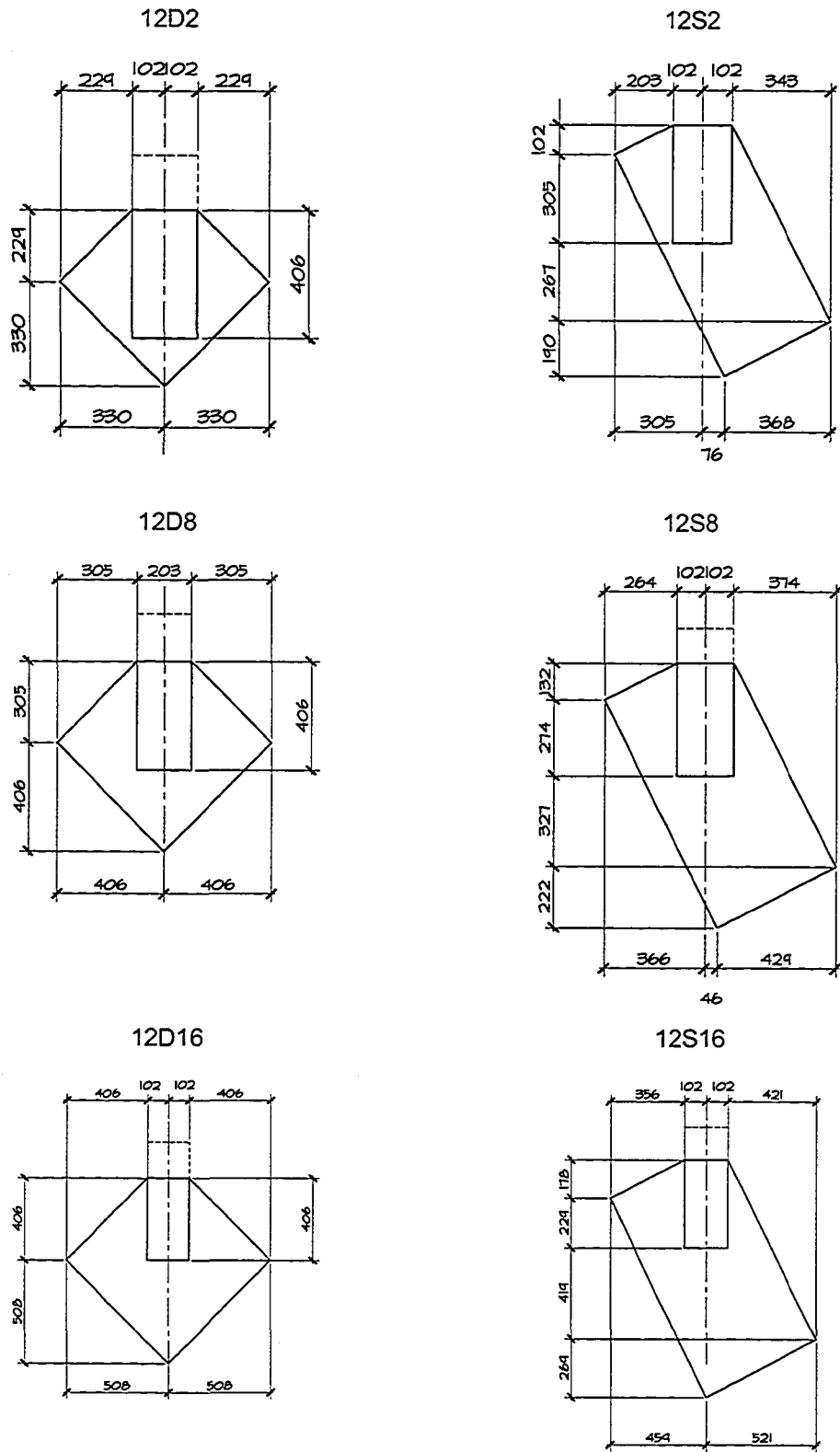


Figure 3.18 – Doubler Plate Reinforced Gusset Geometries

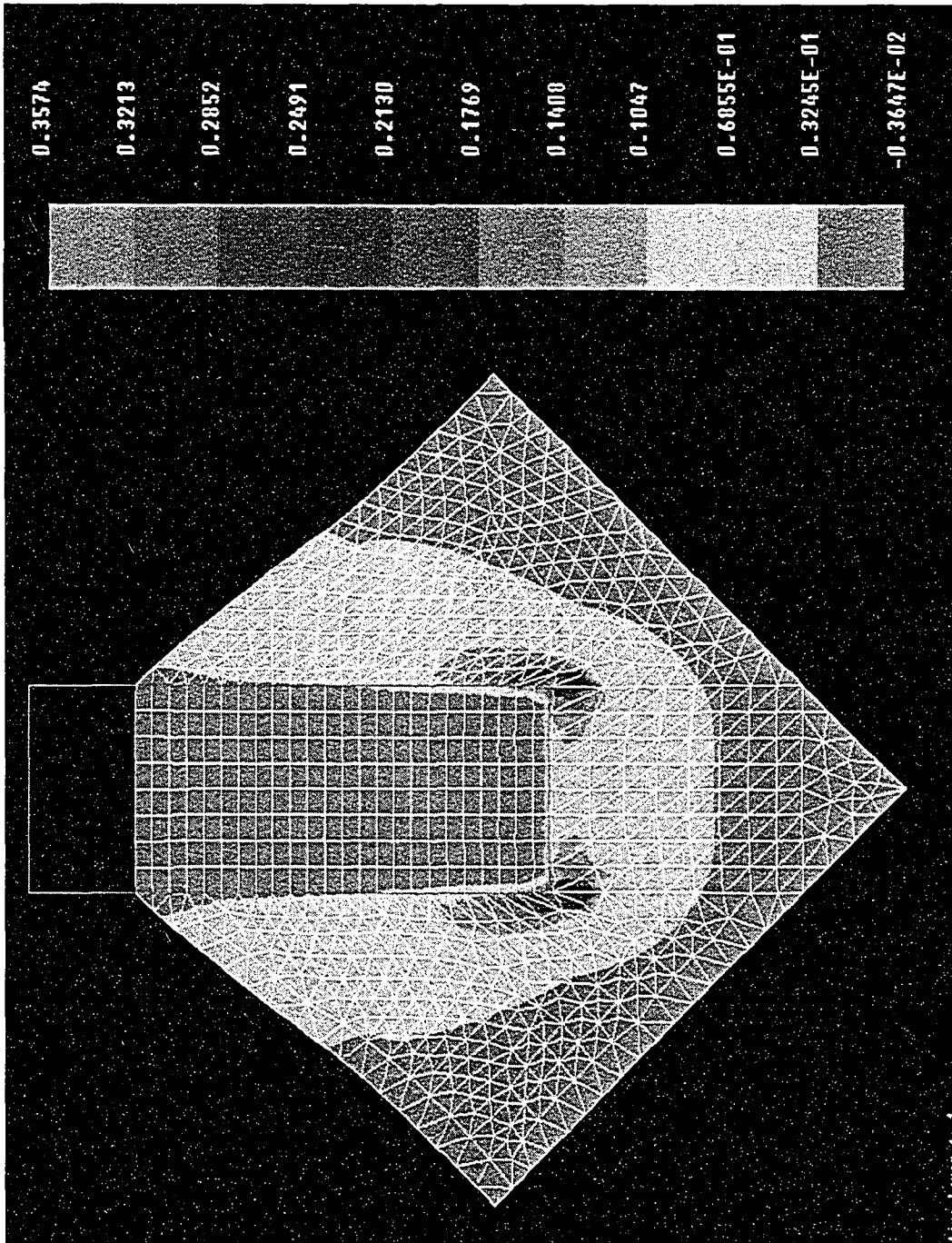


Figure 3.19 – 12D8 Gusset – Deformation 10.2 mm – Maximum Principal Strain

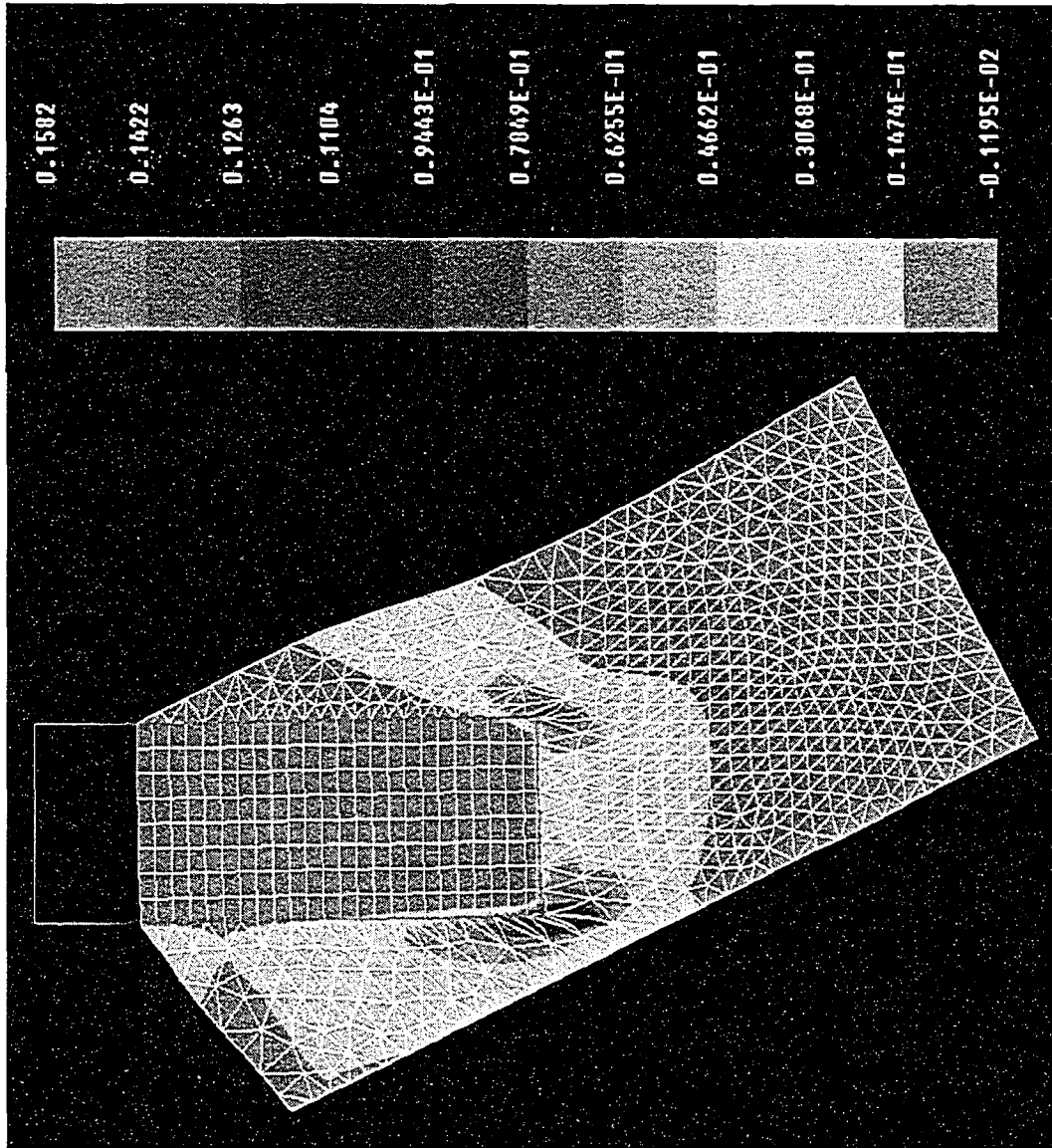
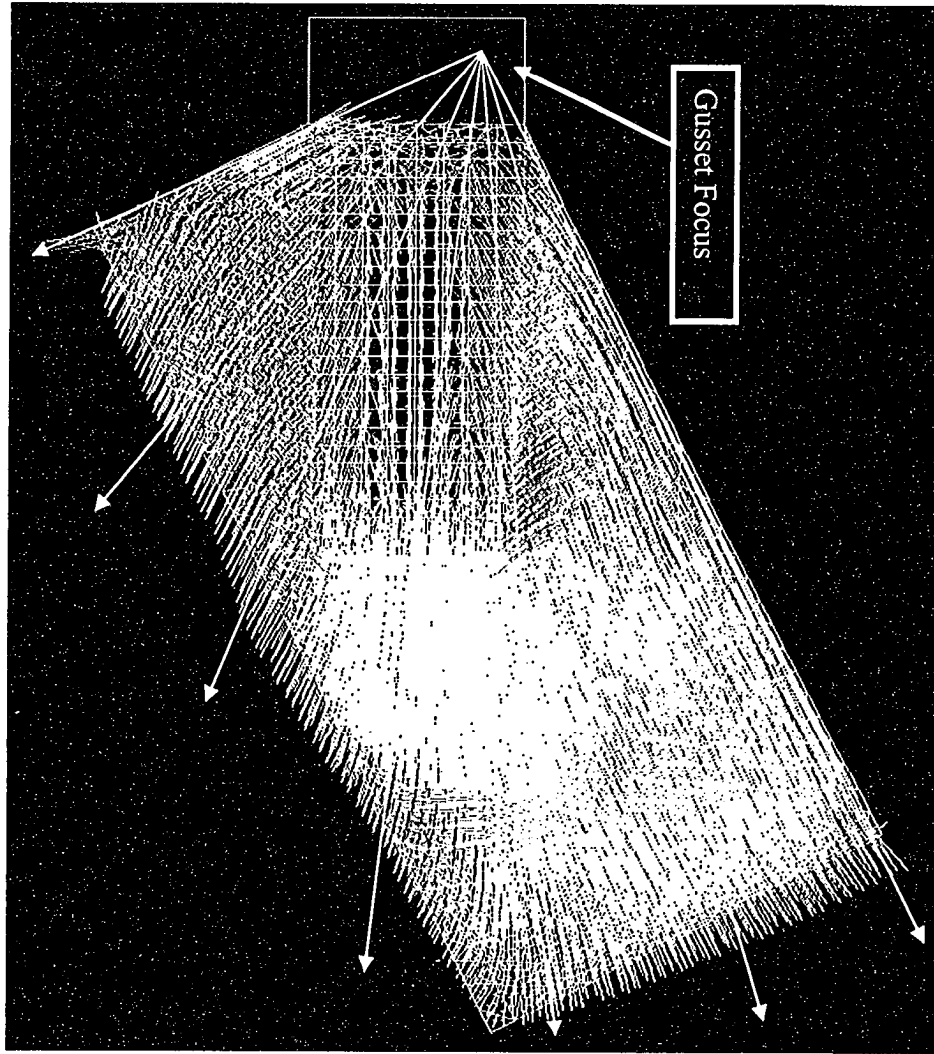
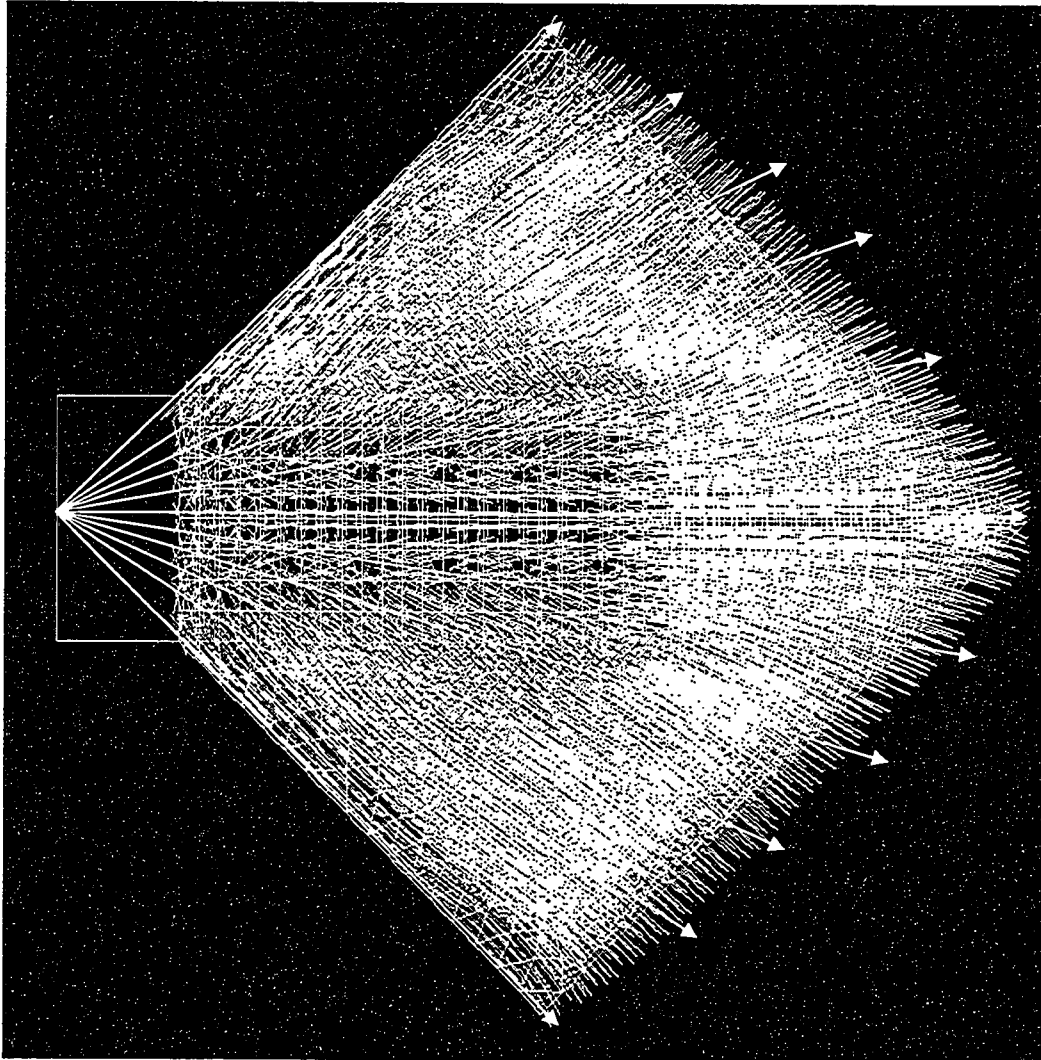


Figure 3.20 – 12S2 Gusset – Deformation 3.3 mm - Maximum Principal Strain



**Figure 3.21 – 12S2 Gusset – Deformation 10 mm – Principal Stress Vector Plot
Includes Radial Lines from Focus of Gusset**



**Figure 3.22 – 12D8 Gusset – Deformation 10.2 mm - Principal Stress Vector Plot
Includes Radial Lines from Focus of Gusset**

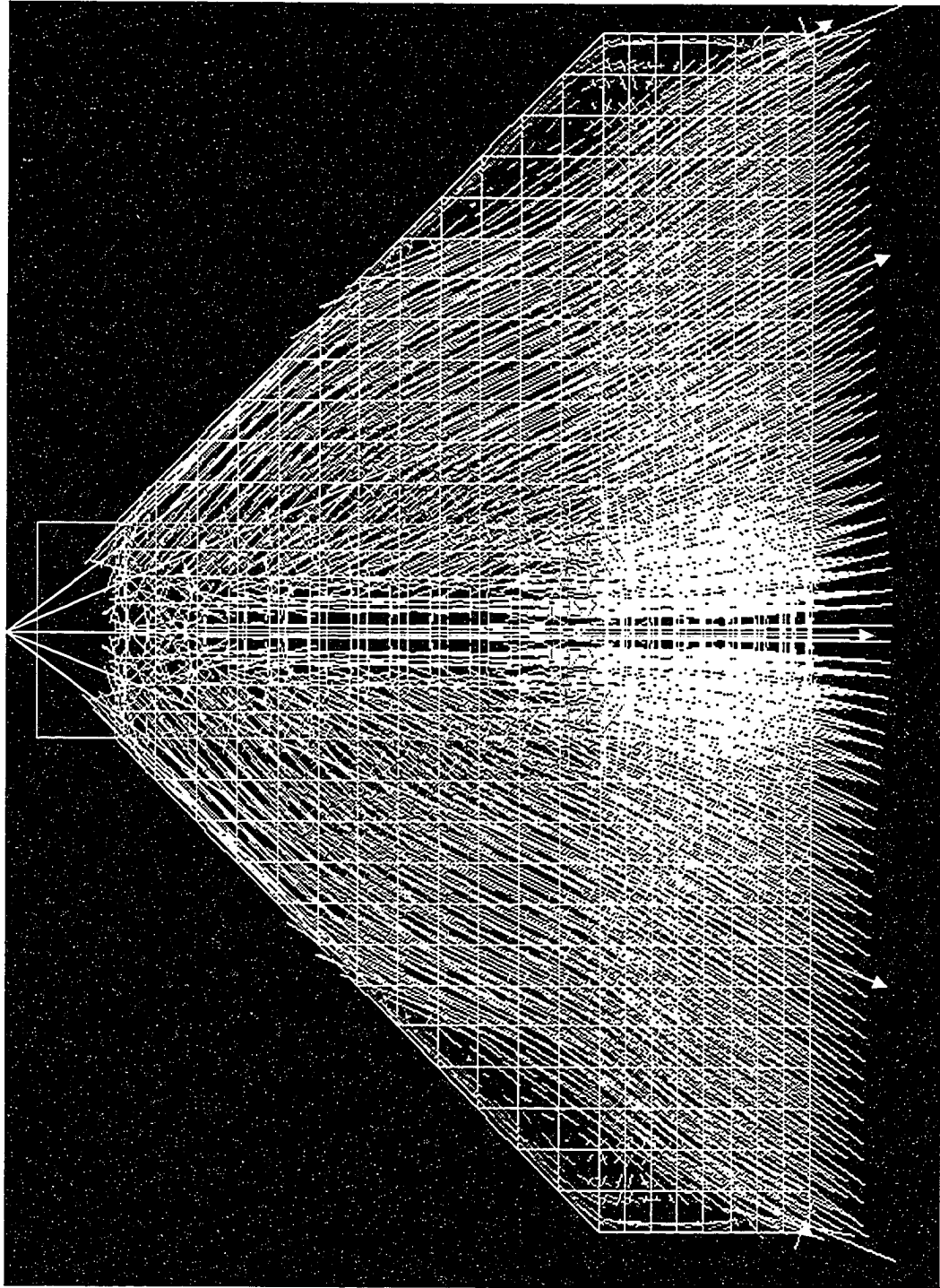


Figure 3.23 - 12R Gusset – Deformation 17.4 mm – Principal Stress Vector Plot
Includes Radial Lines from Focus of Gusset

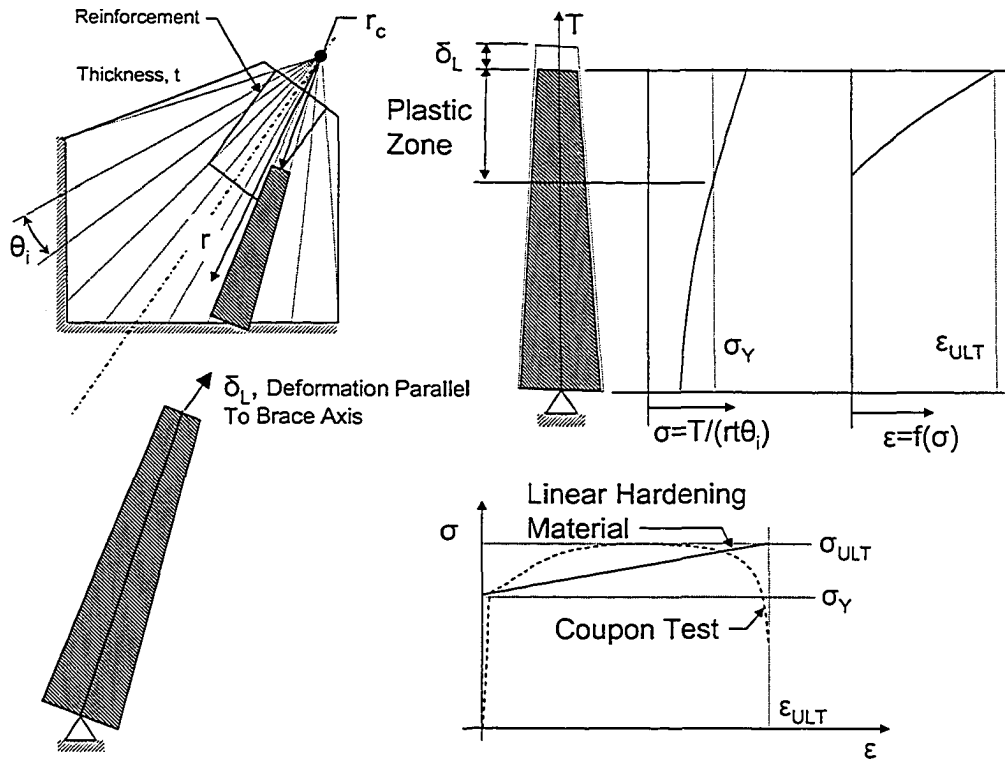


Figure 3.24 – Radial Strip Analysis

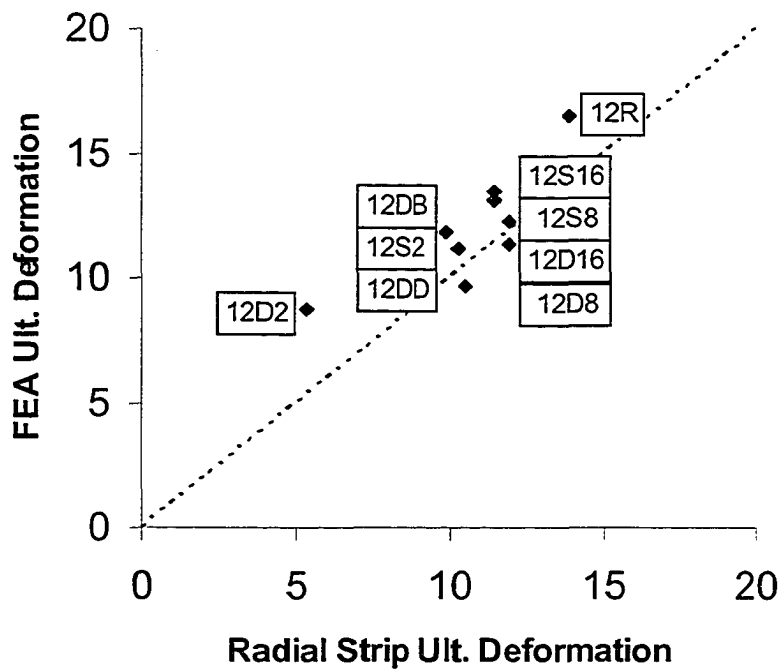


Figure 3.25 – Predicted Ultimate Deformations (mm) – FEA vs Radial Strip

3. 8 References

- AISC, 1999. Manual of Steel Construction. Volume II: Connections, LRFD 2nd Ed. American Institute of Steel Construction, Inc., Chicago IL.
- AISC, 1999. Manual of Steel Construction. Load and Resistance Factor Design. Second Edition. American Institute of Steel Construction, Inc., Chicago IL.
- ASTM A370-96, 1996. Standard Test Methods and Definitions for Mechanical Testing of Steel Products. American Society for Testing and Materials, Philadelphia, PA.
- Bjorhovde, R., and Chakrabarti, S.K., 1985. "Tests of Full-Size Gusset Plate Connections." Journal of Structural Engineering, ASCE, Vol. 111, No. 3, pp. 667-684.
- CAN/CSA-S16-01, 2003. Limit States Design of Steel Structures, Canadian Standards Association, Rexdale, Ontario.
- Chakrabarti, S.K., and Bjorhovde, R., 1983. "Tests of Full Size Gusset Plate Connections." Research Report, Department of Civil Engineering, University of Arizona - Tuscon, Arizona.
- Hardash, S.G., and Bjorhovde, R., 1985. "New Design Criteria for Gusset Plates in Tension." Engineering Journal, AISC, Vol. 22, No. 2, pp. 77-94.
- Hu, S.Z., and Cheng, J.J.R., 1987. "Compressive Behaviour of Gusset Plate Connections." Structural Engineering Report No. 153, Department of Civil Engineering, University of Alberta, Edmonton, Alberta.
- James, M.A., 1998. "A Plane Stress Finite Element Model for Elastic-Plastic Mode I/II Crack Growth." PhD Dissertation, Department of Mechanical and Nuclear Engineering, Applied Computation Laboratory, Kansas State University, Manhattan, Kansas.

Rabinovitch, J.S., and Cheng, J.J.R., 1993. "Cyclic Behaviour of Steel Gusset Plate Connections." Structural Engineering Report No. 191, Department of Civil Engineering, University of Alberta, Edmonton, Alberta.

Swenson, D., and James, M.A., 1997. "FRANC2D/L: A Crack Propagation Simulator for Plane Layered Structures. Version 1.4 Users Guide." Kansas State University, Manhattan, Kansas.

Swenson, D., James, M.A., and Hardeman, B., 1997. "CASCA: A Simple 2-D Mesh Generator. Version 1.4 Users Guide." Kansas State University, Manhattan, Kansas.

Thomason, P.F., 1990. "Ductile Fracture of Metals." Pergamon Press, Oxford, UK.

Walbridge, S.S., Grondin, G.Y., and Cheng, J.J.R., 1998. "An Analysis of the Cyclic Behaviour of Steel Gusset Plate Connections." Structural Engineering Report No. 225, Department of Civil Engineering, University of Alberta, Edmonton, Alberta.

Walbridge, S.S., Grondin, G.Y., and Cheng, J.J.R., 1998. "An Analytical Study of the Cyclic Behaviour of Steel Gusset Plate Connections." Proceedings of the Annual Conference of the Canadian Society for Civil Engineering, Vol IIIa, pp. 107 to 116.

Whitmore, R.E., 1952. "Experimental Investigation of Stresses in Gusset Plates." Bulletin No. 16, Engineering Experiment Station, University of Tennessee.

4. DUCTILE GUSSET PLATE – TESTS AND ANALYSIS^{3,4}

4.1 Introduction

Gusset plates are those elements which form connections between bracing and gravity load resisting elements in steel structures. They are typically fabricated using structural steel plates, bolted or welded to bracing elements and bolted or welded to beams and/or columns. Gussets may be stiffened on their edges, by the addition of stiffener plates welded to the free edges of the gusset, to enhance compression and post-buckling strength. When tested in that configuration by Rabinovitch and Cheng (1993) and Nast, Grondin and Cheng (1999), gusset plates continued to carry significant compression forces after development of a buckled region of gusset plate just beyond the brace connection. This stable post-buckling load-deformation behaviour is desirable for inelastic elements in seismically loaded structures. The use of gusset plates as inelastic elements in seismically loaded structures has been proposed in research by Hu and Cheng (1987), Rabinovitch and Cheng (1993), Yam and Cheng (1994), Walbridge, Grondin and Cheng (1998) and Nast, Grondin and Cheng (1999), based on observed stable and open load-deformation hysteresis in cyclic tests.

In a structure employing inelastic gusset plates as energy absorbing elements for seismic loading, braces may be designed to remain elastic throughout the design seismic event. With bracing members remaining elastic, damage would be concentrated in gusset plates while braces, beams and columns would remain primarily elastic throughout earthquake loading. Such configurations, referred to as “strong brace - weak gusset” systems, are attractive since they would facilitate a wider variety of candidate members for bracing member selection, simplified design and fabrication of brace end connections with required capacity less than $A_G F_Y$ and may simplify post-earthquake repairs when compared to systems employing inelastic brace members.

³ Portions of this chapter were presented at the NASCC / PSSC Conference, Long Beach, California, March, 2004.

⁴ A version of this chapter is currently under revision for publication in the Journal of Constructional Steel Research.

While gusset plates have exhibited desirable cyclic load-deformation behaviour, the deformation they can sustain in seismically loaded structures is limited by their ultimate deformation in tension, which has generally ranged between 10 mm to 20 mm in tests. The inelastic deformation demand anticipated for a seismically loaded inelastic gusset plates has been researched by Mullin (Chapters 5, 6, and 7) for 1, 2, 4 and 8 storey steel structures and for 8 storey concrete structures, retrofit with steel infill bracing. Using non-linear time history analysis, gusset deformations were calculated to exceed observed fracture deformation, of 10 mm to 20 mm, for a range of structures exceeding two storeys in height subjected to design Zone 3 and 5 seismic events.

For gusset plates to be used as energy dissipating elements in seismically loaded structures in the configurations outlined above, deformability in excess of the demand imposed by seismic loading must be available to prevent fracture during a design seismic event.

The purpose of this research is to formulate and evaluate a modified gusset arrangement with deformability exceeding that observed in past continuous gusset tests. A gusset configuration, employing flexural links to distribute inelastic strain, is developed. Finite element modelling of the flexural link is done to assess the effectiveness of the link and to allow evaluation of anticipated ultimate load and ultimate deformation.

Experimentally determined cyclic load-deformation responses are obtained from two prototype gusset specimens employing flexural links.

4.2 Typical Gusset Behaviour

The load-deformation behaviour typically observed in tension tests of gusset plates with bolted brace connections is an initially linear response up to first yield followed by declining stiffness. As yielding progresses, stiffness decreases to zero and a fracture forms in the gusset plate, typically transverse to the brace axis between the innermost pair

of bolts in the brace-gusset connection region. Initiation of fracture coincides with ultimate load. Fracture initiation and ultimate load are typically observed at less than 20 mm deformation. With propagation of cracks, load decreases until cracks circumscribe the bolted connection region. Some yielding may be observed along the sides of the bolted connection region after the completion of the initial fracture across the innermost bolts.

When furnished with reinforcing plates to suppress crack initiation at bolt holes, gusset plate deformation a first fracture has been observed to increase by 3mm to 5 mm over similarly proportioned unreinforced plates, Mullin (Chapter 3). Reinforced gusset plate deformation at first fracture may be reasonably well predicted using a radial strip analysis, Mullin (Chapter 3). Fracture in the case of reinforced gussets has been observed in tests by Mullin (Chapter 3) within the unreinforced portion of the gusset, first across the end of the reinforcement and then propagating diagonally through the plate, toward the free edges. In tests and radial strip analyses by Mullin (Chapter 3), a practical upper deformability limit of approximately 20 mm exists for gusset plates constructed of commonly available steel and using geometry consistent with current industry practice.

4.3 Gusset Modifications for Increased Deformability

It is anticipated that deformation demand on gusset plates in a strong brace – weak gusset CBF would exceed 20 mm in many common structure types and design events.

Modifications of gusset plate geometry, based on the observations made during tests of both reinforced and unreinforced gusset plates, are proposed to increase gusset deformability.

Gusset plate fracture has been described by Hardash and Bjorhovde (1985) and by many others in a large body of research. First fractures are generally perpendicular to the brace axis, along the innermost row of bolts in unreinforced bolted connections or just beyond the end of reinforcement plates in gussets with reinforcement welded over the bolted

brace connection region. Fracture location and orientation consistent with that predicted by the radial strip analogy and by finite element modelling, reported by Mullin, (Chapter 3). After completion of first fracture, unreinforced gussets develop a region of shear yield along the sides of the brace – gusset connection region. With increasing deformation, the yielded region strain hardens and eventually causes fractures to form along the bolted connection perimeter, parallel to the brace axis.

It is reasoned that two modifications, as shown in figure 4.1, may be made to gusset geometry to prevent fracture along the perimeter of the bolted connection, as observed historically in tests of continuous gusset plates. First, to prevent fracture perpendicular to the brace axis along the line connecting the innermost two bolts of the bolted brace connection, the gusset plate material between the brace – gusset connection and the supported boundary may be removed. Second, to prevent fracture along the boundaries of the bolted brace connection parallel to the brace axis, weakening of the shear yield region adjacent to the brace – gusset connection may be accomplished by removal of some plate material in the adjacent region. It is proposed that the weakened region be perforated by slots, such that flexural links remain.

4.4 Extended Hinge Link (EHL) Formulation

The formulation of the candidate flexural link is based on the requirement that, at the inflection point, yielding not occur while elsewhere within the link elongated plastic hinges develop. By maximizing the volume of yielded material in this manner, it is hypothesized that deformation at first fracture and energy absorption will be maximized. The shape, $h(x)$ of the candidate flexural link shown in figure 4.2, can be determined using the following approximate formulation:

Forces acting on a cross section of the link, located x from the neck, are defined by:

$$V = h_0 t \alpha \sigma_Y \quad [1]$$

$$M = h_0 t \alpha \sigma_Y x \quad [2]$$

where $h_0 = h(0)$, the neck depth of the beam and $\alpha \sigma_Y$ is the average shear stress at the minimum section, $x = 0$.

Applying a first order unity interaction equation for allowable shear and plastic moment in the beam, the expression for the shape of the beam can be derived as follows:

$$\frac{V}{V_{ALL}} + \frac{M}{M_P} = 1 \quad [3]$$

where,

$$V_{ALL} = \alpha \sigma_Y h(x) t$$

$$M_P = \frac{h(x)^2 t}{4} \sigma_Y$$

Substituting [1] and [2] in [3] yields the expression:

$$-h(x)^2 + h_0 \cdot h(x) + 4 \cdot h_0 \cdot \alpha \cdot x = 0 \quad [4]$$

Solving the quadratic for the expression $h(x)$ yields:

$$h(x) = \frac{h_0 + \sqrt{h_0^2 + 16 \cdot h_0 \cdot \alpha \cdot x}}{2} \quad [5]$$

Simplifying [5] yields the expression:

$$h(x) = h_0 \cdot \left[0.5 + 0.5 \cdot \sqrt{1 + 16 \cdot \alpha \cdot x / h_0} \right] \quad [6]$$

It should be noted that axial force is omitted from the above formulation since the presence of axial force in this system causes strain localization at the neck, $x = 0$, and therefore is deemed to interfere with the stated goal of maximizing yielded volume.

4.4.1 Preliminary Finite Element Analyses

Using geometry $h(x)$ from [6], a range of α , and the modelling and material parameters described in 4.5, several finite element models were analysed using FRANC2D/L (FRacture ANalysis Code 2D Layered) software, Swenson and James (1997) and a bilinear stress strain relationship with $\sigma_Y = 443$ MPa, $E = 200,100$ MPa, $\epsilon_{ULT} = 0.27$ and $\sigma_{ULT} = 523$ MPa to evaluate the effect of the parameter α on the behaviour of flexural links. It was found that, for structure geometry based on α greater than 0.7, shear yielding and strain localization occurred within the vicinity of the neck ($x = 0$) prior to development of extended plastic hinges. For values of α between 0.6 and 0.7, extended hinges developed early in the loading history but were not fully developed when shear yielding and strain localization occurred in the neck region. Structure geometries based on α between 0.5 and 0.6 were found to develop extended plastic hinges without strain concentration at the neck. This corresponds to the anticipated value of α corresponding to plane stress shear yield, based on von Mises yield criteria, of 0.577.

4.5 EHL Modelling

A series of 16 extended hinge links were modelled using CASCA, Swenson, James and Hardeman (1998), and analysed using FRANC2D/L, Swenson and James (1997). The geometry of each link was based on independent variables of throat depth, h_0 and span – which were varied to permit determination of their effect on deformability. Material properties were based on the measured material properties of steel used in test specimens, reported below. Vertical displacement was increased incrementally on the left edge of the mesh while the right edge remained fixed. The model geometry, maximum predicted

load and predicted deflection at ultimate strain (0.40) are provided in table 4.1. The deformation at predicted fracture initiation, determined by the maximum principal stress criteria ($\max|\sigma_1, \sigma_2, \sigma_3| = \sigma_{ULT}$) as defined by Thomason (1990), ranges from 89 mm to 660 mm for the range of configurations analysed. Deformation at first fracture was observed to increase with span and with decreasing neck depth.

Figures 4.3 and 4.4 show the principal strain and principal stress analysis results for extended hinge gusset link opt9. Both figures clearly illustrate the large extent of uniform inelastic strains along the top and bottom surfaces of the link while, at the neck and ends, strains remain lower. The deformation of the link is shown in proportion to the geometry of the structure in figures 4.3 and 4.4. Axial load was zero for the analyses.

4.6 EHL Predictive Model

Based on the independent variables neck depth, h_0 , and span, l , and the previously defined shape relationships, one can compare finite element model predicted load at fracture initiation to that predicted theoretically. The following expressions were derived from finite element analysis results obtained for configurations opt1 through opt12.

From the unity interaction equation used to derive link shape, link ultimate load is defined as:

$$V_{ULT} = \alpha \cdot h_0 \cdot l \cdot \sigma_y \quad [7]$$

Deformation at fracture initiation (deformability) may be predicted by the empirical formula below, (constants were derived by regression of finite element analysis results):

$$\delta_{ULT} = \frac{3 \varepsilon_{ULT} l^{1.5}}{4 h_0^{0.66}} \quad [8]$$

V_{ULT} (load at fracture initiation) determined by [7] agrees well with load at fracture initiation determined by finite element analysis, with a mean empirical/finite element ratio of 0.977 as shown on table 4.1. δ_{ULT} (deformability) determined by empirical relationship [8] correlated well with deformability determined by finite element analysis, with a mean empirical/finite element ratio of 1.01 as shown in table 4.1.

The relationships between geometry and structural behaviour indicate that ultimate load is dependant on h_0 , t and σ_Y and is independent of link span, l . Deformability of a link gusset constructed of a given material and neck geometry is then solely dependant on span, l . For a design with a given material, ultimate load and deformability, gusset may be determined by selection of appropriate the independent geometric variables, h_0 and l .

4.7 Test Specimens

In proportioning the gusset specimens, the design philosophy was to provide enhanced deformability using a structural configuration which could, with reasonable cost and using readily available materials and manufacturing techniques, be incorporated in a real structure. Two specimens were designed, fabricated and tested to assess the response of extended hinge link gussets to cyclic loading. In a real structure, the required ultimate load for a gusset-brace could be resisted by a single link. To resist loads of the magnitude commonly encountered in real structures, a single link might require a deep neck section. The designer would then require a very long span to provide desired deformability of the link – which would give rise to excessively large connections. An obvious solution to this problem is to introduce several links in parallel which, for a given material, gusset ultimate design load and required deformability, simultaneously reduces the required h_0 and l of each link versus the single link gusset designed using the same parameters. Reflecting this, the specimens were designed with multiple links to maintain a reasonable specimen size provide capacity within the range of that commonly required of gusset plates in real structures. The specimens were configured to emulate the boundary conditions anticipated in a real structure.

It should be noted that, the provision of multiple links gives rise to axial loads in the links above and below the mid-depth of the system – which has been previously identified as deleterious to the deformability of link gussets and results in strain localization at the neck. This can be observed in finite element analysis result of the three link assembly opt21 shown in figures 4.5 and 4.6. In figure 4.5, the maximum inelastic principal strain in the top link extends along the top left of the extreme fibre and through the necked section toward the bottom right. In figure 4.6, the top link neutral axis is shifted down from the mid-depth of the link. The middle link maximum principal strains are located only near the extreme fibres of the bending portions of the link with the strains in the neck remaining much smaller. The bottom link exhibits an upward shift of the neutral axis from the mid-depth of the link and a reduction of the volume of material experiencing significant straining when compared to the middle link. The presence of axial stress in the links is demonstrated by the distribution of stresses along the centerline of the assembly, varying from approximately 50ksi (345MPa) at the top of the assembly to -14ksi (96.5MPa) at the bottom.

During testing, the links will be predominantly inelastic. As such, out-of-plane restraint was provided to prevent local and lateral torsional buckling. The restraint provided in the form of two face plates, detailed in figure 4.7, bolted to contact both sides of the extended hinge gusset cores. A slot was provided in the face plates to allow the connection material between the brace members and the link to displace relative to the face plates. Spacer plates of thickness equal to that of the face plates, and shown in figure 4.8, were placed between the brace members and the extended hinge gusset. The spacer plates were sized to pass just inside the slot, thereby restraining sideways deformation of the load carrying gusset relative to the original alignment of the brace. The face plates provided stiffness required to restrain the brace-gusset assembly from deformation out-of-plane of the gusset system.

The shapes of the components were fabricated using an AutoCAD drawing – transferred electronically to the steel fabricator – and transferred directly to a numerically controlled

cutting table – ensuring that the link profile was accurately reproduced in the structure. The geometries of the two core plates tested are shown in figures 4.8 and 4.9. The geometry of the small plate hole is shown in figure 4.10 and the brace member is shown in figure 4.11.

While the gusset plates tested were significantly more complicated than a similar sized continuous gusset, the average cost of each of the EHL specimens tested was found to be 1.2 times the average cost of similarly sized continuous gussets, purchased from the same fabricator for the testing reported in chapter 3. While significantly more cutting operations are required to manufacture EHL gussets than traditionally configured ones, the numerically controlled cutting process used to fabricate the pieces allow cutting operations to be performed accurately and at low cost.

4.8 Test Apparatus

The tests were conducted in the MTS600 test machine at the University of Alberta IF Morrison Structures Lab. The assembled test apparatus is depicted in figures 4.12 viewed from the front and 4.13, viewed along the edge. The large plate core is shown prior to testing in figure 4.14.

Load, machine stroke and gusset assembly deformation, measured by LVDT, data were collected for the duration of the tests. Cyclic deformations were applied to the specimens in single sinusoidal cycles of increasing amplitude, in steps of 10 mm, similar to the loading specified in SAC Background Document 97/02, Appendix E “Loading Protocol for Stepwise Increasing Cyclic Tests”. Two specimens were tested, referred to as small plate and large plate. The geometry of the specimens is provided in figures 4.8 and 4.9. All components of the specimens were blast cleaned to SP-6 prior to assembly.

4.9 Test Results

4.9.1 Ancillary Tests

Coupons were harvested from the same plate used to fabricate the gusset cores. Coupons were tested in conformance with ASTM A370-96 in a direction parallel to the links. The measured properties of the steel were $\sigma_Y = 402$ MPa, $\sigma_{ULT} = 499$ MPa and $\epsilon_{ULT} = 0.384$, obtained from those coupons which fractured within the 50 mm extensometer gauge length.

4.9.2 Small Plate Test

The small plate specimen consisted of three levels of link beams, spanning 152 mm (6") each with a neck depth of 25.4 mm (1") and a thickness of 12.7 mm (½"). Based on the finite element analysis results of the single link system, the predicted ultimate load if this assembly was 430 kN and the predicted deformation at first fracture was 65 mm. The load deformation response of the small plate specimen is provided in full in figure 4.15. It is also subdivided into three cycle segments in figures 4.16 through 4.18. Upon loading in cycle 1, some seating of the specimen was observed in the 0 to 100 kN range. Once seated, the specimen responded in a linear elastic manner up to a proportional limit of approximately 300 kN, which was followed by gradual stiffness reduction to the maximum deformation of cycle 1 at +10 mm and corresponding load of 370kN. The negative portion of the deformation cycle mirrored the positive, in that the seating behaviour from 0 to -100 kN was repeated and at the minimum deformation of the cycle, -10 mm, a load of -375 kN was carried. The observed proportional limit was in good agreement with the ultimate load and proportional limit predicted by the finite element analysis. With each subsequent cycle, increasing the maximum and decreasing the minimum deformation by 10 mm, the maximum load was observed to increase. By the end of compression cycle 3, the load carried by the gusset-brace assembly was -580 kN – well in excess of that predicted by the finite element analysis. The trend of increasing load continued with each cycle until, at the end of compression cycle 6, the brace

member began to buckle out-of-the-plane of the gusset at a load of 950 kN. The specimen was then unloaded and disassembled to allow the overall brace length to be reduced from 3660 mm (12'-0") to 1830 mm (6'-0") – to increase its capacity and allow the test to continue. When disassembled, the faying surfaces between the face plates and the gusset assembly were observed and found to have galled as shown in figure 4.19. Rough and approximately spherical pieces of steel, from 1 mm to 6 mm in diameter had formed on the interface between the face and core plates and had gouged grooves in the surfaces of the face plate and link gusset material. The specimen was reassembled but without the galled steel in place. During cycle 7, the maximum load carried by the assembly reduced to 410 kN in tension and 404 kN in compression, close to the predicted maximum load based on finite element and empirical analyses. During cycle 7, deformation +50 mm, necking of an upper link was observed, just adjacent to the d_o , and is shown in figure 4.24. During tension cycle 7, at a deformation of approximately 60 mm, a loud bang accompanied by a drop in loading from 350 kN to 200 kN was heard. This corresponded to the fracture of the upper right link near the neck, shown in figure 4.21. With additional tension deformation up to 70 mm, load carried by the specimen increased to 290 kN. During the compression cycle, the specimen sustained a load of approximately 350 kN until, at a deformation of -35 mm the fractured parts of the upper right link contacted each other. Upon contact, the fractured upper right link began to carry load and deform as shown in figure 4.22, increasing the load carried to 400 kN in compression.

During tension cycle 8, at deformation +10 mm to +15 mm, several load bangs were heard from the internal link beams. They were assumed to have fractured but could not be directly observed because of their location. The load carried by the specimen was reduced to approximately 90 kN. Cycle 8 was continued to a total elongation of 80 mm, where the test was halted. The outside of the specimen exhibited few signs of damage after testing (figure 4.23). Upon disassembly of the gusset assembly, no significant new galling was observed. Only small steel particles were found at the surface of the link gusset plate. The link gusset was found to be fractured in several locations as shown in

the photograph. It is notable that the fractures occurred in locations at or near the neck of the links as well as along the length of the links, away from both the neck and ends.

The galling and increase of maximum load carried with passage of load cycles was considered undesirable for the purposes of this testing, since it made accurate determination of the ultimate load of the core plate impossible. The use of blast cleaned surfaces was considered to contribute to the galling and interference between the restraining face plates and the gusset. To prevent similar behaviour in the large plate test, the inside surfaces of the face plates, which had been blast cleaned, were ground by hand held disk grinding to smooth the surfaces in contact with the gusset and reduce the propensity for galling during testing.

4.9.3 Large Plate Test

The large plate specimen consisted of five levels of link beams, spanning 203 mm (8") with a thickness of 12.7 mm ($\frac{1}{2}$ "). The predicted ultimate load and deformation of the assembly, based on the empirical relationships derived from finite element analysis and theoretical strength, were 550 kN and 120 mm respectively.

The specimen as loaded cyclically using the same cyclic loading parameters as the small test specimen. The complete load-deformation response of the assembly is shown in figure 4.24 and is presented in three cycle segments in figures 4.25 through 4.28. In cycles 1 through 3 and after some seating at loads below 100 kN, the specimen exhibited a linear load deformation relationship up to a proportional limit of approximately 450 kN. After the proportional limit was passed, in both tension and compression, the stiffness of the assembly gradually reduced with continued deformation. Maximum load carried by the specimen increased with each completed cycle and, within a given cycle, the specimen carried more load at the maximum compression than at maximum tension deformation. During load cycles 4 through 8, hysteresis became open with near horizontal yield plateaus, at a load of approximately 800 kN. The unloading curve after

peak deformation in each cycle was typically near vertical to zero load with a stiffness similar to that observed in the first cycles upon reloading in the direction of the applied deformation (in quadrants two and four). The first link fracture was observed during the tension excursion of cycle 9, at a load of 590 kN and a displacement of +8 mm. Load carried by the specimen increased after first fracture to a maximum of 760 kN at 90 mm deformation, the maximum tension deformation of cycle 9. A second link fracture occurred during the compression excursion of cycle 9 at load of -700 kN and a displacement of +50 mm with an accompanying reduction in load to -525 kN. Several link element fractures occurred throughout the remainder of cycles 9 and 10. During part of cycle 9 and all of cycles 10 and 11, all links were believed to have fractured and transferred no load by bearing. The assembly continued to carry forces ranging from approximately 400 kN at zero displacement increasing to approximately 600 kN at the maximum deformation in cycles 10 and 11. The load transfer mechanism was friction and interference between the fractured link gusset plate and the outer face plates. The test was halted after the completion of cycle 11, which covered a deformation range from -100 mm to +120 mm, and was halted because of the stroke limitations of the test machine. After disassembly, the core plate was found to have fractured through each link and through one leg, as shown in figure 4.29. Based on the observed behaviour of the test specimen, for additional deformation outside the -100 mm to +120 mm range, load in the 400 to 600 kN range could be anticipated. After fracture of the links, the system was observed to behave as a “friction damper” device. If deformation could have continued to the limit of the slot in the face plates, load transfer would be by direct bearing of the bolts and spacer plate on the slot ends – allowing much larger forces to be transferred.

4.9.4 Face Plate Restraint

During both the large and small plate testing, the link gusset components were restrained from local and overall instability by the face plates. Figure 4.30 is a close-up photograph a portion of the large plate gusset plate in figure 4.29 which, during testing, developed a local buckle. Significant yielding occurred in that location with the final thickness of the

specimen increasing 24% over the measured pre-test thickness. A fold, visible on both sides of the plate in the blown up portion of the photo in figure 4.30, was restrained by the face plates and remained confined in the plane of the gusset – thereby permitting significant inelastic compression deformation without out-of-plane instability.

4.9.5 Energy Absorption

Energy absorbed during testing is shown in figure 4.31 for both the small and large plate specimens. The small plate specimen exhibits a decrease in the energy absorption rate after the disassembly of the face plates, which occurred during the compression excursion of cycle 6 to allow modification of the brace members and inspection. This is consistent with the observation during the test of galled steel interference between the face and core plates providing an alternative load path and increasing maximum load and energy absorption rate.

4.10 Discussion

The hysteresis observed during the two tests reported have many characteristics desirable for inelastic elements in seismically loaded structures. The link gusset assembly is stiff at loads below the proportional limit, which is desirable for control of deflections arising from wind loads on CBF structures. When yielding, the link gusset assembly provides long flat yield plateaus and does not exhibit stiffness degradation with cycling. As deformation capacity is expended, the load carried by the gusset assembly reduces gradually with cycling and remains, through friction transfer, significant after complete loss of cross section of the gusset plate link elements. Upon contact of the brace connection with the end of the face plate slot, face plates provide an alternative load path - enabling the gusset to carry significant loading after having expended its deformable core.

The additional loading carried by friction was not considered in the design of the brace element and resulted in a bracing failure during the first test. Unexpected additional load arising from friction is undesirable in capacity design since it can, as observed in testing, give rise to unexpected failures in elements with undesirable load-deformation characteristics.

The inclusion of deformable gusset assemblies in structures has potential to simplify post disaster rehabilitation by localizing damage to connection elements and limiting member repair or replacement. If bolted in place, the expanded gussets could be removed and replaced with relative ease when compared to the effort required to replace damaged bracing or frame members. Retrofit, using bolted gusset assemblies would also be easily accomplished. The cost of supply each of the tested plate assemblies was found to be 120% of the cost of typical continuous gusset plates used in similar testing, conducted at the same time as this research.

4.11 Conclusions

Anticipated deformation demand on gussets employed as inelastic elements in seismically loaded structures exceeds the known fracture deformation of conventionally configured gusset plates.

A specific link shape, which can be employed in gusset plates, has been identified which, when loaded by equal and opposite end moments and uniform shear, develops an elongated hinge region while remaining elastic at the inflection point. This configuration, referred to as the EHL (Extended Hinge Link), has exhibited excellent deformability, stable post yield hardening behaviour and symmetric hysteresis when subjected to load reversal in experiments and in finite element analyses.

Based on the finite element analysis results, a predictive model for EHL deformability and ultimate load was developed. The model indicated that link ultimate load is related

to neck section area. Deformability, for a given neck depth, may be increased by increasing link length. As indicated by the empirical model, deformability and ultimate load may be independently controlled in design of EHL gusset plates.

Two proof tests were conducted to demonstrate the effectiveness of EHL equipped gussets. The tests utilized external face plates to act as guides for the brace member end connection and to suppress local and overall buckling of the EHL components.

During testing, face plates contributed to load carrying capacity of the system through friction and galling at the interface between the EHL core and the face plates. The two tests employed cyclic deformation, increasing in 10 mm increments, to loss of capacity or the limits of the apparatus. Both tests demonstrated significant improvement in deformability when compared to continuous gusset plates, with tests being halted at 80 mm and 120 mm for the small and large specimens, respectively. This compares to anticipated fracture deformations of 10 mm to 20 mm for traditionally configured continuous gusset plates. EHL gussets were found to exhibit similar stiffness, during elastic response, as observed in similar tests of continuous gussets.

Table 4.1- Distributed Plasticity Gusset Analysis Results

Gusset	h_o (mm)	l (mm)	Finite Element Analysis		Empirical Relationships		$\frac{FEA, V_{ULT}}{Emp., V_{ULT}}$	$\frac{FEA, \delta_{ULT}}{Emp., \delta_{ULT}}$
			FEA V_{ULT} (kN)	FEA δ_{ULT} (mm)	[7] V_{ULT} (kN)	[8] δ_{ULT} (mm)		
opt1	25.4	305	144	201	146	185	0.979	1.08
opt2	38.1	305	223	149	219	141	1.01	1.05
opt3	51	305	297	130	293	117	1.01	1.11
opt4	76	305	441	86.2	436	89	1.00	0.964
opt5	25.4	508	157	399	146	398	0.963	1.02
opt6	38.1	508	246	330	219	304	0.980	1.09
opt7	51	508	317	247	293	250	0.977	1.02
opt8	76	508	419	164	436	192	0.961	0.854
opt9	25.4	711	166	717	146	660	0.949	0.899
opt13	12.7	152	71.2	103	72.8	103	0.971	0.999
opt14	12.7	203	70.8	156	72.8	160	0.965	0.979
opt15	12.7	254	70.9	228	72.8	223	0.967	1.02
opt16	12.7	305	70.8	311	72.8	294	0.965	1.06
Mean							0.977	1.01

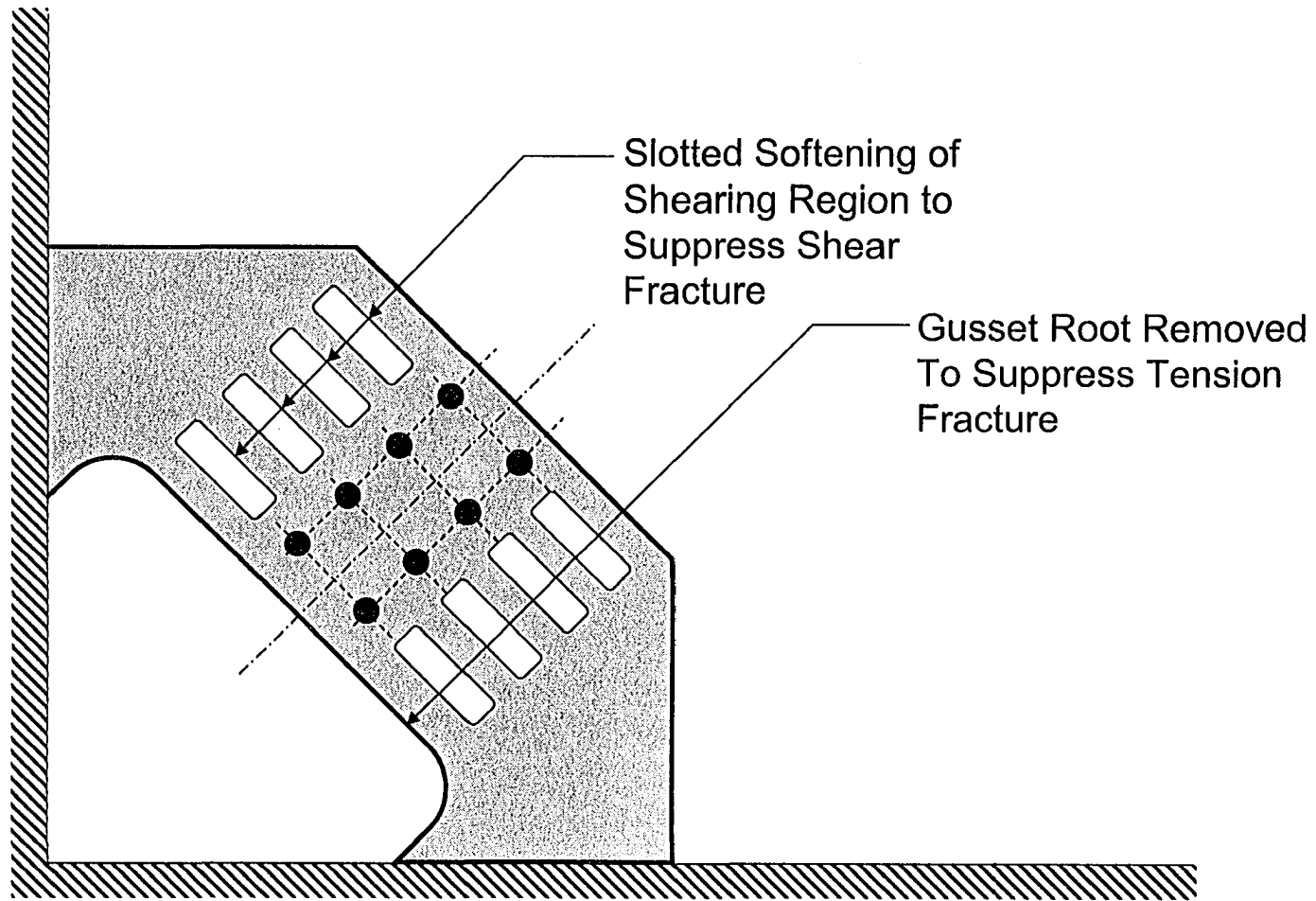


Figure 4.1 – Gusset Modification to Increase Deformability

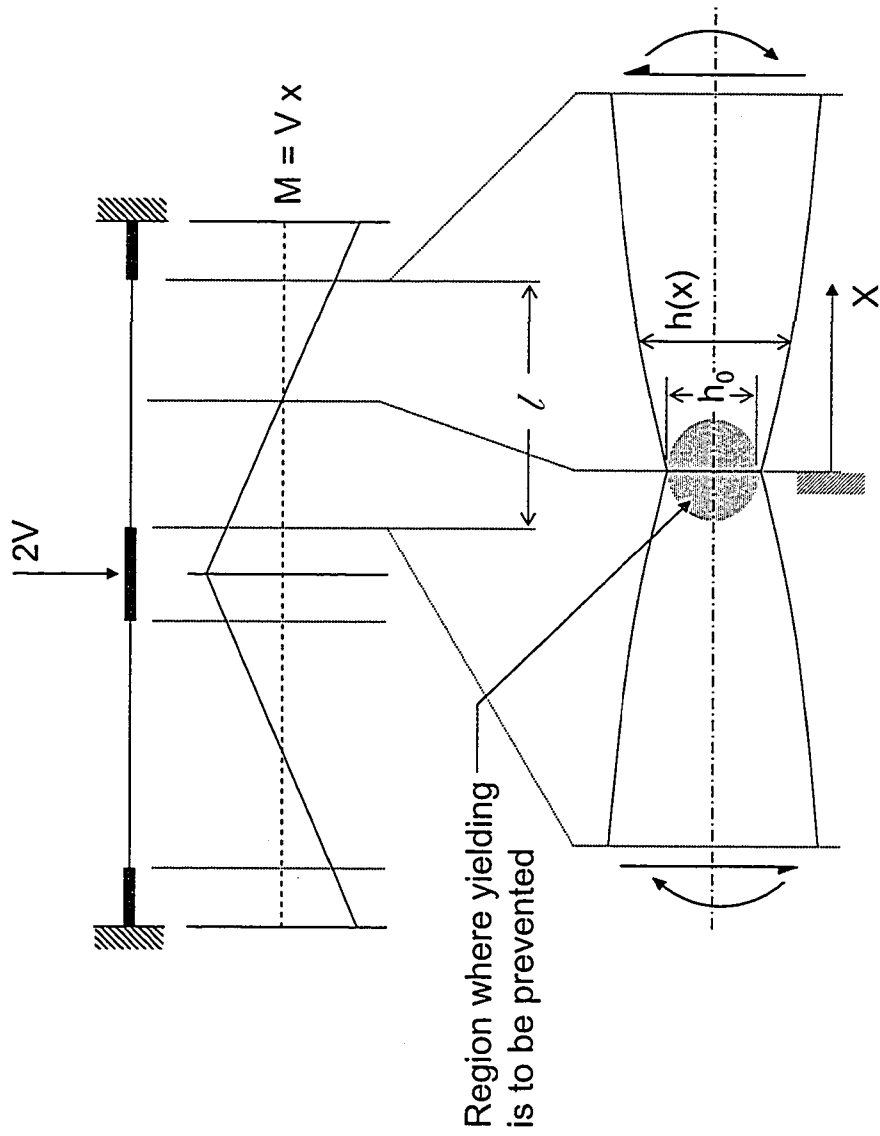


Figure 4.2 – Extended Hinge Link (EHL) Schematic

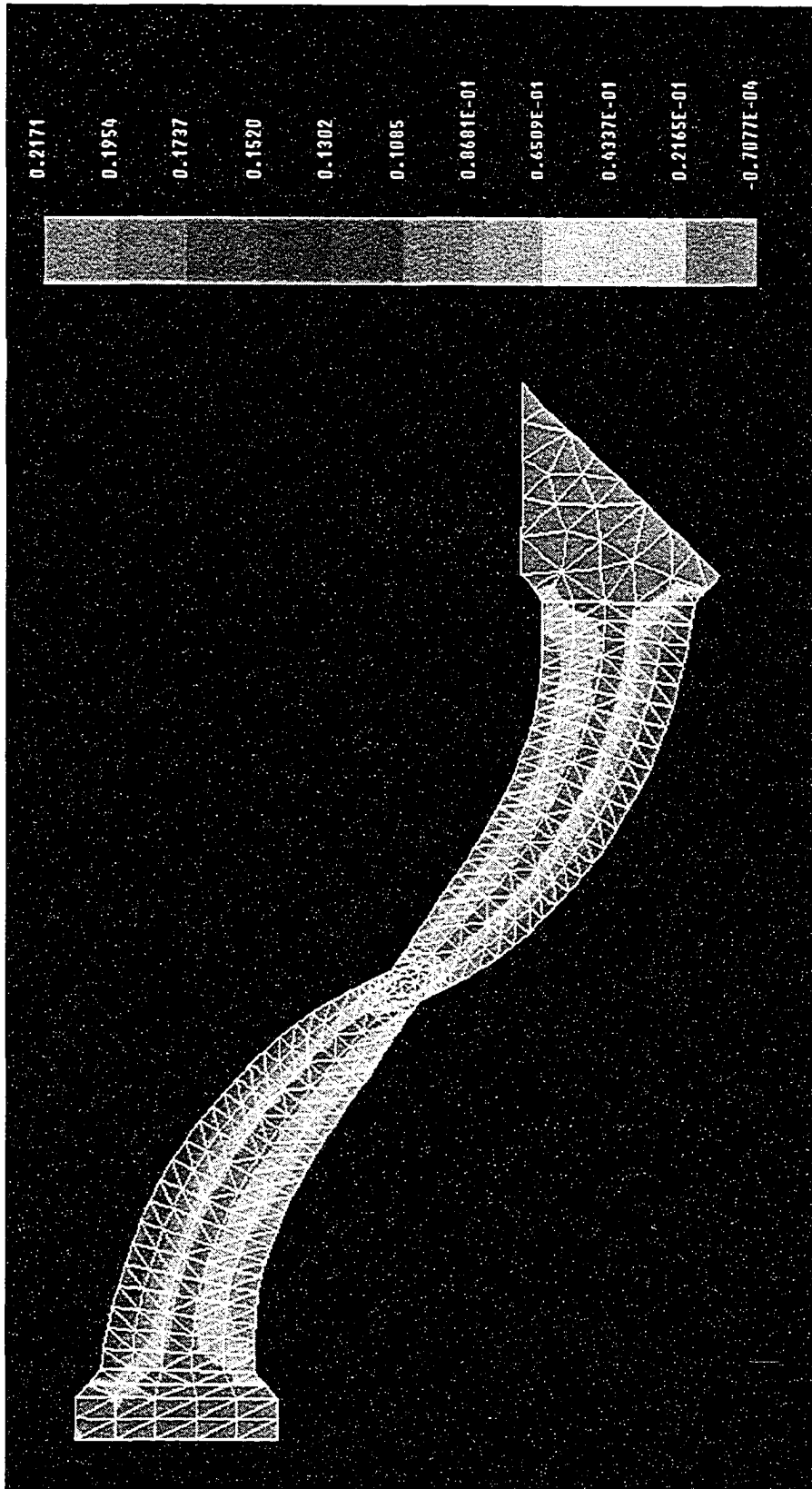


Figure 4.3 - Opt9 Gusset Segment – Principal Strain at 394 mm Deformation

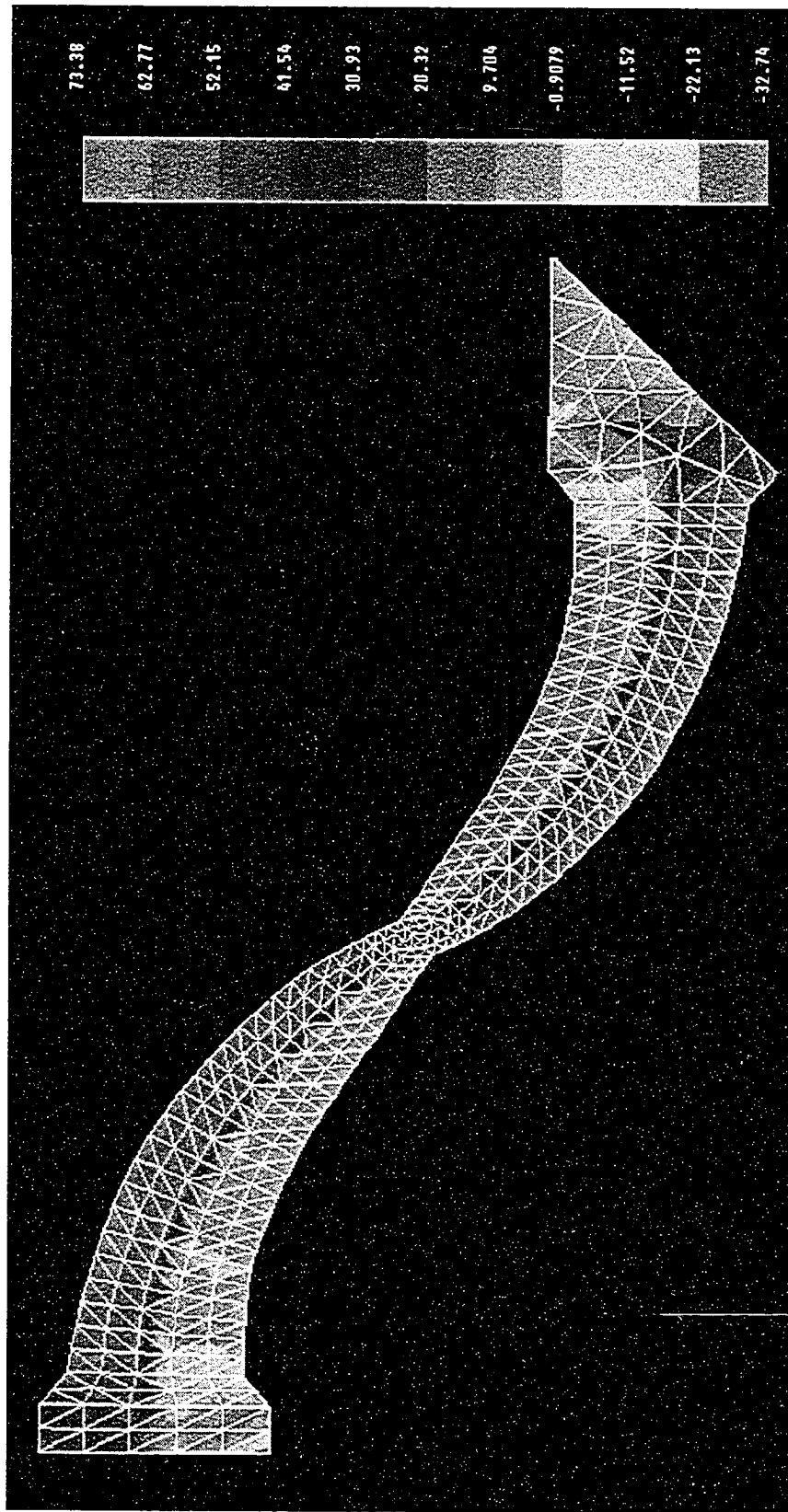


Figure 4.4 - Opt9 Gusset Segment – Principal Stress (ksi) at 394 mm Deformation

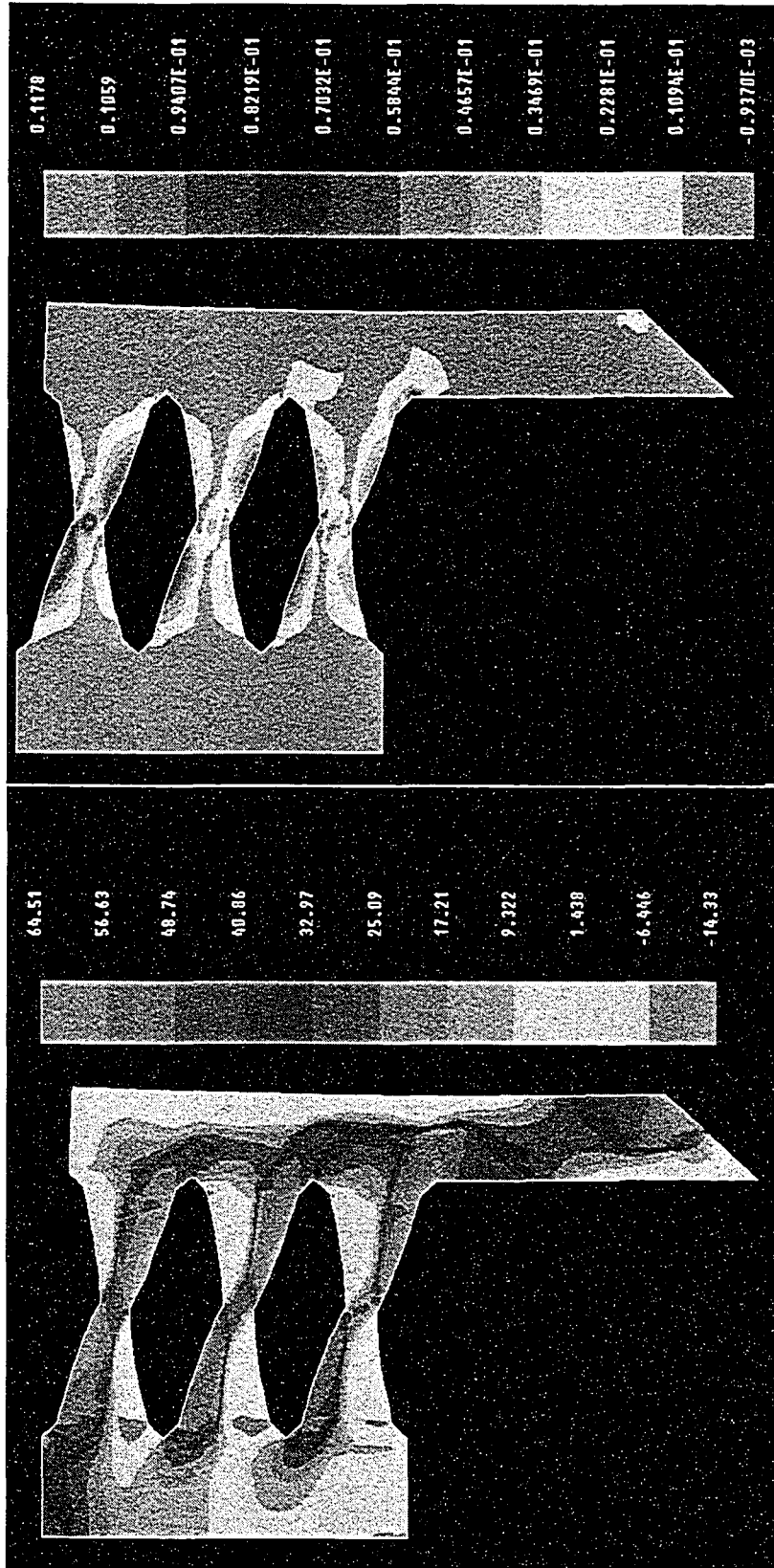


Figure 4.5 - Opt21 Gusset – Principal Stress (ksi) –
Deformation 25.4 mm, Cycle 1

Figure 4.6 - Opt21 Gusset – Principal Strain
Deformation 25.4 mm, Cycle 1

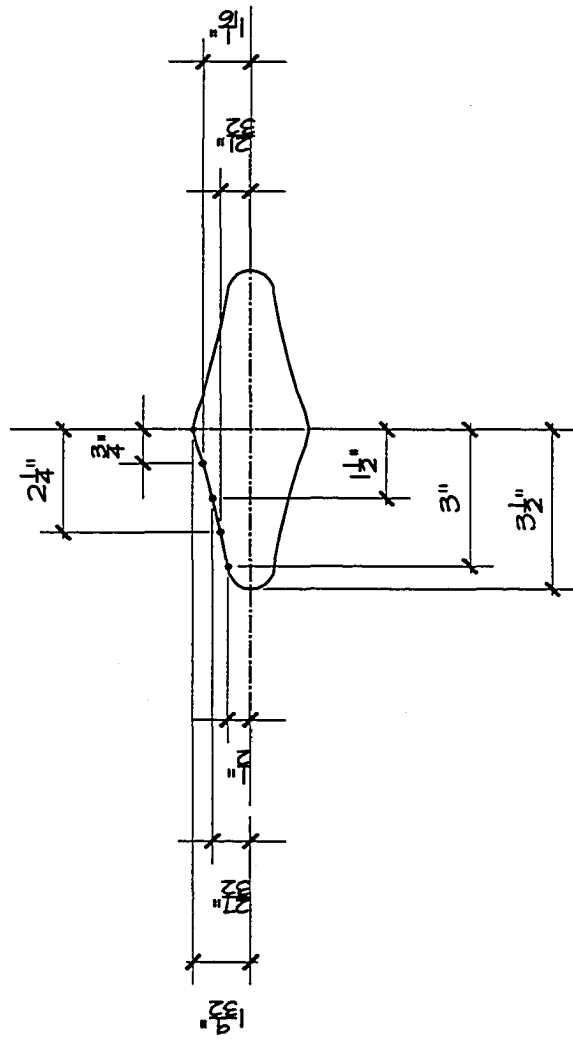


Figure 4.10 - Small Plate Hole Dimensions

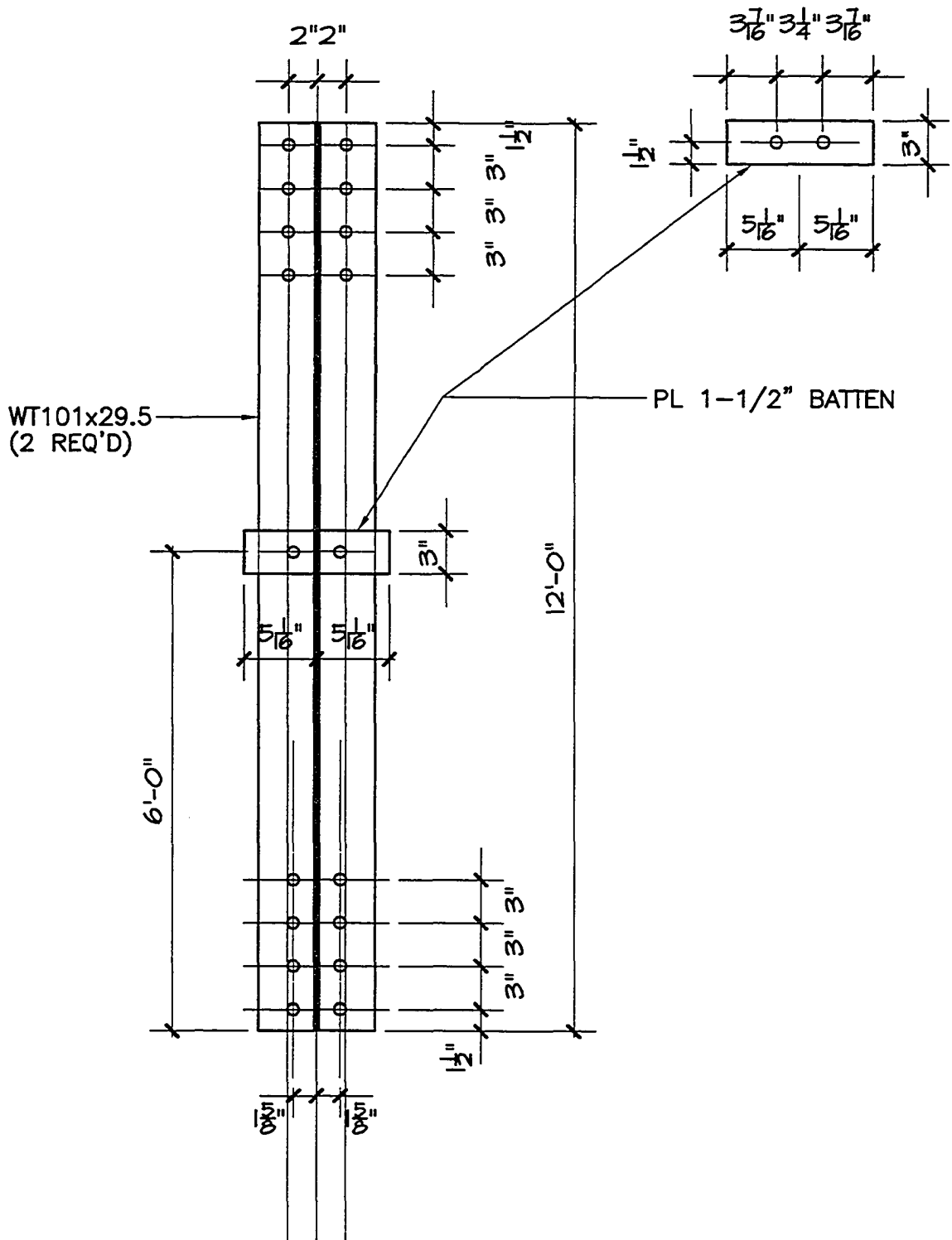


Figure 4.11 – Brace Dimensions (As Originally Fabricated)

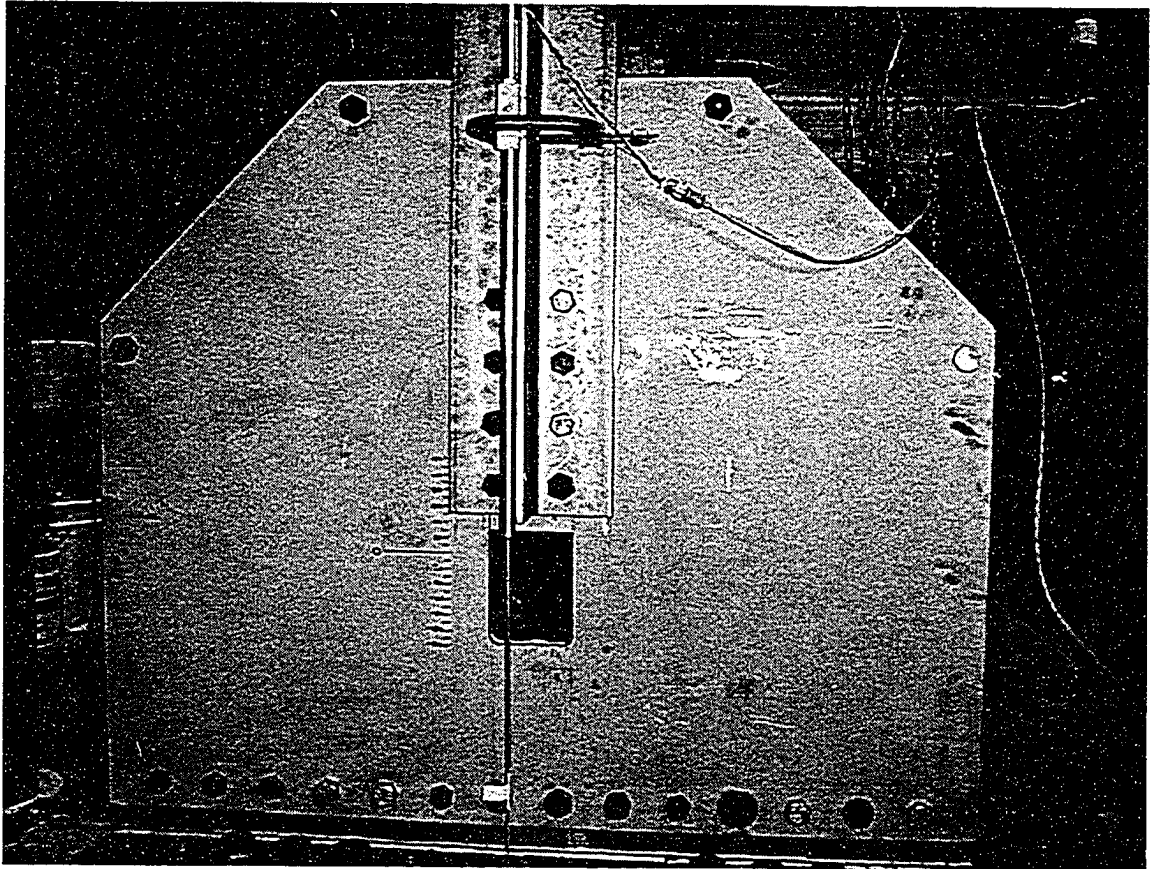


Figure 4.12 - Large Plate – Deformation +52 mm

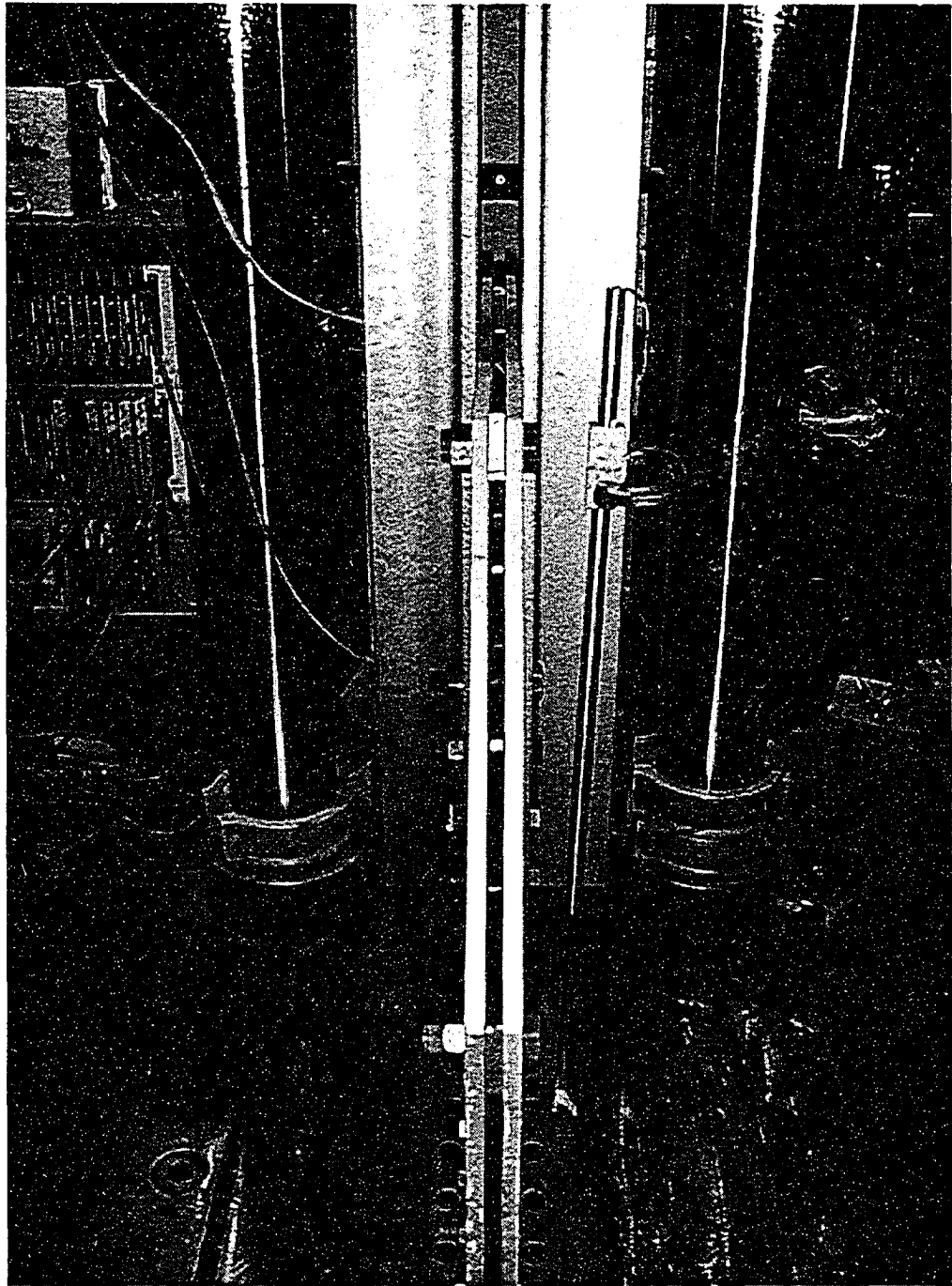


Figure 4.13 – Edge View of Assembled Specimen

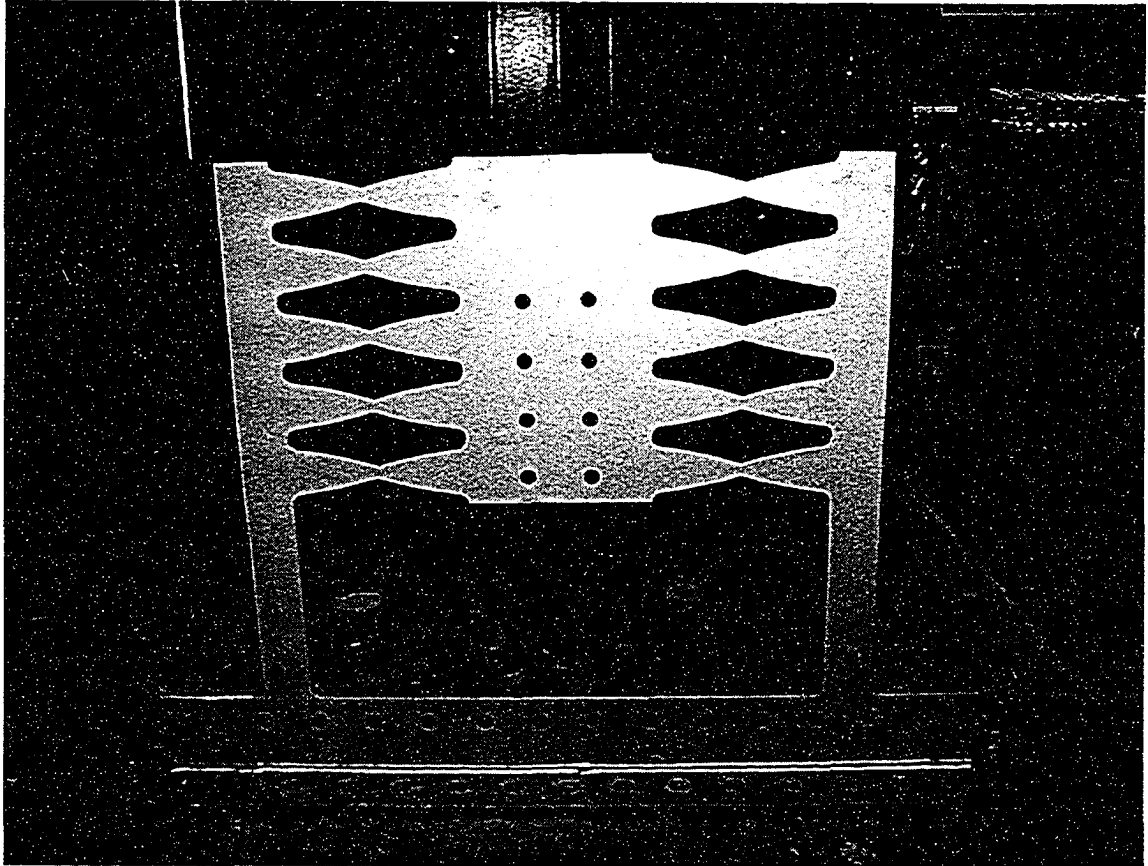


Figure 4.14 - Large Plate – Pretest

Load Deformation Response Small Plate - Full Response

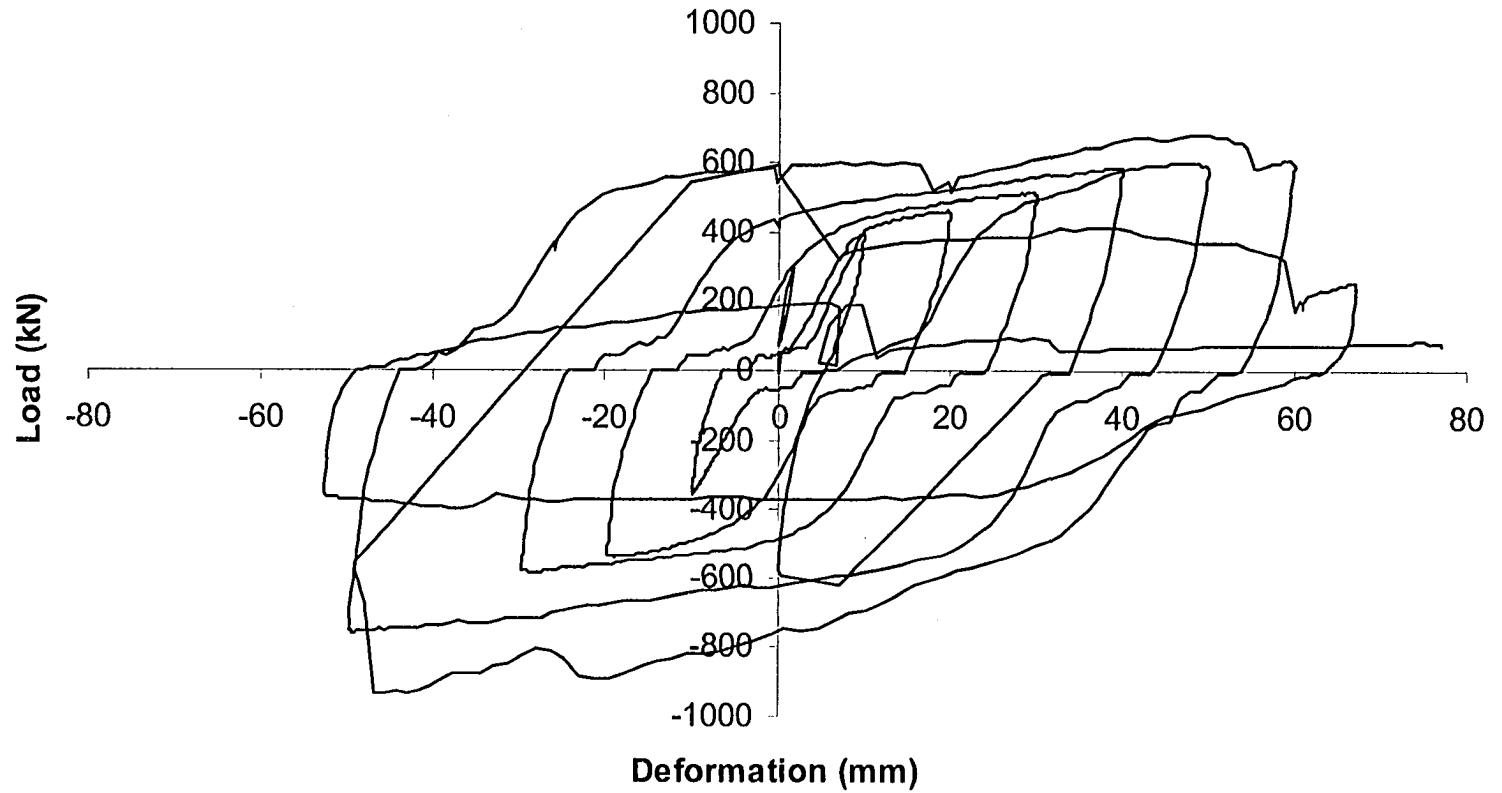


Figure 4.15 - Small Plate Load – Deformation Hysteresis

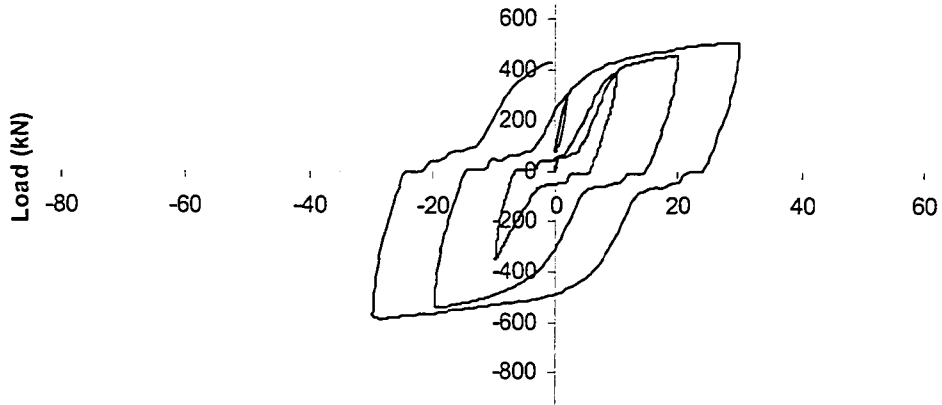


Figure 4.16 – Small Plate Load Deformation Cycles 1 through 3

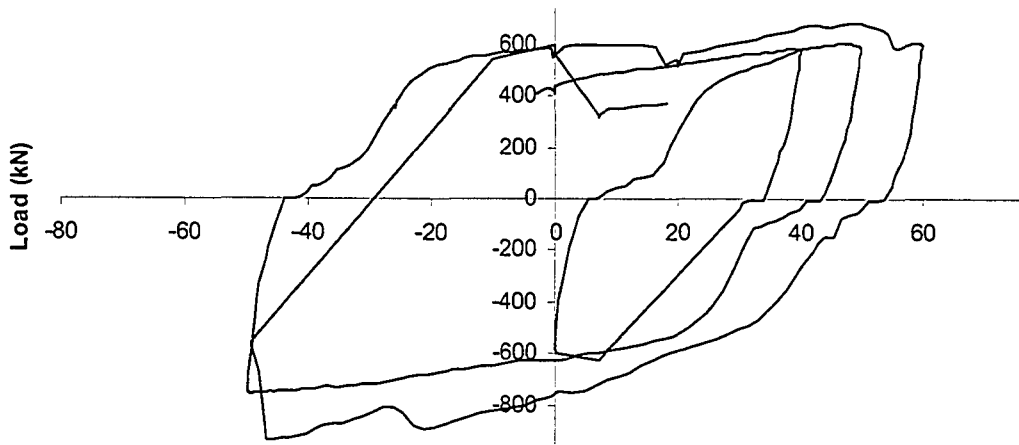


Figure 4.17 – Small Plate Load Deformation Cycles 4 through 6

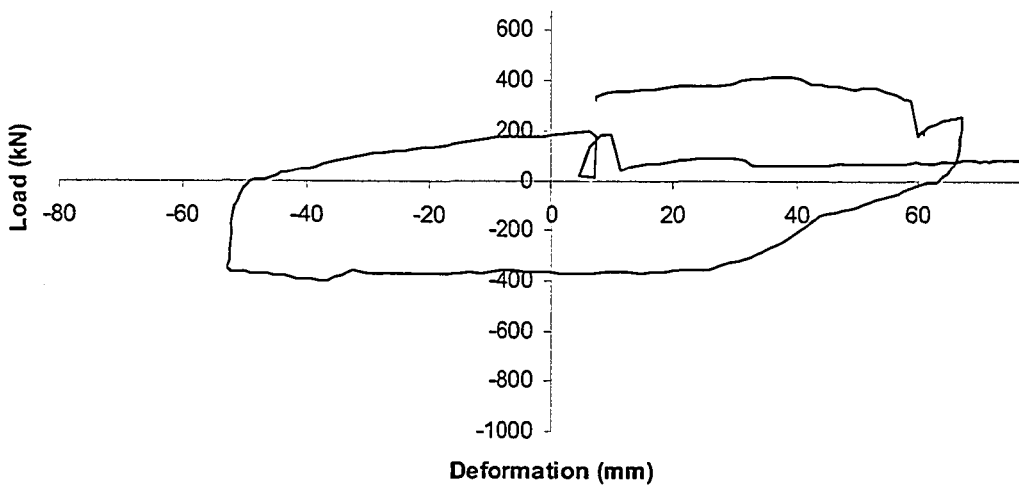


Figure 4.18 – Small Plate Load Deformation Cycle 7

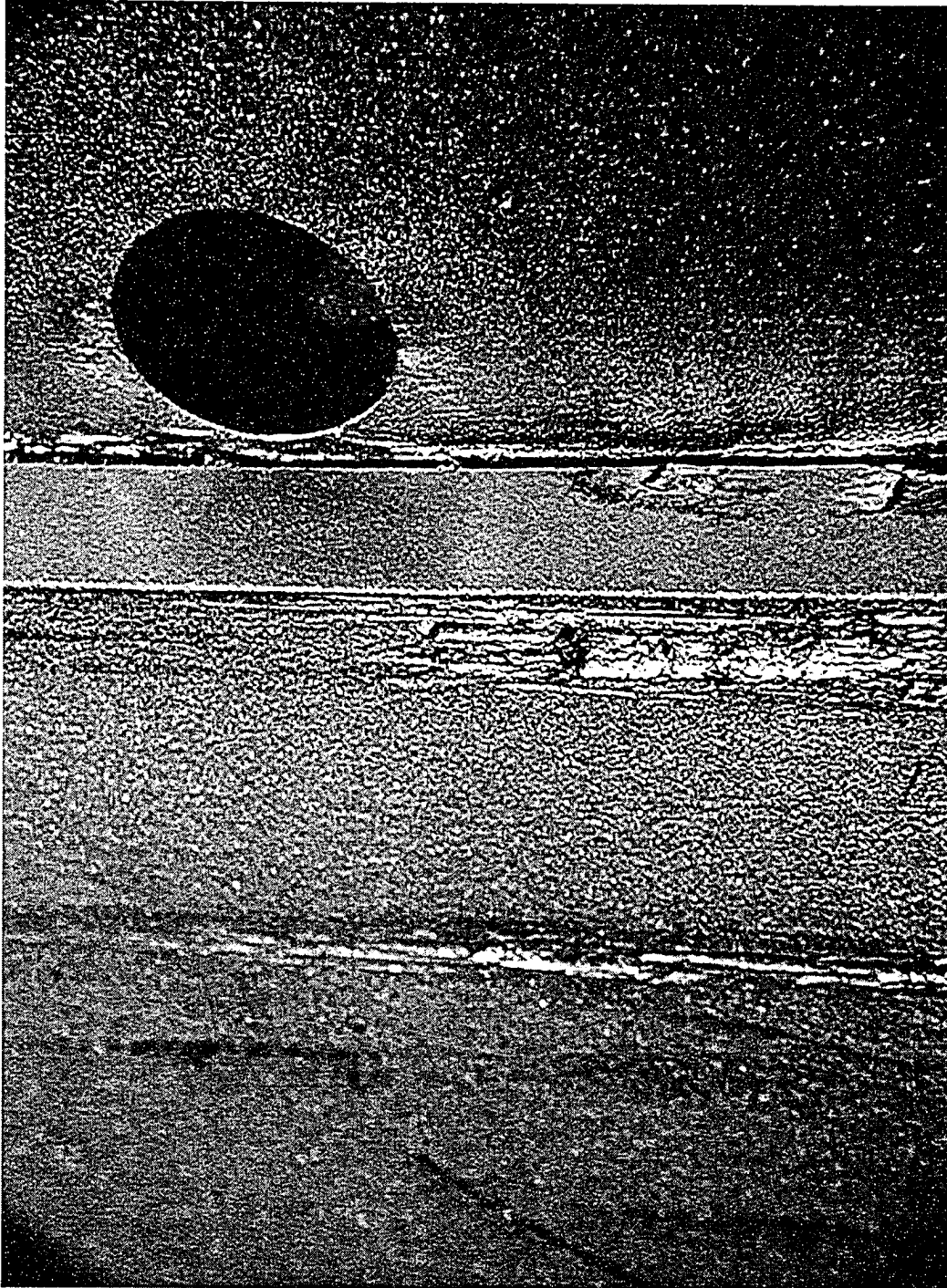
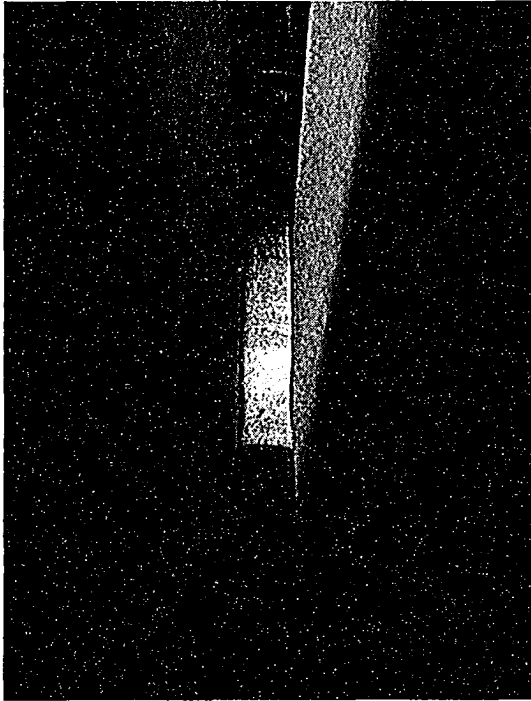
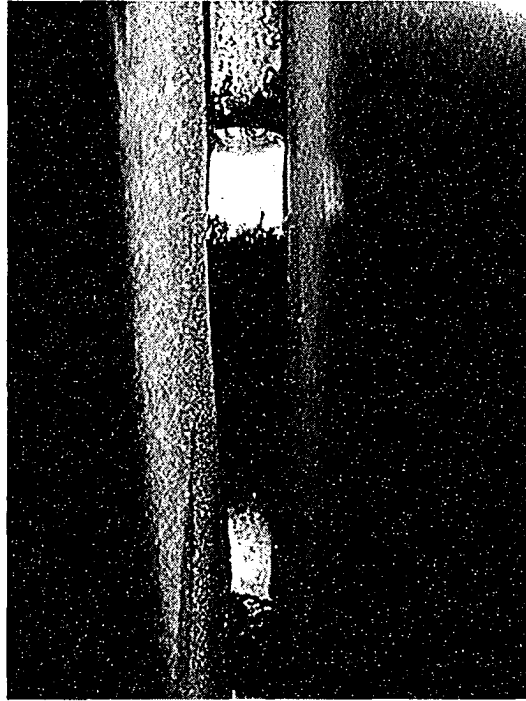


Figure 4.19 – Small Plate Galling of Outside Surface of Face Plate



**Figure 4.20 - Small Gusset
Necking of Upper Link
Cycle 7, Def. +60 mm, Load 350 kN**



**Figure 4.21 - Small Plate – End of
Test – Fractured Links Visible
Between Face Plates**

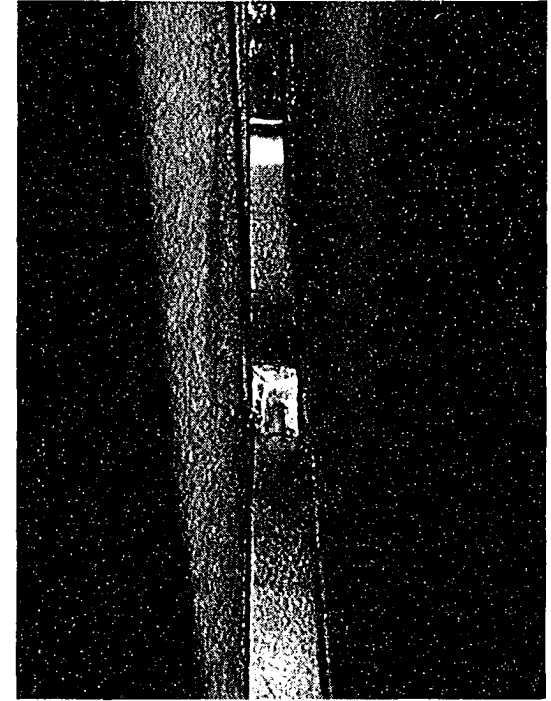


**Figure 4.22 - Small Plate with Fractured
Link Parts in Contact,
Compression Cycle 7**

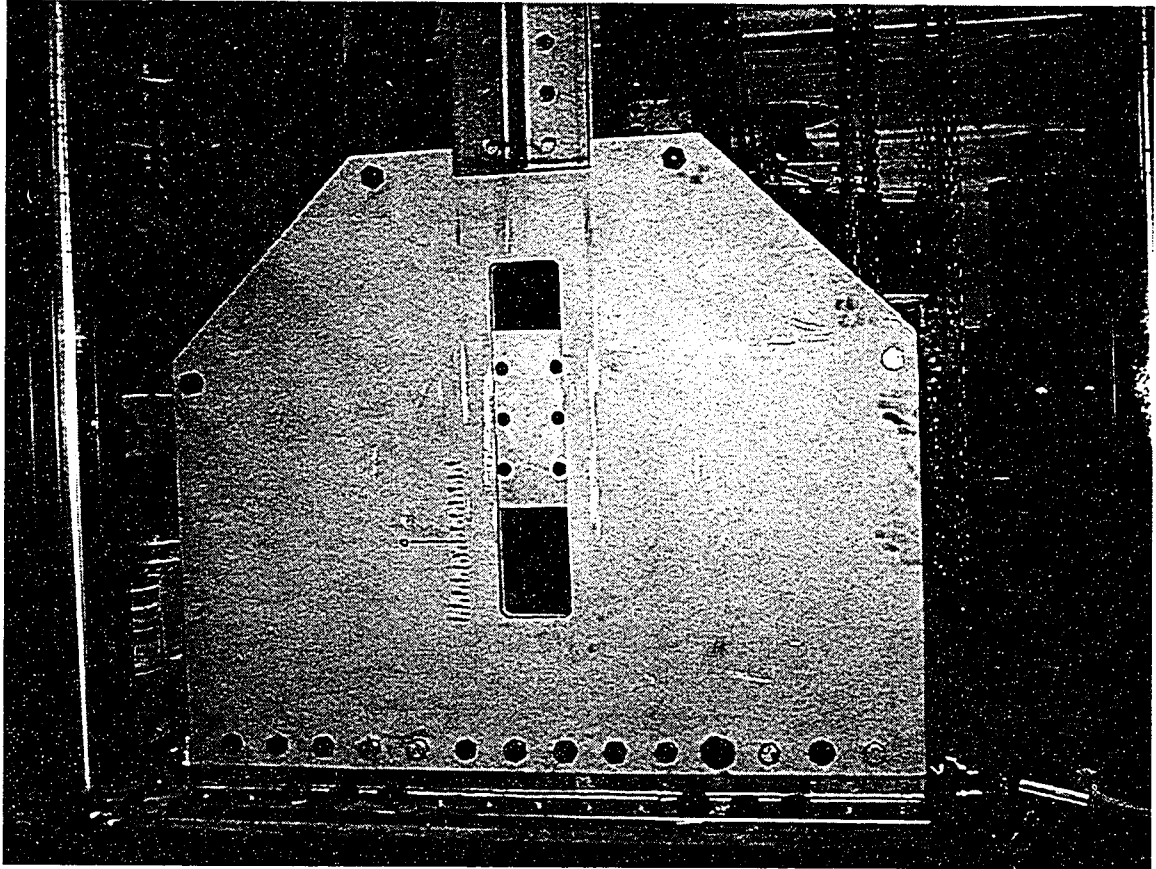


Figure 4.23 - Small Plate – Post Test Before Disassembly

Load Deformation Response Large Plate - Full Response

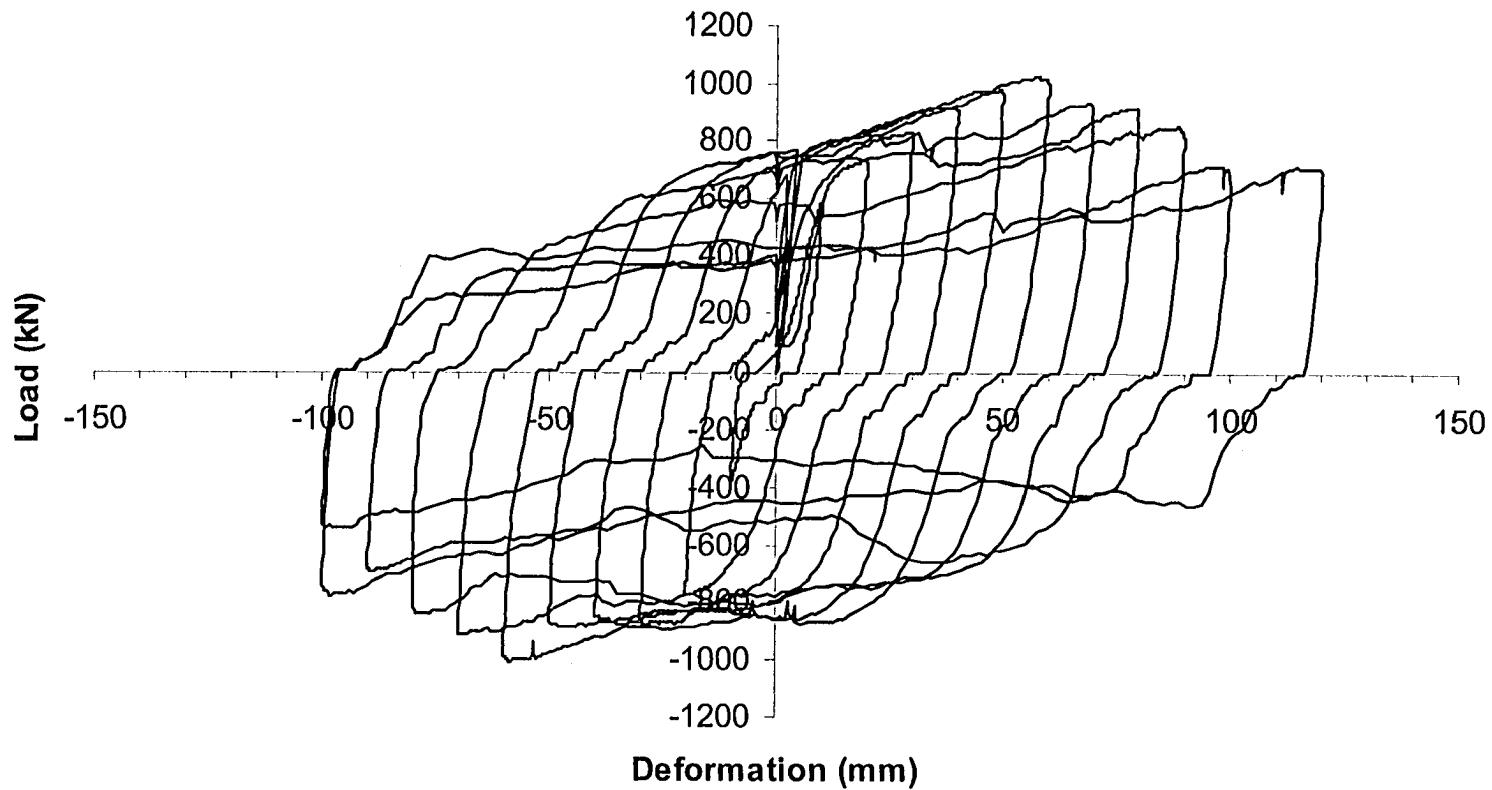


Figure 4.24 – Large Plate – Load Deformation Hysteresis

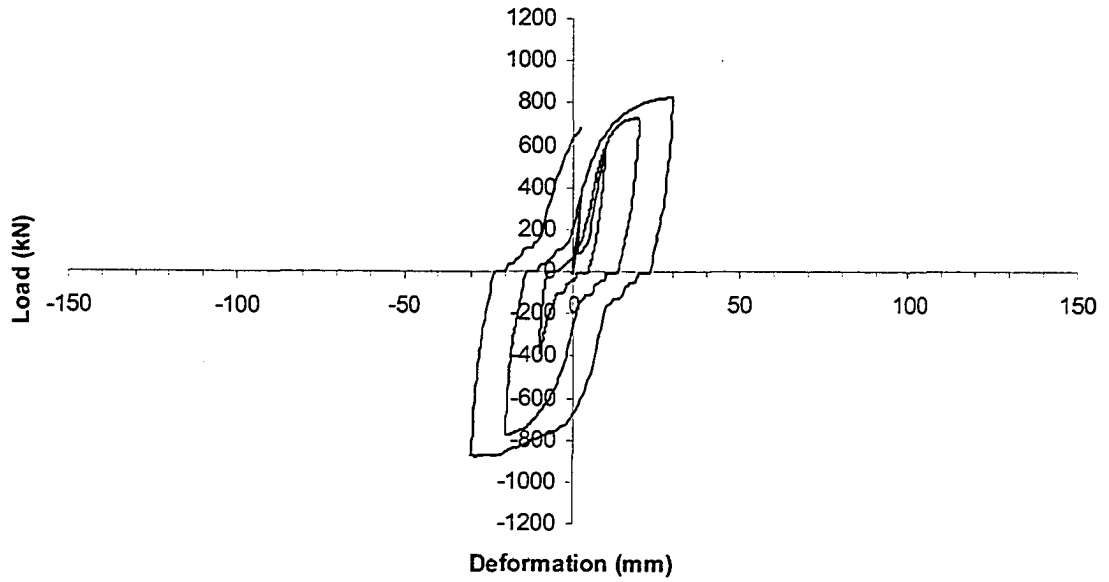


Figure 4.25 – Large Plate – Load Deformation – Cycles 1 through 3

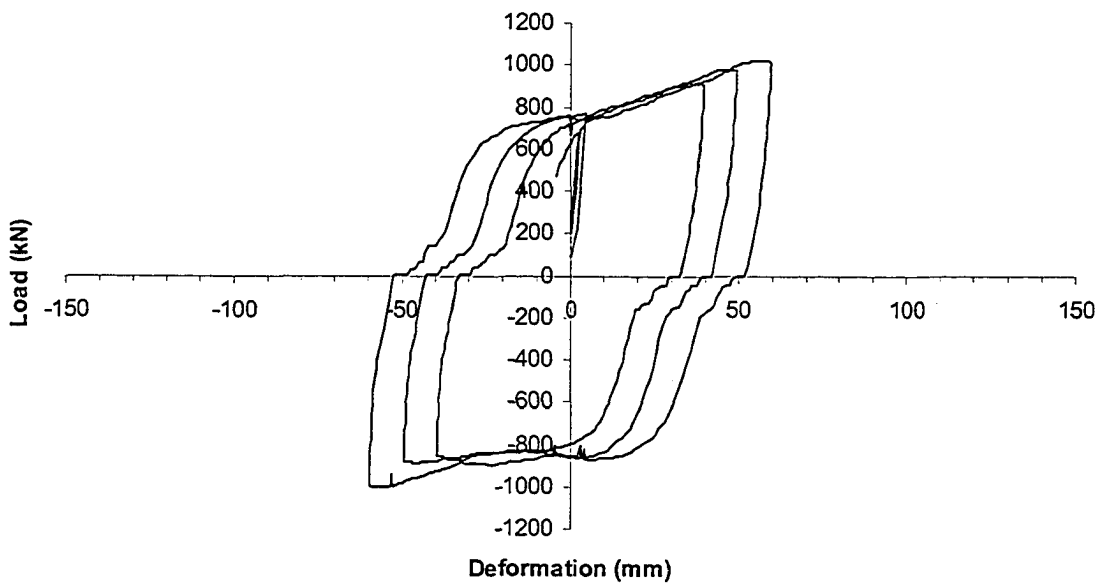


Figure 4.26 - Large Plate – Load Deformation – Cycles 4 through 6

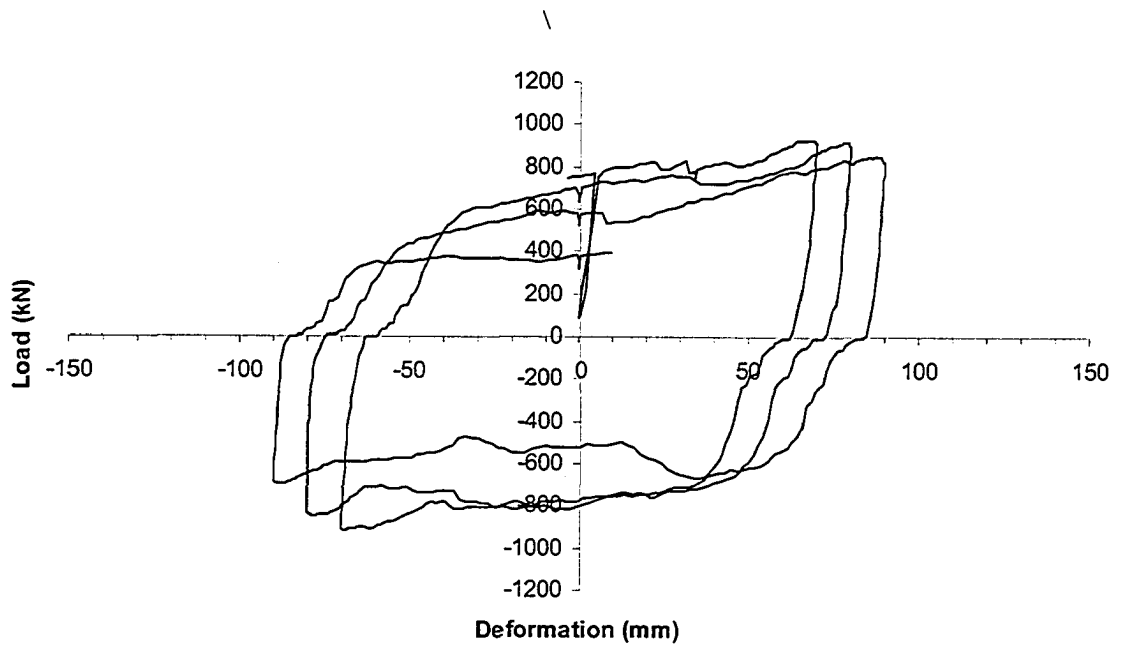


Figure 4.27 - Large Plate – Load Deformation – Cycles 7 through 9

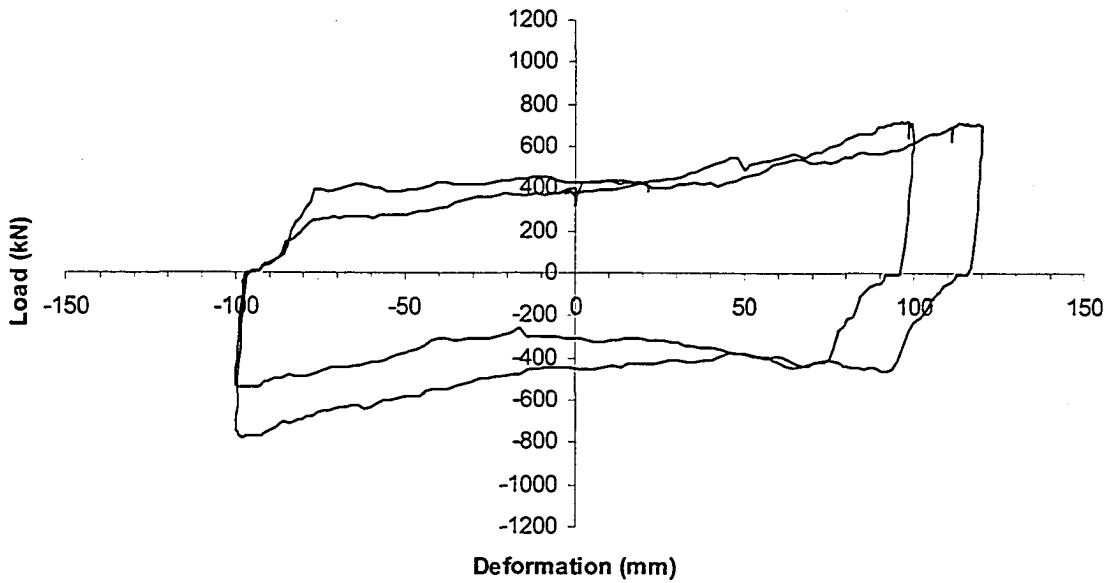


Figure 4.28 - Large Plate – Load Deformation – Cycles 10 and 11

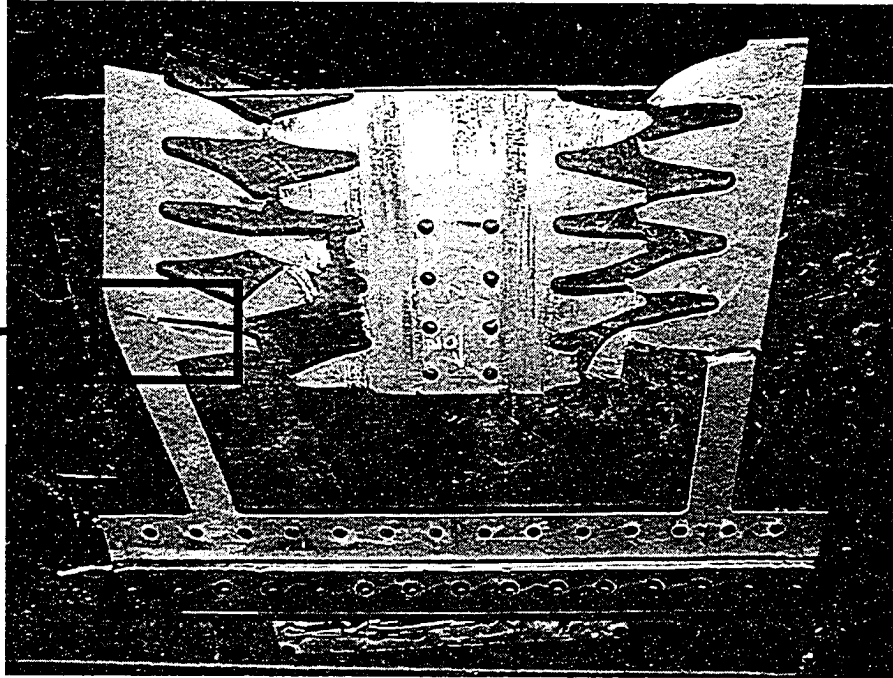


Figure 4.29 – Large Plate Core – Post Test

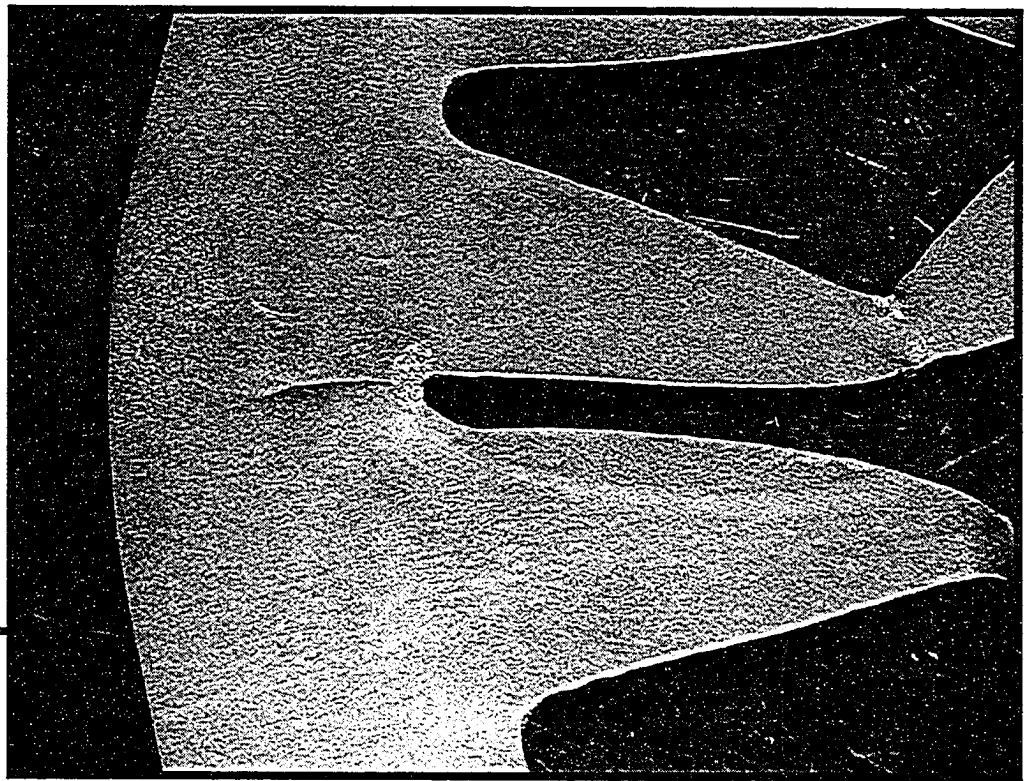


Figure 4.30 – Large Plate Local Buckle Restrained by Face Plates

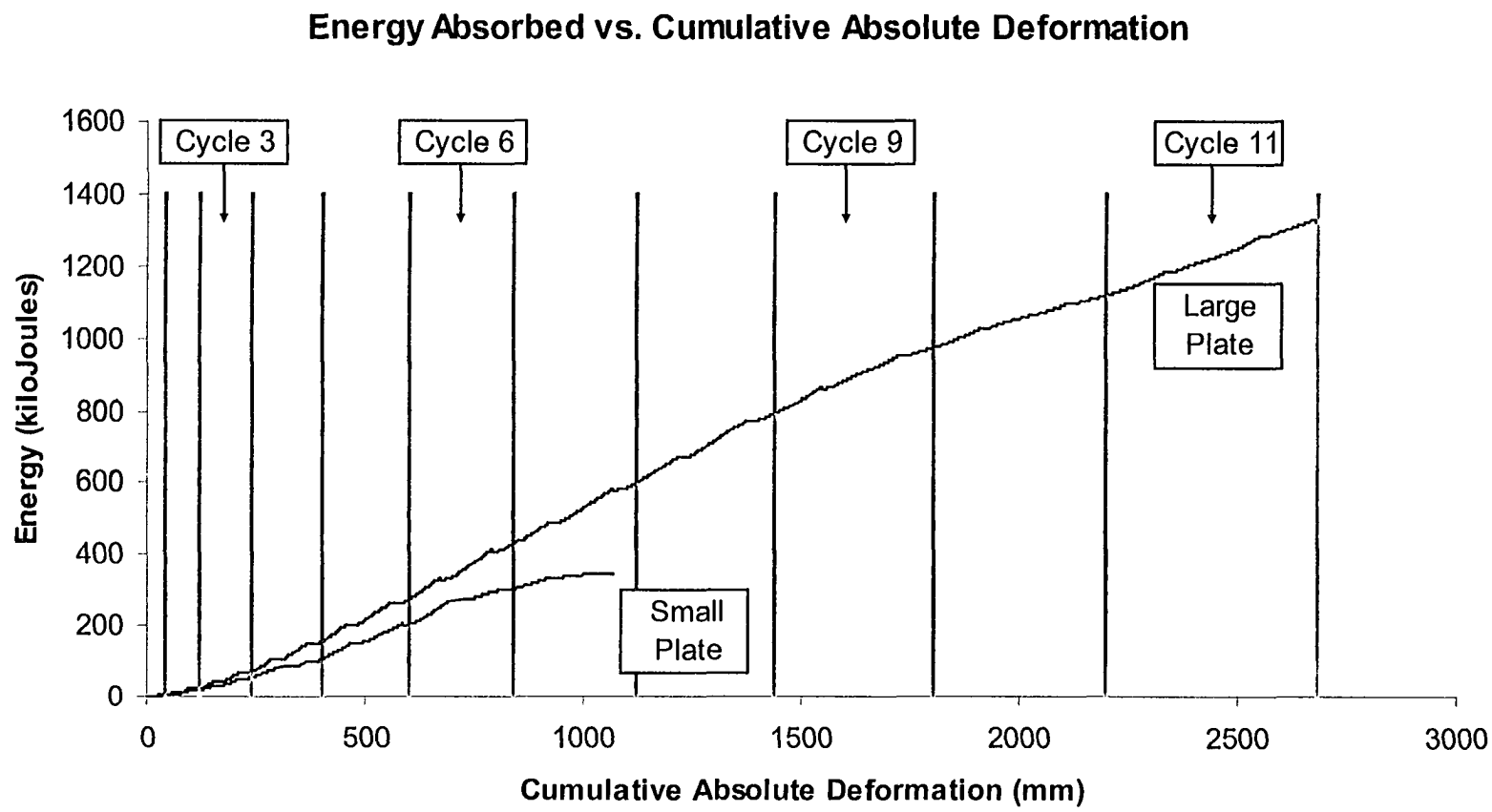


Figure 4.31 - Ductile Gusset Energy Absorption

4.12 References

ASTM A370-96, 1996. Standard Test Methods and Definitions for Mechanical Testing of Steel Products. American Society for Testing and Materials, Philadelphia, PA.

Hardash, S.G., and Bjorhovde, R., 1985. "New Design Criteria for Gusset Plates in Tension." *Engineering Journal*, AISC, Vol. 22, No. 2, pp. 77-94.

Hu, S.Z., and Cheng, J.J.R., 1987. "Compressive Behaviour of Gusset Plate Connections." Structural Engineering Report No. 153, Department of Civil Engineering, University of Alberta, Edmonton, Alberta.

Nast, T.E., Grondin, G.Y., and Cheng, J.J.R., 1999. "Cyclic Behaviour of Stiffened Gusset Plate-Brace Member Assemblies." Structural Engineering Report No. 229, Department of Civil Engineering, University of Alberta, Edmonton, Alberta.

Rabinovitch, J.S., and Cheng, J.J.R., 1993. "Cyclic Behaviour of Steel Gusset Plate Connections." Structural Engineering Report No. 191, Department of Civil Engineering, University of Alberta, Edmonton, Alberta.

SAC Background Document 97/02, Appendix E "Loading Protocol for Stepwise Increasing Cyclic Tests".

Swenson, D., and James, M.A., 1997. "FRANC2D/L: A Crack Propagation Simulator for Plane Layered Structures. Version 1.4 Users Guide." Kansas State University, Manhattan, Kansas.

Swenson, D., James, M.A., and Hardeman, B., 1997. "CASCA: A Simple 2-D Mesh Generator. Version 1.4 Users Guide." Kansas State University, Manhattan, Kansas.

Struik, J.H.A., 1972. "Applications of Finite Element Analysis to Non-Linear Plane Stress Problem." Ph.D. Dissertation, Department of Civil Engineering, Lehigh University, Bethlehem, Pa.

Thomason, P.F., 1990. "Ductile Fracture of Metals." Pergamon Press, Oxford, UK.

Walbridge, S.S., Grondin, G.Y., and Cheng, J.J.R., 1998. "An Analysis of the Cyclic Behaviour of Steel Gusset Plate Connections." Structural Engineering Report No. 225, Department of Civil Engineering, University of Alberta, Edmonton, Alberta.

Walbridge, S.S., Grondin, G.Y., and Cheng, J.J.R., 1998. "An Analytical Study of the Cyclic Behaviour of Steel Gusset Plate Connections." Proceedings of the Annual Conference of the Canadian Society for Civil Engineering, Vol IIIa, pp. 107 to 116.

Whitmore, R.E., 1952. "Experimental Investigation of Stresses in Gusset Plates." Bulletin No. 16, Engineering Experiment Station, University of Tennessee.

Yam, C.H.M., and Cheng, J.J.R., 1993. "Experimental Investigation of the Compressive Behaviour of Gusset Plate Connections." Structural Engineering Report No. 194, Department of Civil Engineering, University of Alberta, Edmonton, Alberta.

Yam, C.H.M., and Cheng, J.J.R., 1994. "Analytical Investigation of the Compressive Behaviour and Strength of Steel Gusset Plate Connections." Structural Engineering Report No. 207, Department of Civil Engineering, University of Alberta, Edmonton, Alberta.

5. RESPONSE OF SEISMICALLY LOADED LOW RISE STEEL CBF STRUCTURES WITH INELASTIC GUSSET PLATE CONNECTIONS^{5,6}

5.1 Introduction

A common design philosophy for earthquake resistant is to absorb earthquake energy through inelasticity of selected structural elements. Inelasticity is best confined to those elements which absorb large amounts of energy and can sustain multiple cycles of inelastic loading without reductions in capacity or fracture. While gusset plates are currently not generally considered as good candidates to act inelastically in seismically loaded structures, they have exhibited characteristics indicating their potential to do so. When tested cyclically by Rabinovitch and Cheng (1993) and Nast, Grondin and Cheng (1999), gusset plates exhibited open load deformation hysteresis and maintained capacity in both tension and compression during cyclic loading.

While gusset plates have demonstrated potential to act inelastically, based on their observed load deformation hysteresis, in seismically loaded structures, there is no research to-date to quantify the deformation demand anticipated within such structures.

The purpose of this research is to evaluate the deformation demands on gusset plates, designed to act inelastically in steel structures of one, two and four storey heights, and proportioned using the NBCC equivalent static lateral load approach and CAN/CSA-S16.1-94. Non-linear time history analysis was employed to calculate the responses of structures, designed for Zone 3 and Zone 5 events and using a variety of force modification (R) factors and structure configurations. Non-linear time history analyses were conducted using DRAIN-2DX and scaled earthquake records covering a range of a/v ratios. Envelopes of gusset deformations, storey drifts and overall structure drifts

⁵ A version of this chapter is under revision for publication in the Canadian Journal of Civil Engineering.

⁶ Portions of this chapter were presented at the NASCC /PSSC Conference, March 2004. Long Beach, California.

were used to evaluate the anticipated deformation demand on gusset for the combinations of design parameters R , v and structure configurations.

5.2 Gusset Plate Behaviour

Gusset plates are those elements which, in concentrically braced frames, connect bracing elements to gravity load resisting frames. They are typically located at beam - column intersections but may be located at other locations along beams and columns, depending on the bracing configuration, as outlined in figure 5.1.

The behaviour of gusset plates has been researched extensively and may be discussed in terms of tension and compression behaviour.

5.2.1 Gusset Plate Behaviour in Tension

When loaded in tension, failures within gusset plates have exhibited consistent characteristics in many tests. With increasing axial tension deformation, load increases linearly until local yielding occurs within the plate, generally in the vicinity of the connection between the gusset and the brace member. The occurrence of first yield in the gusset plate corresponds with the proportional limit of the load deformation relationship. With further axial tension deformations, strain localization(s) occur, typically in the vicinity of the location(s) of first yield, until fracture initiation occurs at those sites. Fracture initiation typically, but not necessarily, occurs at ultimate load. In gussets with bolted brace connections where gusset thickness at the bolted connection region equals the thickness of the surrounding gusset material, fracture typically occurs around the brace connection bolt group perimeter with first fracture occurring along a line between the row of bolts closest to the end of the brace, as described by Hardash and Bjorhovde (1985). In gusset connections where bracing is welded to the gusset plate, fracture typically initiates just past the end of the brace and grows through the remaining gusset

with increasing deformation. Deformation during fracture growth is accompanied by reduction in load. Fractures typically initiate at deformations of 5 to 20 mm.

5.2.2. Gusset Plate Behaviour in Compression

Compression behaviour of continuous gussets differs between those with unstiffened free edges and those gussets with stiffened free edges. Compression behaviour of unstiffened gusset plates may generally be described as linear elastic load deformation response up to a proportional limit load, which corresponds to buckling or first yield of the gusset plate beyond which, stiffness rapidly decreases. With compression deformation beyond buckling, gusset load decreases rapidly and significantly as the buckled plate develops hinge zones and forms a plastic mechanism – permitting out-of-plane displacement of the brace end connection.

The addition of edge stiffeners to gussets has been observed, in tests by Rabinovitch and Cheng (1993) and Nast, Grondin and Cheng (1999) and in analyses by Walbridge, Grondin and Cheng (1998), to have little effect on the linear elastic and early non-linear load deformation response of gusset plates. In tests, it was observed that, after gusset buckling occurs, edge stiffeners act to limit the extent of the buckled region, which forms just beyond the end of the brace member. With the edges of the plate stiffened and remaining straight through post-buckling response, additional compression deformation is accompanied by a nearly constant load; with the buckled region of the plate remaining confined on all sides by unbuckled stiffened plate material and connected boundaries at beams and columns. The presence of edge stiffeners stabilizes the post buckling load vs. deformation response of gussets loaded in compression by confining the buckled regions and permitting load to remain nearly constant through post buckling compressive deformations.

When cyclically loaded, the open hysteresis and deformability associated with edge stiffened gusset plates are desirable characteristics for effective seismic load resistance.

As such, there is some interest in evaluating their use as inelastic elements in seismically loaded structures. While significant research has been conducted on gusset plates in isolation, little is available regarding their anticipated behaviour as inelastic elements in seismically loaded structures. To assess the deformation demand and effectiveness of gusset plates in such structures, a series of non-linear time history analyses were performed on one, two and four storey steel structures – designed according to NBCC, NRCC (1995) and CAN/CSA-S16.1-94, using a variety of parameters.

5.3 Structures Analysed

5.3.1 Proportioning of Structural Members

The one, two and four storey steel structures analysed were comprised of members sized using NBCC 1995 equivalent static lateral force method and mass and geometric parameters consistent with those used in the CISC Single Storey and Low Rise Building Design Guides, Chien (1989) and Chien (1991) respectively. Structures were designed using Zone 3 and 5 design earthquakes and force modification factors, R , of 1.5, 2, 3 and 4. It should be noted that NBCC does not permit the use of $R = 1.5$ in locations with Z exceeding 2. The combination of $R = 1.5$ and higher zones was included to permit comparisons between subsets of the data collected and to maintain consistency with previous research by Redwood, Lu, Bouchard and Paultre (1991) and Kobeovic and Redwood (1997).

The geometry, design parameters and member sizes of the structures are provided in figure 5.2 and Table 5.1. A 3.6 meter high by 8 meter wide bay, similar to the structure geometry used in analyses by Redwood, Lu, Bouchard and Paultre (1991), was used for all storeys of all structures. The lateral load resisting system for each structure was cross braced concentrically braced frame, rising in a single bay, as shown in figure 5.2. Fundamental periods were 0.08 s to 0.12 s for the one storey, 0.17 s to 0.23 s for the two storey and 0.33 s to 0.45 s for the four storey structures.

Member sizing of the gravity framing was based on gravity plus live loading plus axial forces arising from overturning moment. Overturning moment was calculated at each storey as the square root sum-of-squares (SRSS) of the moments of the equivalent lateral seismic design loads above that storey. Gusset plates were modelled to yield at the maximum design bracing force arising from the equivalent lateral seismic loads. Wind forces were assumed to not contribute to the design of any members. Bracing was proportioned to provide compression resistance, as calculated using CAN/CSA-S16.1-94, to equal or exceeding 1.5 times the modelled gusset plate ultimate load. The factor applied to gusset capacity to reflect that, for capacity based bracing design, gusset ultimate load would be treated as a load effect and would be factored to that ensure ultimate limit states not be reached in brace members. Reflecting common design practice, brace members and gusset design loadings did not include axial loads arising from gravity load sharing with columns.

5.3.2 Finite Element Modelling Parameters

Structures were analysed using DRAIN-2DX software, Prakash, Powell and Campbell (1993). Gusset plates were modelled using two parallel nonlinear type 1 truss elements, Powell (1993), as shown in figure 5.3. By combining buckling and yielding behaviour of the elements, the experimentally observed behaviour of gusset plates was modelled. Beam and columns were modelled using type 15 elements using type three (linear) axial load – bending interaction recommended for steel members in the element documentation by Powell (1993). Column bending and axial load ultimate limit states were set equal to cross section capacities calculated using CAN/CSA-S16.1-94 with $\phi = 1.0$. Bracing was modelled using elastic truss elements since gusset elements were modelled to limited axial load in bracing to the elastic range. In this research, both slender and stocky gusset types were modelled. The slender plate was modelled to have a compression ultimate load of 0.85 times tension ultimate load. The stocky plate was modelled to have equal ultimate loads in both tension and compression. This is consistent with observations of

the relationship between gusset tension and compression capacity versus gusset thickness made by Walbridge, Grondin and Cheng (1998).

Analysis was performed using DRAIN-2DX non-linear time history analysis. Base accelerations, derived from earthquake records scaled to provide peak accelerations and velocities consistent with NBCC design values, were applied to the structures. Unscaled earthquake record summaries are provided in table 5.2 and an example unscaled earthquake record is provided in figure 5.4. In a manner consistent with Redwood, Lu, Bouchard and Paultre (1991), earthquake records were scaled to correspond to NBCC design earthquakes for seismic zones 3 and 5. The design a/v ratio was assumed to equal 1.33. For records with $a/v < 1.33$, the scale factors were selected to provide peak velocities consistent with the NBCC design values. For records with $a/v > 1.33$, the scale factors were selected to provide peak accelerations consistent with the NBCC design values. A preliminary time step of 0.02 seconds was used for all analyses. Where errors occurred during solution, time steps were reduced and corrections were applied to the solution as required to improve solution accuracy.

Mass and structural damping was 5% for beams and columns. Structural damping was minimized for gusset plates to reduce viscous forces and maintain static force equilibrium with bracing as recommended in the DRAIN-2DX manual, Prakash, Powell and Campbell (1993).

Lumped masses were assigned to nodes at each floor level at the ends of lean-on columns. The lean-on columns and struts connecting them to the structure models were pin ended elastic elements of large cross sectional area, considered very stiff relative to the structure.

5.4 Analysis

In the first step of analysis, dead, snow and occupancy loads as defined in the NBCC-1995 Clause 4.1.9.1(2) were applied to both the lean-on and structural columns.

Structural columns were loaded at floor and roof levels with forces arising from the design dead and live gravity loads acting on the floor area tributary to those columns. For those gravity loads tributary to the lateral load resisting system but not directly supported by columns in the modelled structure, loads were applied to the lean-on columns. After gravity load effects were modelled, accelerations were applied horizontally at the base of the structures. Vertical accelerations were neglected. A constant time step solution scheme, with 0.02 seconds per step, was used for analysis. P-delta effects were considered in all cases.

5.5 Results

5.5.1 Overall Structure Drift

Maximum overall drift of the stocky gusset plate connected structures are reported in table 5.3 as both absolute maximum displacements and as percentages of the current maximum drift permitted for structures during the design earthquake of 0.02H (NBCC 1995). In all cases, the predicted drift of the structures were within NBCC limits.

The data presented in table 5.3 is arranged, from top to bottom, in three groups – one storey, two storey and four storey structures. Within each group, results are arranged in order of increasing Z and R, with Zone 3 at the top and Zone 5 at the bottom. It is clear from the data that the taller structures experience greater top lateral deflection, measured both absolutely and relative to the NBCC maximum, than shorter structures of similar design. Structures of the same height and using the same design parameters also experience greater top lateral displacement during design earthquakes of zone 5 versus zone 3 intensity. This result would not be anticipated based on the top lateral displacement calculated using NBCC 4.1.9.2.(2) – which increases elastic displacement arising from application of equivalent lateral seismic loads by the design R factor. In this case, the lateral deflection of structures sharing the same height and design R value

would be nearly equal for both Zone 3 and 5 earthquakes. One would also expect that the ratio of the top lateral displacements of two structures, sharing the same design zone and height, would equal the ratio of the design R values. Using four storey structures as an example, the ratio of the $Z = 5, R = 2$ and the $Z = 5, R = 4$ top displacement is $75.5 / 92.8 = 0.814$, while the ratio of the design R values is 0.5. Generally, the top lateral deflections arising from the non-linear time history analysis are not well predicted by NBCC 4.1.9.2.(2).

Maximum predicted drift among the stocky gusset connected one storey structures was 10.0 mm, for the Zone 5, $R = 4$ design structure, during the PKH event. The drift predicted for the slender gusset connected structure subjected to the same earthquake was 10.3 mm. The maximum top drift permitted for the single storey structure was 72 mm. Maximum predicted drift for both the stocky and slender gusset connected two storey structures was 50.4 mm, for the Zone 5, $R = 4$ design structure, during the LPI event. The maximum permissible top drift permitted for the two storey structure was 144 mm using the NBCC provisions. Maximum predicted drift among the stocky gusset connected four storey structures was 92.8 mm, for the Zone 5, $R = 4$ design structure during the LPI event. The maximum predicted drift for the corresponding slender gusseted structure was 89.6 mm. The maximum permissible top drift for the structure was 288 mm using the NBCC provisions.

Overall drift of structures designed using slender and stocky gusset plates were compared to determine the effect of gusset slenderness on seismic response. Generally, more slender gussets absorb less energy per similar inelastic cycle than stocky gussets of equivalent tension capacity because of hysteresis pinching, which arises from the reduced buckling strength of slender gussets relative to their tension strength. In tests, slender gussets have also exhibited degradation of compression strength and stiffness with continued cyclic loading.

Direct comparison of the top lateral displacements of slender and stocky gusseted structures reveals that, in many cases, especially among structures with predominantly

elastic responses, the top displacements are equal or near equal. Among structures with inelastic responses, the differences between stocky and slender gusset connected structures vary significantly. To clarify the effect of gusset slenderness on top lateral displacement, the mean of the ratios of slender vs. stocky gusseted structure top storey lateral displacement was used as a metric. Among the single storey structures, response was predominantly elastic and the mean of the ratios of slender to stocky structure top storey drift was unity. For two and four storey structures, some inelasticity was predicted in the structure's responses to the design excitations. For the two storey structures, the mean of the ratios of stocky to slender structure top storey drift was 0.95. For the four storey structures, the mean of the ratios of stocky to slender structure top storey drift was 0.97. These ratios indicate that the difference in inelastic response between stocky and slender gussets was quite insignificant to the overall response of the class of structures analysed. One storey structures exhibited predominantly elastic response to design events, so practically no difference was found between the responses of stocky and slender gusseted one storey structures. As such, the effect of pinching of lateral load resisting system hysteresis in overall structure drift ranged from no effect in the one storey structures to a 5% increase in drift.

5.5.2 Interstorey Drift

Figure 5.5 depicts the maximum, mean and minimum interstorey drift for all structures analysed versus the a/v ratios of the scaled earthquakes. Among all one storey structures, shown in the topmost plot, the earthquake which gave rise to the maximum interstorey drift was the PKH event with $a/v = 1.67$. It should be noted that among all of the events analysed, single storey structures remained predominantly elastic. For two and four storey structures, the most damaging event, measured by maximum interstorey drift, was the LPI event, with $a/v = 1.14$. It should be noted that the velocity dominated events with $a/v < 1$ were more damaging to the four storey structures than they were to the two storey ones. These observations are consistent with the expectation that velocity dominated

loading is more damaging to structures with longer periods, in this case those of similar mass distribution but of greater height.

5.5.3 Gusset Plate Deformation Demand - General

It has been determined in tests by Rabinovitch and Cheng (1994), Nast and Cheng (1999) and Mullin (Chapter 3) that a wide range continuous gussets, both without edge reinforcement and with local reinforcement in the region of the bracing connection, typically experience first fracture in tension at deformations ranging from 10 to 20 mm. That fracture typically occurs within the plate, either originating at bolt holes nearest the root of the gusset or just beyond the end of local reinforcement. In those gussets with connection length (measured parallel to the brace axis) in the range of 75 to 150 mm, rapid loss of load with post fracture deformation has been observed in tests. For evaluation of gusset plate deformation demand, an anticipated inelastic deformation at first fracture of 15 mm was used.

Inelastic gusset deformations are not reported for one storey structures since, as stated earlier, their responses were predominantly elastic in all cases.

5.5.4 Gusset Plate Deformation Demand - Two Storey Structures

Figure 5.6 depicts maximum inelastic gusset plate deformation for all two storey structures, arranged by gusset stockiness and earthquake intensity, Z . The gusset deformations predicted within the second storey do not vary significantly among the structures sharing a common design zone, remaining consistent at 5 to 8 mm for Zone 3, and 10 to 15 mm for Zone 5 structures, independent of design R . Concentration of damage occurs within the bottom storey of the two storey structures analyzed while upper storey deformation is unaffected by variation of design R . Using 15 mm maximum anticipated gusset deformability, it can be seen that in Zone 3, $R = 1.5, 2$ and 3 structures,

continuous gusset plates would be expected to remain unfractured during all design events analysed. Zone 3, R = 4 gusset deformation of 15.36 mm just exceeded the 15 mm anticipated fracture deformation. If furnished with properly detailed continuous gusset plates manufactured using ductile steel, deformations of this magnitude could be tolerated without fracture. For Zone 5 structures, fractures would not be expected in the R = 1.5 and R = 2 structures. Zone 5, R = 3 and R = 4 structures predicted bottom storey gusset deformations were 19.8 mm and 28.5 mm respectively. Deformations of this magnitude almost certainly exceed the deformation capacity of continuous gussets and would correspond to fracture. As anticipated, the deformations predicted in slender gusset connections exceed those predicted for stocky gusset connections in most cases

5.5.5 Gusset Plate Deformation Demand - Four Storey Structures

Figure 5.7 depicts maximum inelastic gusset deformation among the four storey structures analysed. In all structures, the most severe damage was predicted to occur in the third storey. Increased damage in upper storeys is associated with structures designed without sufficient allowance for the effects of higher order modes, typically caused by an underestimated top force. This, as discussed by Humar and Mahgoub (2000) and Humar and Rahgozar (2000), is a characteristic of the NBCC, 1995 equivalent lateral load approach for steel structures of the type analysed here. Among the zone 3 structures, gusset deformation tended to increase with increasing design R as expected. Within zone 5 structures however, significant concentration of damage was predicted in the third storey of the R = 1.5 case, exceeding the deformation predictions for both the R = 2 and R = 3 structures. This likely indicates a more significant higher order modes effect in the R = 1.5 structure, which possessed the shortest fundamental period of all four storey structures analysed.

Maximum gusset deformation exceeded the anticipated fracture deformation of continuous gusset plates in the third storey of all four storey Zone 5 structures and in the

third storey of the Zone 3, $R = 3$ (15.34 mm) and $R = 4$ (15.39 mm) stocky gusseted structures.

The deformations sustained by gussets within the third storey of the Zone 3, $R = 3$ and $R = 4$ structures were 15.34 mm and 15.39 mm respectively - within the 15 to 20 mm range sustainable by properly detailed gussets fabricated using ductile steel. To ensure such deformability is present in as-built structures, special effort would be required of the designer in specifying gusset geometry and materials.

Zone 5 structures experience gusset deformations in excess of the anticipated fracture deformation of 15mm in all cases of $R = 1.5$ through $R = 4$. In the case of the $R = 3$ and $R = 4$ structures, anticipated fracture deformations were exceeded in storeys 2, 3 and 4 and 1, 2 and 3 respectively. Maximum gusset deformation of 29.97 mm was calculated for storey 3 of the Zone 5, $R = 4$ structure – well in excess of the experimentally observed range of continuous gusset fracture deformation of 10 mm to 20 mm.

5.6 Conclusions

In NBCC, 1995, it is stated that predominantly elastic response may be anticipated for structures designed using $R = 1.5$ while structures designed using larger R values are expected to undergo increasing inelasticity in response to design seismic excitations with increasing design R values. The results of the analyses reported herein do not reflect that relationship.

For one storey structures, elastic response was obtained for structures with design R values up to 4 when subject to a range of design Zone 3 and 5 earthquakes, as indicated in table 5.3.

For similarly designed two storey structures, damage increased with increasing R as anticipated based on current design standards. As anticipated, structures designed with

R = 1.5 were found to experience limited inelasticity and were, in no case, predicted to experience gusset deformations corresponding to fracture. Damage was generally limited to the bottom storey and was found to correspond with gusset plate fracture in the Zone 3, R = 4 and Zone 5, R = 3 and R = 4 cases as indicated by shaded cells in the right column of table 5.3, where grey indicates possible fracture and black indicates gusset deformation sufficiently large to consider fracture likely.

Four storey structures designed for Zone 3 events were predicted to undergo limited inelasticity when designed using R = 1.5 but, for Zone 5 events, were predicted to undergo sufficient inelastic deformation to cause gusset fracture within the third storey.

During Zone 3 design events, gusset plate predicted deformation did not exceed the anticipated fracture deformation of properly designed continuous gusset plates. During Zone 5 events, continuous gusset deformability was exceeded in R = 3 and 4 designed two storey structures and in R = 1.5, 3 and 4 designed four storey structures. In no case did gusset deformation exceed 30 mm. In analyses of eight storey steel (Chapter 6) and concrete frames (Chapter 7), modified bracing configurations, wherein steep angle chevron bracing was employed, were shown to significantly decrease gusset deformations within a braced bay for a given storey drift. In all structures analysed here, modified bracing configurations could result in sufficiently reduced deformation demand to reduce gusset deformation below the fracture limit.

The results of the analysis presented are specific to the structures analysed and may not be generalized. Within the group of structures analysed, lateral load resisting systems employing “strong brace – weak gusset” capacity design were effective at resisting Zone 3 design earthquakes in one, two and four storey structures with design R ranging from 1.5 to 4 and were also effective at resisting Zone 5 design earthquakes in one and two storey structures with design R of 1.5 and 2. A four storey structure, designed for Zone 5 using R=1.5 suffered damage corresponding to gusset fracture. The expectation of a structure so designed is primarily elastic response.

Table 5.1 – Member Size Summary

MEMBER	Zone 3, R = 1.5	Zone 3, R = 2	Zone 3, R = 3	Zone 3, R = 4	Zone 5, R = 1.5	Zone 5, R = 2	Zone 5, R = 3	Zone 5, R = 4
C1-1	W 410 × 46							
B1-1	HSS 127 × 6.4							
BR1-1	L 102×76×9.5	L 102×76×8			L 127×89×13	L 127×89×9.5	L 102×76×9.5	L 102×76×8
C2-1,2	HSS 152 × 6.4			HSS 152 × 8	HSS 152 × 6.4			
B2-1	W 530 × 82							
B2-2	W 410 × 46							
BR2-1	HSS 152 × 6.4	HSS 127 × 6.4	HSS 101 × 6.4	HSS 178 × 8	HSS 178 × 6.4	HSS 152 × 6.4	HSS 127 × 6.4	
BR2-2	L 102×76×6.4			HSS 101 × 6.4	L 102×76×8	L 102×76×6.4		
C4-1,2	W 310 × 79	W 310 × 74	W 310 × 67		W 310 × 107	W 310 × 97	W 310 × 79	W 310 × 74
C4-3,4	W 310 × 60							
B4-1,2,3	W 530 × 82							
B4-4	W 410 × 46							
BR4-1	HSS 203 × 8	HSS 178 × 8	HSS 152 × 6.4		HSS 254×11	HSS 254 × 8	HSS 203 × 8	HSS 178 × 8
BR4-2	HSS 178 × 6.4	HSS 152 × 8	HSS 127 × 8	HSS 127 × 6.4	HSS 203×11	HSS 203 × 6.4	HSS 178 × 6.4	HSS 152 × 8
BR4-3	HSS 127 × 8	HSS 127 × 6	HSS 101 × 8	HSS 101 × 6.4	HSS 178 × 8	HSS 152 × 8	HSS 127 × 8	HSS 127 × 6.4
BR4-4	L 102 × 76 × 6.4							

Notes: All HSS are square. All angles, designated L, are double angle members with long legs back-to-back

Table 5.2 - Summary of Earthquake Records used in Analysis

Record, Date, Site	Abbrev.	Comp.	PHA(g)	PHV(m/s)	a/v
Long Beach, Mar. 10, 1933, (Los Angeles Subway Terminal)	LBL	N39E	0.064	0.173	0.37
El Centro, Dec. 30, 1934 (El Centro Imperial Valley)	ECL	S00W	0.160	0.209	0.52
Taft, July 21, 1952 (Lincoln School)	TFI	N21E	0.156	0.157	0.99
San Fernando, Feb. 9, 1971, (Pacoima Dam)	PDI	S16E	1.171	1.132	1.03
Loma Prieta 2, Oct 17, 1989, (Eureka Canyon Road)	LPI	0	0.629	0.552	1.14
Parkfield, June 27, 1966, (Cholame, Shandon)	PKH	N85E	0.426	0.255	1.67
Loma Prieta 4, Oct 17, 1989, (USCS/Link Lab, Santa Cruz)	LPH	0	0.442	0.212	2.08
Nahanni, Dec. 25, 1985 (Site I: Iverson)	NAH	LONG	1.101	0.462	2.38
Monte Negro, Apr. 9, 1979 (Hotel Albatross Basement)	MNH	N00E	0.042	0.016	2.63

Table 5.3 - Stocky Gusseted Structures – Results Summary

	Design Parameters	Max Top Displ. (mm)	Event	Percent of NBCC Drift Limit (0.02H)	Max Storey Drift (mm)	Inelastic Gusset Deformation (mm)
One Storey	Zone 3, R = 1.5	2.67	LPH	3.71%	2.67	Elastic
	Zone 3, R = 2	3.41	LPH	4.74%	3.41	Elastic
	Zone 3, R = 3	4.12	LPH	5.72%	4.12	Elastic
	Zone 3, R = 4	8.96	TFI	12.44%	8.96	Elastic
	Zone 5, R = 1.5	3.22	LPH	4.47%	3.22	Elastic
	Zone 5, R = 2	5.53	PDI	7.68%	5.53	Elastic
	Zone 5, R = 3	7.25	PDI	10.07%	7.25	Elastic
	Zone 5, R = 4	10	PKH	13.89%	10	Elastic
Two Storey	Zone 3, R = 1.5	15.8	LPI	10.97%	12.3	5.84
	Zone 3, R = 2	20.3	LPI	14.10%	13.8	7.64
	Zone 3, R = 3	23.4	LPI	16.25%	16.6	11.85
	Zone 3, R = 4	26.56	LPI	18.44%	20.3	15.35
	Zone 5, R = 1.5	27.5	LPH	19.10%	18.4	11.13
	Zone 5, R = 2	28.6	LPI	19.86%	18.7	10.21
	Zone 5, R = 3	41	LPI	28.47%	27.7	19.82
	Zone 5, R = 4	50.4	LPI	35.00%	36.7	28.54
Four Storey	Zone 3, R = 1.5	43.1	TFI	14.97%	14.8	9.74
	Zone 3, R = 2	45.6	TFI	15.83%	16.8	11.82
	Zone 3, R = 3	54.1	ECL	18.78%	19.7	16.24
	Zone 3, R = 4	55	TFI	19.10%	19.5	15.89
	Zone 5, R = 1.5	68.4	LPI	23.75%	35.2	22.16
	Zone 5, R = 2	75.5	LPI	26.22%	27.5	18.23
	Zone 5, R = 3	86.9	TFI	30.17%	31.3	22.31
	Zone 5, R = 4	92.8	LPI	32.22%	36.7	29.97

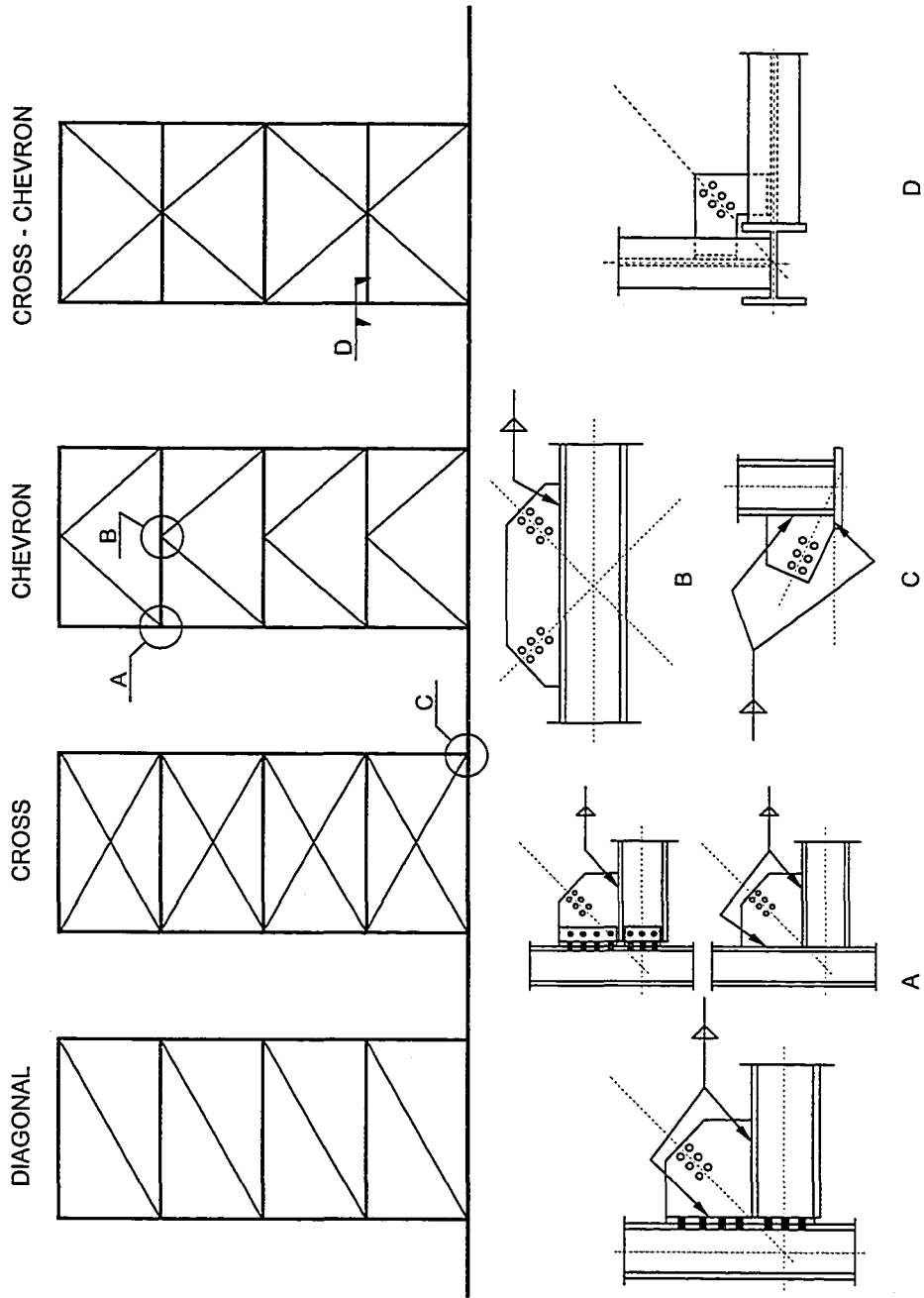


Figure 5.1 – Typical Brace and Gusset Configurations

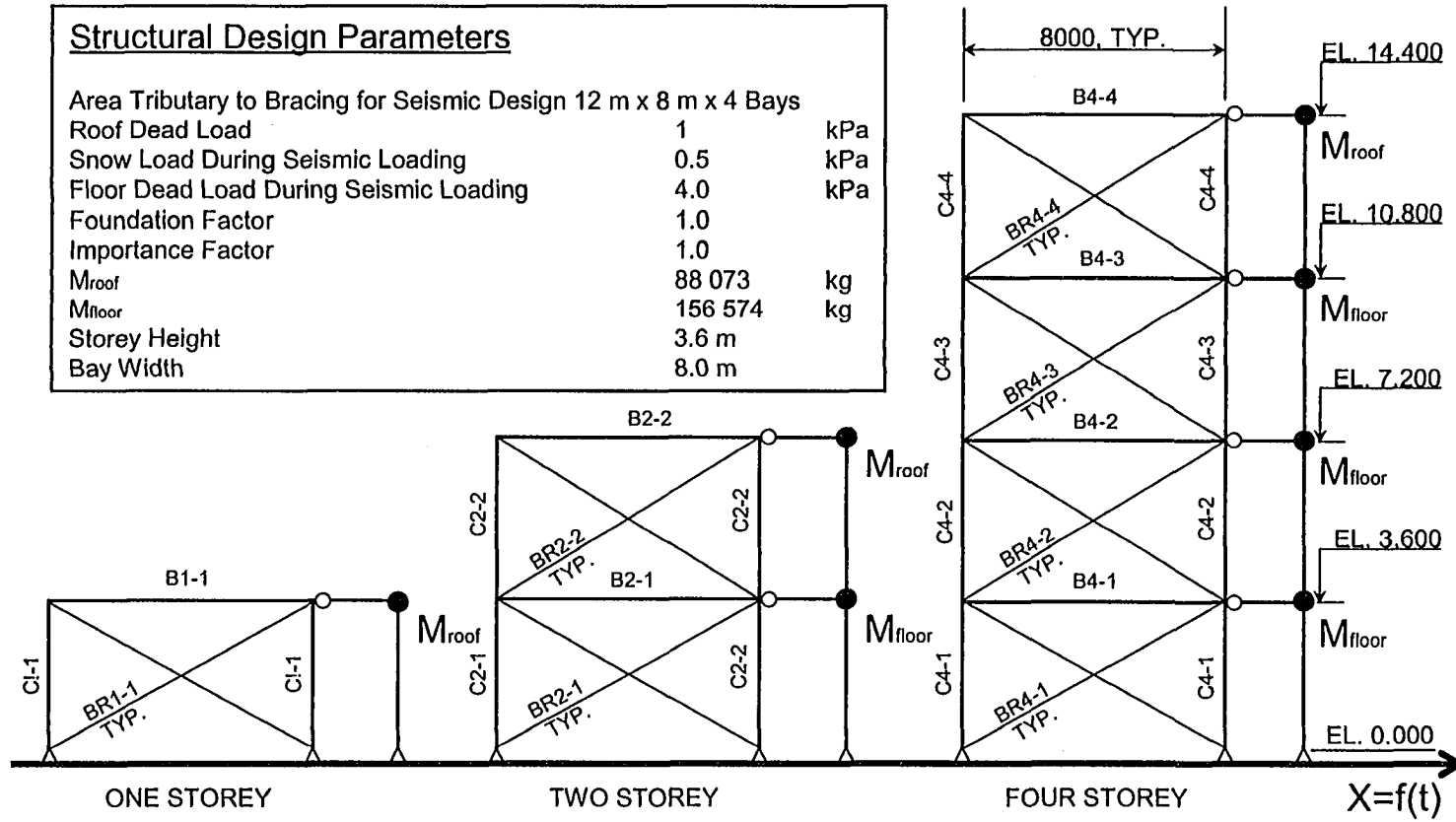
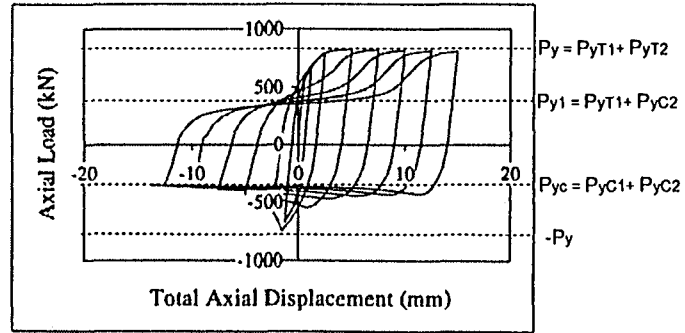


Figure 5.2 - One, Two and Four Storey CBF Structure Geometry and Design Parameters



OBSERVED GUSSET BEHAVIOUR (from Walbridge, 1998)

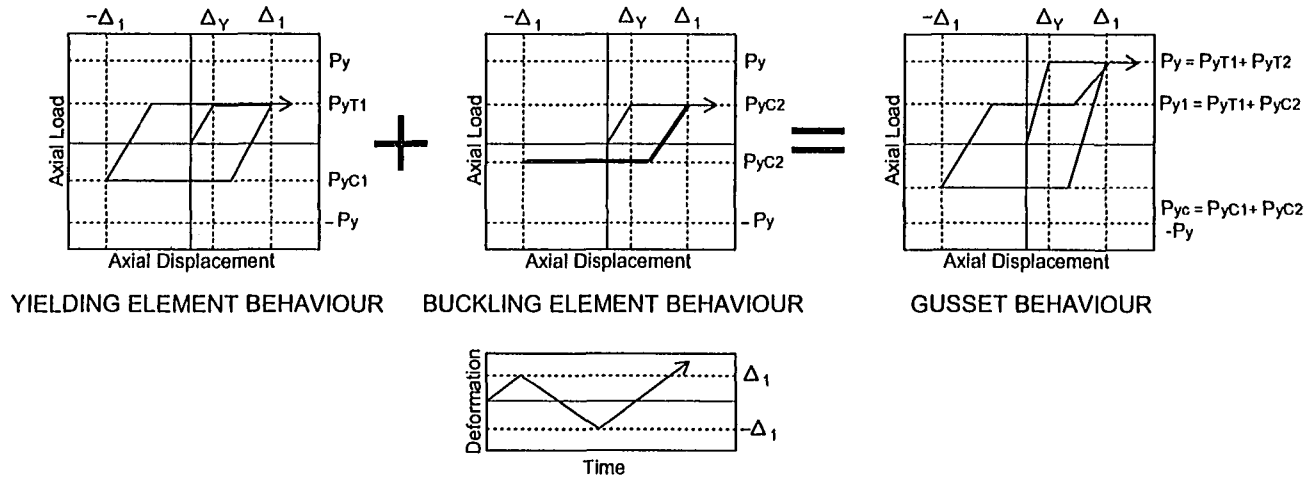


Figure 5.3 – Gusset Behaviour Modelled using Parallel Nonlinear Elements

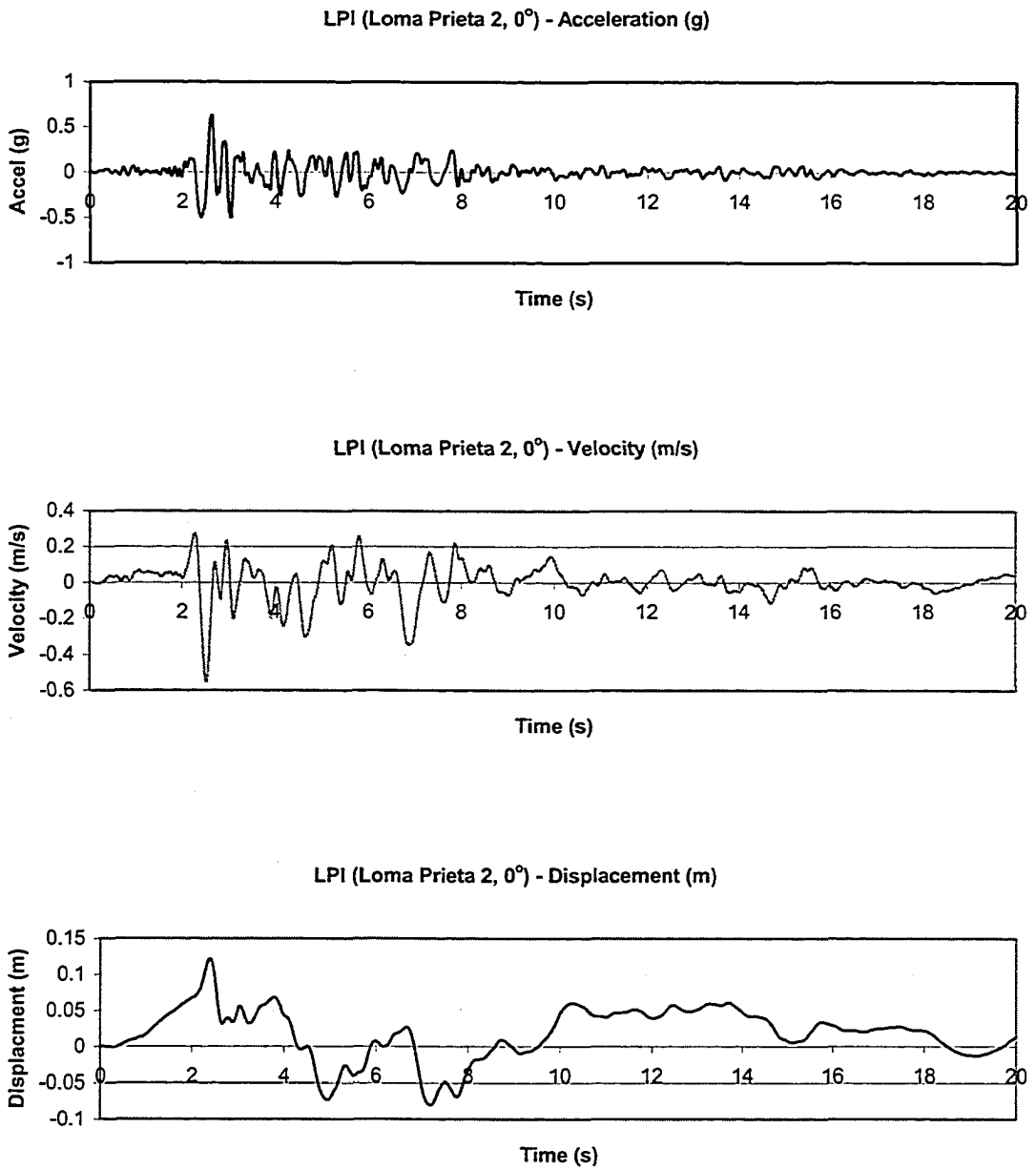


Figure 5.4 – Unscaled LPI Acceleration, Velocity and Displacement

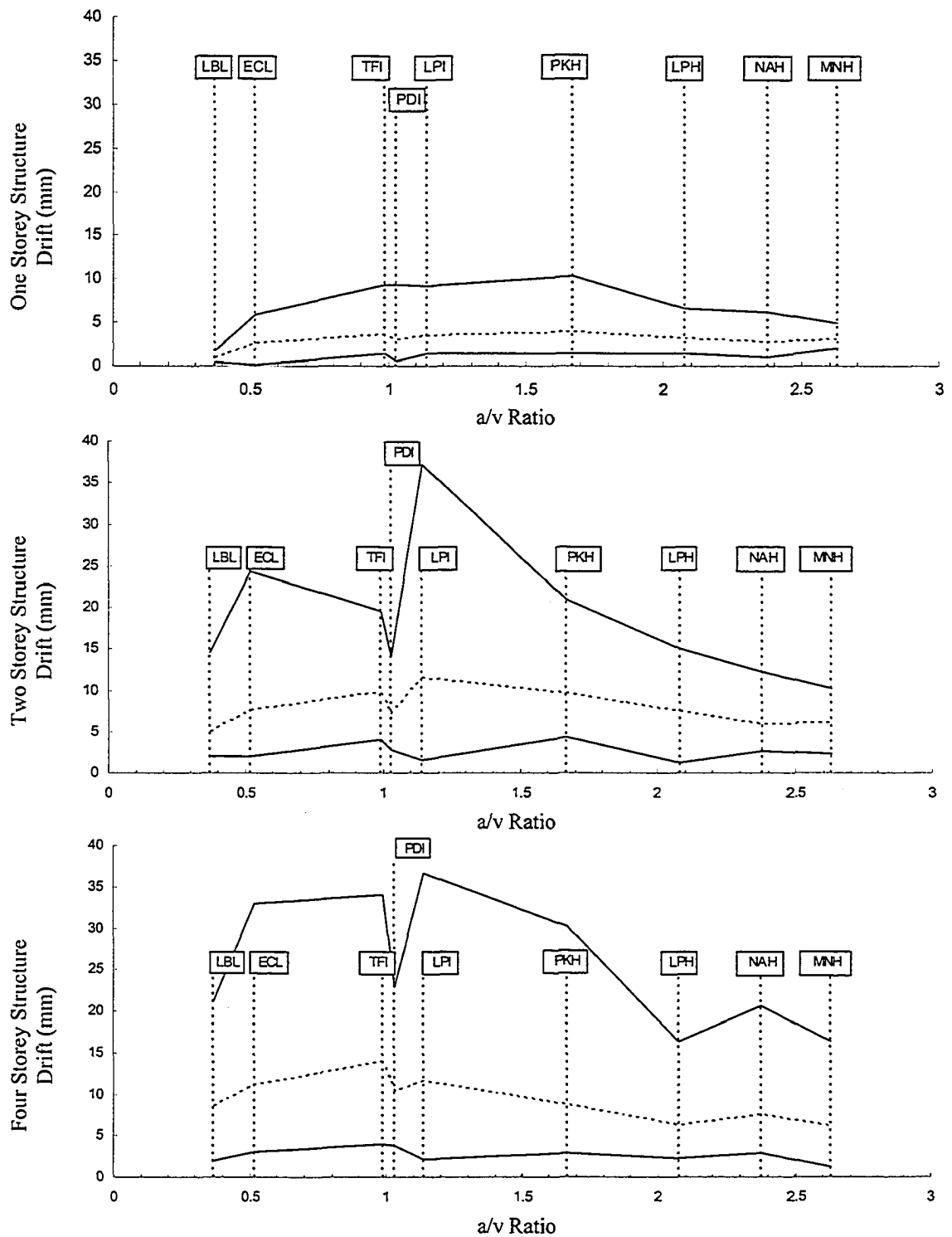
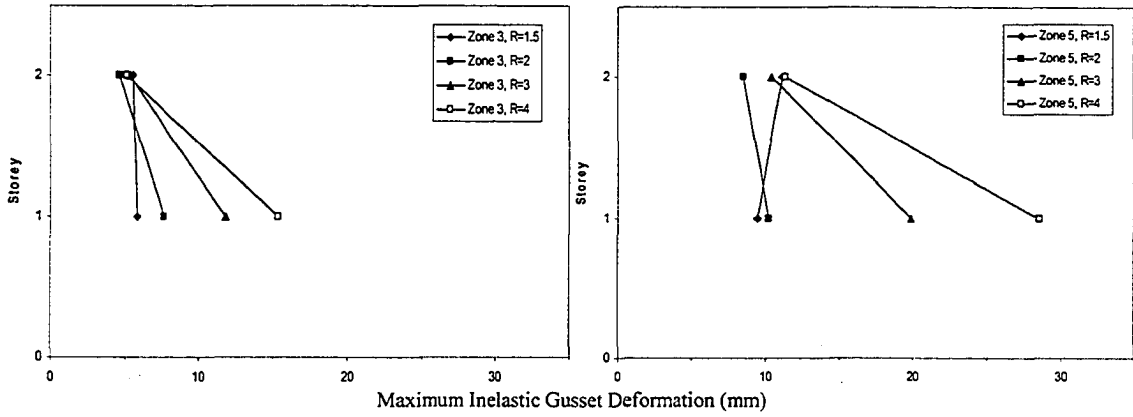


Figure 5.5 – Maximum, Mean and Minimum Interstorey Drift vs. a/v

Storey versus Maximum Stocky Gusset Deformation (mm)



Storey versus Maximum Slender Gusset Deformation (mm)

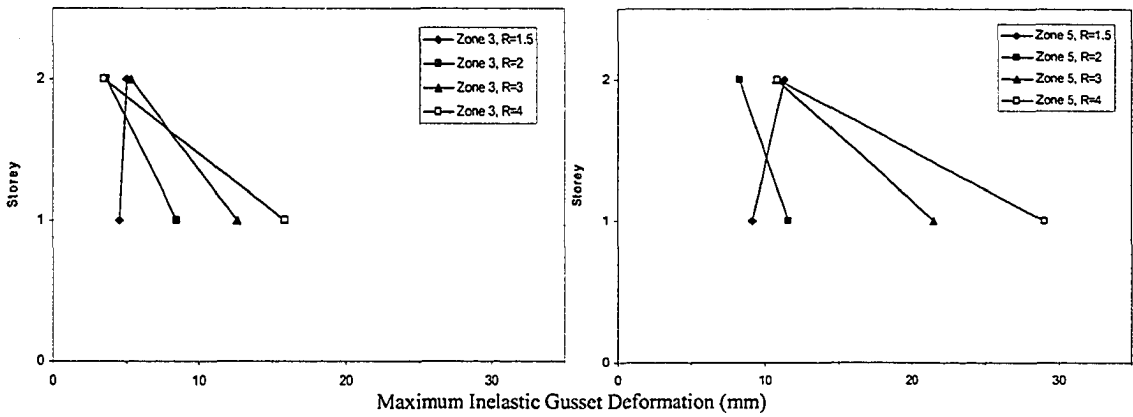


Figure 5.6 - Maximum Gusset Deformation – Two Storey Structures

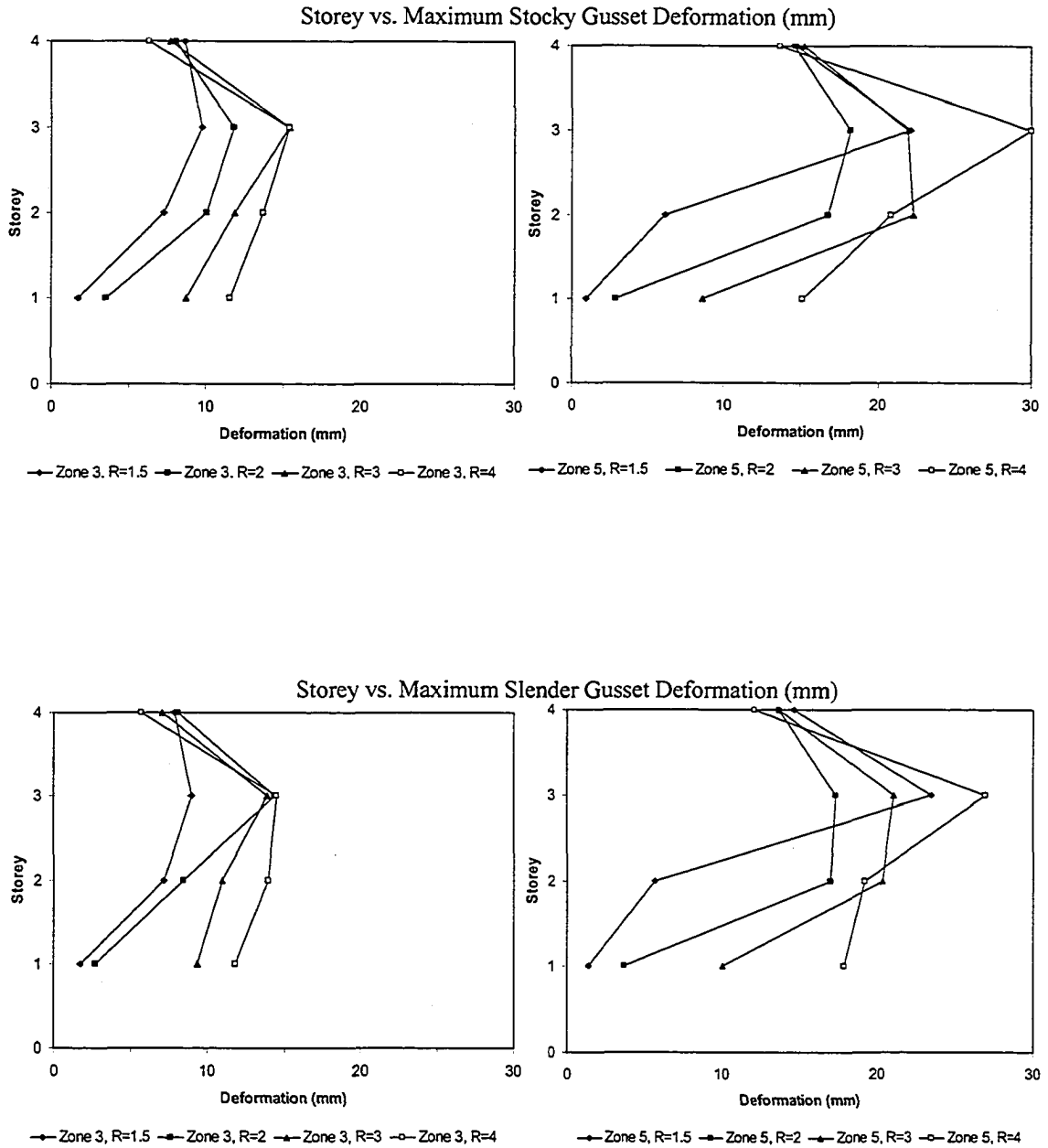


Figure 5.7 – Maximum Gusset Deformation – Four Storey Structures

5.7 References

CAN/CSA-S16.1-M89, 1989. Limit States Design of Steel Structures, Canadian Standards Association, Rexdale, Ontario.

Chien, E., 1991. "Low Rise Office Building Design Aid." Canadian Institute of Steel Construction, Willowdale, Ontario.

Chien, E., 1989. "Single Storey Building Design Aid." Canadian Institute of Steel Construction, Willowdale, Ontario.

Hardash, S.G., and Bjorhovde, R., 1985. "New Design Criteria for Gusset Plates in Tension." Engineering Journal, AISC, Vol. 22, No. 2, pp. 77-94.

Humar, J.L., and Mahgoub, M., 2000. "Accounting for Higher Order Mode Effects in UHS Based Design." Discussion Paper, Canadian National Committee on Earthquake Engineering (CANCEE).

Humar, J.L., and Rahgozar, M.A., 2000. "Application of Uniform Hazard Spectra in Seismic Design of Multistorey Buildings." Canadian Journal of Civil Engineering, 27, pp 1-18.

Kobeovic, S., and Redwood, R., 1997. "Design and Seismic Response of Shear Critical Eccentrically Braced Frames." Canadian Journal of Civil Engineering, 24: 761 – 771.

Nast, T.E., Grondin, G.Y., and Cheng, J.J.R., 1999. "Cyclic Behaviour of Stiffened Gusset Plate-Brace Member Assemblies." Structural Engineering Report No. 229, Department of Civil Engineering, University of Alberta, Edmonton, Alberta.

NRCC, 1995. National Building Code of Canada. Associate Committee on the National Building Code, National Research Council of Canada, Ottawa, Ontario.

Powell, G.H., 1993. DRAIN-2DX Element Description and Users Guide for Element TYPE01, TYPE02, TYPE04, TYPE06, TYPE09 and TYPE15 Ver. 1.10 Report No. UCB/SEMM-93/18, Department of Civil Engineering, University of California, Berkeley, California.

Prakash, V., Powell, G.H., and Campbell, S., 1993. DRAIN-2DX Base Program Description and Users Guide. Ver. 1.10, Report No. UCB/SEMM-93/17, Department of Civil Engineering, University of California, Berkeley, California.

Rabinovitch, J.S., and Cheng, J.J.R., 1993. "Cyclic Behaviour of Steel Gusset Plate Connections." Structural Engineering Report No. 191, Department of Civil Engineering, University of Alberta, Edmonton, Alberta.

Redwood, R.G., Lu, F., Bouchard, G., and Paultre, P., 1991. "Seismic Response of Concentrically Braced Steel Frames." Canadian Journal of Civil Engineering, 18(6), pp 1062 - 1077.

Redwood, R., and Channagiri, V.S., 1991, "Earthquake Resistant Design of Concentrically Braced Steel Frames." Canadian Journal of Civil Engineering, 18, pp 839 - 850.

Walbridge, S.S., Grondin, G.Y., and Cheng, J.J.R., 1998. "An Analysis of the Cyclic Behaviour of Steel Gusset Plate Connections." Structural Engineering Report No. 225, Department of Civil Engineering, University of Alberta, Edmonton, Alberta.

Walbridge, S.S., Grondin, G.Y., and Cheng, J.J.R., 1998. "An Analytical Study of the Cyclic Behaviour of Steel Gusset Plate Connections." Proceedings of the Annual Conference of the Canadian Society for Civil Engineering, Vol IIIa, pp. 107 to 116.

Yam, C.H.M., and Cheng, J.J.R., 1993. "Experimental Investigation of the Compressive Behaviour of Gusset Plate Connections." Structural Engineering Report No. 194, Department of Civil Engineering, University of Alberta, Edmonton, Alberta.

Yam, C.H.M., and Cheng, J.J.R., 1994. "Analytical Investigation of the Compressive Behaviour and Strength of Steel Gusset Plate Connections." Structural Engineering Report No. 207, Department of Civil Engineering, University of Alberta, Edmonton, Alberta.

6. DEFORMATION DEMAND IN SEISMICALLY LOADED CONCENTRICALLY BRACED STEEL FRAMES EMPLOYING INELASTIC GUSSET PLATES^{7,8}

6.1 Introduction

Current design practice for structures in zones of high seismic risk includes use of ductile lateral load resisting systems which, when loaded by intense earthquakes, absorb energy through inelastic response. Lateral load resisting systems which have performed well in past earthquakes include properly detailed and constructed moment resisting frames, concentrically braced frames and shearwalls. Common among these structural systems is open and stable lateral load vs. storey drift hysteresis of cyclically loaded bays. While gusset plates are currently not employed as inelastic elements in earthquake resistant structures, they have exhibited the characteristics typical of those elements which have performed well when seismically loaded. When tested cyclically by Rabinovitch and Cheng (1993) and Nast, Grondin and Cheng (1999), gusset plates exhibited open load-deformation hysteresis and maintained capacity in tension and, when fitted with free edge stiffeners, in compression.

While gusset plates have, based on their observed load deformation hysteresis, demonstrated potential to act inelastically in seismically loaded structures, there is limited research to-date to quantify the deformation demand anticipated within such structures.

The purpose of this research is to evaluate the deformation demand on gusset plates, designed to act inelastically in steel structures eight storeys in height, proportioned using the NBCC-1995, NRCC (1995) equivalent static lateral load approach and CAN/CSA-S16.1-94. Non-linear time-history analysis was employed to calculate the responses of structures, designed for Zone 3 and Zone 5 events and using a variety of structure response modification (R) factors and structure configurations including single diagonal

⁷ A version of this chapter is under revision for publication in the Canadian Journal of Civil Engineering

⁸ Portions of this chapter were presented at the NASCC / PSSC Conference, Long Beach California, March 2004.

braced and cross braced. An additional bracing configuration employing tension/compression bracing aligned at steep angles, referred to as M-braced, was also analysed. Analyses were conducted using scaled earthquake records covering a range of a/v ratios. Envelopes of gusset deformations, storey drifts and overall structure drifts were used to evaluate the anticipated maximum deformation demand on gusset for the combinations of design parameters R , v and bracing configurations.

6.2 Gusset Plate Behaviour

Analytical and experimental studies of individual gusset plates subject to cyclic and monotonic loading have been completed by Rabinovitch and Cheng (1993), Walbridge, Grondin and Cheng (1998), Nast, Grondin and Cheng (1999), Hu and Cheng (1987) and Yam and Cheng (1993). The subject gusset plates included plates with and without stiffeners along the free edges.

Load – deformation hysteresis observed for plates without edge stiffeners is generally not suitable for seismic resistance due to poor energy absorption characteristics in compression arising from low post-buckling strength. The provision of edge stiffeners improves the post-buckling behaviour of the gusset plates. It has been observed in tests by Rabinovitch and Cheng (1993) and Nast, Grondin and Cheng (1999), and in finite element analysis by Walbridge, Grondin and Cheng (1999), that properly proportioned edge stiffened gusset plates exhibit stable post-buckling hysteresis and are capable of enduring multiple inelastic load cycles prior to failure. Based on these characteristics, gusset plates are considered candidates to act as energy dissipating elements in seismically loaded structures, Rabinovitch and Cheng (1993).

Figure 6.1 shows some characteristic load-deformation responses of cyclically loaded gusset plate – brace assemblies, determined by Nast, Grondin and Cheng (1999). In a study of combined brace – gusset assemblies, it was determined that the strong brace – weak gusset combination gave rise to the most energy absorptive behaviour in cyclic load

tests, Nast, Grondin and Cheng (1999). The combination of elastic bracing combined with inelastic stiffened gusset plate behaviour in both compression and tension is the focus of this research.

6.3 Structural Design

The structural bay matched dimensions and loading used in the CISC multi-storey steel building design aid, Chien (1987) and in non-linear time history analysis research by Kobeovic and Redwood (1997) and Redwood, Lu, Bouchard and Paultre (1991).

Gravity loading was applied to the structure in accordance with the design example in the CISC High Rise Building Design Guide, Chien (1987). Seismic loading was applied using the equivalent static lateral load procedure, defined in NBCC – 1995 Clause 4.1.9 “Live Loads due to Earthquakes”. Structures were designed for Zones 3 and 5. For Zone 3 structures, single diagonal and cross braced structures were designed and analysed using $R = 1.5, 2$ and 3 . For zone 5, single diagonal and cross braced structures were designed and analysed using $R = 2, 3$ and 4 . M-braced structures, employing steep angle chevron bracing within each bay, as shown in figure 6.3, were proportioned for Zone 3, $R = 2, 3, 4$ and Zone 5, $R = 3, 4.5$ and 6 . The fundamental periods of the structures were in the 0.7 to 0.9 second range.

Gusset plates were designated to be the only inelastic elements within the structures. Bracing member sizes were selected based on an effective length equal to the diagonal work point to work point dimension of each braced panel. Bracing design forces were calculated by applying a load factor of 1.5 on gusset plate maximum loads in both tension and compression. The load factor was included to provide member sizes representative of those which would be specified in a real structure since, in capacity design of a real structure, load factors would be applied to the predicted ultimate load of gussets to ensure that bracing members remain elastic while gussets behave non-linearly. The cross-section and overall slenderness limits of CAN/CSA-S16.1-94 Clause 27 were not applied

in the selection of bracing members, since they were designed to behave elastically. Members were selected based on CAN/CSA-S16.1-94 Clause 13.

Columns were proportioned for the gravity loads, determined using area based live load reductions from NBCC-1995, NRCC (1995), plus seismic lateral loads combined by SRSS to determine overturning effects. The orientation of the columns was revised from that used by Chien (1987) such that braces were connected to column webs. This was done to minimize the energy absorption potential of the frame action in the event that inelastically extended into beams and columns, thereby placing greater demand on the bracing system.

Because of the configuration of the frames, beam axial loads arising from seismic loading were not significant. Members were sized for gravity loads only and selected sizes were not limited by section class.

6.4 Finite Element Analysis

6.4.1 General

Analyses were conducted using DRAIN-2DX, Prakash, Powell and Campbell (1993). The analyses were conducted on the example braced bays, shown on Figure 6.3, with member sizes summarized in tables 6.1 and 6.2. Time history analyses were conducted using the nine earthquake records listed in Table 6.3. The LPI event is shown, unscaled, in figure 6.4, for reference. In a manner consistent with Redwood, Lu, Bouchard and Paultre (1991), earthquake records were scaled to correspond to NBCC design earthquakes for seismic zones 3 and 5. The design a/v ratio was assumed to equal 1.33. For records with $a/v < 1.33$, the scale factors were selected to provide peak velocities consistent with the NBCC design values. For records with $a/v > 1.33$, the scale factors were selected to provide peak accelerations consistent with the NBCC design values.

Braces were represented in the analysis using element TYPE01, Powell (1993), with yielding possible in both tension and compression. Yield forces were defined as the tension and compression capacity of the bracing members, calculated using CAN/CSA-S16.1-94 design provisions with $\Phi = 1.0$.

Columns were modelled as continuous members over the full height of the structure and were represented in the analysis using element TYPE02, Powell (1993). The column P-M interaction was assumed to be a straight line relationships between C_R and M_{RY} and between T_R and M_{RY} , calculated using CAN/CSA S16.1-94 design provisions with $\Phi = 1.0$. The selected linear interaction slightly underestimates column strength when compared with CAN/CSA-S16.1-94.

Beams were modelled using type 2 elements configured to act as beams only, with no provision for inelasticity arising from axial loads.

P-Delta effects were included in the analysis by including lean-on columns, linked to the braced bay at floor levels, with axial forces and lumped mass at floors representing the loading and mass of the structure braced by the subject bay. Elastic truss elements were used for both the lean-on columns and the members linked to the subject bay. To ensure that lean-on elements behaved rigidly relative to the analysed structure, the cross section area of the lean-on elements was ten times the area of the largest column in each structure.

The bracing and gusset plate elements used in analysis were truss type 01 strut elements. To prevent displacement of the node between the two elements, a zero force link was placed between the node and the adjacent floor beam, as shown in Figure 6.5.

Mass and structural damping was 5% for beams and columns. Structural damping was minimized for gusset plates to reduce viscous forces and maintain static force equilibrium

with bracing as recommended in the DRAIN-2DX manual, Prakash, Powell and Campbell (1993).

6.4.2 Gusset Plate Modelling

To model gusset behaviour, two truss elements (EL01 in DRAIN-2DX) were used in parallel, as shown in Figure 6.5. One element buckled elastically in compression and yielded in tension. The second element yielded in both tension and compression. With this combination of parallel elements, any combination of stiffness, tension yield, buckling strength and post buckling tension reload could be modelled, as shown in figure 6.5. For this analysis, EA of the gusset matched EA of the brace during elastic loading. The tension yield load of the plate was equal to the brace force calculated using NBCC equivalent static method for each combination of seismic risk Zone and structural response factor, R. For the single diagonal braced structures, the buckling load was 85% of the tension yield load. For the cross braced structures, the buckling load was 75% of the tension yield load. For all structures, the post buckling tension reload force was 50% of the tension yield load. The strain hardening modulus was 0.01% of the elastic modulus. The response of the parallel elements shown in figure 6.5 corresponds well with the experimentally and analytically observed behaviour, shown in figure 6.1.

P-Delta effects were considered in all analyses and a constant time step solution scheme was used with a nominal time step of 0.01s. For each analysis the energy imbalance was monitored as an indication of the accuracy of the solution. In a few analyses energy imbalance indicated errors in solution. In those cases, the time step was decreased until the energy imbalance was at least three orders of magnitude less than the total energy - a level which was found to provide a convergent solution. In no case was time history analysis continued beyond the first 30 seconds of the design earthquake record.

In many experiments, single continuous gusset plates loaded in tension have fractured at a total elongation of between 10 mm and 20 mm. In any storey with gusset extension

exceeding 15mm, it is assumed for the purposes of this research that a gusset plate has fractured.

Experimental and analytical results are not available for edge-stiffened gusset plates compressed far beyond 15 mm of inelastic deformation. For this analysis, it is assumed that only one of the two gusset plates connected to any brace may buckle. Inelastic gusset compression is therefore concentrated in the gusset plate which first buckles. Data are not available to support concluding that gussets may carry load in compression beyond 15 mm of inelastic compression. For that reason, a compression deformation limit of 15 mm is imposed.

Combined inelastic gusset deformations beyond the range of -15 mm to +15 mm are considered to represent gusset failure.

6.4 Drift

6.4.1 General

Interstorey drift is presented, by structure type, in figures 6.6 through 6.8. The figures provide drift envelopes for low a/v (LBL, ECL, TFI), medium a/v (TFI, PDI, LPI) and high a/v (LPH, NAH, MNH) events. The NBCC-1995 seismic interstorey drift limit is 2% of storey height, which corresponds to 90 mm for the bottom storey and 72 mm for all other storeys.

6.4.2 Cross Braced Structures

Cross braced structure interstorey drift, summarized in figure 6.6, is generally greatest in the first, seventh and eighth storeys with a uniform and predominantly elastic response

within storeys 2 through 6. Interstorey drift exceeded the 2% limit in the seventh storey of the Zone 3, $R = 3$ structure and in the first and seventh storeys of the Zone 5, $R = 3$ and $R = 4$ structures. The presence of concentration of interstorey drift in the upper storeys generally indicates higher order modes contributing to the structure response more significantly than anticipated by the equivalent static lateral design loads, as described by Humar and Mahgoub, (2000). In the equivalent static lateral design process, the top force V_T accounts for the contribution of higher order modes and, in this case, the method has underestimated the contribution of those modes for medium and low a/v events. The family of curves presented in each of the plots on figure 6.8 show that with increasing a/v , interstorey drift generally decreased. A detailed examination of the maximum storey drift for each event indicates that the ECL and TFI events were most damaging to the structures analysed.

6.4.3 Single Diagonal Braced Structures

Interstorey drift for single diagonal braced structures are summarized in figure 6.7. When compared with the results obtained for cross braced structures, it may be observed that diagonal braced structures suffered more deformation in upper storey and less deformation within the bottom storey – indicating a greater contribution of higher order modes than experienced in the cross braced structures. For a given set of design parameters, diagonally braced structure interstorey drift was less than that predicted for the corresponding cross braced structure. In all cases, calculated interstorey drift was within the 2% NBCC-1995 limit.

6.4.4 M-Braced Structures

M-Braced structure interstorey drift is presented in figure 6.8. As observed for cross braced structures, drift was maximum in the first, seventh and eighth storeys with the most damaging events having in the low a/v group. Calculated drift in the second

through sixth storeys were limited to less than approximately 50 mm. The NBCC-1995 2% drift limit was exceeded in the seventh and eighth storeys of the Zone 5, R = 6 structure and in the seventh storey of the Zone 5, R = 4.5 and Zone 3, R = 4 structures.

6.5 Gusset Plate Deformation

6.5.1 General

Tables 6.4 through 6.9 present the maximum inelastic deformations experienced by gusset plates within each storey for each of the analyses conducted. Nil values indicate that gusset plates remained elastic throughout the entire analysis. Values in bold type indicate tension deformations which exceed the fracture limit of 15 mm total deformation. The scaled earthquakes used for analysis are arranged in increasing order of a/v ratio from left to right. The most damaging earthquakes were those with a/v ratios between approximately 0.5 (ECL) and 1.15 (LPI). Analyses using earthquake records with high a/v ratios generally predicted very little damage. The specific instances of deformations exceeding the fracture limit will be discussed below. The contents of tables 6.4 through 6.9 are presented graphically and in condensed form in figure 6.9.

6.5.2 Gusset Plate Deformations - Cross Braced CBF

Typically, maximum inelastic elongation and compression were approximately equal for the cross braced structures analysed. For any gusset deformation in compression within a storey, an approximately equal tension deformation would occur in the opposing gusset - brace assembly. For that reason, only the maximum of compression and tension deformation are reported in table 6.4.

Calculated gusset plate deformations for cross braced structures generally exceeded those predicted for similar single diagonal braced structures. All structures analysed using Zone 5 earthquakes with a/v between 0.37 (LBL) and 1.67 (PKH) were predicted to have gusset plate failures in both tension and compression in at least one storey, with failure typically occurring in the top two storeys and in the bottom storey. All structures analysed using zone 3 earthquakes were predicted to have failures during at least two events. The fractures were generally predicted in the top two storeys of the structures analysed. Among the zone 3, $R = 1.5$ analyses, only the PDI event have rise to deformations marginally in excess of 15 mm anticipated fracture limit, at 16.2 mm.

6.5.3 Gusset Plate Deformations - Single Diagonal Braced CBF

As expected for the single diagonal braced structures, plates were commonly predicted to buckle but not yield in tension – indicating a bias or asymmetry in the structural response. For example, the zone 5, $R = 3$, PKH time history analysis indicates buckling within the first and fifth storeys without accompanying tension yield. Less frequently, plates were predicted to undergo some tension yielding but remain unbuckled. For example, the zone 5, $R = 2$, LPI time history analysis predicted tension yield without buckling in the seventh storey. Generally, damage was concentrated in upper storeys of structures analysed using earthquake records with a/v ratios between approximately 0.5 and 1.15.

In Zone 3, gusset plate tension failures were not predicted in the $R = 1.5$ structure for any of the time histories analysed. Compression failure of a top storey gusset plate was predicted in the $R=2.0$ structure for both the TFI and LPI events. In both cases the gusset deformation exceeded the deformation limit by only a small margin. For the $R = 3.0$ structure, gusset failures occurred in compression in the seventh storey for the TFI event and in the top storey for the LPI and LBL events. The compression deformation values exceeded the imposed limit by only a small margin in all cases. The predicted gusset elongation in the top storey during the TFI event was 29.5 mm, which significantly exceeds the anticipated fracture limit. The lower storeys of the zone 3, $R = 3$ structure

remained relatively undamaged, however. Predicted gusset elongations in six of the lower seven storeys were less than 2 mm. This concentration of damage in the upper storeys indicates a more significant contribution of higher order modes than predicted using the NBCC equivalent static design method.

The predicted gusset deformation in the seventh storey of the zone 5, the $R = 2$ structure, analysed using the PKH event was 35.9 mm, which significantly exceeds the anticipated extension limit of 15 mm. This structure did not, however, have large predicted gusset tension deformation in any other storey during the PKH event. Combined gusset elongations of less than 1 mm were predicted in the fifth and sixth storeys while the gussets in all other storeys remained elastic in tension. For the $R = 3$ and $R = 4$ structures, numerous gusset plates exceeded both the extension and compression deformation limits during several events. For all cases in zone 5, the extension deformations corresponding to fracture were concentrated on the top storeys with only two occurrences below the sixth storey. In both cases of excessive gusset plate extension below the sixth storey, the maximum deformation was within 10% of the limit value. Those gussets which sustained inelastic extension below the fracture limit in Zone 5, $R = 3$ and 4 structures typically had substantial reserve deformation capacity. In many cases, gussets remained elastic or had small predicted inelastic extension in the second to sixth storeys.

For both the zone 3 and zone 5 structures, failures and large deformations of gusset plates were generally limited to the upper storeys of the structures analysed. This suggests that higher order modes have a more significant influence on the response of these structures than indicated by the equivalent static design method prescribed by the NBCC.

6.5.4 Gusset Plate Deformations – M-Braced Structures

M-Braced structure gusset plate elongations are presented in tables 6.8 and 6.9. It is notable that the structure / event combinations which suffered most severe damage in

compression do not correspond well with those which suffered damage in tension. This is similar to observations made in the single diagonal braced case, where maximum compression deformations did not closely resemble maximum tension deformations. This is characteristic of the seismic events which did give rise to symmetric structural response, especially in the velocity dominated events.

Gusset elongations were typically greatest during the LBL, ECL, TFI and PDI ($a/v < 1.04$) events and were concentrated, as in other bracing configurations, in storeys 1, 7 and 8. Maximum predicted gusset deformation was 25.4 mm extension in storey 7 of the Zone 5, R = 6 structure, during the LBL event. This compares with maximum deformations of 36 mm in storey 7 of Zone 5, R = 4, PDI, Cross Braced and 54.9 mm in storey 8 of Zone 5, R = 4, TFI, Single Diagonal. With reduction of maximum gusset elongation in storeys 1, 7 and 8, increases in gusset elongation in storeys 2 through 6 were also observed among the M-braced structures – indicating a more uniform distribution of damage on structures of this type.

6.6 Beams and Columns

Beams and columns remained predominantly elastic throughout all analyses. In previous studies by Kobeovic and Redwood (1997) and Redwood, Lu, Bouchard and Paultre (1991), it was found that top columns experienced axial forces in excess of capacity during design earthquakes. In the structures analysed herein, column sizes were constant over two storeys, such that the same section is present in the seventh and eighth storeys. This provided a capacity in excess of the minimum capacity required to satisfy the design in the top storey. The provision of stronger-than-required columns in the top storey prevented calculated forces from exceeding their capacity.

6.7 Comparison of Predicted Behaviour with Published Literature

The analytical method and structure geometry used for analysis of concentrically braced frames in this study are consistent with those used by Kobojevic and Redwood (1997) and Redwood, Lu, Bouchard and Paultre (1991) in their analyses of eccentrically braced frame EBF and CBF structures with inelastic brace elements. In this section, a general comparison of the results obtained in this study with those obtained by others is presented.

Redwood, Lu, Bouchard and Paultre (1991) performed analyses of eight storey frames with bay and storey height as shown in figure 6.3. The Redwood, Lu, Bouchard and Paultre (1991) DBF Victoria structure may be compared with the Zone 5, $R = 3$ structure in this study as the design and loading parameters are very similar. It should be noted that the scaled peak ground velocity for the Redwood, Lu, Bouchard and Paultre (1991) study was 0.26 for all records, which differs slightly from the scaling method described in section 6.4.1. The results obtained by Redwood, Lu, Bouchard and Paultre (1991) indicated that, among all earthquake records used for analysis, the Victoria DBF structure would experience the maximum storey drift of ± 40 mm within the seventh storey. This value compares well with the maximum drift of ± 45.8 mm obtained within the seventh storey of the Zone 5, $R = 3$ single diagonal braced structure in this study. The drift reported by Redwood, Lu, Bouchard and Paultre (1991) was greatest in the seventh and first storeys at approximately ± 40 mm and ± 31 mm respectively, followed by the eighth and sixth storeys at approximately ± 25 mm each. Similarly, the maximum drift in the Zone 5, $R = 3$ structure was ± 57.6 mm in the eighth storey, followed by approximately ± 46 mm in the sixth and seventh storeys and ± 33.8 mm in the first storey. The magnitude and distribution of storey drift and, hence, inelasticity found in this study were generally consistent with those obtained for structures similarly designed, loaded and analysed by Redwood, Lu, Bouchard and Paultre (1991).

Comparison of the results obtained in this study with those obtained by Kobojevic and Redwood (1997) also indicated strong similarities in the responses of similarly designed

and loaded structures. In their study, Redwood et al (1991) evaluated the response of shear critical eccentrically braced frames to earthquakes and, as with the Redwood, Lu, Bouchard and Paultre (1991) study, the geometry, design and loading parameters were generally consistent with those used here. Direct comparison of the analytically determined responses of structure in this study with those analysed by Koboevic and Redwood is not possible since the parameters used to describe the response of eccentrically braced frames, such as link deformation and demand to resistance ratios, are not readily comparable to storey drift or inelastic gusset deformation. Consistent with the results obtained here, the results obtained by Koboevic and Redwood for Zone 5, $R = 3$ structures indicated a concentration of inelasticity in the eighth, seventh, sixth and first storeys. It was reported by Koboevic and Redwood (1997) that for Zone 5, $R = 3$ structures, overall drift did not exceed NBCC (1995) limits.

6.8 Discussion – Cross Braced Bay Energy Absorption Characteristics

It may be observed that similar structures designed using similar parameters performed better with single diagonal than with cross braced lateral load resisting systems in the analyses reported herein.

The drift vs. panel shear hysteresis of a single braced panel is similar to the load deformation hysteresis of a single gusset. When deformed such that the bracing is in tension, the tension capacity of the gusset plate may be developed. Upon loading in the opposite direction, the compression capacity of the gusset is reached. The drift versus panel shear hysteresis of the braced panel would be expected to resemble the idealized gusset behaviour shown in figure 6.5. In the case of the deformed cross braced panel, one gusset is always in compression while the other is in tension. Given the idealized behaviour shown in figure 6.5, one would expect pinching of the drift versus panel shear hysteresis in both the second and fourth quadrants – arising from the reduced capacity of the gusset being compressed or the gusset being re-tensioned. Pinching of lateral load-deformation hysteresis of braced panels impairs the energy absorption capacity of cross

braced systems compared to single diagonal systems designed for equal maximum storey shears.

6.9 Conclusions

The responses of twelve steel building structures subject to severe and moderate seismic loading were obtained by non-linear time history analysis. The structures were modelled to represent anticipated behaviour of gusset plates as energy dissipaters. The design loads used to select members and gusset plate load deformation relationships were based on the seismic provisions of the National Building Code of Canada (1995).

Gusset plates located in bottom six storeys of the single diagonal braced structures analysed underwent inelastic deformations in both compression and tension and remained within defined deformation limits in most cases. Beam, column and bracing elements remained predominantly elastic.

Inelastic gusset deformation was generally predicted in the top two storeys and was most severe for earthquakes with a/v between 0.5 and 1.15. Gusset deformation was relatively minor for earthquakes with $a/v > 1.15$ and in the second to sixth storeys of all structures.

For the single diagonal braced structures analysed, the influence of higher order modes imposed demand on the upper storeys which concentrated deformations and failures in those storeys. In many cases of failure in upper storeys, lower storey gusset plates remained elastic.

Cross braced structures were not as effective as single diagonal braced structures at resisting earthquakes. For zone 3 and 5, all cross braced structures analysed were predicted to have gusset plate failures in at least two events. The combination of inelastic gusset compression and elongation within a storey reduces the energy absorption capability of the system.

In the analyses conducted, structures designed using edge-stiffened gusset plates as energy dissipaters were not effective at dissipating energy when subject to zone 5 events. For zone 3 events, single diagonal braced structures designed using $R=1.5$ and $R=2$ were effective at resisting most earthquakes. Cross braced CBF structures using edge stiffened gusset plates as energy dissipaters were generally not effective at absorbing energy when subject to zone 3 or zone 5 loading.

CBF structures employing inelastic gusset plates exhibit seismic responses closely resembling those observed for similarly designed and loaded structures with weak brace – strong gusset and eccentrically braced frame lateral load resisting systems.

It should be noted that the results may not be generalized to other bracing configurations or structure heights since the analysis was conducted on only two bracing configurations and one gravity load structure configuration. Additional research is required to determine the behaviour of other structural configurations as well as the potential use of edge-stiffened gusset plates in seismic retrofit.

Effectiveness of the existing configuration of edge-stiffened gusset plates is limited by deformation capacity, primarily in tension. Additional deformation capacity may be obtained by modifying the arrangement of bracing or by modifying gusset connection geometry. Previously tested Extended Hinge Link (EHL) Gussets by Mullin (Chapter 4) have exhibited deformability in excess of the maximum calculated gusset deformation reported herein.

Table 6.1. Member Sizes – Single Diagonal and Cross Braced Structures

Structure Design Parameters	Storey	Column Size	Single Diagonal Brace Size	Cross Brace Size
Zone 5, R=2	1	WWF 500 x 381	WWF 450 x 342	HSS 304 x 304 x 12.5
	2		WWF 450 x 308	HSS 304 x 304 x 11.5
	3	WWF 500 x 267		
	4		WWF 400 x 303	
	5	W 310 x 158	WWF 400 x 273	HSS 254 x 254 x 8.0
	6		WWF 400 x 220	
	7	W 310 x 67	WWF 400 x 157	HSS 203 x 203 x 8.0
	8		HSS 305 x 305 x 9.5	HSS 152 x 152 x 9.5
Zone 5, R=3 Zone 3, R=1.5	1	WWF 500 x 267	WWF 400 x 243	HSS 203 x 203 x 12.5
	2			HSS 203 x 203 x 11.5
	3	W 310 x 226	WWF 400 x 220	HSS 203 x 203 x 9.5
	4		WWF 400 x 202	
	5	W 310 x 129	WWF 400 x 178	HSS 178 x 178 x 9.5
	6		HSS 305 x 305 x 13	
	7	W 310 x 60	HSS 305 x 305 x 9.5	HSS 178 x 178 x 6.5
	8		HSS 254 x 254 x 9.5	HSS 152 x 152 x 6.5
Zone 5, R=4 Zone 3, R=2	1	WWF 350 x 263	WWF 400 x 202	HSS 203 x 203 x 9.5
	2			
	3	W 310 x 179	WWF 400 x 178	HSS 203 x 203 x 8.0
	4			
	5	W 310 x 107	HSS 305 x 305 x 11	HSS 178 x 178 x 8.0
	6		HSS 305 x 305 x 9.5	HSS 152 x 152 x 9.5
	7	W 310 x 60	HSS 254 x 254 x 11	HSS 152 x 152 x 6.5
	8		HSS 254 x 254 x 8.0	HSS 127 x 127 x 6.5
Zone 3, R=3	1	WWF 400 x 178	HSS 305 x 305 x 11	HSS 178 x 178 x 8.0
	2		HSS 305 x 305 x 9.5	
	3	W 310 x 129		HSS 305 x 305 x 9.5
	4			
	5	W 310 x 86	HSS 305 x 305 x 8.0	HSS 152 x 152 x 6.5
	6		HSS 254 x 254 x 9.5	
	7	W 310 x 60	HSS 254 x 254 x 8.0	HSS 152 x 152 x 6.5
	8		HSS 203 x 203 x 8.0	

Table 6.2 - Member Sizes for M-Braced CBF Structures

Structure Design Parameters	Storey	Column Size	Brace Size
Zone 3, R=3	1	WWF 400 x 303	HSS 254 x 254 x 11
	2		
	3	WWF 400 x 202	HSS 203 x 203 x 11
	4		
	5	W 310 X 143	HSS 178 x 178 x 11
	6		HSS 178 x 178 x 9.5
	7	W 310 X 67	HSS 178 x 178 x 6.4
	8		HSS 127 x 127 x 9.5
Zone 3, R=4.5	1	WWF 400 x 303	HSS 203 x 203 x 11
	2		HSS 178 x 178 x 11
	3	WWF 400 x 202	HSS 128 x 178 x 9.5
	4		
	5	W 310 X 143	HSS 178 x 178 x 8
	6		
	7	W 310 X 67	HSS 152 x 152 x 6.4
	8		HSS 127 x 127 x 6.4
Zone 3, R=6 Zone 5, R=3	1	WWF 400 x 303	HSS 178 x 178 x 9.5
	2		HSS 178 x 178 x 8
	3	WWF 400 x 202	HSS 178 x 178 x 6.4
	4		HSS 152 x 152 x 8
	5	W 310 X 143	HSS 152 x 152 x 6.4
	6		
	7	W 310 X 67	HSS 127 x 127 x 6.4
	8		HSS 101 x 101 x 9.5
Zone 5, R=4.5	1	WWF 400 x 303	HSS 178 x 178 x 8
	2		HSS 152 x 152 x 6.4
	3	WWF 400 x 202	
	4		
	5	W 310 X 143	HSS 127 x 127 x 6.4
	6		
	7	W 310 X 67	HSS 101 x 101 x 9.5
	8		
Zone 5, R=6	1	WWF 400 x 303	HSS 127 x 127 x 9.5
	2		HSS 127 x 127 x 6.5
	3	WWF 400 x 202	
	4		
	5	W 310 X 143	HSS 127 x 127 x 6.5
	6		
	7	W 310 X 67	HSS 101 x 101 x 9.5
	8		

Table 6.3 - Summary of Earthquake Records used in Analysis

Record, Date, Site	Abbreviation	Component	PHA (g)	PHV (m/s)	a/v
Long Beach, Mar. 10, 1933 (Los Angeles Subway terminal)	LBL	N39E	0.064	0.173	0.37
El Centro, Dec. 30, 1934 (El Centro Imperial Valley)	ECL	S00W	0.160	0.209	0.52
Taft, July 21, 1952 (Lincoln School)	TFI	N21E	0.156	0.157	0.99
San Fernando, Feb. 9, 1971, (Pacoima Dam)	PDI	S16E	1.171	1.132	1.03
Loma Prieta 2, Oct 17, 1989 (Eureka Canyon Road)	LPI	0	0.629	0.552	1.14
Parkfield, June 27, 1966 (Cholame, Shandon)	PKH	N85E	0.426	0.255	1.67
Loma Prieta 4, Oct 17, 1989 (USCS/Link Lab, Santa Cruz)	LPH	0	0.442	0.212	2.08
Nahanni, Dec 25, 1985 (Site I: Iverson)	NAH	LONG	1.101	0.462	2.38
Monte Negro, Apr 9, 1979 (Hotel Albatross Basement)	MNH	N00E	0.042	0.016	2.63

Table 6.4 - Maximum Inelastic Gusset Deformation (mm) - Cross Braced CBF

	Storey	LBL	ECL	TFI	PDI	LPI	PKH	LPH	NAH	MNH	
Zone 5	R=2	1	29	1.4	6.2	8.9	3.7	6.6	3.8	8.1	-
		2	22	-	2.9	5	1.7	-	-	-	-
		3	1.5	-	1.1	-	-	-	-	-	-
		4	1.7	-	3.4	-	1.9	-	-	-	-
		5	2	-	1.9	4.3	1.1	-	-	-	-
		6	-	-	1	-	-	-	-	-	-
		7	4.1	-	4	17	3.3	2.3	-	4.3	-
		8	4.6	-	4.5	2.3	5.3	8.6	2.5	3.4	5
	R=3	1	36	10	9.5	24	6.9	7.1	9.5	6.9	-
		2	3.6	-	3.7	3.9	-	1.5	-	1.5	-
		3	1.6	-	-	-	-	-	-	-	-
		4	-	-	-	-	-	-	-	-	-
		5	2.4	-	4	4.9	-	-	-	-	-
		6	-	1	-	1.2	-	-	-	-	-
		7	13	13	17	35	3.6	5.5	-	7.9	-
		8	7.6	9.6	17	12	4.6	7.4	-	5.2	5.7
	R=4	1	38	12	21.7	28	7.2	6.6	14	5.4	-
		2	4.2	-	3.8	3.5	1.4	-	-	1.1	-
		3	1.7	-	-	-	-	-	-	-	-
		4	-	-	1	-	-	-	-	-	-
		5	3.2	-	5.5	5.4	1.9	-	-	1.2	-
		6	-	-	2.4	23	2.2	-	-	-	-
		7	23	13	25	36	8.5	4.4	3.4	6	-
		8	11	16	16	27	9.7	6.5	1.6	7.4	6.9
Zone 3	R=1.5	1	19	5.9	5.8	9.2	1.1	-	3.6	-	-
		2	2.5	-	1.3	1.2	-	-	-	-	-
		3	-	-	-	-	-	-	-	-	-
		4	-	-	-	-	-	-	-	-	-
		5	-	-	1.3	1.4	-	-	-	-	-
		6	-	-	-	-	-	-	-	-	-
		7	6.6	4.3	8	16.2	7.9	-	-	-	-
		8	6.8	5.5	9.5	6.9	13	3.2	-	1.5	1.2
	R=2	1	17	6.5	7.6	10	1	2.9	7.2	-	-
		2	1.4	-	-	-	-	-	-	-	-
		3	-	-	-	-	-	-	-	-	-
		4	-	-	-	-	-	-	-	-	-
		5	1.1	-	1.5	1.3	-	-	-	-	-
		6	-	-	-	-	-	-	-	-	-
		7	11	5.8	18	22	2.3	-	-	1.9	-
		8	8.7	7	7.1	15	9.5	2.8	-	3.1	1.1
	R=3	1	13	3.5	9.3	9.4	2	4.3	6.3	-	-
		2	1.2	-	1	-	6	-	-	-	-
		3	-	-	-	-	-	-	-	-	-
		4	-	-	-	-	-	-	-	-	-
		5	1.9	-	1.7	2.2	-	1.1	-	-	-
		6	-	-	-	1	-	-	-	-	-
		7	23.5	6.7	19.7	23	2.8	8.7	1.2	1	-
		8	8.5	9.6	8.5	20	8.5	4.2	1.1	2.1	1.1

Table 6.5 - Maximum Inelastic Gusset Compression (mm) - Single Diagonal CBF

	Storey	LBL	ECL	TFI	PDI	LPI	PKH	LPH	NAH	MNH		
Zone 5	R=2	1	-	-	-	-	0.85	-	-	-	-	
		2	-	-	-	-	-	-	-	-	-	
		3	-	-	-	-	-	-	-	-	-	
		4	1.52	-	-	-	-	-	-	-	-	
		5	0.17	-	-	-	-	-	0.35	-	-	-
		6	1.61	-	-	3.55	2.25	-	0.45	-	-	-
		7	10.25	8.55	6.25	2.25	1.45	35.55	-	-	-	-
		8	-	-	-	-	2.15	-	-	-	-	-
	R=3	1	8.25	0.95	0.65	1.15	21.55	-	-	-	-	
		2	0.19	-	0.32	-	-	-	-	-	-	
		3	5.05	-	-	-	-	-	-	-	-	
		4	1.65	-	-	-	-	-	-	-	-	
		5	7.45	-	-	-	-	-	-	-	-	
		6	3.25	-	-	1.05	2.35	-	0.01	-	-	-
		7	13.45	5.15	0.25	1.35	5.65	-	-	-	0.43	-
		8	0.9	18.45	1.85	17.35	36.75	2.05	-	1.14	-	-
	R=4	1	9.15	3.75	12.05	13.15	31.95	-	0.71	0.3	-	
		2	5.45	-	-	-	-	-	-	-	-	
		3	6.85	-	-	-	-	-	-	-	-	
		4	3.65	-	-	-	-	-	-	-	-	
		5	11.85	0.45	-	-	-	-	-	-	-	
		6	6.65	2.65	17.85	1.35	-	1.35	-	-	-	-
		7	15.45	8.05	4.55	5.35	10.25	7.45	-	1.4	-	-
		8	2.45	25.55	54.85	20.55	38.25	18.15	-	3.26	1.05	-
Zone 3	R=1.5	1	-	-	-	-	-	-	-	-	-	
		2	-	-	-	-	-	-	-	-	-	
		3	-	-	-	-	-	-	-	-	-	
		4	-	-	-	-	-	-	-	-	-	
		5	-	-	-	-	-	-	-	-	-	
		6	-	-	-	-	-	-	-	-	-	
		7	0.64	-	-	-	-	0.2	-	-	-	-
		8	-	-	13.19	-	-	4.05	-	-	-	-
	R=2	1	-	-	1.35	-	2.05	-	-	-	-	
		2	-	-	-	-	-	-	-	-	-	
		3	-	-	-	-	-	-	-	-	-	
		4	-	-	-	-	-	-	-	-	-	
		5	-	-	-	-	-	-	-	-	-	
		6	0.93	-	-	-	-	-	-	-	-	
		7	1.28	-	4.85	-	2.95	-	-	-	-	
		8	4.45	6.35	11.53	-	10.85	0.98	-	-	-	
	R=3	1	7.98	-	1.52	0.85	2.25	-	-	-	-	
		2	-	-	-	-	-	-	-	-	-	
		3	-	-	-	-	-	-	-	-	-	
		4	-	-	-	-	-	-	-	-	-	
		5	-	-	-	-	-	-	-	-	-	
		6	5	-	1.35	-	-	-	-	-	-	
		7	4.97	1.15	16.35	4.35	2.85	-	-	-	-	
		8	9.55	4.55	29.15	8.85	7.05	0.35	-	-	-	

Table 6.6 - Maximum Inelastic Gusset Extension (mm) - Single Diagonal CBF

		Storey	LBL	ECL	TFI	PDI	LPI	PKH	LPH	NAH	MNH
Zone 5	R=2	1	-	3.55	0.35	-	0.06	1.55	-	-	-
		2	0.36	2.15	-	-	0.42	-	-	-	-
		3	-	-	-	-	-	-	-	-	-
		4	0.42	-	-	-	-	-	-	-	-
		5	0.32	-	1.25	1.35	-	0.12	-	-	-
		6	1.07	-	-	-	-	0.19	-	-	-
		7	-	12.05	8.55	2.35	-	7.35	-	-	-
		8	0.25	6.65	1.85	-	1.25	9.35	0.55	0.67	-
	R=3	1	11.45	6.05	0.75	-	-	0.25	-	-	1.01
		2	11.35	1.35	-	1.95	8.65	-	-	-	-
		3	3.15	0.65	0.13	-	-	0.35	-	-	-
		4	10.65	1.35	-	5.75	-	-	-	-	-
		5	2.25	-	0.25	-	-	2.95	-	-	-
		6	16.35	-	-	26.15	2.65	0.65	-	-	-
		7	7.05	18.95	2.15	24.35	5.15	9.05	-	-	-
		8	8.05	10.65	-	22.55	30.45	0.65	0.55	9.72	-
	R=4	1	21.05	5.65	14.45	-	-	4.45	0.6	0.81	1.75
		2	6.65	3.55	3.25	3.85	7.15	0.75	0.13	-	-
		3	10.95	1.05	-	-	-	0.25	-	-	-
		4	10.75	1.55	2.75	10.35	-	1.45	-	-	-
		5	8.55	4.05	5.75	-	-	4.85	-	-	-
		6	15.15	2.95	14.85	28.45	2.25	1.95	-	0.18	-
		7	10.35	23.95	43.75	7.35	4.05	23.05	-	-	-
		8	7.05	15.95	12.75	30.65	27.45	8.9	2.05	6.32	-
Zone 3	R=1.5	1	-	-	2.75	-	-	-	-	-	-
		2	-	-	-	-	0.5	-	-	-	-
		3	-	-	-	-	-	-	-	-	-
		4	-	-	-	-	-	-	-	-	-
		5	-	-	-	-	-	-	-	-	-
		6	10.25	-	-	-	-	-	-	-	-
		7	6.95	-	4.05	-	-	0.42	-	-	-
		8	12.55	1.15	12.45	-	16.85	-	-	-	-
	R=2	1	3.38	-	7.35	-	-	-	-	-	-
		2	1.96	-	4.35	-	2.65	-	-	-	-
		3	1.57	-	-	-	-	-	-	-	-
		4	3.81	-	-	-	-	-	-	-	-
		5	2.39	-	-	-	-	-	-	-	-
		6	13.85	-	2.52	0.75	-	-	-	-	-
		7	1.75	1.05	11.05	-	-	3.23	-	-	-
		8	16.05	6.15	24.25	2.55	19.85	-	-	-	-
	R=3	1	18.85	-	0.34	-	-	-	-	-	-
		2	8.35	-	5.85	-	2.35	-	-	-	-
		3	2.35	-	1.35	-	-	-	-	-	-
		4	8.61	-	2.65	-	-	-	-	-	-
		5	13.85	-	-	-	-	-	-	-	-
		6	7.75	-	3.15	18.15	2.55	0.75	-	-	-
		7	20.65	11.55	23.05	-	-	-	-	-	-
		8	7.25	3.65	9.85	18.65	21.25	0.45	0.92	-	-

Table 6.7 - Maximum Inelastic Gusset Compression (mm) – MBF

	Storey	LBL	ECL	TFI	PDI	LPI	PKH	LPH	NAH	MNH	
Zone 5	R=3	1	16.5	1.1	6.7	12.2	3	10.9	-	4.1	-
		2	8	-	3.9	6.4	1.8	6.4	-	1.8	-
		3	9.3	-	4.2	6.3	2.2	5.1	-	2.8	-
		4	6.9	1.2	7.3	13.3	5.4	3.9	-	2.8	-
		5	5	-	2.7	6	2.1	1.9	-	2.4	-
		6	1.5	-	1.9	3.1	0	0	-	-	-
		7	5.7	-	5.5	14.4	3.9	10.9	-	9.9	2.6
		8	4.4	-	5.4	5.3	5.8	8.6	4.2	4.2	5.8
	R=4.5	1	16.9	3.8	1.2	14.8	3.5	6.4	2.8	7.7	-
		2	9	1.6	6.3	7.6	2	2.3	-	3.2	-
		3	11.5	3.1	5.2	6.9	2.6	2.5	-	1.7	-
		4	9.1	4.5	10	14.1	3.7	3.1	-	1.7	-
		5	4.5	3.5	5	6	2.2	1.6	-	1.6	-
		6	1.7	1.5	3.1	4.6	2.1	-	-	-	-
		7	12.8	9.4	13.8	22.8	6.9	12.6	1	7.6	-
		8	6	9	8.9	12.5	6.5	10.8	2.5	6.2	7.5
	R=6	1	16.5	3.7	17.8	16.4	3.1	4	7.3	6.1	-
		2	9.8	2.3	8.7	8.4	1.4	1	2.1	2.4	-
		3	11.4	2	5.2	6.9	2.3	-	1.1	-	-
		4	12.7	2.5	7.1	13.9	7.3	1.5	1.1	2	-
		5	4.8	2.3	8.3	6.3	3.4	2.2	1.2	1.7	-
		6	1.9	1	4.4	5.6	2.5	1.1	-	-	-
		7	13.7	9.8	24.8	24.8	7.4	12.9	4.6	6.9	2.9
		8	8.9	18.1	20.7	20.9	6.9	7.5	4.3	4.7	6.9
Zone 3	R=3	1	14	-	4.9	4.7	1.6	1.4	1.8	3.2	-
		2	7.8	-	-	2.2	0	0	-	-	-
		3	6.7	-	-	1.4	0	0	-	-	-
		4	5.3	1	-	2.7	1.1	1.2	-	-	-
		5	2.5	-	-	3.2	2.5	1.9	-	-	-
		6	-	-	-	-	-	-	-	-	-
		7	7.4	7.1	10.7	19.6	9.2	2.2	-	2.1	-
		8	6.5	6.6	10.2	8.7	13.4	5.4	-	2.7	1.1
	R=4.5	1	13.5	2.7	6.4	5.9	1.4	-	5.3	-	-
		2	8.4	-	2.9	2.5	-	-	2	-	-
		3	9	1.3	1.7	2	-	-	2.2	-	-
		4	8.7	0	2.7	2.9	-	-	1.9	-	-
		5	5.3	1.5	2.6	3.4	-	-	1.3	-	-
		6	-	-	-	10.4	-	-	-	-	-
		7	8.4	13.4	19.4	24.6	4.4	1.5	1.5	4.4	-
		8	10.5	7.9	6.8	16.7	11.1	3.1	1.1	3.7	1.6
	R=6	1	9.3	2.7	8.2	6.6	1.3	1.8	6.7	-	-
		2	6.1	-	3.8	2.8	-	-	3.4	-	-
		3	6.9	-	2.1	3.2	-	-	2.7	-	-
		4	7.2	-	3.1	3.7	-	-	1.7	-	-
		5	5.7	2.1	3.1	4.5	-	-	-	-	-
		6	1.2	-	-	2.1	-	-	-	-	-
		7	14	13.7	19.7	24.6	4.7	6.7	2.4	1.9	-
		8	10	10.1	11.8	21.3	9.7	7.1	1.3	4	1.3

Table 6.8 - Maximum Inelastic Gusset Extension (mm) – MBF

	Storey	LBL	ECL	TFI	PDI	LPI	PKH	LPH	NAH	MNH	
Zone 5	R=3	1	12.8	-	3.6	1.5	-	-	-	1.5	-
		2	7.9	-	-	-	-	-	-	-	-
		3	10.4	-	1.1	-	-	-	-	-	-
		4	9.3	-	4.3	-	-	-	-	-	-
		5	6.8	-	1.6	1.1	-	-	-	-	-
		6	-	-	1.5	-	-	-	-	-	-
		7	4.9	-	6.7	3.4	2.1	2.1	-	1.2	-
		8	1.6	-	6.6	1.9	3.4	1.7	-	-	1.3
	R=4.5	1	16.8	6.8	5.4	1.5		4.2	2.8	9.8	
		2	8.6		2.9					2	
		3	11.1		2.7						
		4	12.4	2.4	2.4					1.1	
		5	7.9	3	1.5						
		6	1.8	1.7	0						
		7	21.2	10.4	12.5	6.7	3.8	2.9		5.9	
		8	7.6	7.8	9.9	1.9	5.1	5.5		3.2	1.8
	R=6	1	19.7	10.6	8.3	2.9	1.1	5.3	6.3	7.3	-
		2	11.3	-	3.6	-	-	1.1	-	3.4	-
		3	13.7	-	1.5	-	-	1.9	-	1.7	-
		4	16.2	1.2	3.1	-	-	1.5	-	1.5	-
		5	9.4	1.3	3.3	1.8	-	1.6	-	1.2	-
		6	4.1	1.1	-	-	-	-	-	-	-
		7	25.4	15.1	6.9	7.2	3.4	3.3	-	6.4	1.8
		8	13.1	8.5	10	4.9	6.2	2.8	1.1	4	1.3
Zone 3	R=3	1	7.8	-	12.8	-	-	-	-	2.9	-
		2	2.7	-	-	-	-	-	-	-	-
		3	1.6	-	-	-	-	-	-	-	-
		4	1.4	-	-	-	-	-	-	-	-
		5	1.4	-	-	-	-	-	-	-	-
		6	-	-	-	-	-	-	-	-	-
		7	3.6	3.7	7.5	3.1	-	-	-	-	-
		8	3.3	4.6	6.1	1.8	2.3	1.4	-	1.5	-
	R=4.5	1	8.7	1.9	1.3	1.2	-	1	-	-	-
		2	4.2	-	-	-	-	-	-	-	-
		3	4.4	-	-	-	-	-	-	-	-
		4	3.2	-	-	-	-	-	-	-	-
		5	3.1	-	-	-	-	-	-	-	-
		6	-	-	-	-	-	-	-	-	-
		7	15.1	9.6	5	6.2	-	-	-	6.3	-
		8	6.9	3.8	2.5	2.5	2.3	-	-	2.6	-
	R=6		8.6	2.5	-	-	-	2.2	2.4	-	-
			4.6	-	-	-	-	-	-	-	-
			5.1	-	-	-	-	-	-	-	-
			4.6	-	-	-	-	-	-	-	-
			4.8	-	-	-	-	-	-	-	-
			-	-	-	-	-	-	-	-	-
			23	10.2	3.2	1.9	1.4	1.7	2.1	1.4	-
			9.4	4.4	5.6	4.2	4.7	2.3	1.4	2.6	-

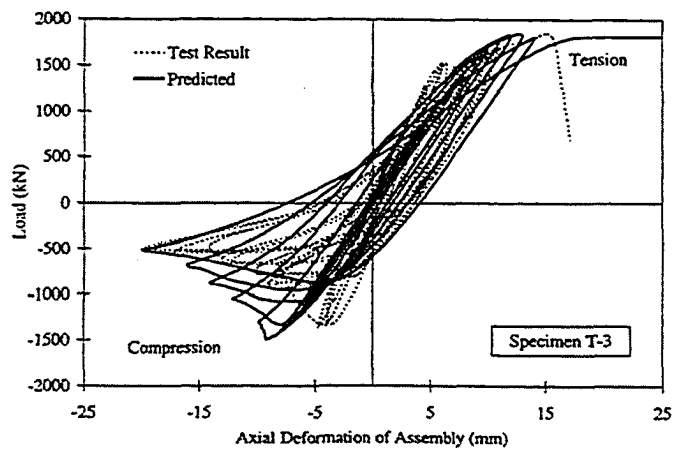
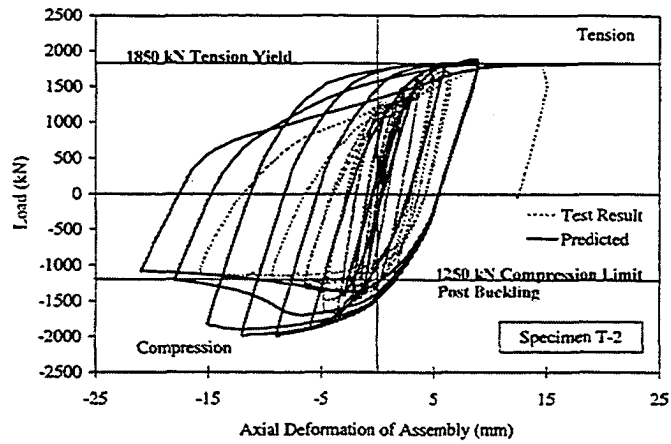
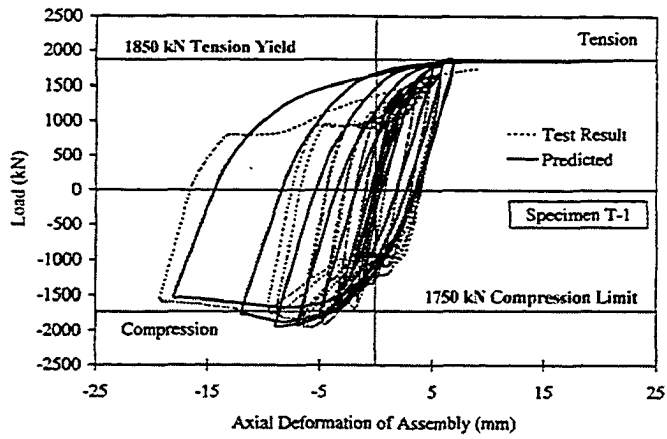
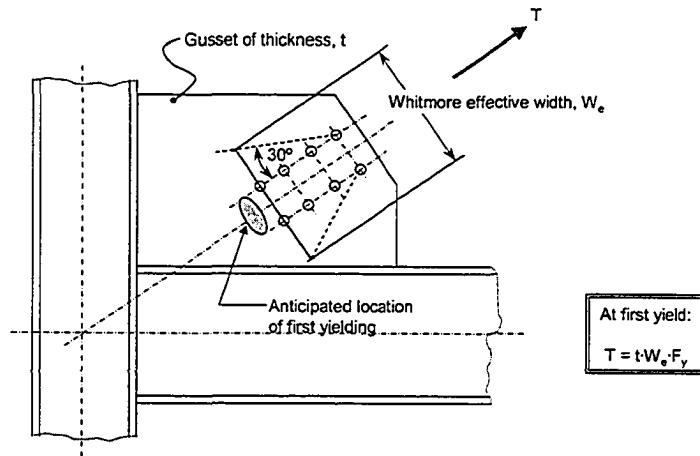
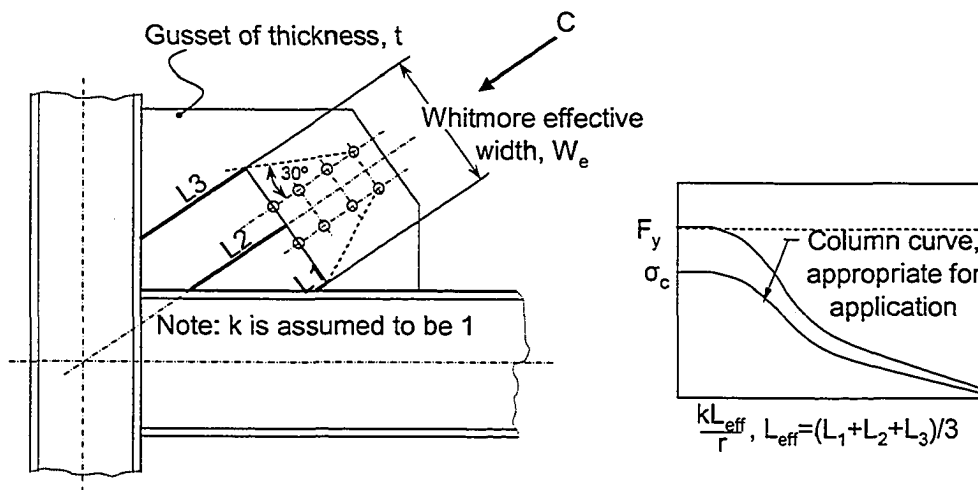


Figure 6.1 – Gusset Hysteresis, taken from Nast (1999)



Whitmore



Thornton

Figure 6.2 – Whitmore (Tension) and Thornton (Compression) Gusset Ultimate Load Models

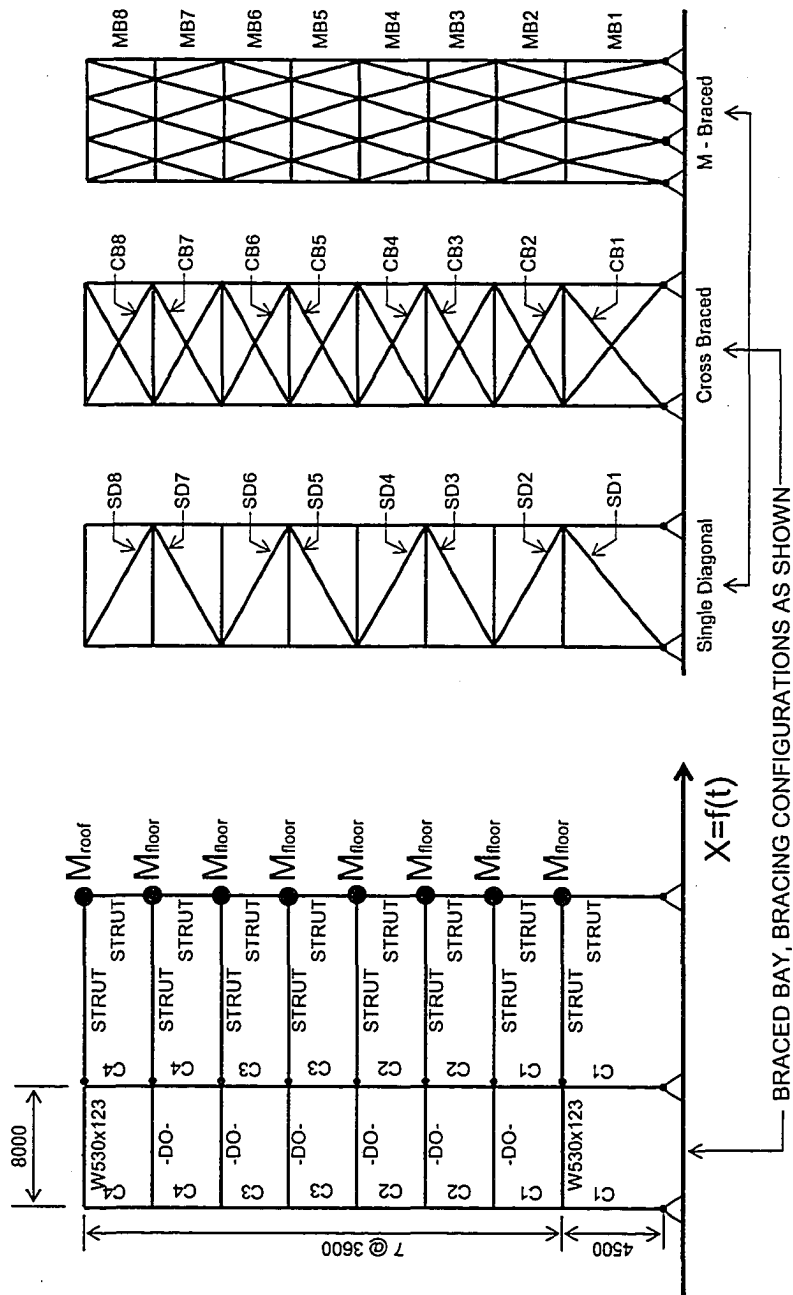
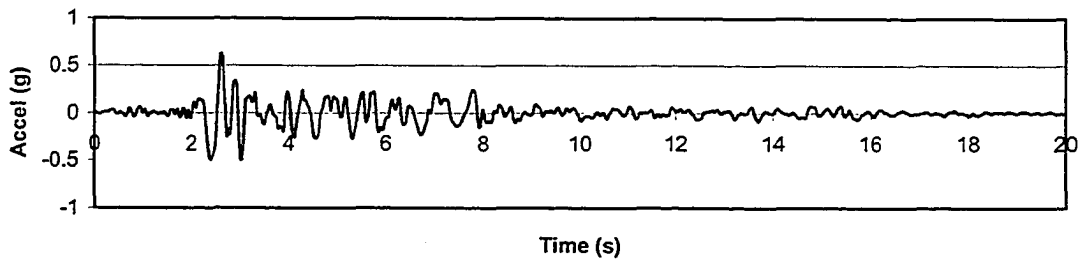
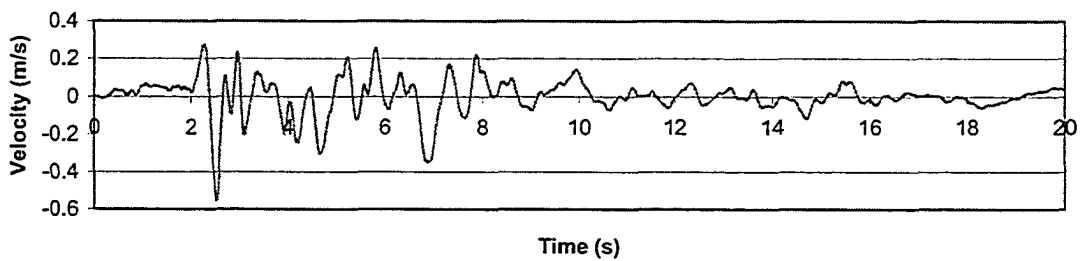


Figure 6.3 – Structure General Arrangement and Bracing Configuration

LPI (Loma Prieta 2, 0°) - Acceleration (g)



LPI (Loma Prieta 2, 0°) - Velocity (m/s)



LPI (Loma Prieta 2, 0°) - Displacement (m)

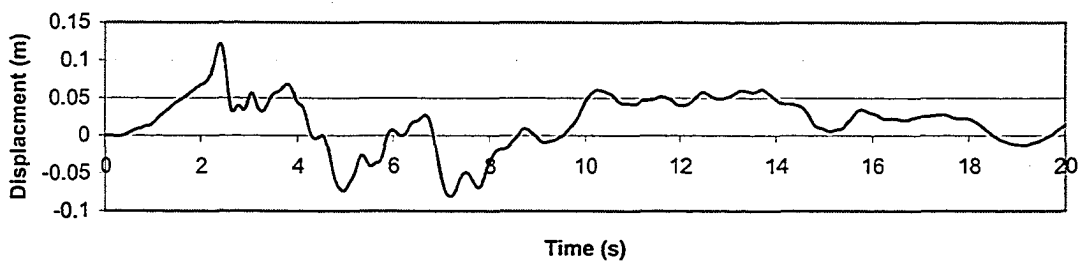


Figure 6.4 – Loma Prieta (LPI) Event Unscaled Acceleration, Velocity and Displacement

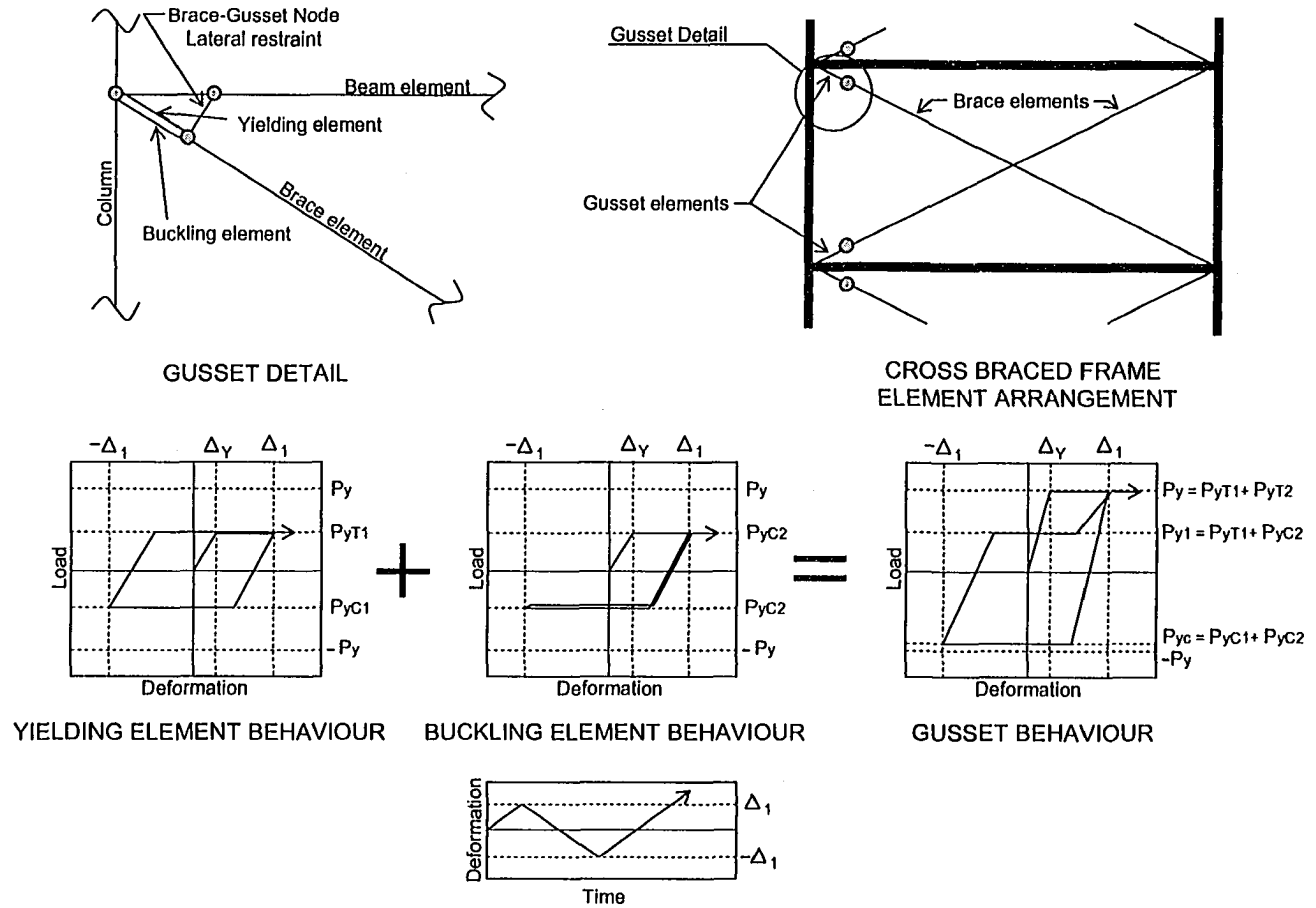


Figure 6.5 – Gusset Plate Model Employing Parallel Inelastic Bar Elements

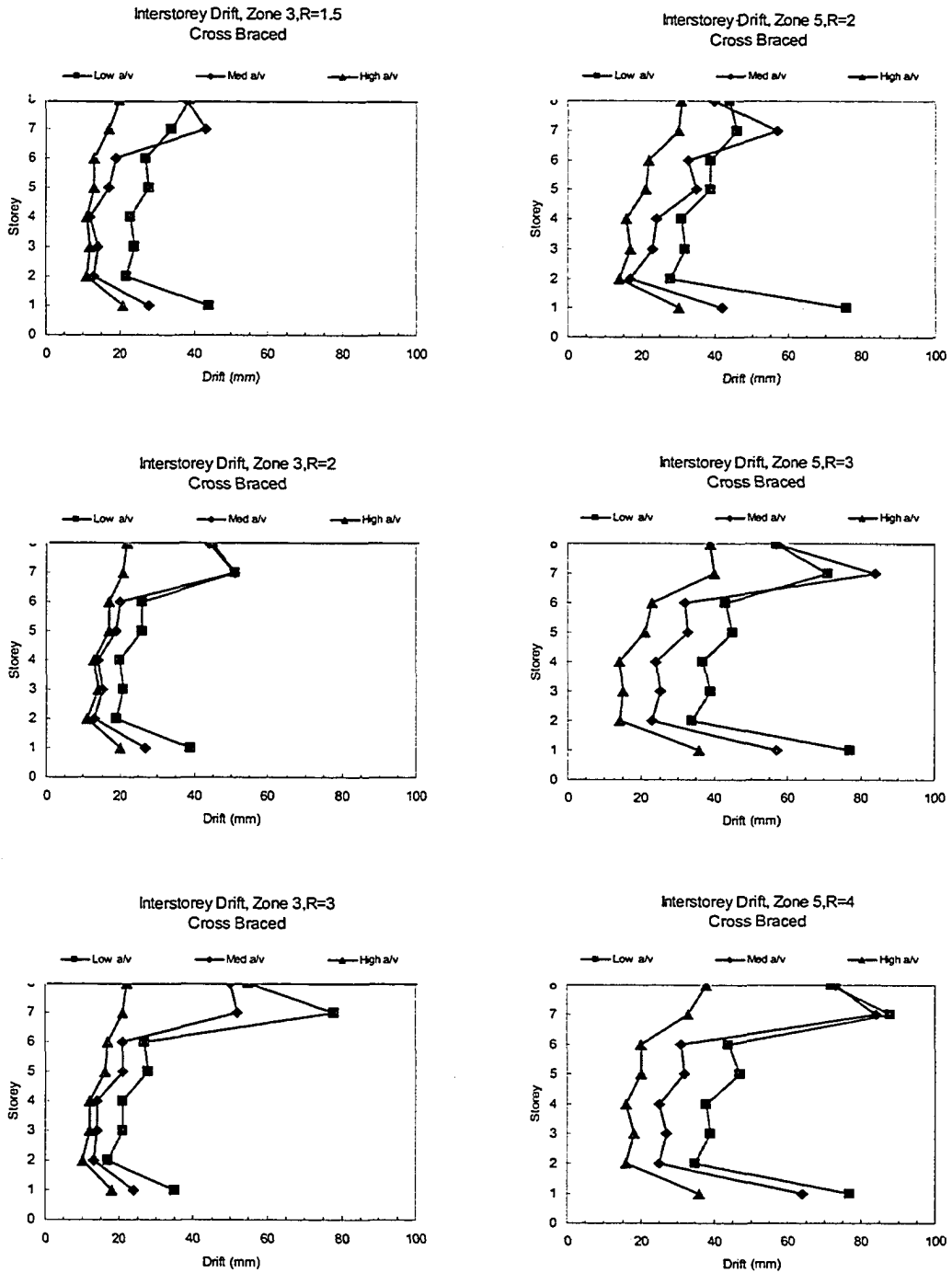


Figure 6.6 – Cross Braced Structures Interstorey Drift Envelopes

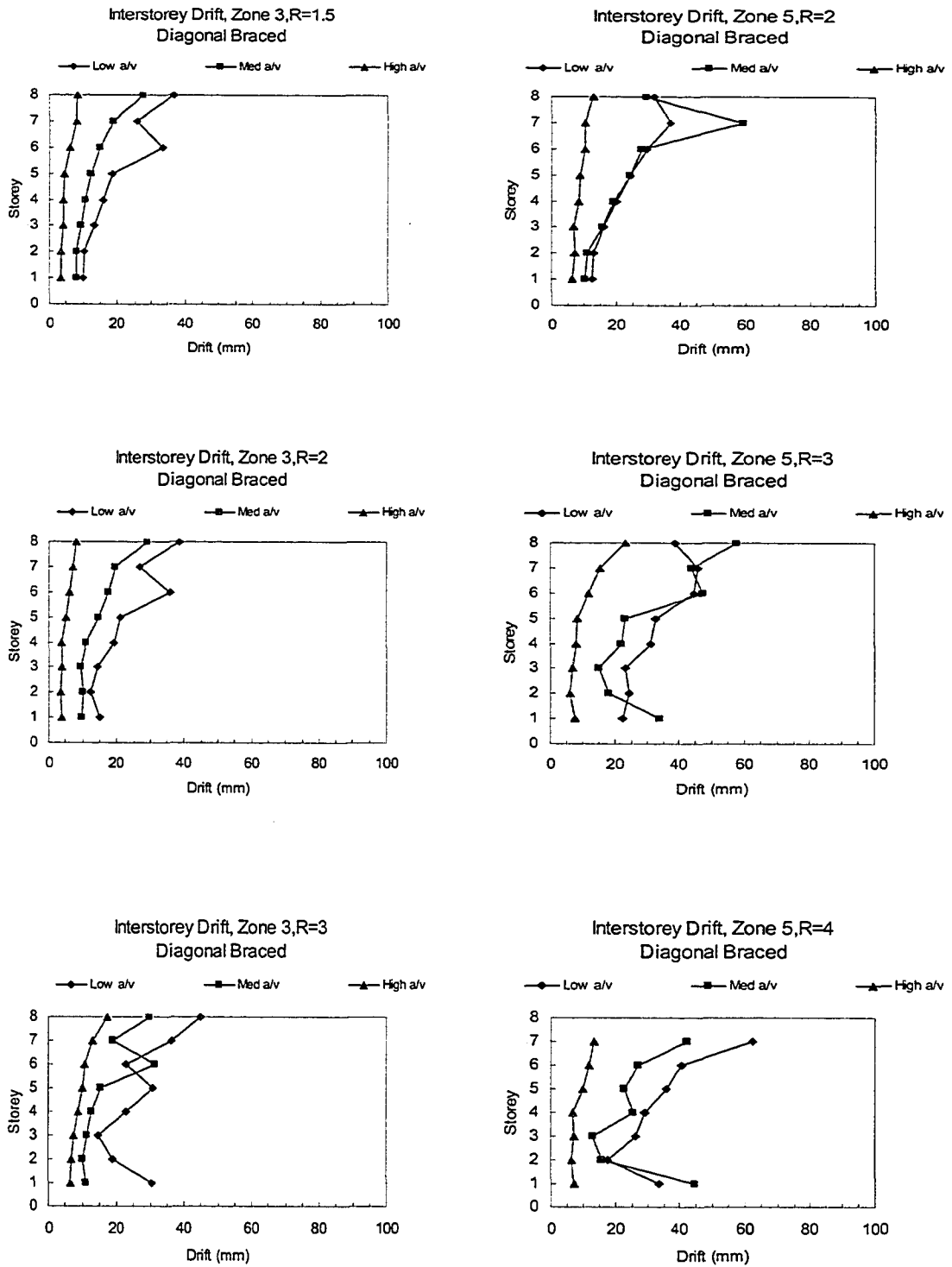


Figure 6.7 – Diagonal Braced Structures Interstorey Drift Envelopes

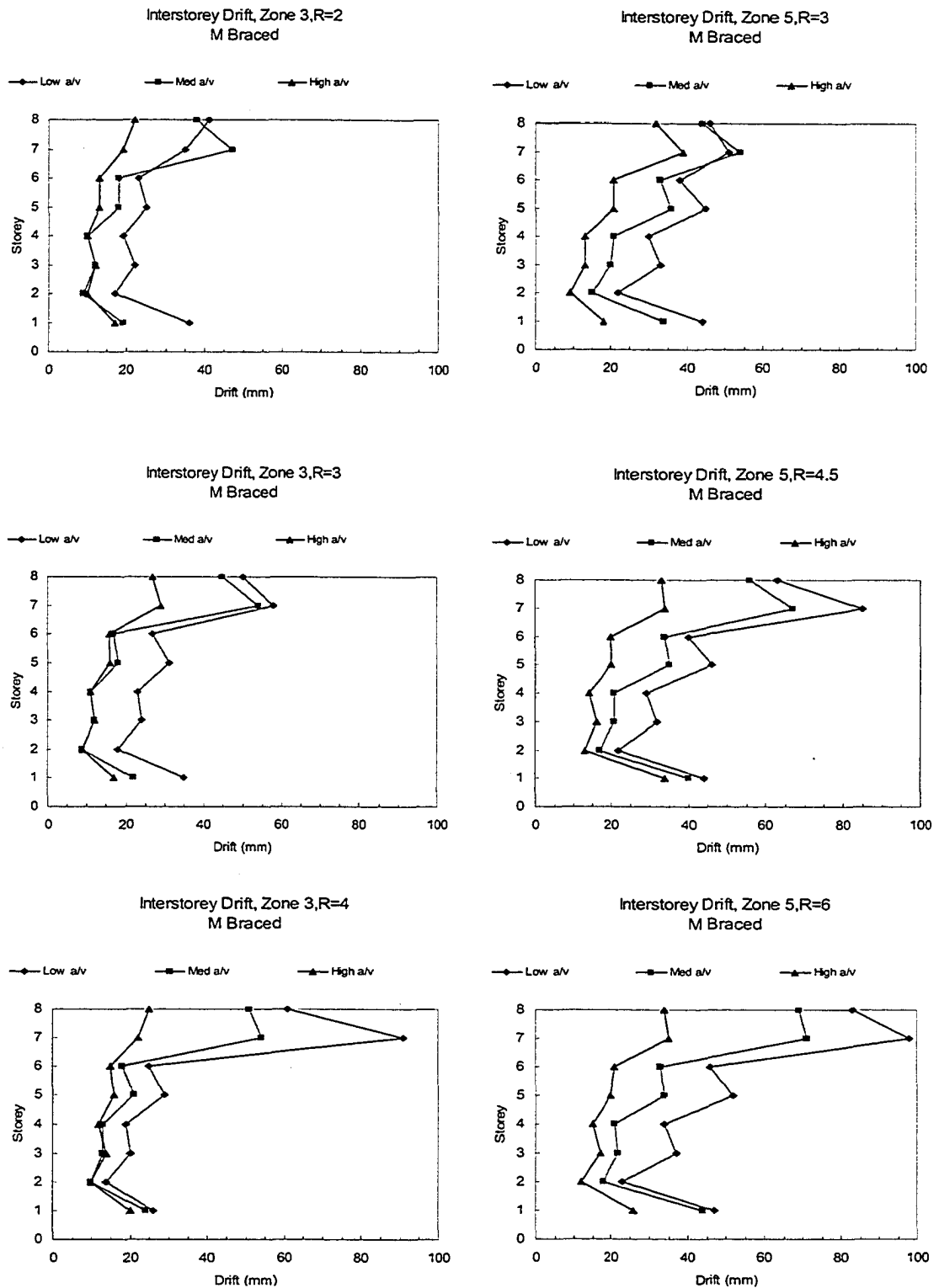


Figure 6.8 – M-Braced Structures Interstorey Drift Envelopes

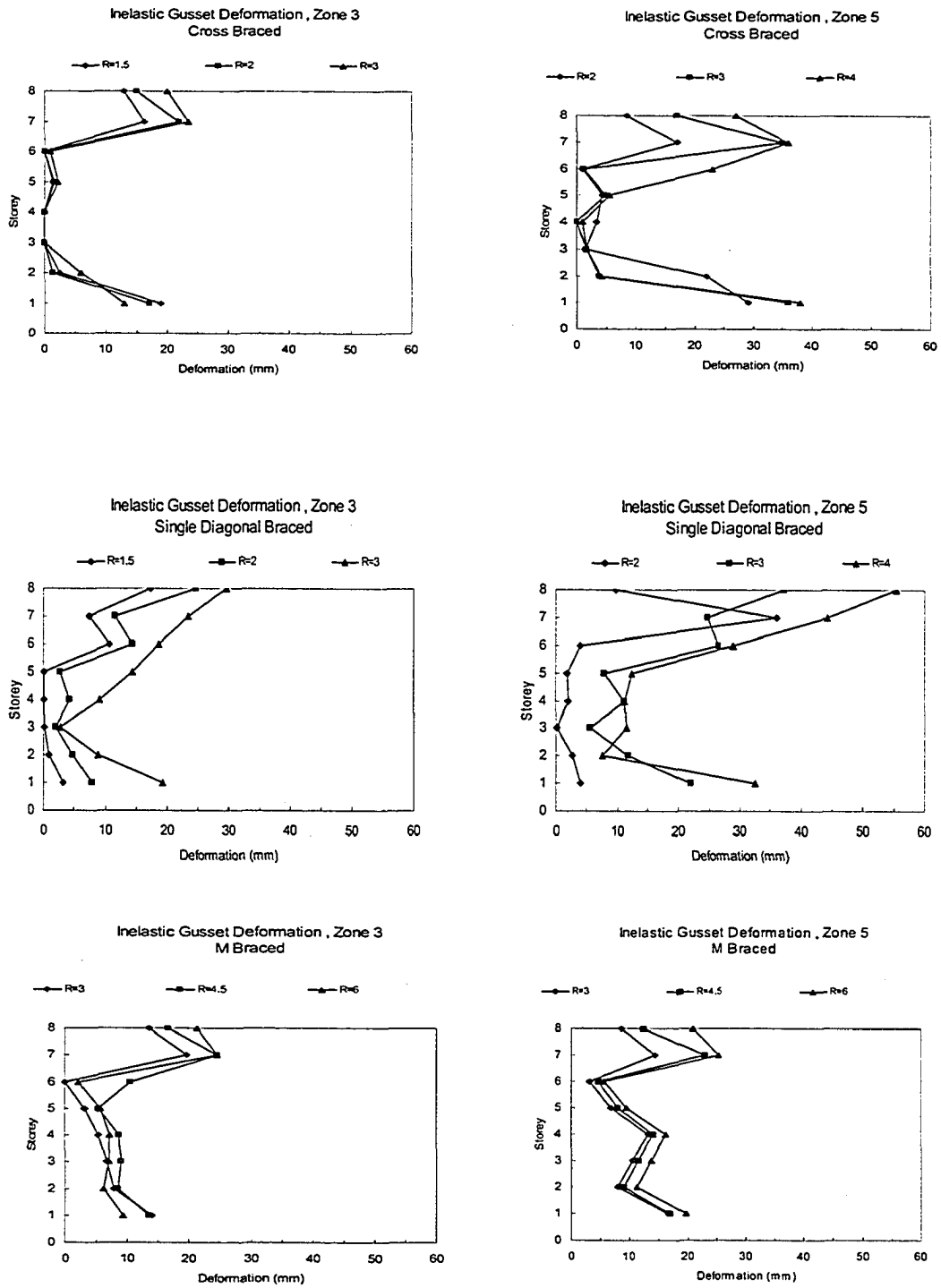


Figure 6.9 - Gusset Inelastic Deformation Envelopes

6.10 References

CAN/CSA-S16.1-94, 1995. Limit States Design of Steel Structures, Canadian Standards Association, Rexdale, Ontario.

Chien, E., 1987. "Multi-Storey Building Design Aid." Canadian Institute of Steel Construction, Willowdale, Ontario.

Hu, S.Z., and Cheng, J.J.R., 1987. "Compressive Behaviour of Gusset Plate Connections." Structural Engineering Report No. 153, Department of Civil Engineering, University of Alberta, Edmonton, Alberta.

Humar, J.L., and Mahgoub, M., 2000. "Accounting for Higher Order Mode Effects in UHS Based Design." Discussion Paper, Canadian National Committee on Earthquake Engineering (CANCEE).

Kobeovic, S., and Redwood, R., 1997. "Design and Seismic Response of Shear Critical Eccentrically Braced Frames." Canadian Journal of Civil Engineering, 24: 761 – 771.

Nast, T.E., Grondin, G.Y., and Cheng, J.J.R., 1999. "Cyclic Behaviour of Stiffened Gusset Plate-Brace Member Assemblies." Structural Engineering Report No. 229, Department of Civil Engineering, University of Alberta, Edmonton, Alberta.

NRCC, 1995. National Building Code of Canada. Associate Committee on the National Building Code, National Research Council of Canada, Ottawa, Ontario.

Powell, G.H., 1993. DRAIN-2DX Element Description and Users Guide for Element TYPE01, TYPE02, TYPE04, TYPE06, TYPE09 and TYPE15 Ver. 1.10 Report No. UCB/SEMM-93/18, Department of Civil Engineering, University of California, Berkeley, California.

Prakash, V., Powell, G.H., and Campbell, S., 1993. DRAIN-2DX Base Program Description and Users Guide. Ver. 1.10, Report No. UCB/SEMM-93/17, Department of Civil Engineering, University of California, Berkeley, California.

Rabinovitch, J.S., and Cheng, J.J.R., 1993. "Cyclic Behaviour of Steel Gusset Plate Connections." Structural Engineering Report No. 191, Department of Civil Engineering, University of Alberta, Edmonton, Alberta.

Redwood, R.G., Lu, F., Bouchard, G., and Paultre, P., 1991. "Seismic Response of Concentrically Braced Steel Frames." Canadian Journal of Civil Engineering, 18(6), pp 1062 - 1077.

Redwood, R., and Channagiri, V.S., 1991, "Earthquake Resistant Design of Concentrically Braced Steel Frames." Canadian Journal of Civil Engineering, 18, pp 839 – 850.

Walbridge, S.S., Grondin, G.Y., and Cheng, J.J.R., 1998. "An Analysis of the Cyclic Behaviour of Steel Gusset Plate Connections." Structural Engineering Report No. 225, Department of Civil Engineering, University of Alberta, Edmonton, Alberta.

Walbridge, S.S., Grondin, G.Y., and Cheng, J.J.R., 1998. "An Analytical Study of the Cyclic Behaviour of Steel Gusset Plate Connections." Proceedings of the Annual Conference of the Canadian Society for Civil Engineering, Vol IIIa, pp. 107 to 116.

Yam, C.H.M., and Cheng, J.J.R., 1993. "Experimental Investigation of the Compressive Behaviour of Gusset Plate Connections." Structural Engineering Report No. 194, Department of Civil Engineering, University of Alberta, Edmonton, Alberta.

Yam, C.H.M., and Cheng, J.J.R., 1994. "Analytical Investigation of the Compressive Behaviour and Strength of Steel Gusset Plate Connections." Structural Eng. Report No. 207, Department of Civil Engineering, University of Alberta, Edmonton, Alberta.

7. DUCTILE GUSSET PLATES AS SEISMIC RETROFIT ELEMENTS IN GRAVITY LOAD DESIGNED CONCRETE FRAMES⁹

7.1 Introduction

Reinforced concrete frames proportioned primarily on the basis of gravity load effects and without consideration of ductility in detailing are referred to a Gravity Load Designed (GLD) frames. Reinforced concrete GLD frames can behave in a non-ductile manner when subjected to earthquake induced cyclic loading, Kunnath, Hoffmann, Reinborn and Mander (1995). GLD frames constructed with columns possessing flexural capacity less than that of connected beams are especially susceptible to severe damage or collapse in strong earthquakes. The damage to these structures is typically concentrated at the ends of the columns - where moment arising from earthquake induced deformation is greatest. With significantly inelastic cyclic loading, such columns accumulate damage, exhibit reduced flexural capacity and reduced stiffness as shown in figure 7.1. With strength and stiffness degradation, inter-storey drift increases, resulting in increased damage to non-structural components and increased likelihood of collapse.

By retrofitting a lateral load resisting system within non-ductile GLD frames, storey drift may be reduced. If the storey drift is kept sufficiently small, damage to columns may be reduced or eliminated, thus preventing collapse or severe damage to GLD structured during earthquakes.

Properly proportioned gusset plates have been shown in analysis by Walbridge, Grondin and Cheng (2000) and testing by Rabinovitch and Cheng (1993) and Nast, Grondin and Cheng (1999) to exhibit stable and open load deformation hysteresis as shown in figure 7.2. When edge stiffened gusset plates are combined with bracing such that inelasticity is confined within the gusset plates and braces remain elastic during seismic loading, the system is referred to as a “strong brace – weak gusset” system. The characteristics of

⁹ A version of this chapter is under revision for submission to the Canadian Journal of Civil Engineering.

strong brace - weak gusset systems include stable post buckling load and open hysteresis, appropriate for energy absorbing elements in seismically loaded structures Nast, Grondin and Cheng (1999). While significant research regarding the behaviour of individual gusset plates and gusset-brace assemblies has been completed, little information is available regarding the response of, or demand on, inelastic gussets in seismically loaded structures.

The purpose of this research is to evaluate the effectiveness of edge stiffened gusset plates within strong brace - weak gusset systems as energy absorbing elements in GLD frames, retrofit with concentrically braced steel frames.

An analytical study was conducted to assess the effectiveness of concentric bracing, designed to employ gusset plates as energy dissipaters within a specific GLD concrete frame. An eight storey, five bay reinforced concrete frame, with the characteristics of a GLD structure, was modelled and subjected to nine scaled earthquake acceleration records, scaled to correspond with the intensity of an NBCC, NRCC (1995), zone 5 design event.

The bay in which retrofit bracing was placed with for analysis was of the same dimensions and loading used in previous steel frame analyses by Kobeovic and Redwood (1997) and Redwood, Lu, Bouchard and Paultre (1991) and for the structure designed in the Canadian Institute of Steel Construction high rise building design guide Chien (1987). Unconfined concrete columns were modelled using DRAIN -2DX, Prakash, Powell and Campbell (1993), Element TYPE 15, Powell (1993). A lumped plasticity approach was used to model inelastic flexural behaviour during seismic loading.

Three retrofit concentric bracing scenarios were analyzed and are depicted in figure 7.3. The first scenario was retrofit of cross bracing, rising in one storey increments within the center bay, and connected to the GLD frame with elements configured to model the load-deformation behaviour of stocky edge stiffened gusset plates. The second scenario was similar to the first, except the gusset behaviour model corresponded with observed

behaviour of slender gusset plates. The third scenario employed a double chevron bracing configuration which, within each braced panel, takes the form of a letter “M”. That configuration, hereinafter referred to as the “M-braced” configuration, was connected to the gravity framing using connection elements configured to model stocky gusset behaviour. Structural retrofit elements were proportioned based on $R=2$ and $R=3$ and lateral loading as defined in NBCC 1995, NRCC (1995).

7.2 Gusset Plate Behaviour

Analytical and experimental studies of individual gusset plates subject to cyclic and monotonic loading have been completed by Hu and Cheng (1987), Yam and Cheng (1993), Rabinovitch and Cheng (1993), Walbridge, Grondin and Cheng (1998) and Nast, Grondin and Cheng (1999). Some of gusset plates tested and analysed included stiffeners along the free edges. The load-deformation hysteresis observed for plates without edge stiffeners generally exhibits post-buckling compression capacity which is significantly less than the first buckling load and tension ultimate load of the plate. Decreasing stiffness, or softening, of unstiffened gusset plates can also be observed during post-buckling compression excursions. Softening and loss of compression capacity is not desirable for energy dissipating elements in seismically loaded structures. As such, unstiffened gussets will not be considered in this analysis. Edge stiffened gusset plates generally have increased post-buckling compression capacity when compared to similar gusset plates without edge stiffening, and can maintain that capacity through multiple compression excursions when cyclically loaded. Example load deformation hysteresis, derived from finite element analyses by Walbridge (1999) are provided in figure 7.4. It can be seen in figure 7.4 that stocky plates, i.e. those that have a lower slenderness (kl/r) as defined by Thornton (1984), exhibit a higher ratio of T_R/C_R than more slender plates as well as a smaller loss of compression capacity after buckling.

In tension, gusset plates exhibit near linear load-deformation relationships up to a limit load, which correlates yield stress acting on the Whitmore (1952) effective area of the

gusset plate. Further tensioning deformation produces a plateau where load increases slowly with increasing deformation. During the compressing cycle, edge stiffened gussets exhibit a linear load deformation relationship to a buckling load, corresponding to the Thornton (1984) compression capacity of the gusset plate. That buckling load corresponds to the maximum compression load reached during out-of-plane displacement of the central region of the gusset plate. The out-of-plane displacement of the plate is confined, by the stiffened edges, to that part of the plate just beyond the end of the brace connection. As shown in figure 7.4, for slender gussets, the buckling load observed in the first buckling cycle is much greater than that maximum load observed in subsequent compression cycles. After buckling, compression load decreases slowly with increasing deformation. For stocky gussets, post buckling compression capacity remains more nearly constant with continued load cycling. Upon reloading in tension edge stiffened gusset plates sustain a force somewhat less than the Whitmore tension capacity until the buckled region straightens. Straightening occurs approximately when the axial displacement of the gusset plate just exceeds the maximum elongation experienced by the plate in its loading history. After straightening, the plate tension capacity again corresponds with the Whitmore load.

In tests by Mullin (Chapter 3), edge stiffened gusset plates have reached a limit state of fracture in tension. Fracture has consistently been observed in gusset plates across the bolt line nearest the free end of the connected brace member. The axial deformation at first fracture has typically ranged from 10mm to 20 mm in tests. The ultimate load observed in tests corresponds approximately with the initiation of fracture along the line between the bolts nearest the end of the brace member. With continued deformation beyond ultimate, load decreases until cracks coalesce along the line across the inner most row of bolts. After completion of the crack along the inner most row of bolts and with increasing deformation cracks typically grow between bolt holes along the sides of the connection region. As cracks in that region grow, load decreases until cracks coalesce to complete the separation of the gusset region bounded by bolt holes. This failure mode is commonly referred to as “block tearing” or “block shear” and is evaluated in AISC-ASD

(1989), AISC-LRFD (1995) and CAN/CSA-S16.1-00 (2003) standards using equations developed by Hardash and Bjorhovde (1985).

In tests by Mullin (Chapter 3), the deformation required to complete the fracture around the bolted region varied with connection length, with short connections sustaining less deformation than long connections prior to complete fracture. Very short connections (2 rows of bolts, 76 mm on center) have rapidly lost capacity after completion of first fracture in tests by Mullin (Chapter 3), with complete loss of capacity at 30 mm deformation. Very long connections (7 rows of bolts, 76 mm on center) have sustained deformations up to 75 mm before completion of fracture. Based on the body of data available, deformation at first fracture typically ranges from 10mm to 20mm, for a wide variety of gusset configurations and connection sizes. For this research, an assumed deformability of 15mm will be used for evaluation of individual gussets.

Since gusset plates exhibit an increasing load versus deflection behaviour after yielding, one might assume that gusset plates on opposite ends of a single brace, using material of controlled strength and toughness, could each deform inelastically at opposite ends of the connected brace. In design and fabrication of real structures, it may be difficult or impossible to ensure that gussets on opposite ends of braces are sufficiently similar to ensure inelasticity in both prior to fracture in one. On that basis, it will be assumed for the purposes of this research that all inelasticity is concentrated in one gusset plate per brace member.

Based on experimental and analytical results obtained to date, it can be concluded that by varying the gusset plate geometry, gusset plate thickness and material strength, a designer may specify a connection which provides desired connection capacities in both tension and compression. For capacity design of lateral load resisting systems, loads are based on the equivalent static lateral loading, calculated according to NBCC-1995, NRCC (1995). For a given loading, brace design forces can be determined and a gusset plate can be proportioned to resist exactly that force. Unlike ductile concentrically braced frames

with inelastic bracing elements, no lateral load resisting system seismic over-strength would be anticipated in a properly designed system, not governed by wind forces.

7.3 Concrete Behaviour and Modelling Parameters

Reinforced concrete members, when subjected to cyclic inelastic loading, may exhibit stiffness and strength degradation, depending on the magnitude and number of cycles experienced by the member (Wang and Shah, 1987). A typical response of a non-ductile concrete member to cyclic loading is shown in figure 7.1. The use of simplified modelling approaches, such as elasto-plastic and bilinear moment-curvature relationships for reinforced concrete members undergoing inelastic cyclic loading produces poor correlation between experimental and analytical results, as reported by Saiidi (1982). For the analyses reported herein, concrete element behaviour was defined to simulate experimentally observed hysteresis of reinforced concrete columns with limited confinement, typical of GLD structures. To properly model this behaviour in the structures analysed, stiffness degradation, unloading stiffness degradation and capacity loss were included in the moment vs. rotation behaviour of the elements used in analysis. DRAIN-2DX element type 15, Powell (1993), which can employ various non-linear material types, assigned to cross section fibres for definition of reinforced concrete cross sections, as shown in figures 7.5, 7.6 and 7.7, is well suited for modelling cyclically loaded reinforced concrete member behaviour.

Distributed plasticity modelling was performed by employing non-linear concrete and steel material properties and modelling a typical concrete column cross section using five fibres - a central core of three unreinforced concrete fibres with two outer fibres employing both steel and concrete material types. Concrete material stress strain relationships included a negative modulus descending branch in compression with zero tensile strength. As recommended in the DRAIN-2DX manual, Prakash, Powell and Campbell (1993), anti flip-flop solution schemes, small time steps and corrections were applied to stabilize the solution, which can be destabilized by the inclusion of negative

modulus stress-strain segments. The element behaviour was tested using single and multiple element patch tests, as depicted in figure 7.8. The patch tests were found to provide unstable solutions over a large range of time steps, damping and material property variations, which gave rise to errors and aborted solutions. Based on the results of the patch tests, distributed plasticity was abandoned in favour of a lumped plasticity approach. Type 15 elements were used to model concrete members with cross section properties based on uncracked section properties. The hinge fibres may be defined to model stiffness degradation, unloading softening, fibre pullout and accumulated strain related strength loss, as observed in tests of poorly confined reinforced concrete frame joints and members. When subjected to the same patch test parameters as the distributed plasticity model, solutions with small energy errors could be reliably obtained.

Both detailed and simplified hinge models were evaluated for modelling of concrete column cross section behaviour. The detailed hinge model comprised modelling the full cross section in six layers of steel and concrete, using steel and concrete material properties and including fibres to represent both materials within the hinge region, as depicted in figure 7.6. The simplified hinge model represented the cross section using an elastic web, comprising 4 hinge fibres, with an inelastic extreme fibre, comprising 2 hinge fibres, having the combined properties of steel and concrete. In this way the flexural behaviour of the cross section was controlled by the properties of the inelastic extreme fibre. The specific parameters and capabilities required to define hinge behaviour are outlined in Jain and Goel (1978).

Both hinge models were subjected to the same patch test as used for the distributed plasticity element. When compared to experimentally observed responses (figure 7.1), both hinge models were found to provide reasonable moment - rotation hysteresis. The simplified hinge model allowed direct calculation of the parameters required to generate desired element response and reduced solution time. For modelling of the analyzed frames, the simplified hinge model was used.

7.4 Frame Model

The modelled structure is an eight storey high by five bay wide frame, as depicted in figure 7.9 and based on geometry from the CISC Multi-Storey Building Design Aid Chien (1987) and research by Kobeovic and Redwood (1997) and Redwood, Lu, Bouchard and Paultre (1991). Consistent with analysis performed by Jain (1985), the frame model did not include any lateral load resistance provided by other lateral load resisting structures, for example, shear walls, located beyond the plane of the model. Each of the column members had an inelastic hinge at each end and elastic cross section properties along their lengths. Static gravity loads were applied as point forces at each beam - column intersection. Masses were modelled as lumped masses at each storey on a leaning column line. The leaning column line comprised a series of pin ended struts which did not contribute to the lateral load resistance of the system

The sizes of the beams and columns were based on CAN/CSA-A23.3-94 (1994) and on dead and live gravity load effects only, which were determined using linear finite element plane frame analysis. The design member sizes and reinforcing are provided in table 7.1.

The design of retrofit bracing was based on NBCC 1995, NRCC (1995), zone 5 loading and the lumped masses used in analysis of the unbraced frame case. Bracing forces were calculated using force modification factors, $R = 2$ and $R = 3$. The cross sectional area of the bracing members were selected such that tension yield of gusset plates would not produce a stress exceeding $0.6F_y$ in the bracing. This is considered to reasonably represent the bracing sizes anticipated in a real structure, designed using the capacity design principle, with gusset plates as the designated inelastic elements. Fundamental period of the braced structures were in the 0.8 to 1 second range.

Gusset plates were modelled using DRAIN-2DX TYPE01 elements. Stocky gussets were modelled using the inelastic bar element with equal tension and compression yield stresses. Slender gussets were modelled using two DRAIN-2DX TYPE01 elements in parallel - one yielding element and one buckling element. The yielding element was

defined with tension and compression yield forces equal to one half the total gusset plate tension proportional limit. The buckling element was defined with a tension yield force equal to one half the total gusset plate tension proportional limit and the buckling force to be negligible. This gusset modelling approach compares favourably to experimentally determined gusset behaviour, as shown in figure 7.4, for both stocky and slender gussets.

7.5 Earthquake Records

Time history analyses were conducted using the nine earthquake records listed in Table 2. The earthquake records were scaled to correspond to NBCC-1995 design earthquakes for seismic zone 5. The LPI event, typical of the records used in this analysis, is shown unscaled in figure 7.10. Consistent with the approach used by Redwood, Lu, Bouchard and Paultre (1991), the design a/v ratio was assumed to equal 1.33. For records with $a/v < 1.33$, the scale factors were selected to provide peak velocities consistent with the NBCC-1995 design values. For records with $a/v > 1.33$, the scale factors were selected to provide peak accelerations consistent with the NBCC-1995 design values. The records were selected to provide a range of event histories from strongly acceleration dominated to strongly velocity dominated.

7.6 Analysis

Analysis was performed using DRAIN-2DX software using a constant time step solution scheme with a typical time step of 0.01 seconds. If, in a given solution, energy errors were found to exceed total energy $\times 10^{-3}$, time step was reduced until energy errors became acceptably small and the solution was found to converge. Velocity, acceleration and displacement corrections were applied to the solution. P-delta effects were included in all analyses. Analyses were terminated if any absolute nodal displacement exceeded 500 mm, which was assumed to represent structural collapse.

7.7 Results - General

For each analysis, a full time history response was calculated. The full content of the responses are of no particular interest in evaluating the overall effectiveness of the lateral load resisting systems analysed. For each of the analyses of structures designed using $R = 2$, the envelope of displacements, interstorey drift, gusset elongation and column axial load are reported in tables 7.3 through 7.6 with the results for each type of retrofit structure reported separately. Unbraced structure type results are provided as a baseline response to which comparisons may be made for evaluation of retrofit structures.

7.8 Unbraced Frame

As anticipated, unbraced GLD frames did not perform well when subjected to seismic loading with the greatest structural damage occurring in the velocity dominated events. For this analysis, collapse has been defined as storey drift exceeding $0.04h$ - the rotation beyond which the modelled columns experience severe stiffness and capacity degradation. This corresponds to significant stiffness and capacity degradation in GLD concrete elements and shown in figure 7.1. In the first storey, this corresponds to storey drift exceeding 160 mm.

The MNH record, which was the most acceleration dominated of the records used ($a/v = 2.63$), resulted in fully elastic response. In other events, structural damage was generally concentrated in the first storey, and was sufficient to cause “soft storey collapse” during the velocity dominated LBL, ECL, TFI and PDI events. Overall structure drift, interstorey drift and angular drift envelopes are presented in figure 7.11 and clearly indicate soft storey collapses. It should be noted that the analyses were halted when any interstorey drift exceeded 500 mm. Such a large magnitude of drift indicates structures which have clearly failed. It is notable that in most cases, storeys 2 through 8

remained elastic or experienced only minor inelasticity through the duration of the events analysed.

Interstorey angular drift envelope is presented in figure 7.11 for low, medium and high a/v ratio events. While the acceleration dominated events did not give rise to soft storey collapse as observed in velocity dominated events, some damage predicted from those events. Degradation of column strength and stiffness has been noted in cyclic tests at rotations between 0.01 and 0.02 radians. Column rotations in that range, which corresponds to damage without collapse, were observed in events LBL, ECL, TFI and PDI in the third and sixth storeys.

7.9 Cross Braced Retrofit with Slender Gussets

Structure drift, interstorey drift and angular drift envelopes for structures retrofit with slender gusset connected cross bracing are shown in figure 7.12 with $R = 2$ structures on the left and $R = 3$ structures on the right of the figure. It is clear from the response envelopes that maximum interstorey drift remained within the bottom or “soft” storey as observed in the unbraced frame analyses. Maximum interstorey drifts are generally similar for the $R = 2$ and $R = 3$ structures above the bottom storey with increases in storey drift associated with higher design R being concentrated in the “soft storey”. The maximum interstorey drift calculated among all of the earthquakes analysed was 67.1 mm for design $R = 3$ and occurred within the first storey during a low a/v event. The design drift limit of $0.02h$ (80mm) was not exceeded in any of the $R = 2$ structures analysed.

For the slender gusset connected cross braced frames, calculated gusset deformation, shown in figure 7.15, exceeded the previously defined fracture limit (15 mm) in several instances. For the $R = 2$ structure, first storey gusset elongation of 53.4 mm was calculated. In the $R = 3$ structure, gusset deformation at that location increased to 81.2 mm. In many cases, gussets within storeys 2 through 8 remained elastic throughout

the events analysed. Where inelasticity did occur in storeys 2 through 8, deformation remained less than 15 mm.

7.10 Cross Braced Retrofit with Stocky Gussets

Stocky gusset – cross brace retrofit frame analyses results are summarized in figure 7.13. Predicted maximum overall drift for cross braced retrofit structures employing stocky gussets were, in all cases, less than those calculated for similar structures employing slender gussets, shown in figure 7.12. When compared to slender gusset connected structures, maximum first storey drift was generally reduced by the use of stocky gussets but, in many cases, gussets in the upper storeys of structures employing stocky gussets experienced more inelasticity than the corollary plates in the structures employing slender gussets. This indicates that the stocky gusseted structure more evenly distributed yielding throughout the structure during design seismic events. This can be clearly seen by comparing the interstorey drift envelopes of slender and stocky gusset structures in figures 7.12 and 7.13. The interstorey drift distributions between the two structure types are similar but the variation between storeys is less for the stocky gusseted structure.

For the stocky gusset connected braced frames, calculated gusset deformation within the first storey exceeded the 15mm fracture limit deformation, as shown in figure 7.13, during the low a/v events. The maximum gusset deformations for the $R = 2$ and $R = 3$ structures were 36.2 mm and 44.1 mm respectively. This is significantly reduced from the 53.4 mm and 81.2 mm deformations predicted for the slender gusset connected structures. Gusset deformations above the first storey were all less than the fracture limit deformation in all events analysed for stocky gusseted X-braced structures.

7.11 M-Braced Retrofit

A summary of the analysis results obtained for M-Brace retrofit structures are presented in figures 7.14 and 7.15. As observed among the cross-braced structures, the most damaging events for the M-braced structures were the LBL, ECL, TFI and PDI events - the velocity dominated events. The distribution of damage throughout the M-braced structures analysed was more uniform than observed in the cross braced cases.

Comparison of the interstorey and angular drift envelopes in figures 7.12, 7.13 and 7.14, it can be observed that the most even distribution of drift was predicted for the M-braced structures.

For each of the LBL, ECL, TFI and PDI events, inelasticity occurred within every storey of the analysed structures. In comparison, the cross braced structures analysis results indicated very little inelasticity in storeys 2 through 5 for the same velocity dominated events. This may be observed in figure 7.15 where, for the cross braced structures, no inelasticity is indicated for storeys 2 through 5 of the $R = 3$ structure.

Concentration of deformation in the bottom storeys of the M-braced structures analysed remained significant, although considerable inelastic deformation was also predicted in storeys 6, 7 and 8. Maximum observed gusset deformations of 24.6 mm occurred in the seventh storey of the $R = 2$ M-Braced Retrofit structure during the TFI event. Gusset plates in other storeys and during all other events deformed less than the 15 mm fracture limit. Unexpectedly, the gusset deformations calculated for the $R = 3$ structure were less than those for the $R=2$ structure with deformations exceeding 15 mm in three locations: 21.2 mm in the seventh storey, 16.5 mm in the sixth storey and 21.6 mm in the bottom storey. While the absolute maximum predicted gusset deformation decreased with increasing design R in this case, the overall deformation in the structure did increase – which is consistent with expectations for increasing R .

It should be noted that, within the storeys containing a gusset deformed beyond the anticipated fracture limit, other gussets remained well below the fracture deformation

limit. This would indicate that, in a real structure with M-bracing, the loss of a single gusset plates would not represent the loss of the lateral load resisting system. Additional energy absorption capacity would be available from remaining gussets. This is not necessarily the case within a single bay of cross braced structures and is not the case within a single bay of single diagonal braced structures.

7.12 Column Loads

For GLD frames, overturning moments resulting from lateral loads are distributed among the columns of the building. The resulting increase in column axial load, over gravity loads only, arising from seismic actions on GLD structures is relatively small. The introduction of a stiff lateral load resisting system within one bay of a GLD structure significantly alters the column axial load distribution arising from seismic loading because of the accumulated brace reactions acting on the columns acting in the lateral load resisting system. The increased axial load present in braced bay columns during seismic loading has potential to overload those columns during seismic loading. As shown in figure 7.16, the column axial load envelopes for the braced bay columns in the structures analysed were compared to the capacity of the columns in the assumed gravity load design frame as well as the predicted axial load calculated using the NBCC-1995 procedure for combining overturning with gravity loads. In no case was the predicted ultimate axial load carrying capacity of a modelled column exceeded. Column axial loads were consistent with those calculated using the NBCC-1995 specified procedure for overturning moment. The ratio of maximum column load to ultimate ranged between 0.53 and 0.91 in the bottom storey of cross braced frames. No column tension forces were predicted during the earthquakes analysed.

For a capacity design, the factored axial loads predicted for the columns in both the analysis and NBCC-1995 design equations would exceed the capacity of the columns without retrofit. In a real structure, the columns would require retrofit to function as part of the lateral load resisting systems analysed. If column retrofit is to be avoided,

sufficient reduction of column axial load might be realized by increasing the width of the braced panel or sharing lateral loads by bracing in more than one bay.

7.13 Conclusions

Modelling of poorly confined reinforced concrete columns can be accomplished most easily, and with acceptable accuracy in DRAIN-2DX, by using lumped plasticity type15 elements and employing strength and stiffness degradation. A patch test should be conducted to confirm that element behaviour accurately represents that observed in real structures and to confirm that desired element behaviour is produced by the selected element parameters.

Among the unbraced structures modelled, soft storey collapse within the bottom storey was predicted in four of the nine events analysed. The predicted failures are consistent with expectations for seismically loaded GLD structures.

Cross braced steel retrofit lateral load resisting systems, employing gusset plates as inelastic elements in GLD frames significantly reduced bottom storey drift and overall drift during design earthquakes. When compared to the unbraced frame, a more even distribution of damage was observed throughout the braced structures analysed. Cross braced structures with slender gusset plates did not behave significantly differently from those employing stocky gusset plates.

M-Braced steel retrofit lateral load resisting systems, employing gusset plates as inelastic elements in GLD frames perform better than X-braced retrofit structures when subjected to the same seismic excitation. For the force modification factor, overall structure drift is reduced, interstorey drift is more uniform over the height of the structure and deformation demand is significantly reduced for M-braced structures when compared to cross braced structures.

In many cases, the deformation demand predicted for gusset plates in cross braced structures exceeded the deformability of continuous gussets, which varies between 10mm and 20mm. Modified gussets, using Extended Hinge Links (EHL), have been tested and analysed by Mullin (Chapter 4). In tests, EHL gussets have sustained cyclic maximum deformation of up to 120 mm, well in excess of the deformation demand calculated for retrofit GLD frames analysed herein.

Table 7.1 - Gravity Load Design Concrete Frame Member Sizes

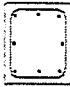





Member	Cross Section (mm x mm)	Flexural Reinforcement
C1 - Interior Base Columns (Level 1)	500 x 500	 $A_s = 2500 \text{ mm}^2$
C2 - Base Columns (Levels 1,2)	500 x 500	 $A_s = 1500 \text{ mm}^2$
C3 - Interior Columns (Level 3)	400 x 400	 $A_s = 900 \text{ mm}^2$
C4 - Columns (Levels 3, 4, 5)	400 x 400	 $A_s = 600 \text{ mm}^2$
C5 - Upper Columns (Levels 6, 7, 8)	300 x 300	 $A_s = 600 \text{ mm}^2$
B1 - Typical Floor and Roof Beams	400 x 800	 $A_s = 900 \text{ mm}^2$

Table 7.2 - Summary of Earthquake Records Used in Analysis

Record, Date, Site	Abbreviation	Component	PHA(g)	PHV(m/s)	a/v
Long Beach, Mar. 10, 1933 (Los Angeles Subway Terminal)	LBL	N39E	0.064	0.173	0.37
El Centro, Dec. 30, 1933 (El Centro Imperial Valley)	ECL	S00W	0.160	0.209	0.52
Taft, July 21, 1952 (Lincoln School)	TFI	N21E	0.156	0.157	0.99
San Fernando, Feb. 9, 1971 (Pacoima Dam)	PDI	S16E	1.171	1.132	1.03
Loma Prieta 2, Oct 17, 1989 (Eureka Canyon Road)	LPI	0	0.629	0.552	1.14
Parkfield, June 27, 1966 (Cholame, Shandon)	PKH	N85E	0.426	0.255	1.67
Loma Prieta 4, Oct 17, 1989 (USCS/Link Lab, Santa Cruz)	LPH	0	0.442	0.212	2.08
Nahanni, Dec. 25, 1985 (Site I: Iverson)	NAH	LONG	1.101	0.462	2.38
Monte Negro, Apr. 9, 1979 (Hotel Albatross Basement)	MNH	N00E	0.042	0.016	2.63

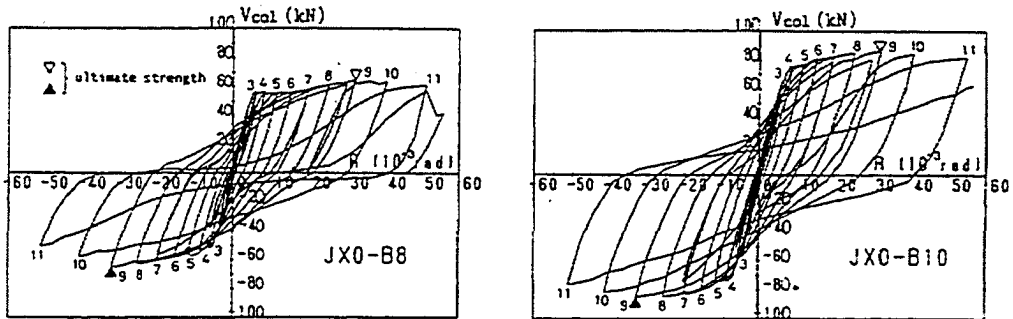


Figure 7.1 – GLD Column Behaviour, from Joh, O., Goto, Y., and Shibata, T. (1991)

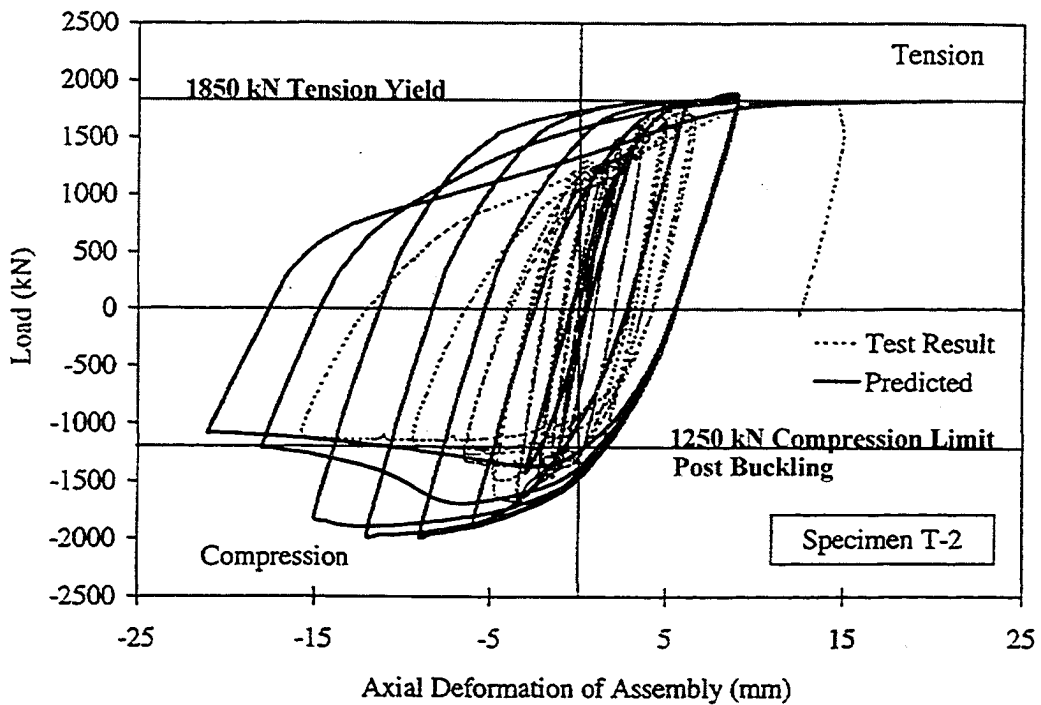


Figure 7.2 - Gusset Hysteresis, from Walbridge (1999)

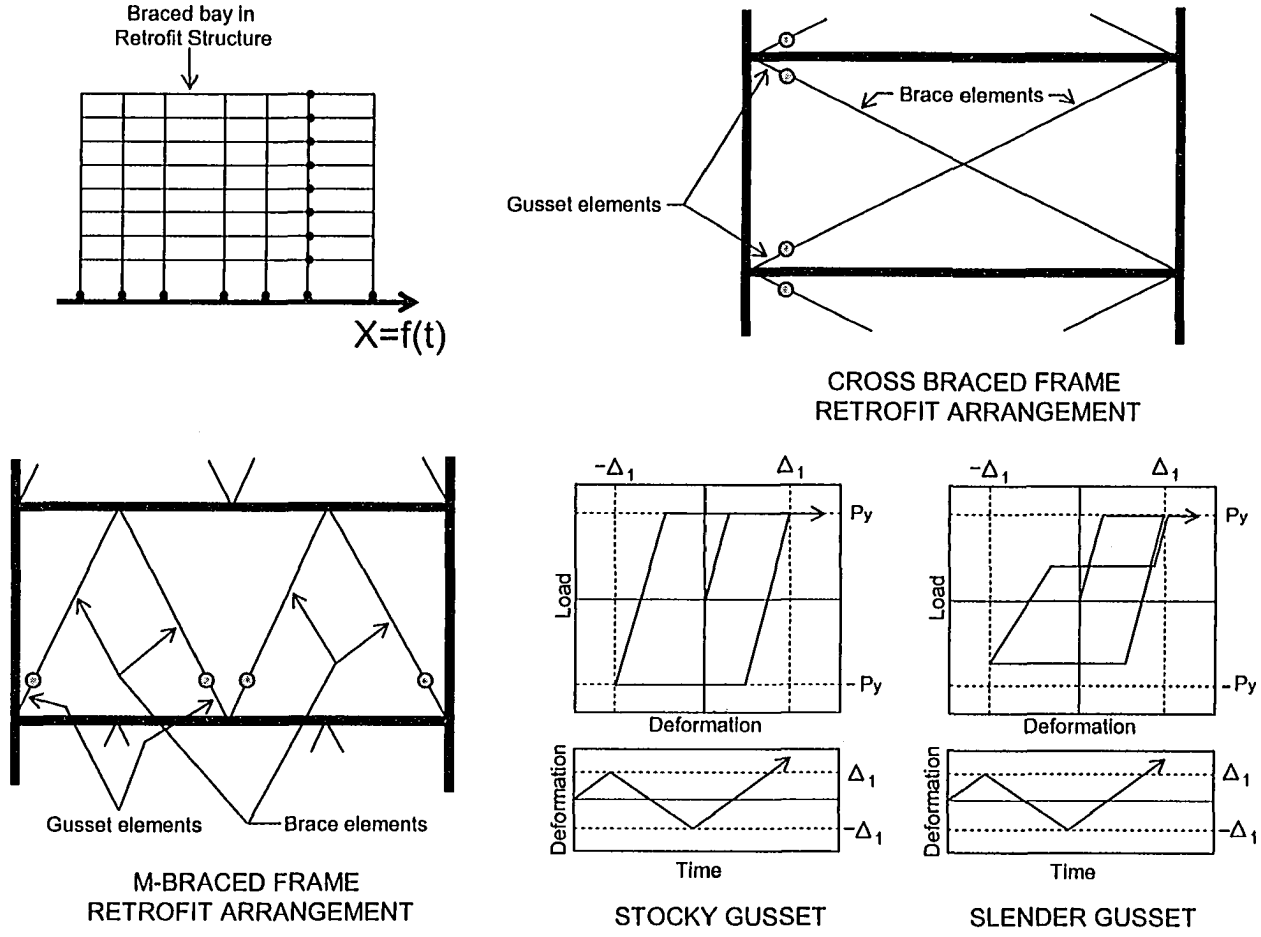
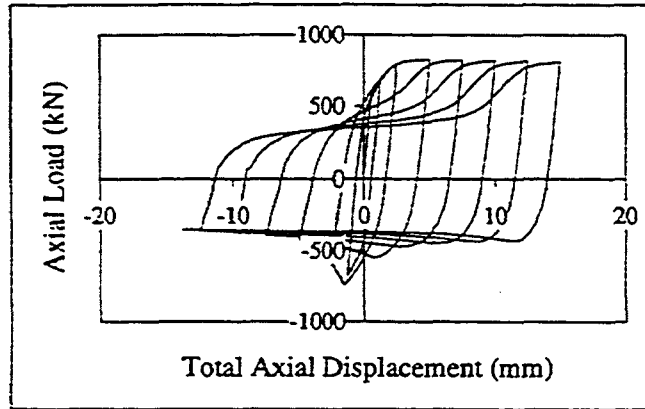
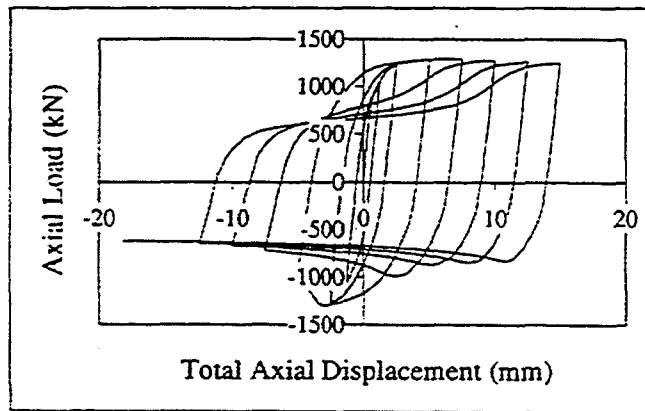


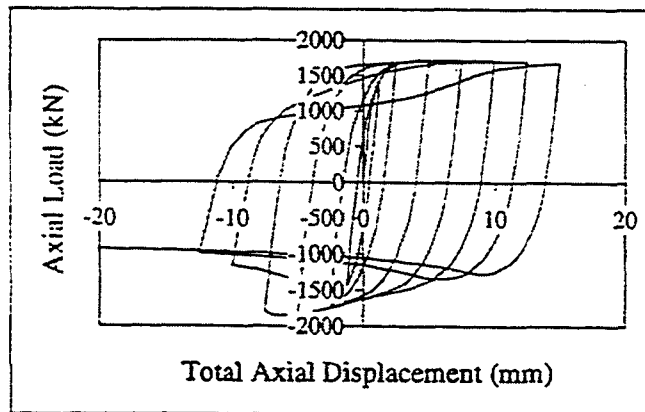
Figure 7.3 – Concrete Frame Retrofit General Arrangement



(a) - Gusset plate GP1 (no brace member): Nominal $t = 6.4$ mm



(b) - Gusset plate GP2 (no brace member): Nominal $t = 9.5$ mm



(c) - Gusset plate GP3 (no brace member): Nominal $t = 12.7$ mm

**Figure 7.4 - Load - Deformation Behaviour of Gussets of Varying Thickness
From Walbridge, Grondin and Cheng (1998)**

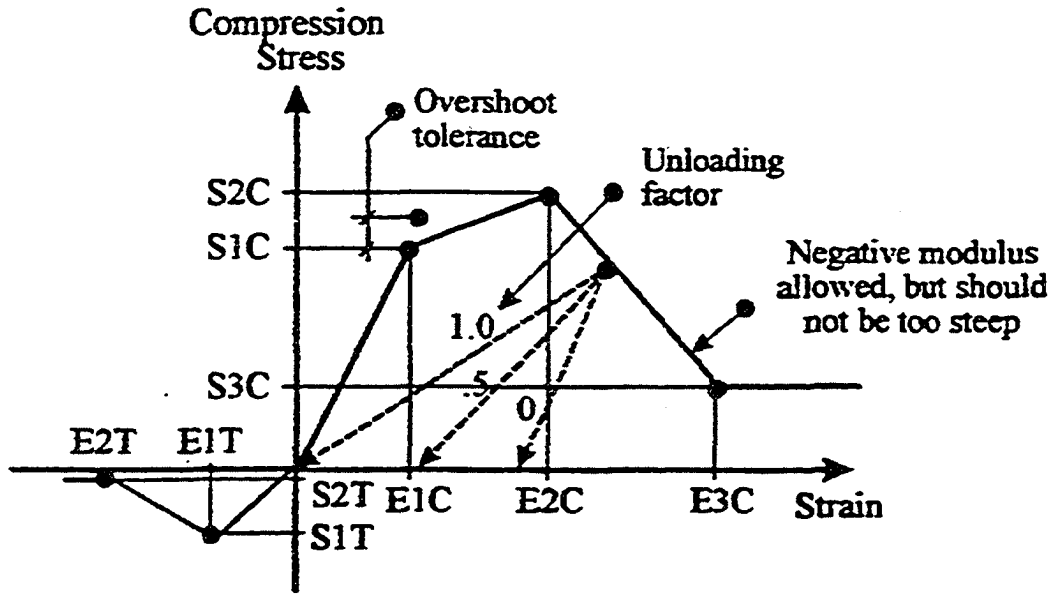


Figure 7.5 – DRAIN2DX Uniaxial Stress-Strain Relationship for Concrete from Powell, G.H. (1993)

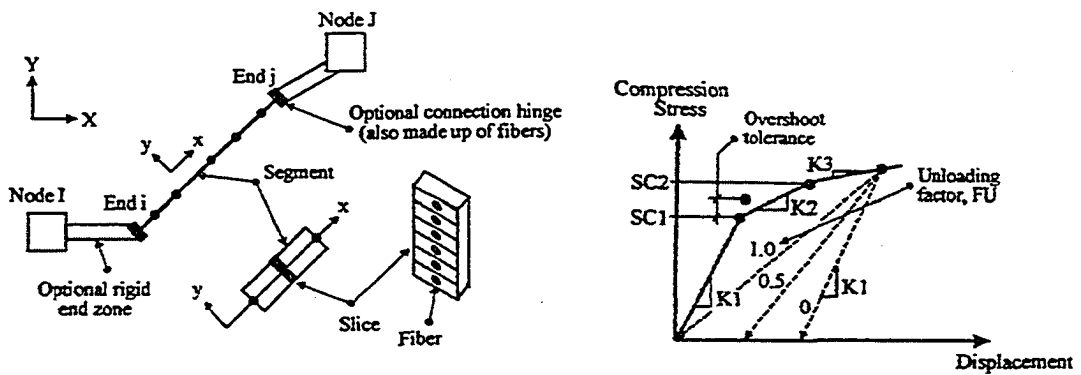
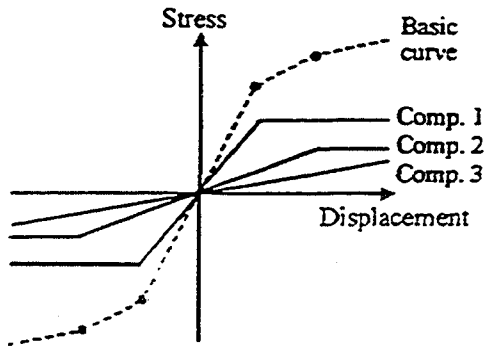
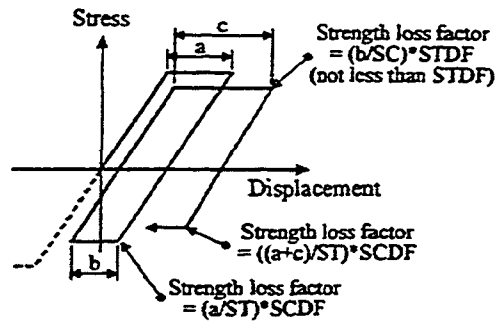


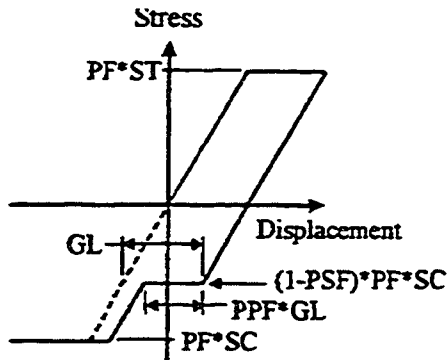
Figure 7.6 – DRAIN2DX Type 15 Element Configuration with Non-linear Hinge from Powell, G.H. (1993)



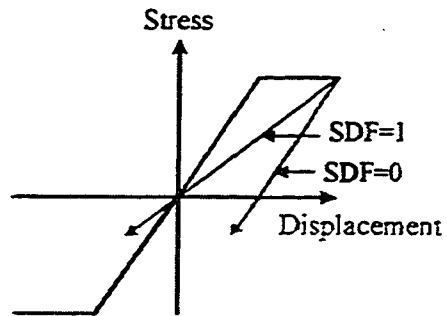
(a) Basic trilinear curve is first decomposed into three parallel components



(c) Strength loss in each component depends on strength degradation factor (STDF or SCDF) and ratio of accumulated plastic displacement to saturated displacement (ST or SC)



(d) Pinch factor (PF) divides each component into pinching and non-pinching parts. Pinch strength factor (PSF) and plateau factor (PPF) are then applied.



(b) Stiffness degradation factor applies to both elastic-plastic components

Figure 7.7 – DRAIN2DX Hinge Fibre Response Modification Factors from Powell, G.H. (1993)

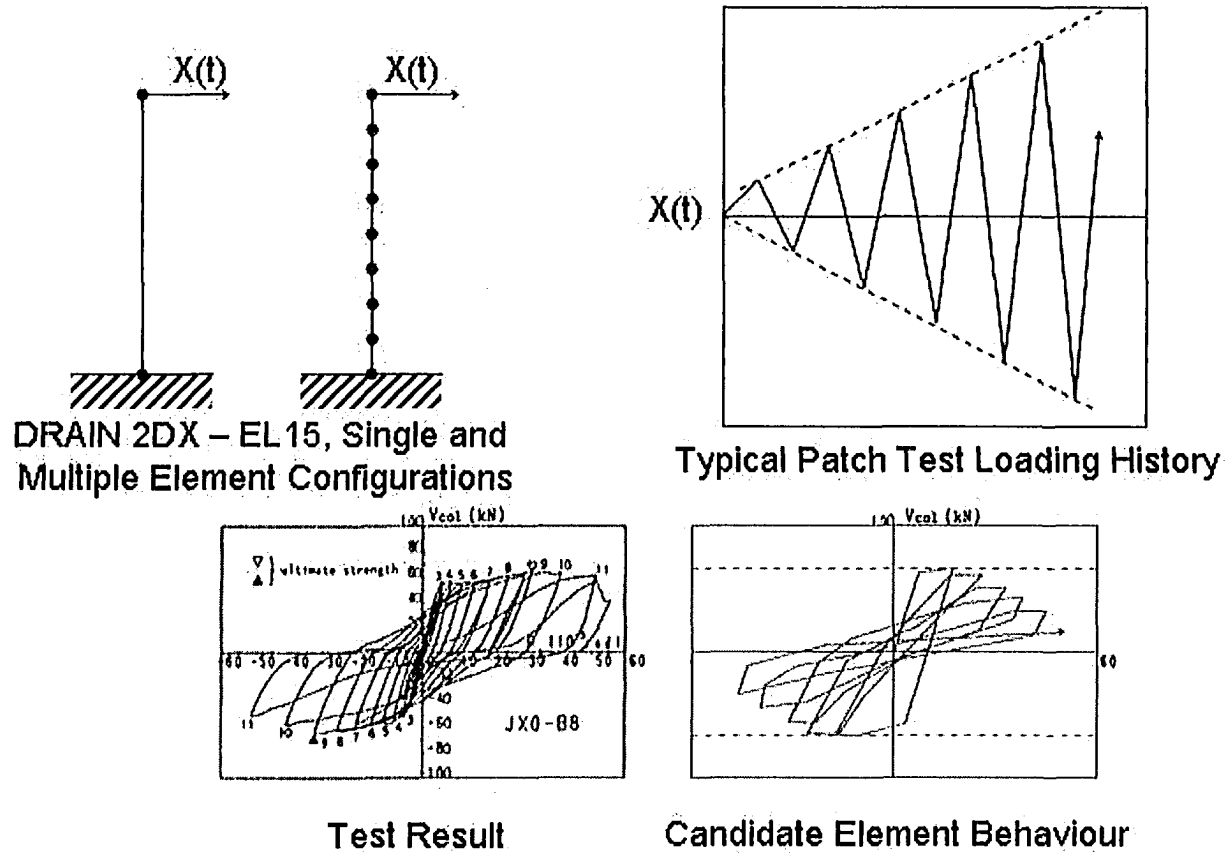


Figure 7.8 – DRAIN-2DX Element 15 Patch Test Schematic
 Test Result from Joh, O., Goto, Y., and Shibata, T. (1991)

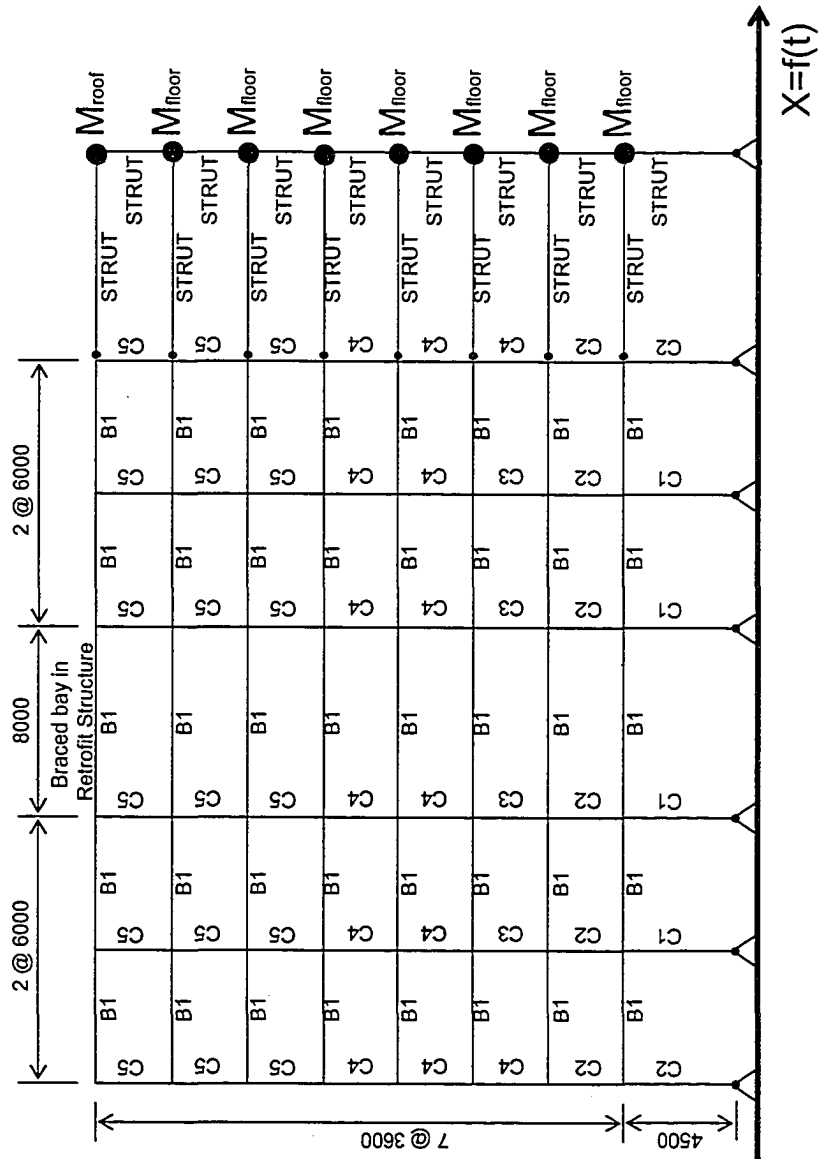
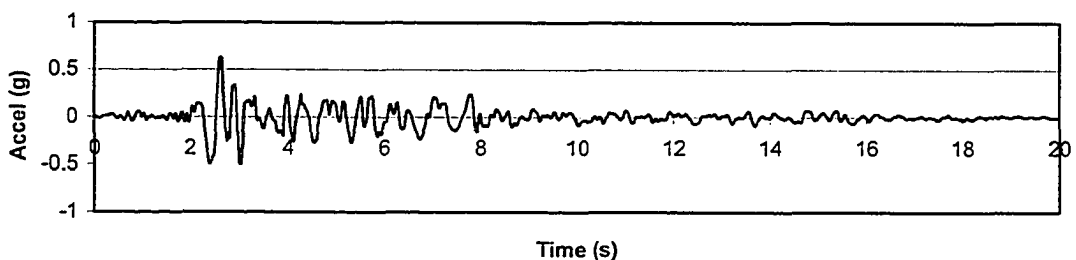
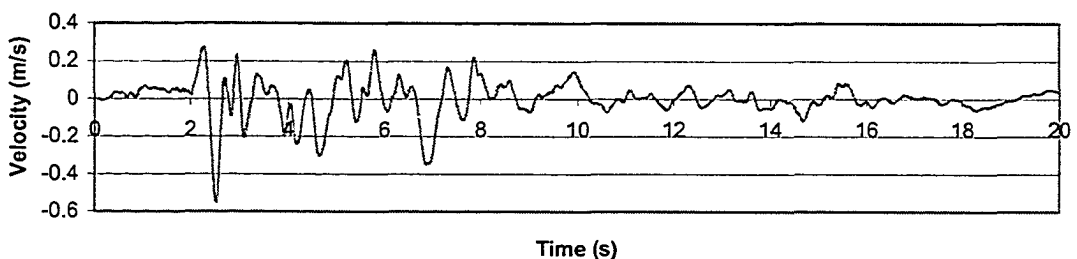


Figure 7.9 -- Concrete Frame Model General Arrangement

LPI (Loma Prieta 2, 0°) - Acceleration (g)



LPI (Loma Prieta 2, 0°) - Velocity (m/s)



LPI (Loma Prieta 2, 0°) - Displacement (m)

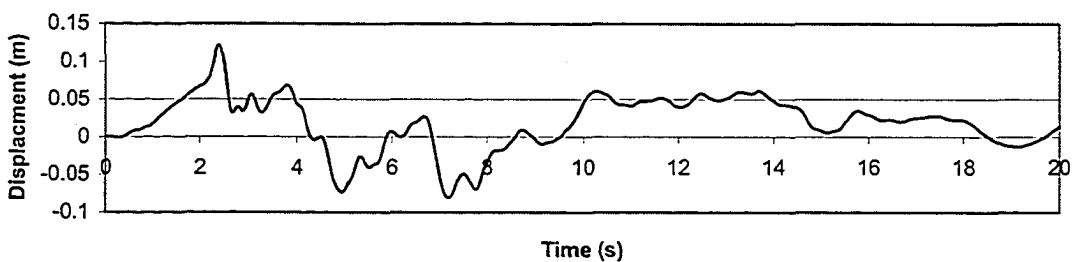


Figure 7.10 - Unscaled LPI Event, Acceleration (g), Velocity (m/s), and Displacement (m)

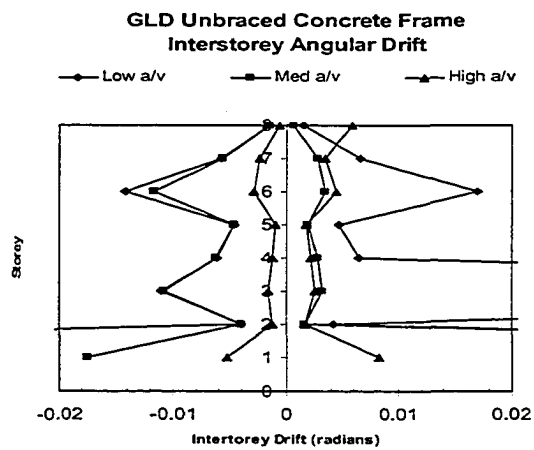
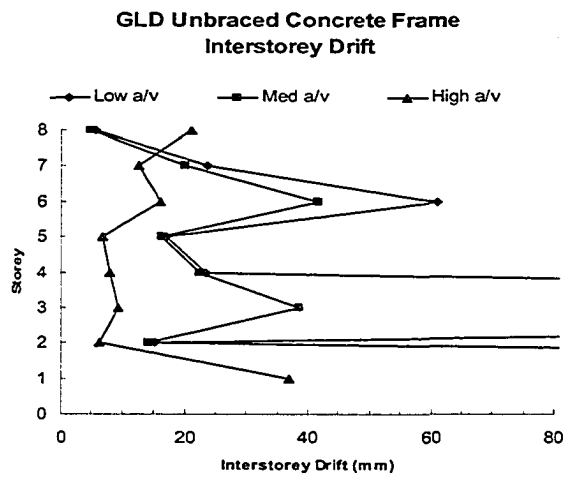
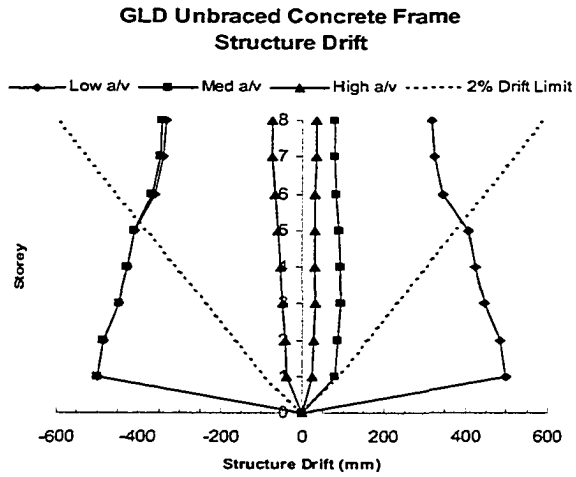


Figure 7.11 - Unbraced GLD Concrete Frame Response Summary

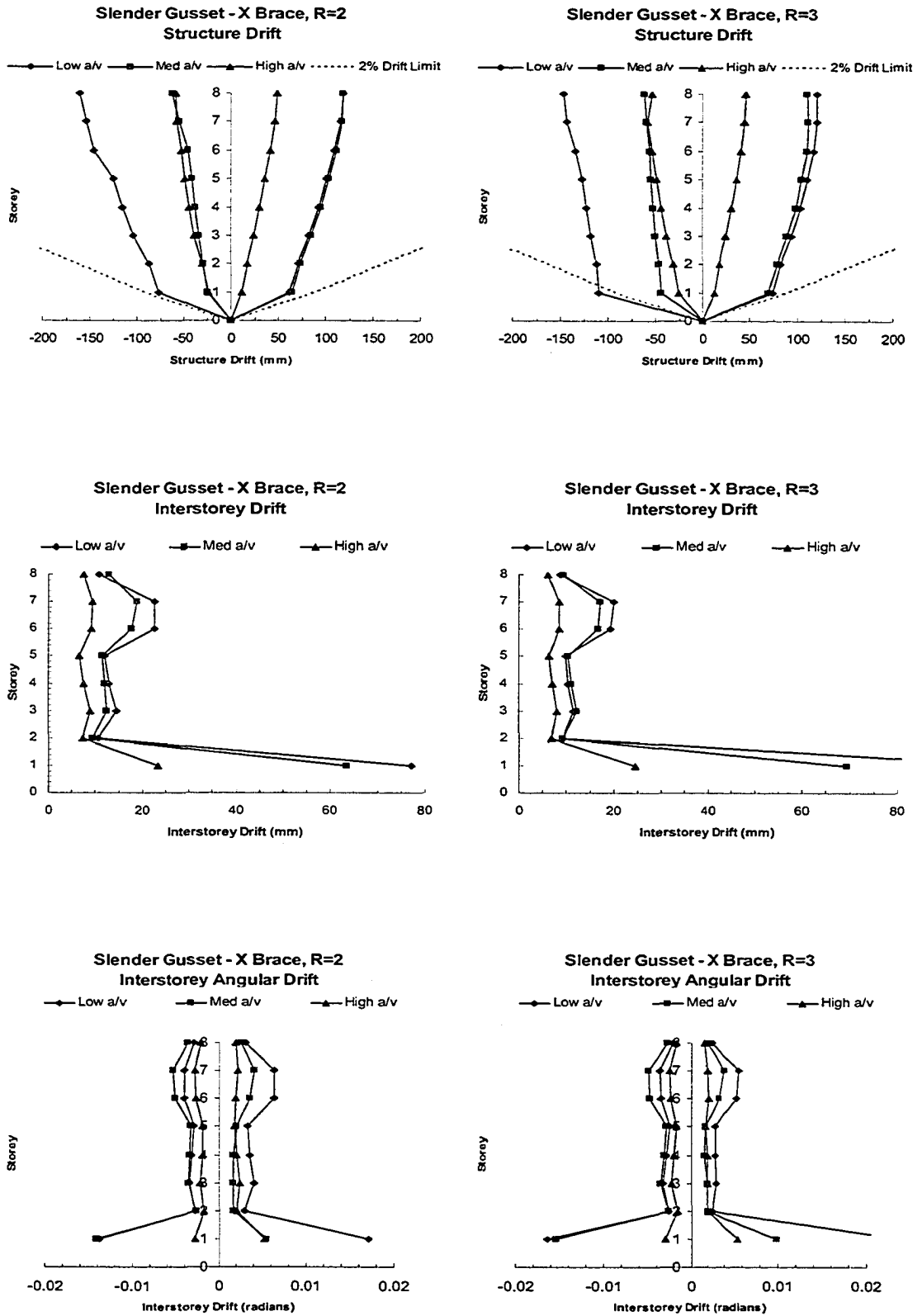


Figure 7.12 – Slender Gusset – X Braced Concrete Frame Response Summary

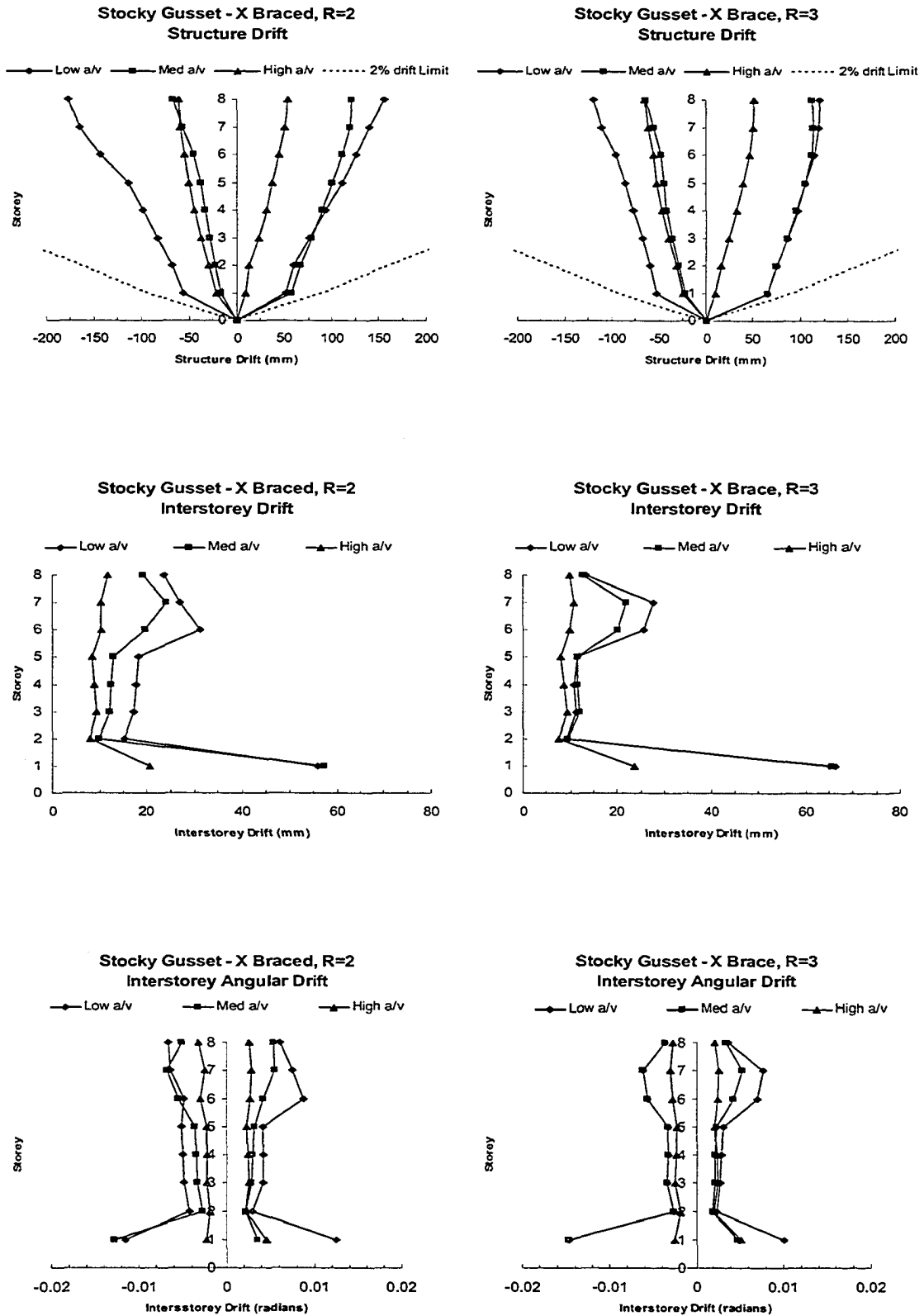


Figure 7.13 – Stocky Gusset – X Braced Concrete Frame Response Summary

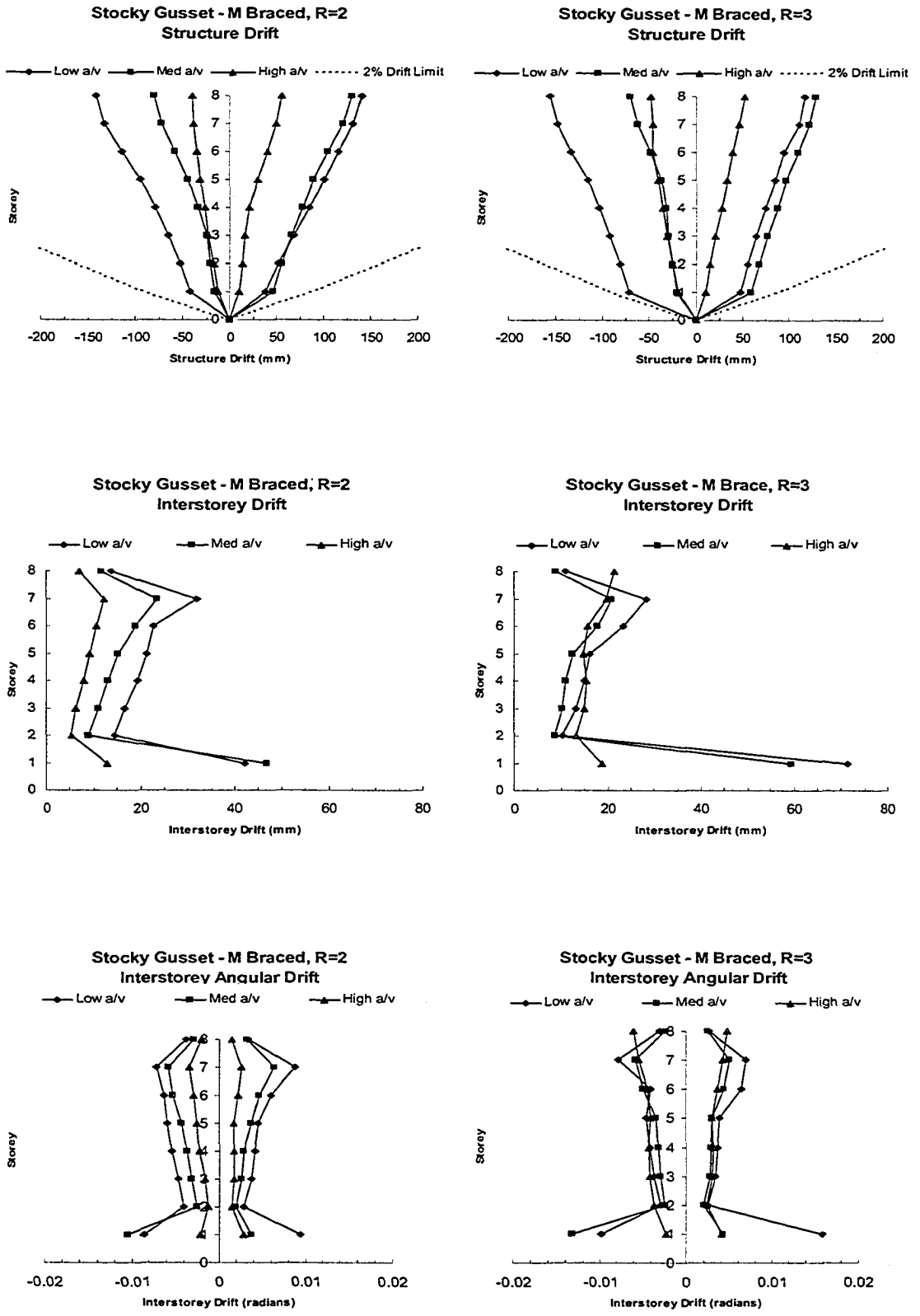
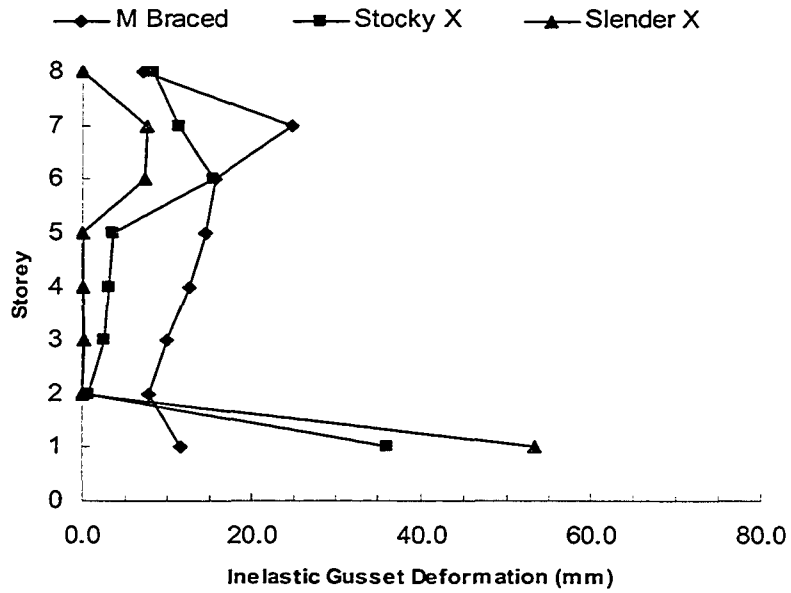


Figure 7.14 - Stocky Gusset - M Braced Frames Response Summary

Retrofit Frames, R=2
Maximum Inelastic Gusset Deformation



Retrofit Frames, R=3
Maximum Inelastic Gusset Deformation

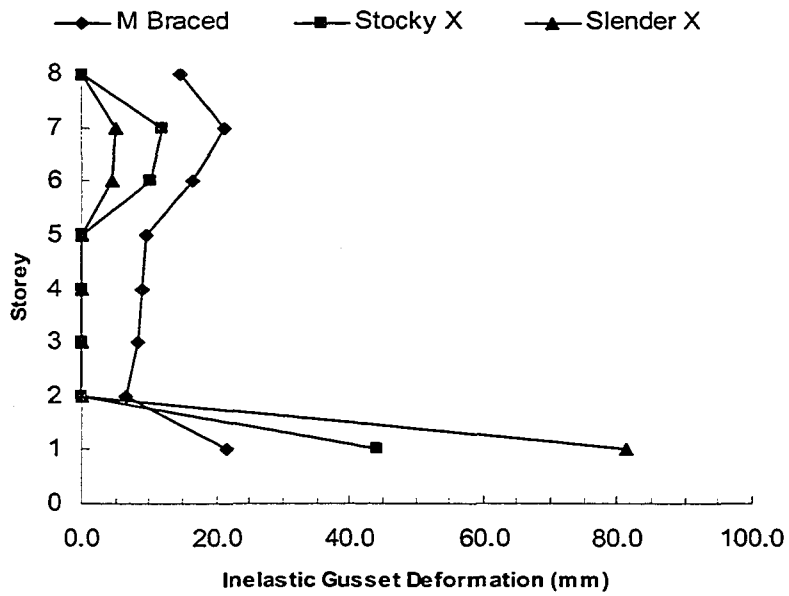
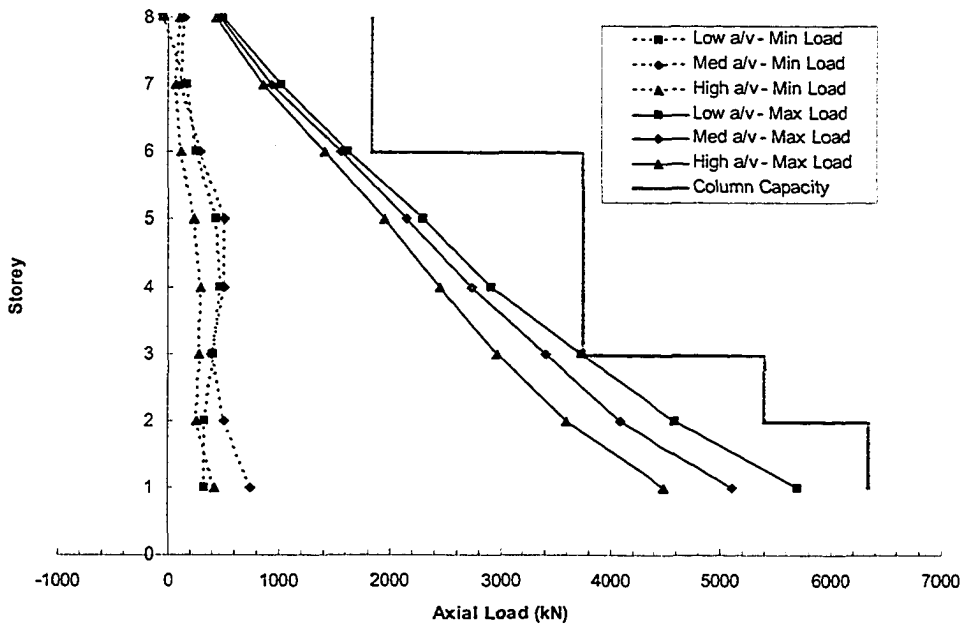


Figure 7.15 - Retrofit Frames,, Gusset Deformation Envelopes

**Column Axial Load Envelope
Cross Braced GLD - Stocky Gussets - R=2**



**Column Axial Load Envelope
Cross Braced GLD - Slender Gussets - R=2**

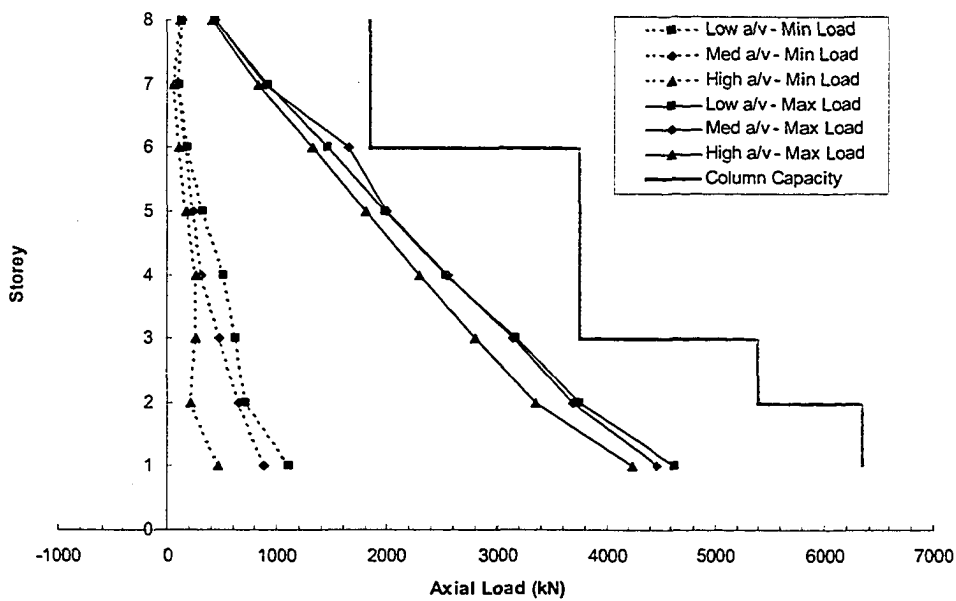


Figure 7.16 – Column Axial Loads , R=2 Structures

7.14 References

AISC, 1989. Manual of Steel Construction. Allowable Stress Design. Ninth Edition. American Institute of Steel Construction, Inc., Chicago IL.

AISC, 1995. Manual of Steel Construction. Load and Resistance Factor Design. Second Edition. American Institute of Steel Construction, Inc., Chicago IL.

AISC, 1992. Manual of Steel Construction. Volume II: Connections, ASD 9th Ed. / LRFD 1st Ed. American Institute of Steel Construction, Inc., Chicago IL.

CAN/CSA-A23,3-94, 1984. Design of Concrete Structures, Canadian Standards Association, Rexdale Ontario.

CAN/CSA-S16.1-94, 1995. Limit States Design of Steel Structures, Canadian Standards Association, Rexdale, Ontario.

Chien, E., 1987. "Multi-Storey Building Design Aid." Canadian Institute of Steel Construction, Willowdale, Ontario.

Chung, Y.S., Meyer, C., and Shinozuka, M., 1989. "Modeling of Concrete Damage." ACI Structural Journal, V. 86, No. 3, May-June 1989, pp 259 – 271.

Hardash, S.G., and Bjorhovde, R., 1985. "New Design Criteria for Gusset Plates in Tension." Engineering Journal, AISC, Vol. 22, No. 2, pp. 77-94.

Hu, S.Z., and Cheng, J.J.R., 1987. "Compressive Behaviour of Gusset Plate Connections." Structural Engineering Report No. 153, Department of Civil Engineering, University of Alberta, Edmonton, Alberta.

Jain, A.K., 1985. "Seismic Response of RC Frames with Steel Braces." ASCE Journal, of Structural Engineering, Vol. .111, No. 10 pp 2138 – 2148.

Jain, A.K., and Goel, S.C., 1978. "Hysteresis Models for Steel Members Subjected to Cyclic Buckling or End Moments and Buckling – Users Guide for DRAIN 2D." Report No. UMEM 78R6, Department of Civil Engineering, University of Michigan, Ann Arbor, MI.

Joh, O., Goto, Y., and Shibata, T., 1991. "Influence of Transverse Joint and Beam Reinforcement and Relocation of Plastic Hinge Region on Beam-Column Joint Stiffness Deterioration." Design of Beam-Column Joints for Seismic Resistance, Edited by James O. Jirsa, American Concrete Institute, Detroit, Michigan., pp 187-223.

Kobeovic, S., and Redwood, R., 1997. "Design and Seismic Response of Shear Critical Eccentrically Braced Frames." Canadian Journal of Civil Engineering, 24: 761 – 771.

Kunnath, S.K., Hoffmann, G., Reinhorn, A.M., and Mander, J.B., 1995. "Gravity-Load-Designed Reinforced Concrete Buildings – Part 1: Seismic Evaluation of Existing Construction." ACI Structural Journal, V. 92, No. 3, May-June, 1995.

Nast, T.E., Grondin, G.Y., and Cheng, J.J.R., 1999. "Cyclic Behaviour of Stiffened Gusset Plate-Brace Member Assemblies." Structural Engineering Report No. 229, Department of Civil Engineering, University of Alberta, Edmonton, Alberta.

NRCC, 1995. National Building Code of Canada. Associate Committee on the National Building Code, National Research Council of Canada, Ottawa, Ontario.

Powell, G.H., 1993. DRAIN-2DX Element Description and Users Guide for Element TYPE01, TYPE02, TYPE04, TYPE06, TYPE09 and TYPE15 Ver. 1.10 Report No. UCB/SEMM-93/18, Department of Civil Engineering, University of California, Berkeley, California.

Prakash, V., Powell, G.H., and Campbell, S., 1993. DRAIN-2DX Base Program Description and Users Guide. Ver. 1.10, Report No. UCB/SEMM-93/17, Department of Civil Engineering, University of California, Berkeley, California.

Rabinovitch, J.S., and Cheng, J.J.R., 1993. "Cyclic Behaviour of Steel Gusset Plate Connections." Structural Engineering Report No. 191, Department of Civil Engineering, University of Alberta, Edmonton, Alberta.

Redwood, R.G., Lu, F., Bouchard, G., and Paultre, P., 1991. "Seismic Response of Concentrically Braced Steel Frames." Canadian Journal of Civil Engineering, 18(6), pp 1062 - 1077.

Saiidi, M., 1982. "Hysteresis Models for Reinforced Concrete." Journal of the Structural Division, Proceedings of the American Society of Civil Engineers, Vol. 108, No. ST5, May 1982. pp 1077 - 1087.

Walbridge, S.S., Grondin, G.Y., and Cheng, J.J.R., 1998. "An Analysis of the Cyclic Behaviour of Steel Gusset Plate Connections." Structural Engineering Report No. 225, Department of Civil Engineering, University of Alberta, Edmonton, Alberta.

Walbridge, S.S., Grondin, G.Y., and Cheng, J.J.R., 1998. "An Analytical Study of the Cyclic Behaviour of Steel Gusset Plate Connections." Proceedings of the Annual Conference of the Canadian Society for Civil Engineering, Vol IIIa, pp. 107 to 116.

Wang, M.L., Shah, S.P., 1987. "Reinforced Concrete Hysteresis Model Based on the Damage Concept." Earthquake Engineering and Structural Dynamics, Vol. 15, pp 993-1003.

Whitmore, R.E., 1952. "Experimental Investigation of Stresses in Gusset Plates." Bulletin No. 16, Engineering Experiment Station, University of Tennessee.

Yam, C.H.M., and Cheng, J.J.R., 1993. "Experimental Investigation of the Compressive Behaviour of Gusset Plate Connections." Structural Engineering Report No. 194, Department of Civil Engineering, University of Alberta, Edmonton, Alberta.

Yam, C.H.M., and Cheng, J.J.R., 1994. "Analytical Investigation of the Compressive Behaviour and Strength of Steel Gusset Plate Connections." Structural Engineering Report No. 207, Department of Civil Engineering, University of Alberta, Edmonton, Alberta.

8. DISCUSSION, CONCLUSIONS AND RECOMMENDATIONS

8.1 General

The research presented in this thesis can be divided into two categories, deformability assessment of inelastic gusset plates and assessment of deformation demand in seismically loaded structures employing inelastic gusset plates.

In the deformability category, experimental and analytical data were presented in Chapters 3 and 4 regarding ultimate deformation of traditional gussets, gussets with reinforced connection regions and a modified gusset configuration, referred to as an Extended Hinge Link gusset, specifically arranged to maximize deformability.

In the demand category, data have been presented in chapters 5, 6 and 7 presented which characterize the anticipated gusset deformation demands for a range of “strong brace weak gusset” lateral load resisting structures subject to design events and designed using a range of parameters. This category may be further subdivided into steel structures and concrete structures. The conclusions of the research will be presented in the order of the chapters in which they are presented. The first conclusion section describes conclusions regarding gusset deformability and the second describes conclusions regarding deformation demand for the various types of structures analyzed. The conclusions reached in the first section are incorporated into the conclusions of the second and provide, in terms of this research, the limits of applicability of gussets as inelastic elements in seismically loaded structures.

8.2 Deformability of Continuous Gusset Plates

The first focus of this research, reported in chapter 3, was to assess the deformability of continuous gusset plates in arrangements typically employed in modern steel construction

and to quantify the effects of changes to that arrangement on deformability. The results of the research, both analytical and experimental, led to the development of radial strip analysis, wherein the first fracture deformation of reinforced continuous gusset plates of given geometry and material properties can be calculated. The yielding and deformation behaviour of gusset plates at first fracture are explained by the analogy and, when compared to experimentally observed deformation, reasonable predictions of deformation can be made. It may be concluded from the radial strip analogy that gusset deformability is dependant on:

1. The ductility of the steel used in fabrication.
2. The geometry of the gusset plate.
3. The proximity of fixed boundary conditions to the brace connection region.

A further conclusion of the radial strip method is that, for material properties and gusset geometry representative of current construction practices, a deformability limit of approximately 20 mm exists.

For purposes of evaluation of overall structure dynamic analysis results, it was concluded that a continuous gusset deformation of 15 mm could be reasonably assumed to correspond to first fracture.

While, in tests reported in chapter 3, continuous gussets with seven and eight rows of bolts (specimens 14U and 16U) in the brace – gusset connection continued to carry significant loads and deform significantly after first fracture, the same is not true of gussets with shorter brace – gusset connection lengths. Continuous gussets with compact brace connection bolt groups exhibit very abrupt loss of capacity with deformations beyond first fracture. Since connections of this type represent a majority of those encountered in real structures, it was concluded that reliance on post fracture capacity in inelastic continuous gusset plates is not advisable. It should be pointed out that, at the time of writing, no cyclic load-deformation response data are known to the author for post fracture continuous gussets and, as such, it is not clear what the effect of fractures is

on compression response. It appears reasonable to assume that the fractured continuous gusset plates would exhibit reduced compression load vs. deformation responses when compared to the unfractured state.

8.3 Deformability of EHL Gusset Plates

Based on the observations of analyses done on continuous gusset plates (Chapter 3), it was concluded that gussets configured in with discontinuities around the brace – gusset connection could provide deformability much greater than that observed on continuous gussets. A specific gusset link shape was identified which maximized yielded volume during loading, thereby maximizing fracture deformation. Two tests were conducted to prove the validity of the concept. The behaviour of gussets so configured was not researched in great detail since they were considered an aside to the main focus of the research. The results of the two cyclic tests indicated deformability in excess of 100 mm could be sustained by EHL gussets. The large plate test was halted at 120 mm because the stroke limit of the apparatus was reached. The cost of supply of the EHL plates was found to be about 20 % higher than the cost of similar continuous gussets, purchased for testing reported in chapter 3. For the purposes of this research it is sufficient to conclude that EHL gusset plates are capable of deformations well in excess of that anticipated for continuous gussets. The fabrication cost for EHL gusset plates is increased when compared to traditional gussets. Significant additional research is required to characterize EHL gusset behavior and to develop design requirements for them.

8.4 Gusset Plate Deformation Demand

8.4.1 General

Gusset plate deformation demand values obtained in this research are based on non-linear time history analysis using scaled records of past earthquakes. As such, the predictions are specific to the structural types and scaled events used in analysis and cannot be generalized. Within the results obtained, however, several interesting observations can be made.

8.4.2 Low Rise Steel Structures

Among the single storey structures analyzed, which were designed using $R = 1.5$ through 4 and were subjected to Zone 3 and 5 design events, few inelastic responses were predicted. This result was unexpected in that for structures designed using $R > 1.5$ it is typically expected that there will be some inelasticity during a design seismic event. In the case of $R = 4$, one would anticipate a highly inelastic response. The results are consistent with historical post-earthquake structural damage assessments wherein single storey CBF steel structures have been found to exhibit limited damage.

The analysis of two storey steel structures indicated that, for force modification factors, $R = 1.5$ and 2, structure responses were inelastic with gusset deformations in the range of 5 mm to 12 mm. For $R = 3$ and $R = 4$ structures, predicted maximum gusset deformations were in the 10 mm to 30 mm range for the most damaging events analyzed. Such deformations correspond to fracture of continuous gusset plates and would be expected to lead to fractures in real structures employing continuous gusset plates inelastically during seismic loading. The extended hinge link gussets tested (reported in Chapter 4) demonstrated deformability of 60 mm to 100 mm, well in excess of the calculated deformation demand among the two storey steel structures analyzed.

Four storey steel structures exhibited gusset deformations in excess of anticipated fracture deformation (15 mm) when designed for Zone 5 events using $R = 1.5, 2, 3$ and 4 . The prediction of significant inelasticity in Zone 5 $R = 1.5$ structures supports the requirement of NBCC 1995 Clause 4.1.9.3.1 which requires that buildings more than 3 storeys in height and in Zone 2 or higher shall have lateral load resisting systems designed using $R = 2$ or greater. For those structures designed using $R = 2, 3,$ and $4,$ gusset deformation exceeded the anticipated fracture deformation of continuous gusset plates predominantly in the third and fourth storeys. The predicted gusset deformations were within those sustained by EHL gussets during cyclic testing, reported in chapter 4. Four storey steel structures subjected to Zone 3 earthquakes typically exhibited much smaller predicted gusset deformations than structures designed using similar parameters for Zone 5 events. Generally, the largest predicted deformations were located in the third storey of the structures analyzed and typically did not exceed the anticipated fracture deformation of continuous gussets. When predicted deformations did exceed the anticipated fracture deformation of 15 mm used in the analysis, it was only by a small amount. As observed in tests of continuous gussets, reported in chapter 2, continuous gusset deformation can exceed 20 mm at first fracture when proper detailing and material properties are used.

For each of the 1, 2 and 4 storey structures analyzed, a stocky (compression and tension capacity equal) and slender (compression capacity reduced compared to tension) gusset model were employed in separate analyses. Comparison of the results of those analyses indicates that the slenderness of gusset plates has a very small effect on the responses of structures to earthquakes. In the one storey case, which can be characterized as primarily elastic response, the differences between the stocky and slender responses were negligible. While the responses observed in two and four storey structures contained more gusset inelasticity, the effect of reduced gusset compression capacity (increased gusset slenderness) was not more than 5% increase in mean interstorey drift.

It can be concluded from the results of analysis of one, two and four storey CBF structures that:

1. One storey structures, designed using $R = 1.5$ to 4 , did not exhibit significant inelasticity in Zone 3 or 5 design events.
2. Among two and four storey structures subjected to Zone 3 earthquakes and designed using $R = 2$ or 3 , continuous gussets were effective as inelastic elements. For that group of structures, predicted deformations were within the range of deformability observed experimentally for continuous gussets.
3. For two storey structures designed using $R = 2$ and subjected to Zone 5 events, continuous gusset plates were effective as inelastic elements. For that group of structures, predicted deformations were within the range of deformability observed experimentally for continuous gussets.
4. Two storey structures designed using $R = 3$ or 4 and for all four storey structures subjected to Zone 5 events, calculated maximum gusset deformation exceeded that sustainable by continuous gussets. Modified EHL gussets have been tested and have been shown to possess adequate deformability to act inelastically in this group of structures.

8.4.3 Eight Storey Steel Structures

A series of eight storey structures, employing X, diagonal and M-bracing configurations, were analyzed using non-linear time history analysis and scaled earthquake records, as described in chapter 7. The X and diagonal braced structures were designed using $R = 2$, 3 and 4 for Zone 3 and 5 design events. In those structures, gusset deformations in excess of the assumed fracture deformation were predicted and, in many cases, gusset deformations exceeded 30 mm. For the M-braced structures, which employed a steep angle chevron bracing configuration to reduce gusset deformation, structures were designed using $R = 3$, 4.5 and 6 and were designed for Zone 3 and 5 events. In the zone 3, $R = 3$ and 4.5 and zone 5, $R = 3$ structures, gusset deformation remained less than

the continuous gusset deformation limit during all analyses in all but one case (Zone 3, R = 4.5, LBL event, 7th Storey), where deformation exceeded the limit by 0.1 mm. For other structures (Zone 5, R = 4.5 and 6; Zone 3, R = 6), gusset deformations exceeded the continuous gusset deformation limit in multiple locations and during low a/v events. It may be concluded from these results that, continuous gussets would not be effective as inelastic elements in cross or diagonal braced structures similar to those analyzed. The use of steep angle chevron, or M-bracing, reduced deformation demand on gussets. Continuous gusset plates would be effective as inelastic elements in structures similar to those analyzed when designed for Zone 3 earthquakes using R up to 4.5 and for Zone 5 earthquakes using R up to 3. In those structures where predicted gusset deformations exceed the anticipated fracture deformation for continuous gussets, EHL gusset plates have demonstrated sufficient deformability to act inelastically.

Comparison of CBF structures employing gusset plates as inelastic elements with the responses of similar structures employing inelastic brace members reveals similar magnitude and location of inelasticity between the two structure types.

8.4.4 Eight Storey Concrete Structures

An eight storey concrete gravity load designed structure was analyzed in the unbraced configuration and as braced by retrofit diagonal braces, connected with both stocky and slender gusset plates, and by retrofit M configured bracing. Design R values were 2 and 3 and design zone 5. As anticipated, unbraced GLD frames exhibited “soft storey” collapse, with little structural damage to upper storeys in many of the events analyzed. Damage in those structures retrofit with diagonal bracing was typically greatest within the first storey, with gusset deformation exceeding anticipated continuous gusset fracture deformation in earthquakes with low and medium a/v ratios. Predicted deformations in the seventh storey were generally less than those predicted in the bottom storey and still typically exceeded the anticipated continuous gusset fracture limit. Inelastic

deformations of gussets within the second to fifth storeys of diagonal braced structures were small.

GLD structures retrofit with M configured bracing exhibited gusset deformations ranging from 5 to 15 mm in the $R = 2$ structure and from 7 to 22 mm in the $R = 3$ structure. While the $R = 3$ structure predicted maximum deformation exceeded the continuous gusset deformation limit, several gussets have deformed more than 22 mm in tests prior to first fracture. As such it may be concluded that, in GLD retrofit diagonal brace configurations, continuous gusset plates would be expected to fracture within the bottom storey for structures similar to those analyzed, during design earthquakes with low to medium a/v ratios. For similar structures retrofit with M configured bracing, gusset deformations are reduced such that, for $R=2$ designed structures continuous gussets would be expected to function as inelastic elements. For M-braced $R = 3$ structures, continuous gussets designed with special considerations to ensure good deformability would be expected to function inelastically without fracture. For all cases, the diagonally braced structures could employ EHL gussets, which have demonstrated deformability in excess of the maximum predicted gusset deformation in all cases.

Generally, it has been demonstrated that M-braced structures have a more uniform distribution of damage along their height than similarly designed cross or diagonally braced structures. M-braced structures also possess redundancy within the bracing system in that, if one brace is lost through gusset fracture and the floor beams have sufficient capacity to redistribute loads, the lateral load resisting system remains intact.

8.5 Conclusions

The use of gusset plates to absorb energy in seismically loaded structures is attractive for several reasons. By confining inelasticity to connection material, design, construction, post earthquake repair and retrofit of existing structures may be simplified and made more economical than current systems, which rely on member inelasticity to absorb

energy. When compared with moment resisting frames, CBF structures are generally less costly, simpler to erect and provide enhanced stiffness, reducing deflections arising from wind.

Of particular importance in the design of earthquake resistant structures is the ability of the designer to accurately predict the maximum forces in the structure. Currently, at the design phase of a project, engineers must estimate the anticipated strength of members since dimensional, material and construction variables may only be exactly determined at the time of construction. EHL or similar enhanced ductility gusset plates may be proportioned, when constructed using material of known properties, to provide very specific load-deformation response, as specified by the designer to fulfill the requirements of a given structural design. This may be accomplished in practice since the variables which controls the response of the gusset assembly are the shape and size of the core plate link elements and the stress-strain response of the plate material, which may be determined prior to gusset manufacture, at a time when the characteristics of the core plate and the requirements of the design are known. Other variables such as bracing work point, brace end connection location and size and frame geometry are independent of gusset performance and can be determined in using a more conventional design approach. The ability to tightly control the load-deformation response of inelastic elements in seismically loaded structures is of great benefit to designers and can be achieved at small cost to owners where enhanced ductility gusset plates are employed.

While the potential benefits of EHL gusset plates are significant, the application of more standard gusset configuration as inelastic structural elements in seismically loaded frames also holds potential. When furnished with edge stiffeners and constructed using materials of reasonable ductility, gusset plates can be effective inelastic elements in one and two storey structures located in zones of high seismic risk and in taller structures of proper design in zones of lower risk. If constructed using materials possessing enhanced ductility or if configured properly, gusset plates can be effective energy dissipaters in a much wider range of seismically loaded structures.

The potential benefits of using gusset plates as inelastic elements in seismically loaded structures extend beyond new construction. Inelastic gusset plates are particularly suitable for the retrofit of existing structures. Where existing structures are constructed using concentrically braced frame lateral load resisting systems, the replacement of existing gusset plates with enhanced ductility gusset plates could be accomplished with minimum disruption of occupants. Where existing structures are moment resisting frames in need of upgrade for seismic loading, bolt in retrofit gussets could connect new bracing to existing beams and columns to provide highly controlled response to lateral loading.

8.6 Recommendations

Additional research is required to determine the seismic responses of a wider range of structures employing gusset plates as energy dissipaters. It was observed that the response of CBF structures employing inelastic gusset plates is similar to the response of similar structures employing inelastic brace members. More detailed study is required to properly compare the two approaches.

It is anticipated that gussets at opposite ends of a single brace will simultaneously deform inelastically during loading. For the purposes of this research, it was assumed that simultaneous inelasticity would not occur in two gussets connected to a single brace since information is not available to justify assuming otherwise. Further research is required to determine the extent of combined deformation which might be expected of gussets at opposite ends of a brace, prior to fracture of one gusset.

M-braced frames have been found to perform better than similarly designed structures employing other bracing configurations. Further research is required to delineate the effects of brace angle, bracing pattern, the cyclic behaviour of chevron gussets and post fracture response of M-brace systems.

EHL gusset plates have been demonstrated to provide significantly enhanced deformability when compared to continuous gusset plates. Gussets of this type have capability to act as inelastic elements in all of the structures analyzed herein. Significant additional research is required to characterize the behaviour of EHL gusset plates and to generate design recommendations. The role of friction in the response of EHL gussets is of particular interest.

Appendix A – Patch, Beam and Extended Gusset Analysis Results

A.1 Preamble

This appendix provides a summary of analysis results obtained for modified continuous gusset plates, proportioned to increase deformability. Referring to the radial strip analogy, one can increase the radius to the gusset force, r , by increasing the width of the reinforced connection region. By increasing r , the deformation at onset of fracture can be increased. Gussets among the “beam” group were analyzed using finite element analysis and are shown in figures A.1 through A.14. Three extended gussets were analyzed to assess the effect of increasing the length of the yielded portion of the gusset plate. Patch gussets, reported at the bottom of the table, are those employing reinforcement in the brace connection region only. It can be seen that the FEA predicted fracture deformations for plates in that category are significantly less than those in the patch and extended categories.

Table A.1 - Analysis Results

Gusset	Ref. Figure	Type	Ult Load (kN)	δ_{ult} Displ. (mm)
12DE	A.1	beam	3233	22.3
12DF	A.2	beam	4249	31.0
12DG	A.3	beam	2336	28.7
12DH	A.4	beam	2915	32.0
12DI	A.5	beam	2172	24.7
12DJ	A.6	beam	2141	24.3
12DK	A.7	beam	3781	41.4
16ROM	A.8	beam	965	15.4
20RCL	A.9	beam	1155	17.8
20RCM	A.10	beam	1762	21.0
20RCS	A.11	beam	1918	19.3
24RCL	A.12	beam	1490	18.1
24RCM	A.13	beam	1962	24.4
24RCS	A.14	beam	2285	21.3
EXT1	A.15	ext/beam	2310	33.7
EXT2	A.16	ext/beam	2561	61.0
EXTEND	A.17	ext/beam	1783	33.0
12WM	A.18	patch	1348	19.8
12D2	A.19	patch	1873	8.8
12D8	A.20	patch	1895	11.4
12D16	A.21	patch	1905	12.3
12S2	A.22	patch	1774	11.2
12S8	A.23	patch	1777	12.1
12S16	A.24	patch	1779	13.5
12DB	A.25	patch	2332	11.9
12DC	A.26	patch	1989	12.2
12DD	A.27	patch	1873	9.7
12R	A.28	patch	2017	16.4
12W	A.29	patch	1424	12.5

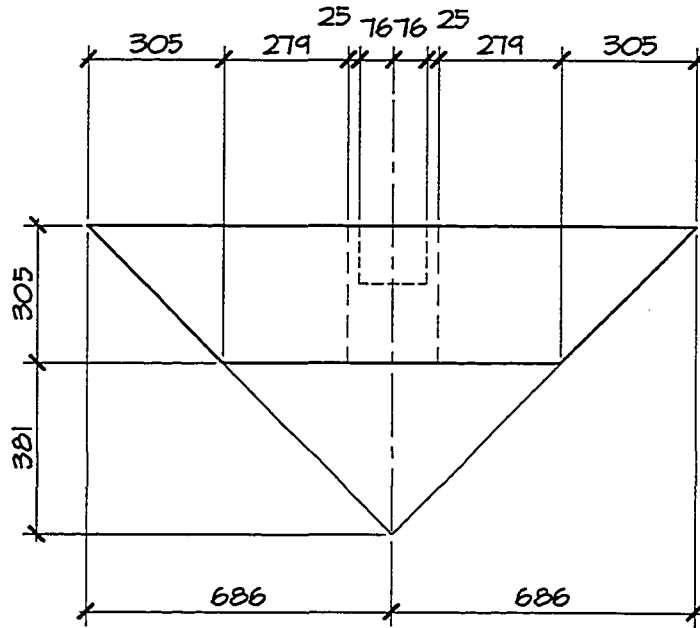


Figure A.1 – Gusset 12DE Geometry

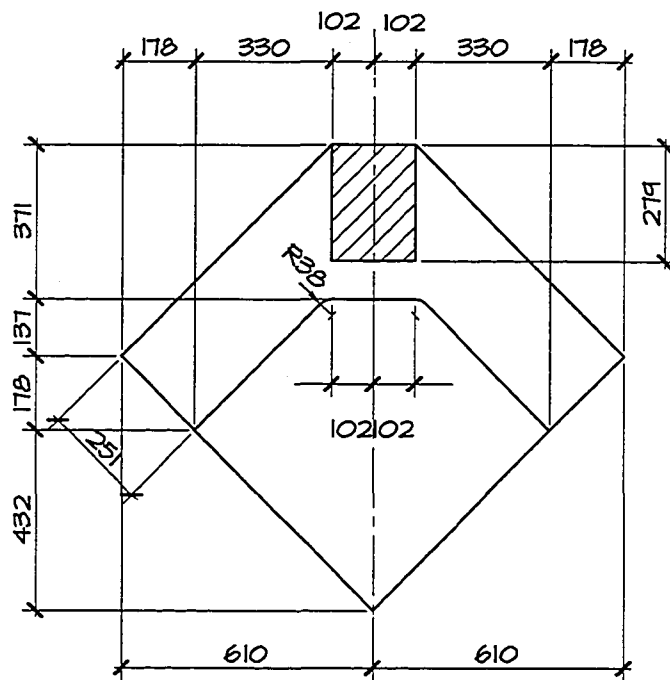


Figure A.2 – Gusset 12DF Geometry

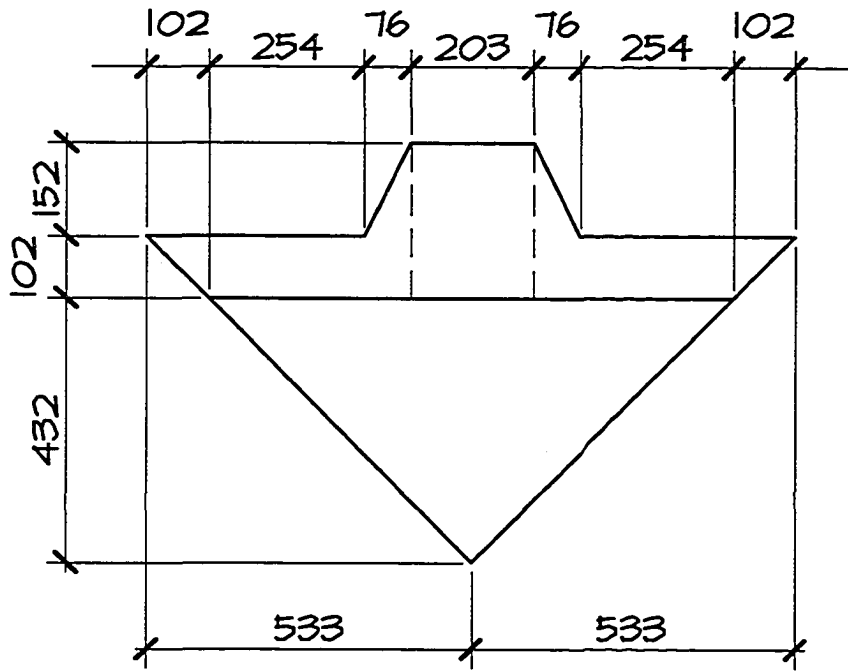


Figure A.3 – Gusset 12DG Geometry

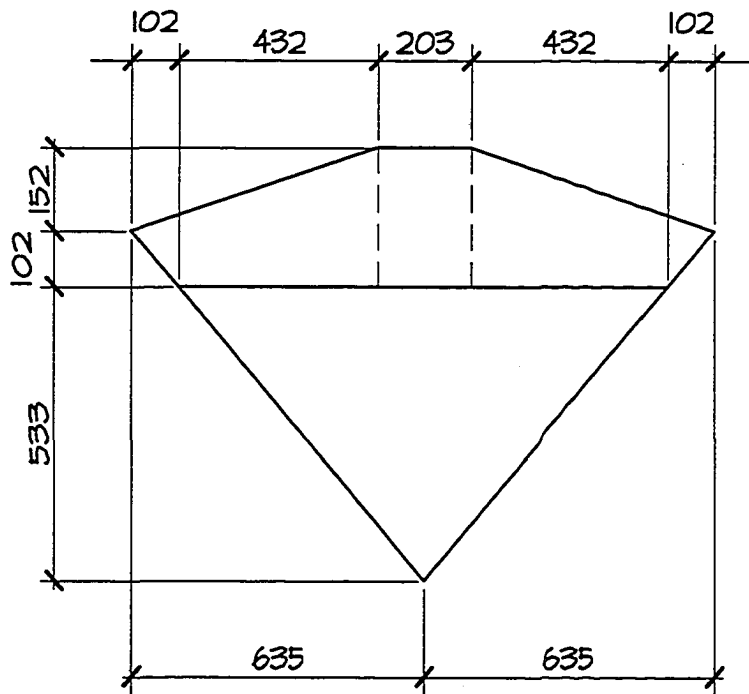


Figure A.4 – Gusset 12DH Geometry

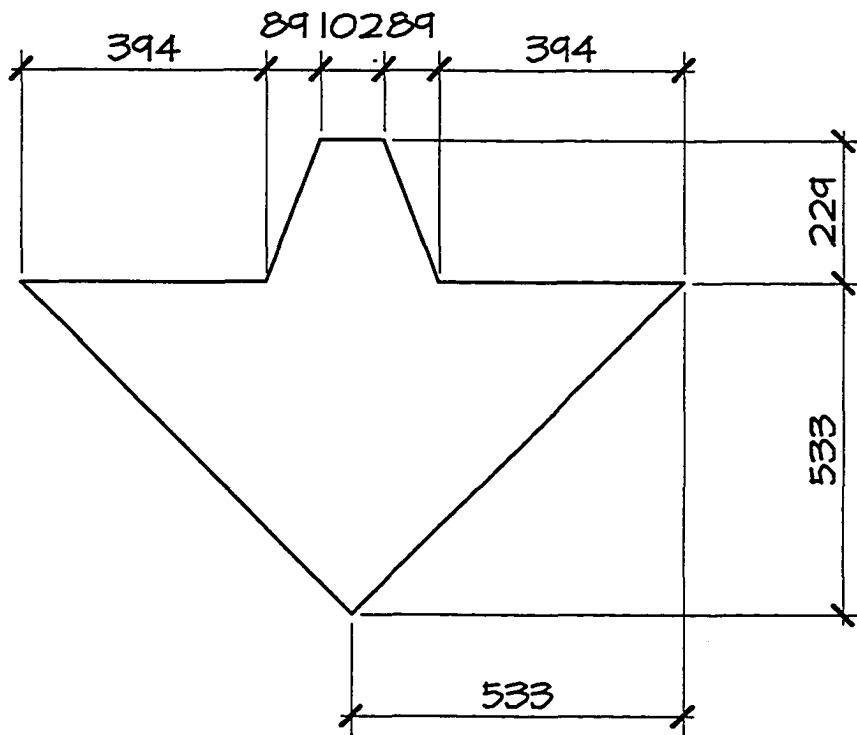


Figure A.5 – Gusset 12DI Geometry

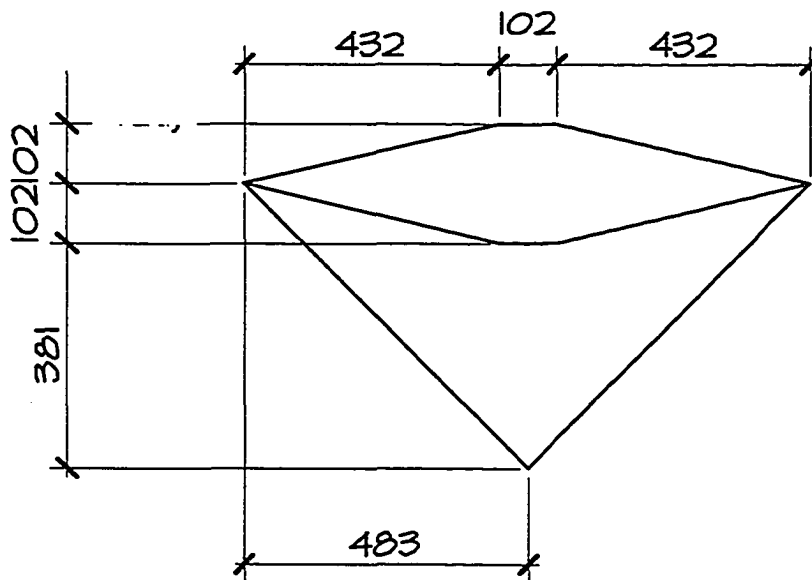


Figure A.6 – Gusset 12DJ Geometry

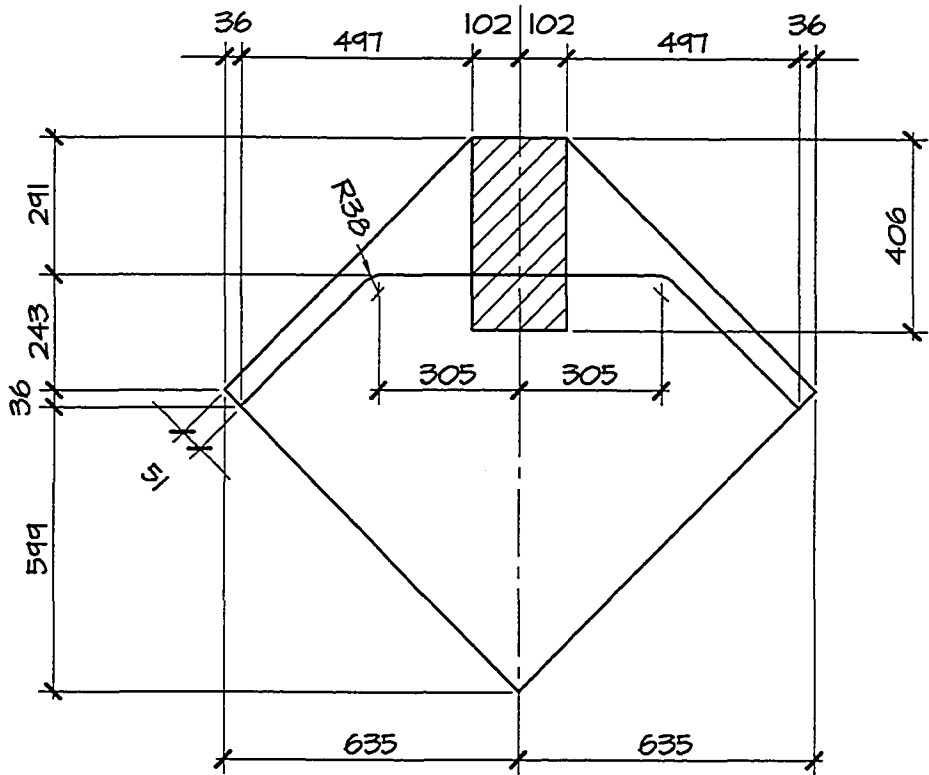


Figure A.7 – Gusset 12DK Geometry

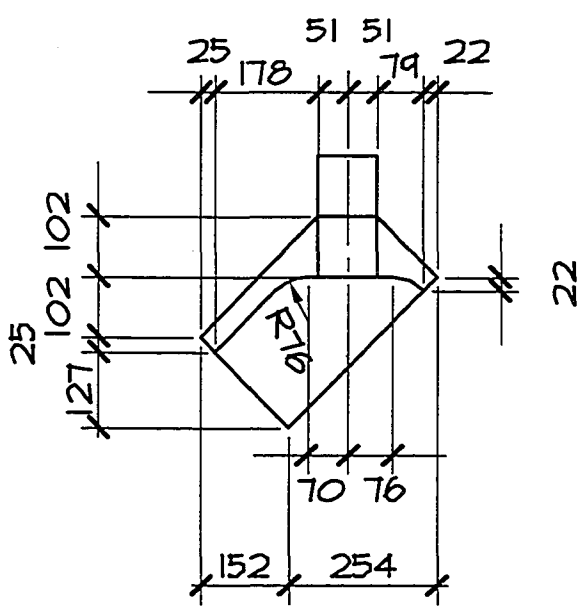


Figure A.8 – Gusset 16ROM Geometry

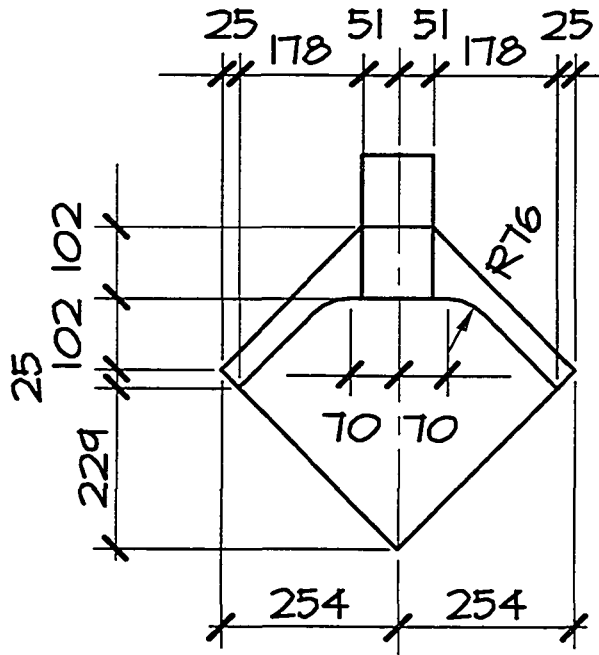


Figure A.9 – Gusset 20RCL Geometry

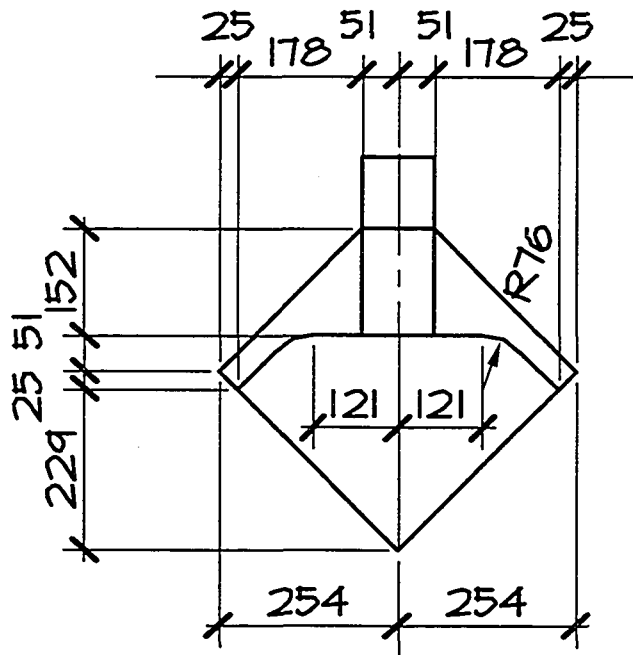


Figure A.10 – Gusset 20RCM Geometry

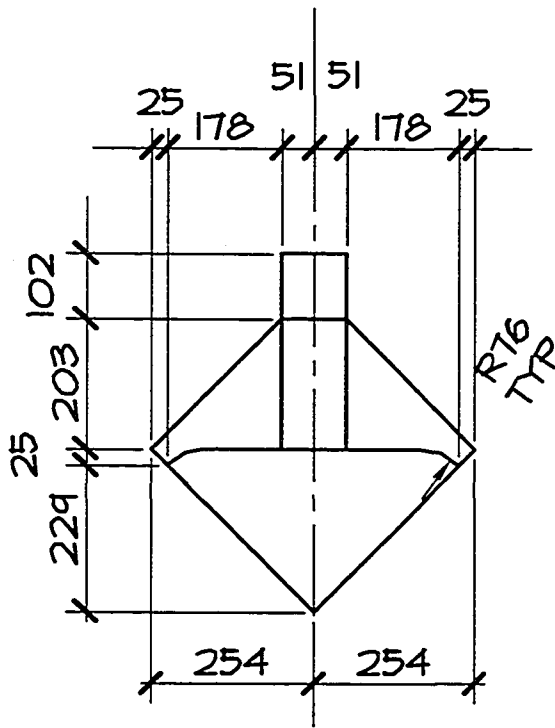


Figure A.11 – Gusset 20RCS Geometry

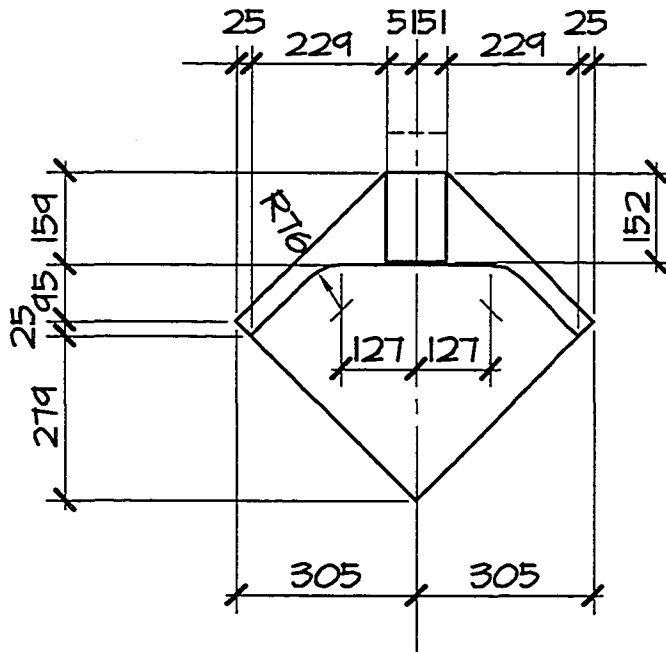


Figure A.12 – Gusset 24RCL Geometry

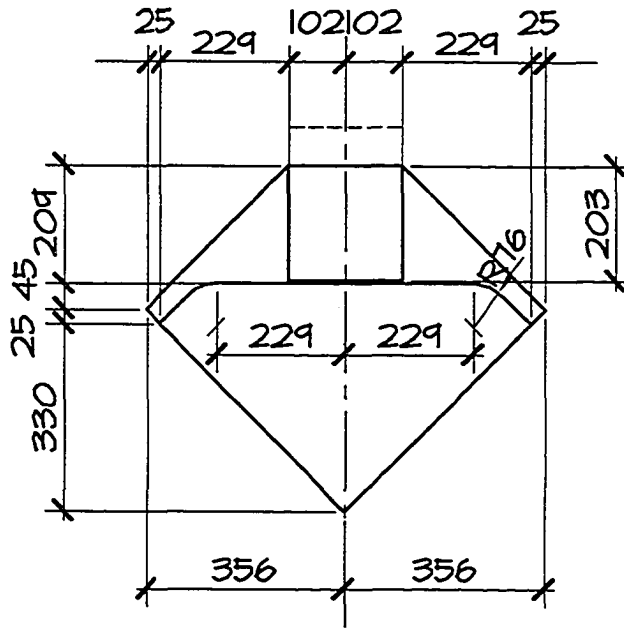


Figure A.13 – Gusset 24RCM Geometry

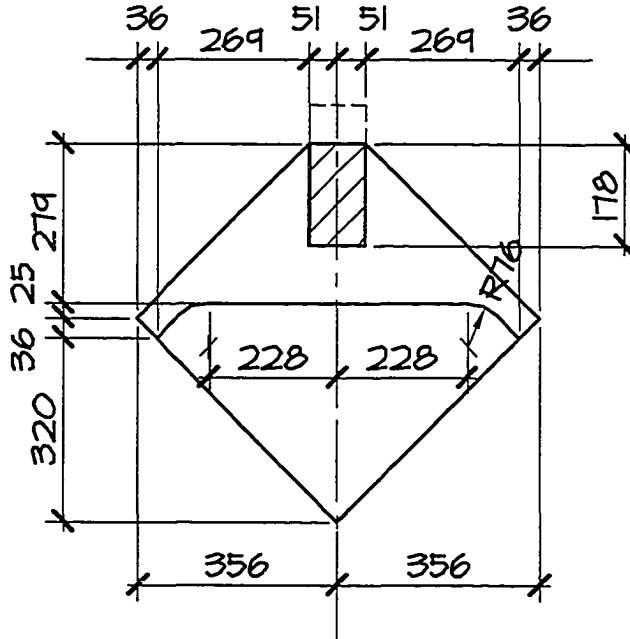


Figure A.14 – Gusset 24RCS Geometry

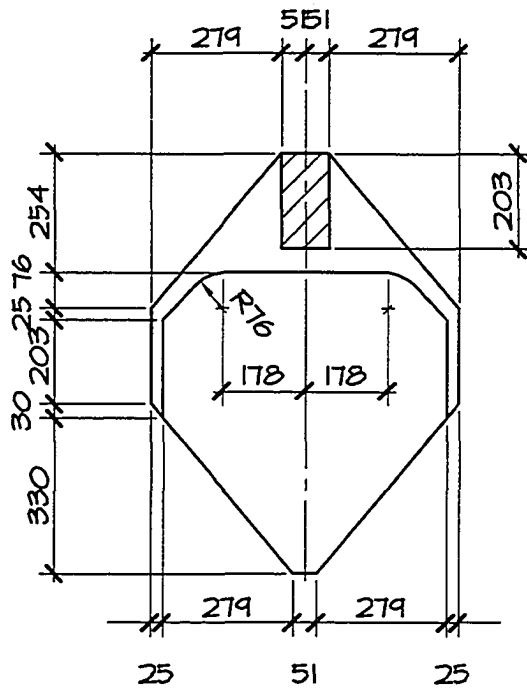


Figure A.17 – Gusset EXTEND Geometry

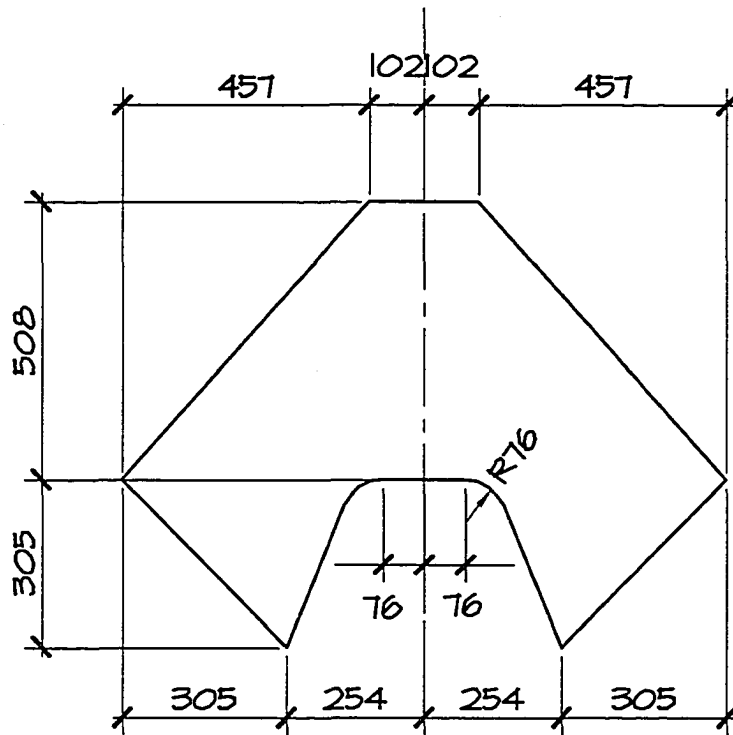


Figure A.18 – Gusset 12WM Geometry

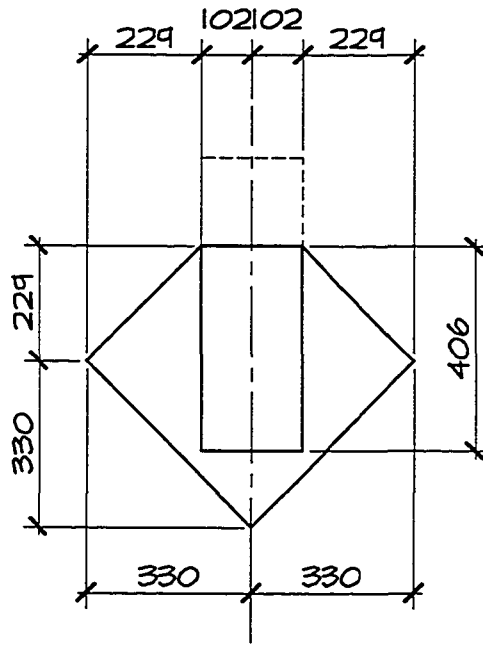


Figure A.19 – Gusset 12D2 Geometry

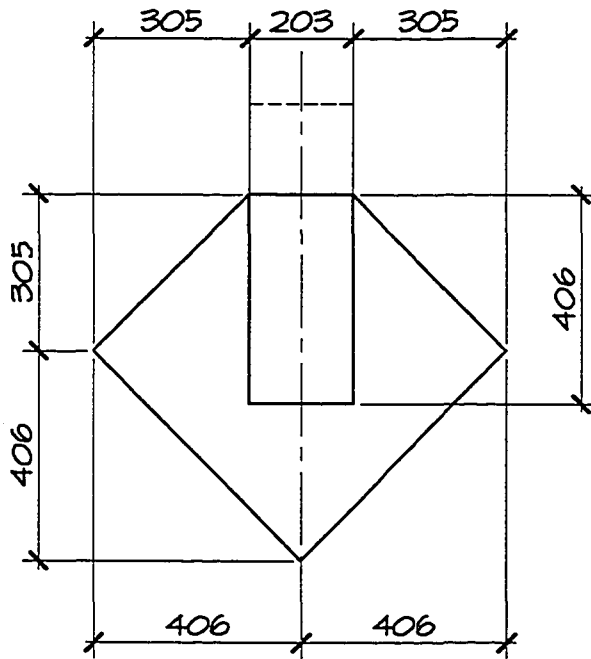


Figure A.20 – Gusset 12D8 Geometry

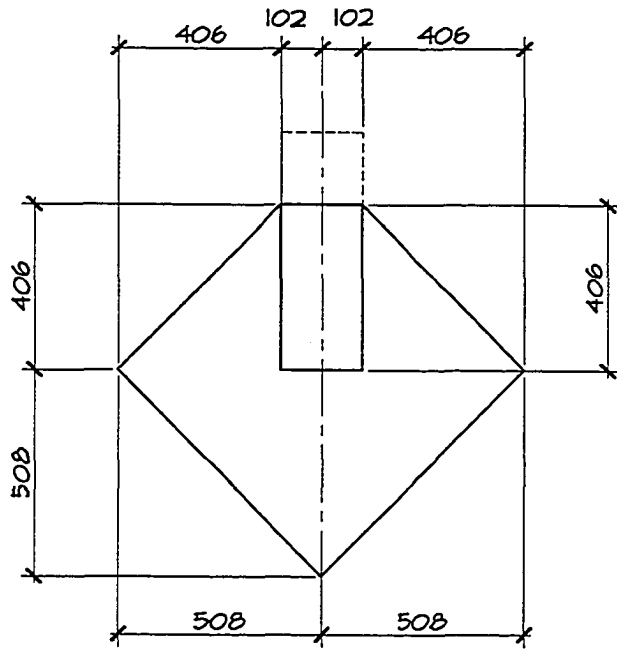


Figure A.21 – Gusset 12D16 Geometry

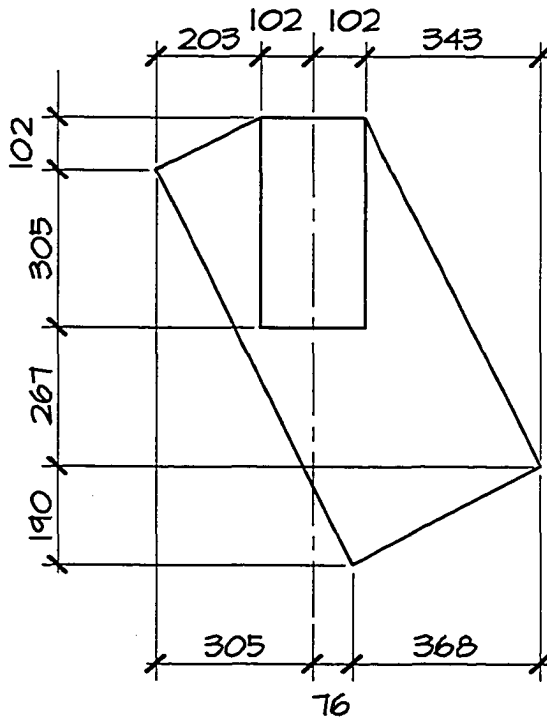


Figure A.22 – Gusset 12S2 Geometry

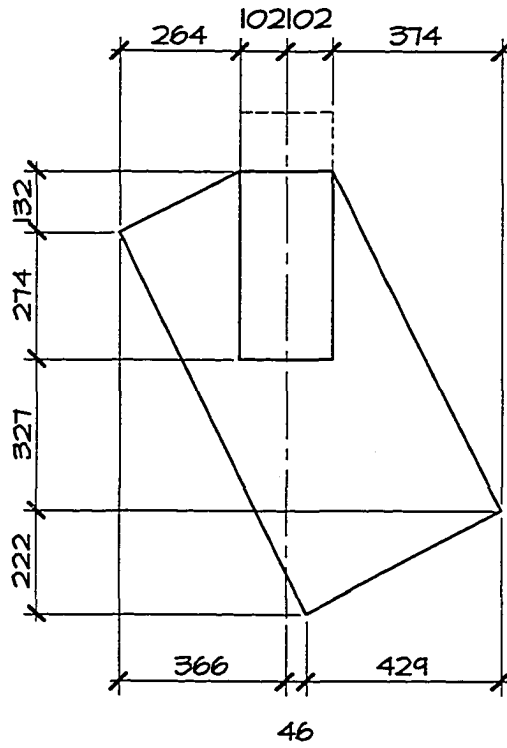


Figure A.23 – Gusset 12S8 Geometry

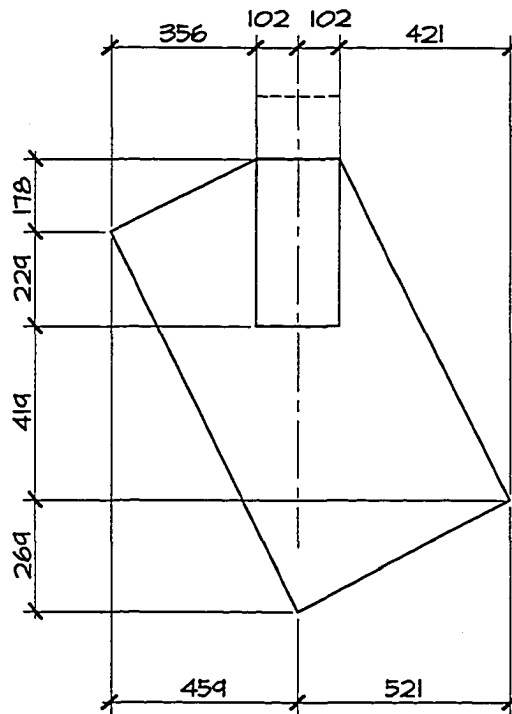


Figure A.24 – Gusset 12S16 Geometry

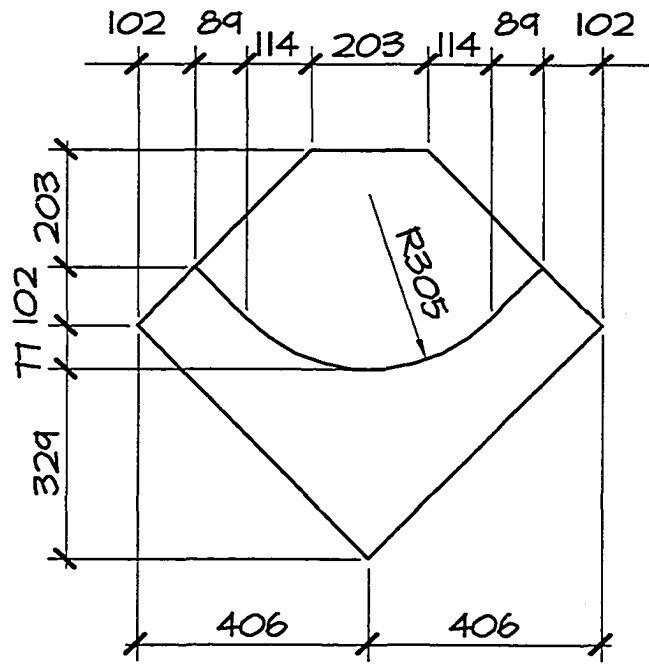


Figure A.25 – Gusset 12DB Geometry

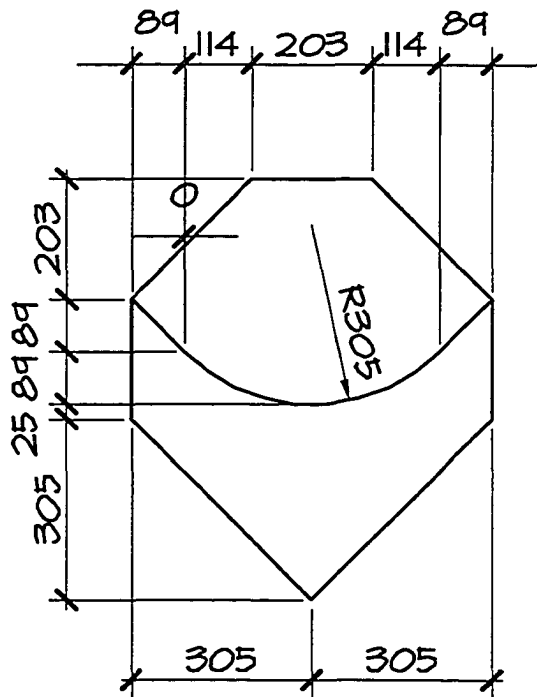


Figure A.26 – Gusset 12DC Geometry

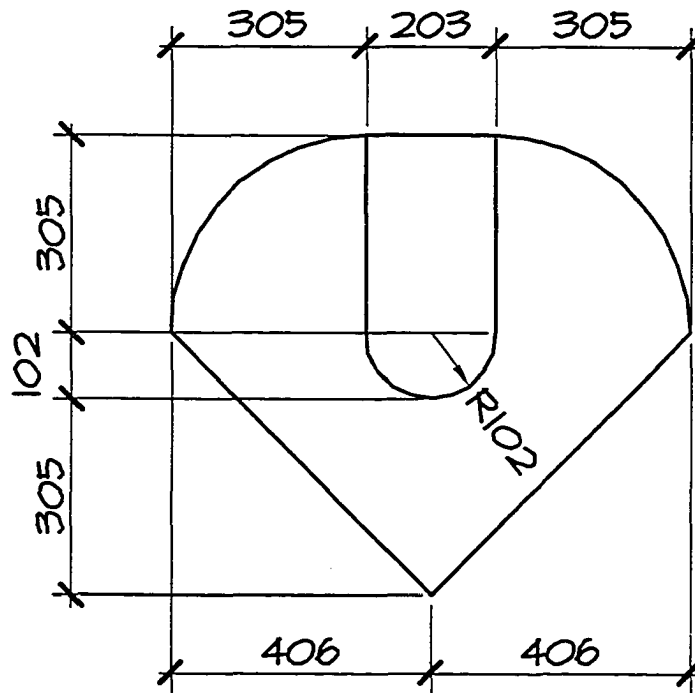


Figure A.27 - Gusset 12DD Geometry

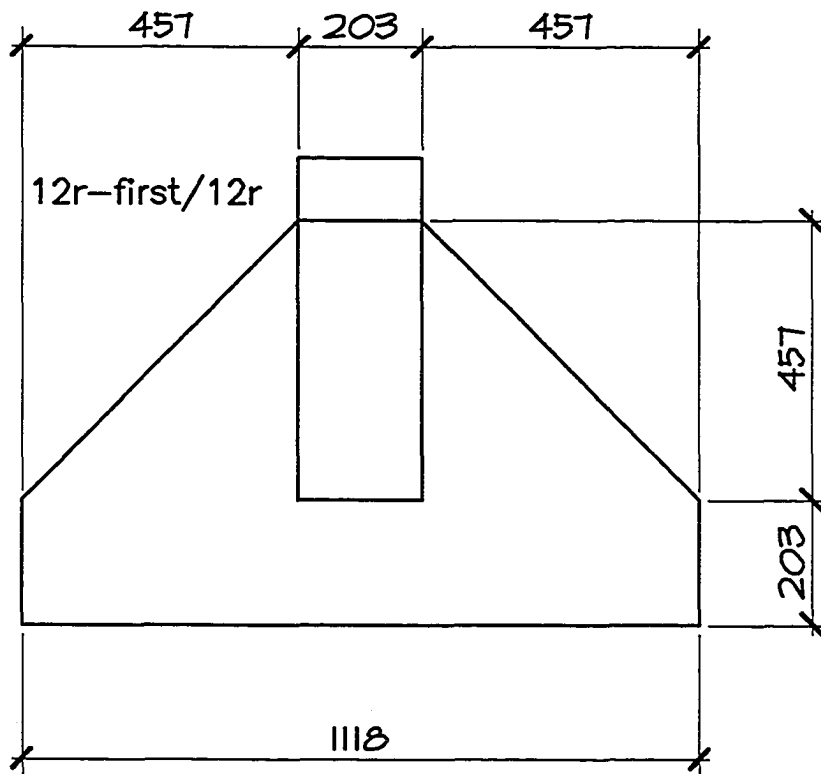


Figure A.28 - Gusset 12R Geometry

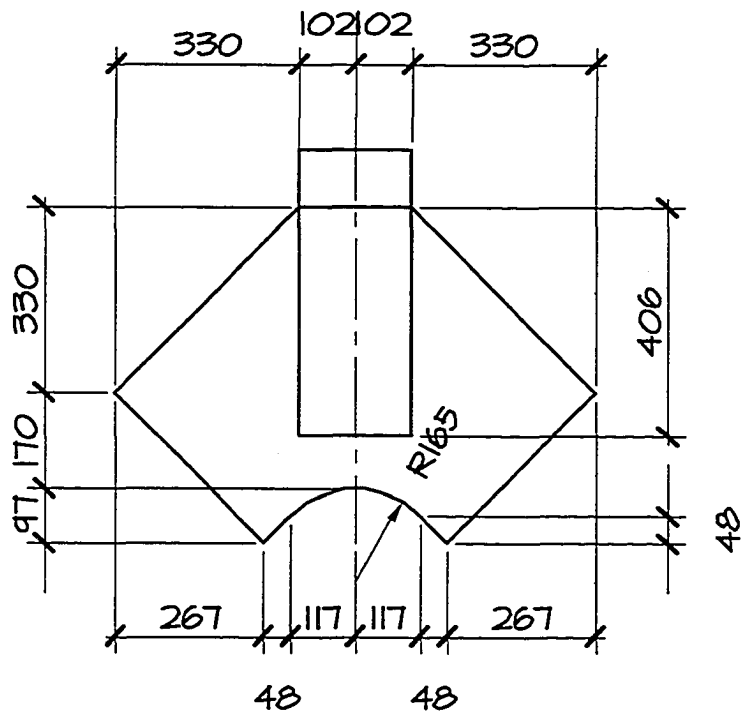


Figure A.29 – Gusset 12W Geometry

Appendix B – Beam Gusset Analysis Results

B.1 Preamble

This appendix summarizes analytical results from a series of exploratory link beam analyses conducted to provide background information for formulation of the Extended Hinge Link gusset, reported in Chapter 4. The geometry of bend11 was found to approximate the desired uniform strain distribution along the top and bottom fibers of the link while remaining elastic within the necked region. It is notable that bend11, the only configuration which did not exhibit early strain localization, had a predicted ultimate deformation of 256 mm. This is significantly larger than the next largest predicted ultimate deformation of 186 mm.

Table B.1 - Analysis Results

Gusset	Reference Figure	Type	Max Load (kN)	δ_{ult} Displ. (mm)
BEND1	-	bend	670	78.5
BEND2	B.1	bend	438	95.6
BEND3	B.2	bend	187	64.2
BEND4	B.3	bend	457	72.9
BEND5	B.4	bend	487	86.7
BEND6	-	bend	259	67.2
BEND7	B.5	bend	496	75.2
BEND8	B.6	bend	978	26.9
BEND9	B.7	bend	731	40.3
BEND10	B.8	bend	942	38.9
BEND11	B.9	bend	596	256
BEND12	B.10	bend	663	96.9
BEND13	B.11	bend	648	151
BEND14	B.12	bend	305	186
BEND15	B.13	bend	168	48.2
BEND15A	-	bend	188	98.0
BEND16	-	bend	165	87.2

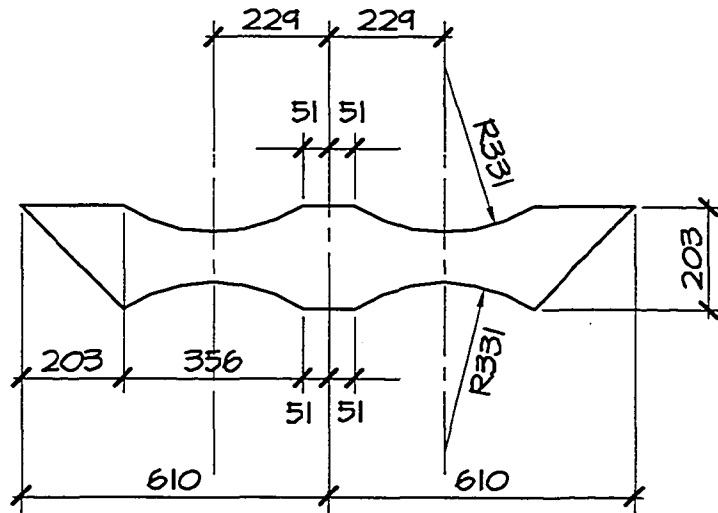


Figure B.1 - BEND2 Geometry

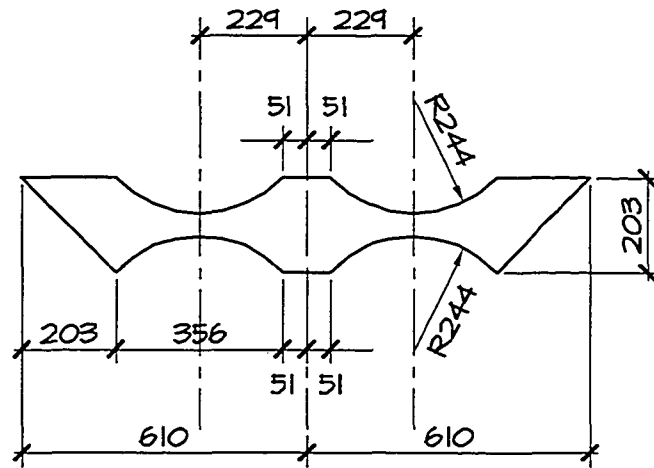


Figure B.2 - BEND3 Geometry

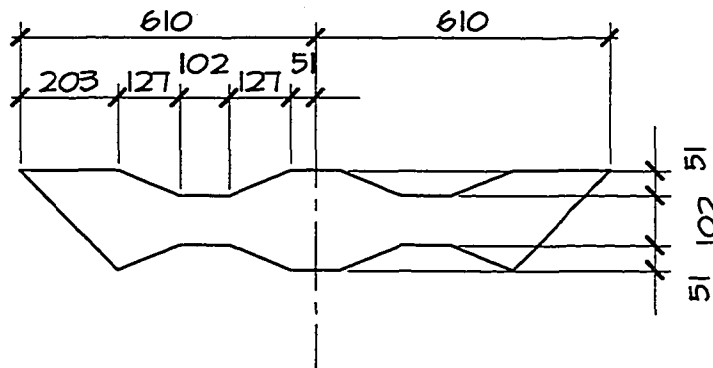


Figure B.3 - BEND4 Geometry

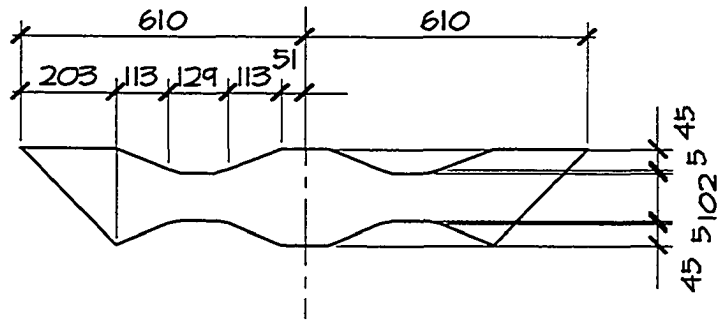


Figure B.4 – BEND5 Geometry

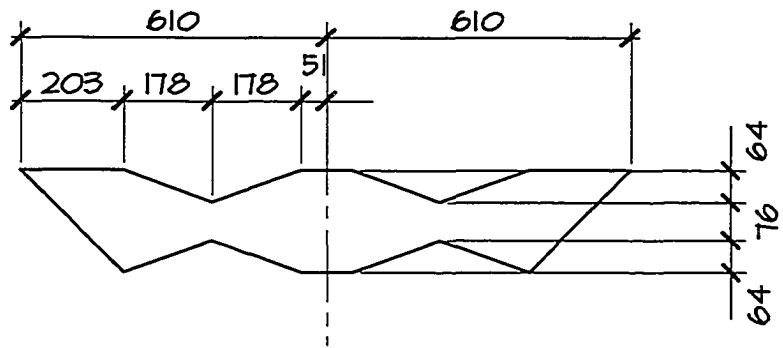


Figure B.5 – BEND7 Geometry

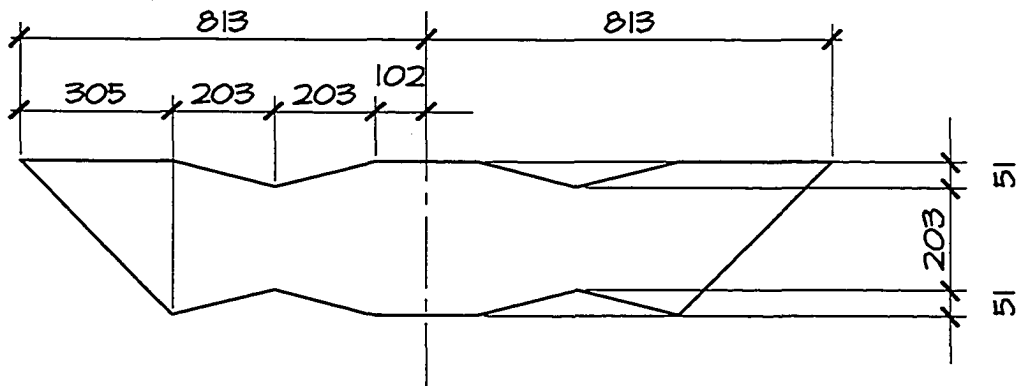


Figure B.6 – BEND8 Geometry

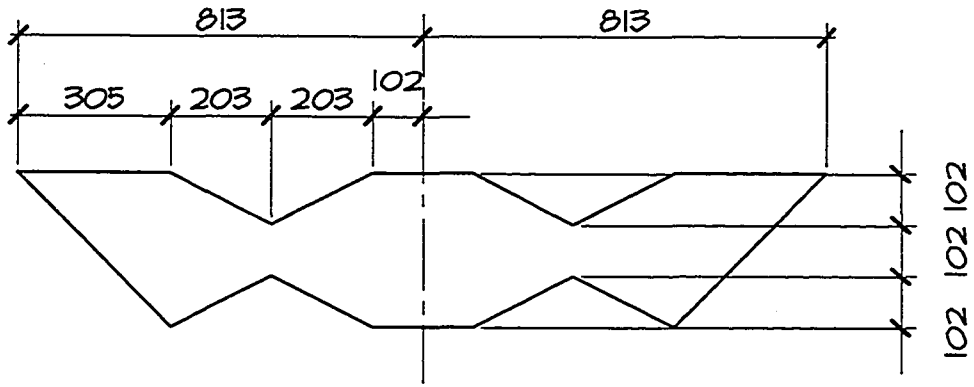


Figure B.7 – BEND9 Geometry

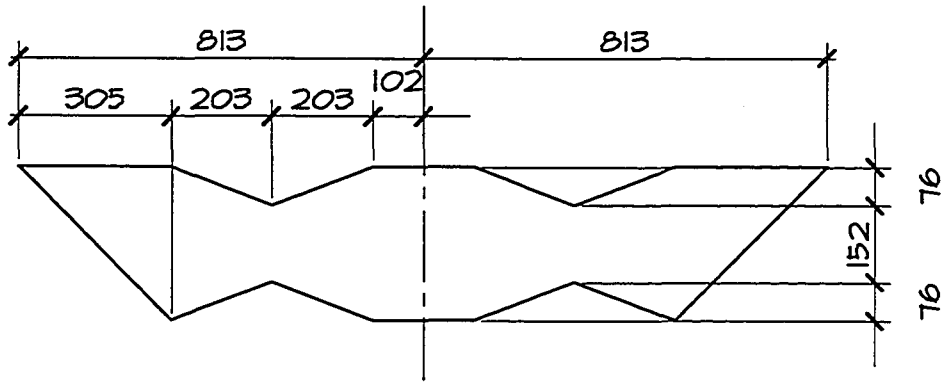


Figure B.8 – BEND10 Geometry

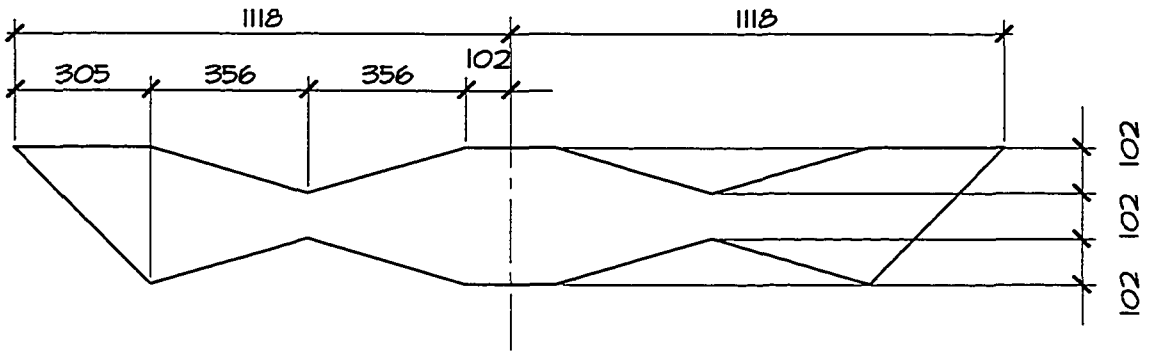


Figure B.9 – BEND11 Geometry

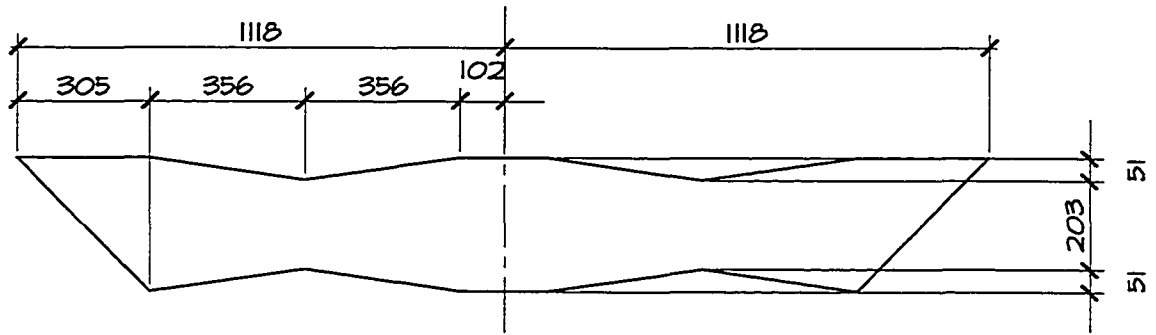


Figure B.10 – BEND12 Geometry

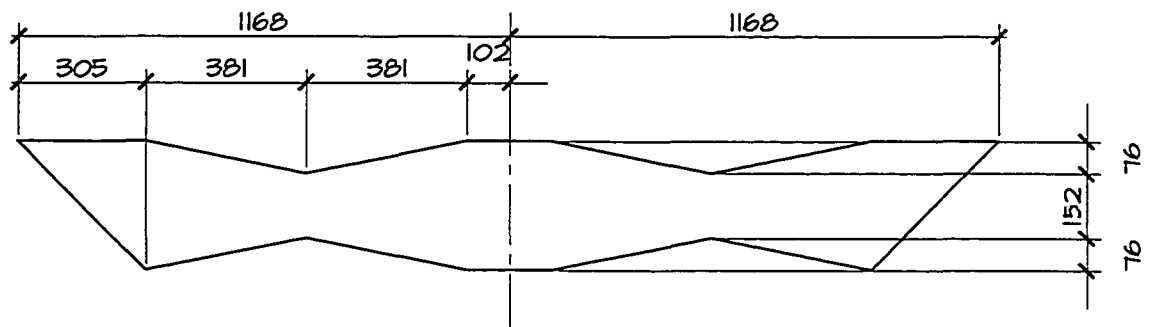


Figure B.11 – BEND13 Geometry

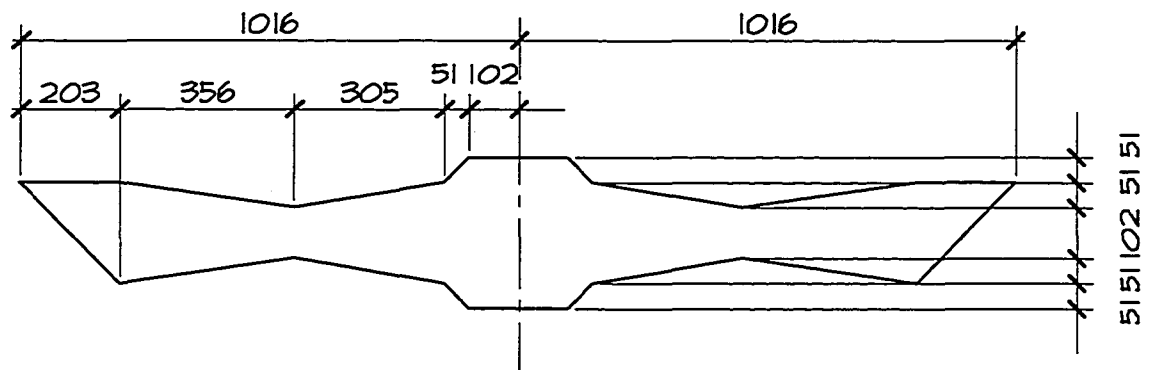


Figure B.12 – BEND2 Geometry

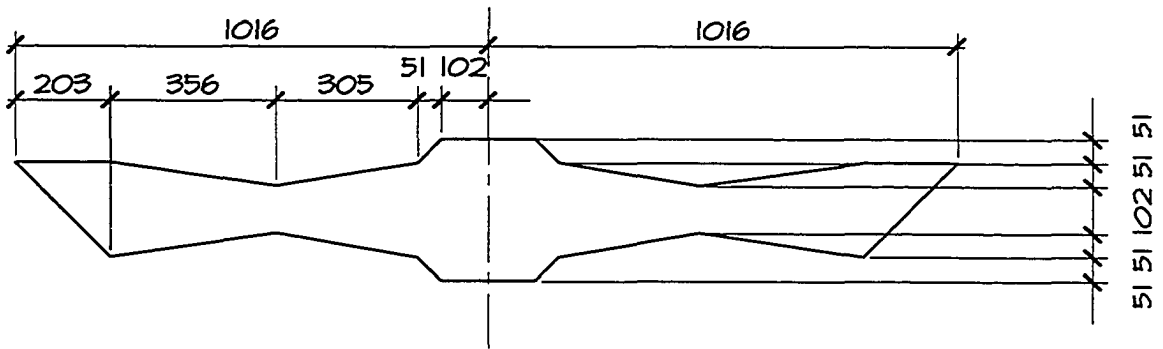


Figure B.13 – BEND15 Geometry